HAL open science

Yang-Mills and Quantum Chromodynamics correlation functions from the Curci-Ferrari model at two-loop accuracy

Nahuel Barrios

To cite this version:

Nahuel Barrios. Yang-Mills and Quantum Chromodynamics correlation functions from the Curci-Ferrari model at two-loop accuracy. High Energy Physics - Theory [hep-th]. Institut Polytechnique de Paris; Universidad de la República (Montevideo), 2022. English. NNT : 2022IPPAX081 . tel-04105546

HAL Id: tel-04105546

https://theses.hal.science/tel-04105546v1

Submitted on 20 Jun 2024

HAL is a multi-disciplinary open access archive for the deposit and dissemination of scientific research documents, whether they are published or not. The documents may come from teaching and research institutions in France or abroad, or from public or private research centers.

L'archive ouverte pluridisciplinaire **HAL**, est destinée au dépôt et à la diffusion de documents scientifiques de niveau recherche, publiés ou non, émanant des établissements d'enseignement et de recherche français ou étrangers, des laboratoires publics ou privés.

INSTITUT POLYTECHNIQUE DE PARIS

NNT : 2022IPPAX081

Thèse de doctorat

Yang-Mills and Quantum Chromodynamics correlation functions from the Curci-Ferrari model at two-loop accuracy

Thèse de doctorat de l'Institut Polytechnique de Paris
préparée à l'École polytechnique et à l'Universidad de la República

École doctorale n°626 Institut Polytechnique de Paris (EDIPP)
Spécialité de doctorat: Physique

Thèse présentée et soutenue à Montevideo, Uruguay, le 21/09/2022, par

NAHUEL BARRIOS

Composition du Jury :

Leticia Palhares Professeur, Unviersidade do Estado do Rio de Janeiro (DFT)	Rapporteur
Axel Weber Professeur, Universidad Michacana de San Nicolás de Hidalgo (IFM)	Rapporteur
Miguel Campiglia Professeur, Universidad de la República (IFFC)	Président
Jan Pawlowski Professeur, Ruprecht-Karls-Universität Heidelberg (ITP)	Examinateur
Marcela Peláez Professeur, Universidad de la República (IFFI)	Directrice de thèse
Urko Reinosa Chargé de Recherche au CNRS, École Polytechnique (CPHT)	Directeur de thèse

Acknowledgments

First and foremost I am very grateful to my advisors, Marcela Peláez and Urko Reinosa, for always being willing to answer my questions, for their continuous support, help and guidance. All of the work presented in this thesis has been made in collaboration with Marcela and Urko. I have learned so much from you.

I am very grateful to my mother, Rosario Acosta, my siblings Tatiana Barrios, Dilan Campos and Milagros Barrios, my niece Nicole Silva, my very good friend Johana Leivas and little Juanma for their permanent support and love over all these years.

I would like to thank Nicolás Wschebor, for his support, specially in the early stages of this doctorate, for many interesting discussions and for collaborating with us in the first work of this thesis.

I am grateful to John Gracey, with whom I had the pleasure of collaborating for one of the works presented in this manuscript and for several illuminating discussions.

I thank Mattheu Tissier for several enhancing discussions and insights. I thank Cédic Lorcé and Julien Serreau for participating of the thesis follow-up committee.

I also would like to thank Arturo Amor, Patricia Ortega, Duifje van Egmond, and the members of the CPHT of École Polytechnique for their kindness, the nice discussions and for making my stays in Paris warmer. I also want to thank Magdalena Fuentes for kindly receiving me at her home in Paris.

I am grateful to Virginia Feldman, Lucía Amy, Andrés Vallejo, Gastón Ayubi, Lucía Duarte, Florencia Benítez, Esteban Mato and Daniel Gau for the lectures and discussions we shared together. I also thank the Pedeciba - Física secretary, Jimena Rodríguez, for her help in the doctorate paperwork.

I would like to thank the financial support of Pedeciba - Física, the Agencia Nacional de Investigación e Innovación (ANII), the Laboratoire International Associé of the CNRS, Institut Franco-Uruguayen de Physique, the French Embassy in Uruguay and the Comisión Académica de Posgrado (CAP - UdelaR). Also, I would like to thank the Instituto de Física, Facultad de Ingeniería, UdelaR, for supporting me in my stays at École Polytechnique.

Finally, I would like to thank the members of the jury, for kindly agreeing to participate of it, and for their valuable comments and corrections: Miguel Campiglia, Leticia Palhares, Jan Pawlowski and Axel Weber.

Abstract

Quantum Chromodynamics (QCD) is a well established gauge theory which describes the dynamics of quarks and gluons. At the analytical level, physical observables can be computed only after the gauge is fixed. The textbook procedure to do so is the Faddeev-Popov (FP) method, which introduces, as a byproduct, auxiliary non-physical fields known as ghosts. Moreover, the QCD gauge coupling becomes small at very high momenta, making of perturbation theory (PT) a suitable calculation tool within that region of momenta. The combination of the FP theory and PT has turned out to be extremely useful and has been tested experimentally in many occasions. However, in the opposite momentum range, the FP method is no longer fully valid due to the presence of Gribov copies. Consequently, in order to access QCD in the infrared, new approaches are needed.

This thesis is devoted to one of such approaches: the Curci-Ferrari (CF) model in Landau gauge. It consists in a simple gluon mass extension of the FP theory. Its main motivation comes from the lattice simulations for correlation functions in the Landau gauge, which clearly indicate that the gluon acquires a mass in the deep infrared. In addition to this striking phenomenon, lattice simulations feature a gauge coupling compatible with a perturbative analysis for the whole range of momenta, at least in the pure gauge - or Yang-Mills (YM) - sector. Thus, with the purpose of testing the model, several two- and three-point correlation functions have been perturbatively evaluated at one-loop order. In general terms, the results show a very good agreement with the lattice data. More recently, the two-point functions from the pure YM theory were evaluated at two-loop order, improving the agreement with lattice data. The goal of this thesis is to extend the two-loop calculations to other correlation functions. This is a way to further test the perturbative use of the model as well as to clarify its limits.

In the case of pure YM theory, we evaluate the ghost-antighost-gluon vertex and the three-gluon vertex in a particular kinematical configuration in four dimensions, for the SU(2) and SU(3) gauge groups. Both quantities emerge as a pure prediction of the CF model, since its two free parameters are determined by fitting the two-point functions. Broadly speaking, the predicted vertices are able to improve the agreement with their numerical counterparts in comparison with the one-loop correction. We also investigate the renormalization scheme dependence of our results, which shows consistency with the perturbative approach. As for the three-gluon vertex, the calculation allows us in particular to gain insight on the zero-crossing as well as to test an exact prediction for its leading behavior in the infrared.

We end this investigation by fitting the ghost, gluon and quark two-point functions in QCD, with two degenerate quark flavors, to available lattice data.

Our evaluation is consistent with such data in all cases, except for the quark mass function in the case of light quarks. The result is particularly relevant for the quark dressing function, since the CF model is unable to reproduce the lattice data at one-loop order. This discrepancy is corrected by the two-loop evaluation, which agrees with the data both at a qualitative and at a quantitative level.

Résumé

La Chromodynamique Quantique (QCD) est une théorie de jauge bien établie qui décrit la dynamique des quarks et des gluons. Au niveau analytique, les observables physiques ne peuvent être calculées que lorsque la jauge est fixée. La méthode standard pour y parvenir est la méthode de Faddeev-Popov (FP), qui introduit comme sous-produit des champs auxiliaires non physiques, les "fantômes". D'autre part, le couplage de jauge de la QCD devient faible pour des impulsions très élevées, ce qui fait de la théorie des perturbations (TP) un outil de calcul approprié dans cette limite. L'approche perturbative dans le cadre de la méthode de FP s'est avérée extrêmement utile et a été testée expérimentalement à de nombreuses reprises. Cependant, dans la gamme opposée d'impulsions, la méthode de FP n'est plus entièrement valide en raison de la présence de copies de Gribov. Par conséquent, pour accéder à l'infrarouge de la QCD, une approche alternative est nécessaire.

Cette thèse est consacrée à une de ces approches : le modèle de Curci-Ferrari (CF) dans la jauge de Landau. Elle consiste en une simple extension de la théorie de FP, à laquelle est ajouté un terme de masse pour le champ de gluons. Sa principale motivation provient des simulations numériques de fonctions de corrélation dans la jauge de Landau, qui indiquent clairement que le gluon acquiert une masse dans l'infrarouge profond. En plus de ce phénomène frappant, les simulations numériques montrent un couplage de jauge compatible avec une analyse perturbative pour toute la gamme d'impulsions, au moins pour le secteur pure jauge - ou de Yang-Mills (YM). Ainsi, afin de tester le modèle, plusieurs fonctions de corrélation à deux et trois points ont été évaluées de manière perturbative à une boucle. D'une manière générale, ces résultats montrent un bon accord avec leurs homologues numériques. Plus récemment, les fonctions à deux points de la théorie YM pure ont été évaluées à deux boucles, améliorant ainsi l'accord avec les données des simulations. L'objectif de cette thèse est d'étendre les calculs à deux boucles à d'autres fonctions de corrélation. Il s'agira ainsi de tester plus avant l'approche perturbative dans le modèle de CF, tout en clarifiant ses limites.

Dans le cas de la théorie YM pure, nous évaluons le vertex fantôme-antifantôme-gluon et le vertex à trois gluons dans une configuration cinématique particulière, en quatre dimensions, pour les groupes de jauge SU(2) et SU(3). Ces deux quantités sont une pure prédiction du modèle de CF, puisque les deux paramètres libres du modèle sont déterminés à partir de l'ajustement des fonctions à deux points. De manière générale, les corrections à deux boucles améliorent l'accord avec les numériques par rapport aux corrections à une boucle. La dépendance de nos prédictions par rapport au schéma de renormalisation, diminue également une fois les corrections à deux boucles incluses, ce qui conforte l'approche perturbative. En ce

qui concerne le vertex à trois gluons, le calcul nous permet notamment d'obtenir des informations sur le passage à zéro ainsi que de tester une prédiction sur le comportement dominant exact de cette quantité dans l'infrarouge.

Nous concluons cette étude en calculant les fonctions à deux boucles pour le fantôme, le gluon et le quark dans le cadre de la QCD, en présence deux saveurs dégénérées de quarks, et en les comparant aux données des simulations numériques. Les résultats à deux boucles montrent un accord au résultats numériques systématiquement meilleur par rapport aux évaluations à une boucle, à l'exception de la fonction de masse des quarks légers. Ce résultat est particulièrement pertinent pour la fonction d'habillage des quarks, puisque les calculs à une boucle est incapable de reproduire les données des simulations. Cette incohérence est levée à deux boucles tant sur le plan qualitatif que quantitatif.

Resumen

La Cromodinámica Cuántica (QCD por sus siglas en inglés) es una teoría de gauge bien establecida que describe la dinámica de quarks y gluones. A nivel analítico, los observables físicos solo pueden calcularse una vez fijado el gauge. La manera estándar de hacer esto es a través del método de Faddeev-Popov (FP), que como subproducto introduce campos auxiliares no físicos, los llamados fantasmas. Por otra parte, el acoplamiento de gauge de la QCD se vuelve pequeño para momentos muy altos, lo que hace de la teoría de perturbaciones (TP) una herramienta de cálculo adecuada en dicha región de momentos. La combinación de la teoría de FP y de la TP ha resultado ser extremadamente útil y ha sido probada experimentalmente en numerosas ocasiones. Sin embargo, en el rango opuesto de momentos, el método de FP deja de ser totalmente válido debido a la presencia de copias de Gribov. En consecuencia, para acceder al infrarrojo de la QCD, es necesario algún tipo de enfoque alternativo.

Esta tesis está dedicada a uno de estos enfoques: el modelo de Curci-Ferrari (CF) en el gauge de Landau. Consiste en una simple extensión de la teoría de FP, a la que se añade un término de masa para el campo de gluones. Su principal motivación proviene de las simulaciones numéricas, que indican claramente que el gluón adquiere una masa en el infrarrojo profundo. Además de este llamativo fenómeno, las simulaciones numéricas muestran un acoplamiento de gauge compatible con un análisis perturbativo para todo el rango de momentos, al menos para el sector de gauge -o Yang-Mills (YM) - puro. Es así que, con el fin de poner a prueba el modelo, se han evaluado perturbativamente varias funciones de correlación a dos y tres puntos a un loop. En términos generales, dichos resultados muestran una buena concordancia con sus contrapartes numéricas. Más recientemente, las funciones a dos puntos de la teoría de YM pura fueron evaluadas a dos loops, mejorando el acuerdo con los datos de las simulaciones. El objetivo de esta tesis es extender el cálculo a dos loops a otras funciones de correlación. Se trata de una forma exigente de testear el uso perturbativo del modelo así como de clarificar sus límites.

En el caso de la teoría de YM pura, evaluamos el vértice fantasma-antifantasma-gluón y el vértice de tres gluones en una configuración cinemática particular, en cuatro dimensiones, para los grupos de gauge SU(2) y SU(3). Ambas cantidades surgen como una predicción pura del modelo de CF, ya que los dos parámetros libres del modelo quedan determinados a partir del ajuste de las funciones a dos puntos. De manera general, las evaluaciones a dos loops de los vértices son capaces de mejorar la concordancia con sus contrapartes numéricas en comparación con las correcciones a un loop. Asimismo, investigamos la dependencia de los vértices con el esquema de renormalización. En cuanto al vértice de tres gluones, el cálculo

nos permite, en particular, obtener información sobre el cruzamiento del cero así como testear una predicción exacta para el comportamiento dominante de esta cantidad en el infrarrojo.

Terminamos esta investigación calculando las funciones a dos puntos para el fantasma, el gluón y el quark en QCD, con dos sabores degenerados de quarks, ajustándolas con los datos de las simulaciones numéricas. Los resultados a dos loops muestran sistemáticamente un mejor acuerdo con estas simulaciones en comparación con las evaluaciones a un loop, a excepción de la función de masa para los quarks livianos. El resultado es particularmente relevante para la función de vestidura del quark, ya que el modelo de CF es incapaz de reproducir los datos de las simulaciones a un loop. Esta discrepancia es corregida por la evaluación a dos loops, que concuerda con los datos tanto a nivel cualitativo como cuantitativo.

Résumé substantiel

La Chromodynamique Quantique (QCD) est la théorie de jauge quantique non abélienne, basée sur le groupe SU(3), qui décrit l'interaction forte. Cette théorie dicte la physique des hadrons, un vaste ensemble de particules comprenant, par exemple, des neutrons et des protons. Cependant, les entités fondamentales de la QCD ne sont pas les hadrons eux-mêmes, mais leurs constituants, les quarks et les gluons. Les premiers sont des fermions de spin 1/2 avec une charge électrique fractionnaire et existent en six types ou saveurs différents. Les gluons sont des bosons de jauge de spin 1 sans charge électrique. La charge associée à l'interaction forte est la couleur. Les quarks et les gluons portent tous deux une charge de couleur, ce qui implique que ces derniers peuvent interagir avec les quarks mais aussi entre eux.

L'étude des théories de jauge non abéliennes basées sur le groupe SU(N) a commencé des années avant l'apparition de la QCD en tant que telle, avec les travaux de C.N. Yang et R.L. Mills en 1954 [1]. En 1967, L. Faddeev et V. Popov ont publié leur célèbre procédure de fixation de jauge de telles théories [2], dont la renormalisabilité a été prouvée par G. t'Hooft en 1971 [3]. Deux ans plus tard, D. Gross et F. Wilczek et, indépendamment, D. Politzer ont découvert que la QCD est asymptotiquement libre [4, 5], ce qui signifie que, à hautes énergies, la valeur du couplage de jauge est une fonction décroissante de l'énergie. La nature non abélienne de la QCD est essentielle pour que cette propriété soit satisfaite en quatre dimensions, comme l'ont démontré S. Coleman et D. Gross [6].

Une conséquence remarquable de la liberté asymptotique est que, pour des moments suffisamment élevés, le couplage de jauge devient si petit qu'il est compatible avec un traitement perturbatif. Dans cette approche, les quarks et les gluons sont considérés comme des champs libres effectifs à l'ordre principal. Les corrections proviennent des interactions et sont incorporées au moyen d'une expansion perturbative. L'utilisation de cette technique en combinaison avec la théorie de Faddeev-Popov (FP) s'est avérée très fructueuse, par exemple, dans le traitement des sections transversales. La validité de la QCD dans le régime perturbatif a été corroborée dans plusieurs cas expérimentaux, tels que la dépendance en énergie du couplage de jauge et dans les taux d'annihilation électron-proton.

En revanche, la QCD donne une image très différente pour les processus caractérisés par une échelle de momentum de 1 GeV ou moins, dans ce que l'on appelle la région de faible momentum ou infrarouge de la QCD. Premièrement, le couplage devient de plus en plus fort vers la région de faible momentum, n'étant plus, après une certaine échelle, dans le domaine de validité de l'approximation perturbative. Cette affirmation doit toutefois être prise avec précaution, car la dépendance du couplage par rapport au momentum est évaluée par la théorie de

FP, ce qui conduit à notre deuxième observation. La théorie de FP n'est pas entièrement justifiée dans l'infrarouge, en raison de l'existence de les copies de Gribov. Ils ont été observés pour la première fois par V. Gribov dans son article fondateur de 1977 [7], étant le résultat d'une condition de fixation de jauge qui sélectionne plus d'un représentant du champ de jauge. Comme le démontre I. Singer [8], toutes les conditions de fixation de la jauge continue tombent dans cette catégorie. À haut momentum, l'effet des copies de Gribov est minime par rapport à la procédure de FP, contrairement au régime à faible momentum, où ces copies remettent sérieusement en question l'une des hypothèses sous-jacentes de la procédure.

Le fait que les outils analytiques utilisés pour décrire le régime à haut moment de la QCD ne puissent être extrapolés sans critique au régime infrarouge n'implique en aucun cas un conflit avec le contenu de la théorie, mais plutôt la nécessité d'une approche différente pour y accéder. En outre, on pense que deux phénomènes importants, qui n'ont pas été entièrement compris à ce jour, peuvent être expliqués par la QCD à faible momentum. Premièrement, il y a le confinement, caractérisé par le fait que les quarks et les gluons ne sont jamais observés libres mais forment des états liés incolores. Deuxièmement, il y a la rupture spontanée de la symétrie chirale (χSB). Il s'agit en fait d'une symétrie d'une théorie de type QCD avec des quarks sans masse. Dans le cas de la QCD, les quarks sont massifs, ce qui fait que cette condition n'est pas exactement remplie. Cependant, il s'agit d'une bonne approximation en ce qui concerne les quarks légers. Une conséquence de χSB est que dans la phase brisée, les hadrons acquièrent une masse bien plus grande que la simple somme des masses des quarks qui les composent. Un résultat surprenant est que le χSB est responsable d'environ 98% de la masse de la matière visible.

Au cours des dernières décennies, plusieurs stratégies ont été développées afin d'approfondir l'infrarouge de la QCD et, par conséquent, d'expliquer les questions intrigantes décrites ci-dessus. La QCD sur le réseau est sans doute la plus importante d'entre elles. Il s'agit d'une approche totalement non-perturbative, basée sur les premiers principes et manifestement invariante de jauge, qui repose sur des simulations de Monte-Carlo. Cette technique a été utilisée pour calculer de nombreuses propriétés hadroniques, comme le spectre de masse hadronique [9], avec un très bon accord avec les mesures empiriques. De plus, elle est compatible avec le confinement [10] et le χSB [11]. Cependant, malgré son succès, la QCD sur le réseau fonctionne comme une sorte de boîte noire, cachant les interactions possibles entre les différents éléments de la théorie et ne fournissant pas d'informations sur l'importance relative de chaque contribution au résultat final. De plus, elle est limitée par les énormes ressources de calcul qu'elle nécessite et ses résultats sont toujours affectés par des incertitudes lorsqu'ils sont extrapolés à la limite du continuum.

Ces raisons ont motivé la recherche d'approches du continuum pour accéder à l'infrarouge de la QCD. Contrairement à l'approche sur le réseau, dans le continuum, on est obligé de fixer la jauge pour évaluer les observables physiques. Selon la façon dont on aborde cette question, les stratégies de continuum peuvent être divisées en deux grandes catégories.

Dans l'une de ces classes, nous pouvons inclure des méthodes fonctionnelles, qui font passer la théorie de jauge fixe *à la* FP au niveau non-perturbatif, comme

les équations de Dyson-Schwinger (DSE) [12–19] et le groupe de renormalisation fonctionnelle [20–23]. Cela conduit généralement à un ensemble infini d'équations reliant toutes les fonctions de corrélation possibles de la QCD. Une fois ce système résolu, toute observable physique peut être reconstruite à partir des fonctions de corrélation. En pratique, cependant, il est nécessaire d'introduire une sorte de troncature dans la tour infinie d'équations afin de la résoudre. Malheureusement, le choix de la troncature a un impact sur le résultat final de ces méthodes. Cela a motivé la communauté du réseau à évaluer les fonctions de corrélation à deux et trois points, les quantités fondamentales des méthodes fonctionnelles, afin de fournir un guide pour les approximations du continuum. Ces simulations sont généralement mises en œuvre dans la jauge de Landau, en raison des diverses symétries dont bénéficie cette jauge, et parce qu'elle a une définition non perturbatrice bien établie qui peut être facilement réalisée sur le réseau. L'étude du propagateur du gluon constitue un exemple paradigmatique de la riche interaction entre les études sur le réseau et les approches de continuum. Avant que des simulations concluantes ne soient disponibles, le comportement précis de cette quantité dans l'infrarouge n'était pas clair dans les études de l'DSE. Les premiers calculs ont conduit à un propagateur qui s'approche de zéro lorsque le momentum disparaît, dans ce qui est connu comme la solution d'échelle, voir *e.g.* [24, 25]. Outre ces recherches, par la suite, certaines études sont arrivées à la conclusion qu'un autre type de comportement était également possible, le découplage ou la solution massive, voir [26, 27]. Cette solution est caractérisée par un propagateur de gluon saturant à une valeur finie à momentum zéro. Au fil du temps, les simulations numériques ont clairement favorisé ce dernier scénario [28–37], permettant ainsi de formuler les études sur l'DSE sur une base plus solide.

Une deuxième classe de stratégies opte plutôt pour l'abandon de l'action standard de FP dans l'infrarouge en faveur d'une action alternative qui vise à incorporer les effets des copies de Gribov ou qui est motivée phénoménologiquement par des données expérimentales ou du réseau.

Le principal représentant des approches traitant des copies de Gribov a été conçu par V. Gribov et poursuivi par D. Zwanziger. Leur but ultime est de restreindre les intégrales fonctionnelles apparaissant dans le calcul des fonctions de corrélation à une région de l'espace de configuration sans copies. La région qu'ils ont proposée à l'origine est connue sous le nom de première région de Gribov et il a été démontré que, même en réduisant considérablement le nombre de copies, elle en contient toujours certaines. Cependant, suite à la conjecture selon laquelle l'effet de ces copies supplémentaires peut être négligé [39], plusieurs évaluations ont été effectuées dans la première région de Gribov et comparées aux données du réseau. La contrainte a été mise en œuvre en introduisant des champs auxiliaires, ce qui a donné lieu à l'action dite de Gribov-Zwanziger (GZ) [39]. Les propagateurs dérivés de cette action se sont révélés incompatibles avec les simulations sur le réseau. Cependant, une généralisation de l'action de GZ, appelée action GZ raffinée [40], a corrigé cela, montrant un bon accord avec les simulations.

Le principal représentant des modèles à motivation phénoménologique est un cas particulier des Lagrangiens de Curci-Ferrari dans la jauge de Landau [41]. Il est motivé par le comportement du propagateur du gluon sur le réseau, qui est cohérent avec un champ massif. La manière la plus simple d'incorporer cet effet et d'étudier ses conséquences est de considérer un modèle effectif dont l'action est

une extension avec des gluons massifs de l'action standard de FP [42, 43]. Nous désignerons le modèle ainsi défini simplement comme le modèle de Curci-Ferrari (CF) dans la jauge de Landau. Il a été montré que le modèle est renormalisable [41, 44–46] et qu'il est équivalent à l'action de FP de jauge fixe à des moments élevés. Proposé à l'origine au milieu des années soixante-dix, il a été écarté parce que la construction standard de l'espace physique de la théorie contient des états de normes négatives: [45, 47]. Cependant, on pourrait aussi rendre la construction standard responsable de l'apparition de ces états, puisqu'il se pourrait qu'une construction alternative puisse les éliminer. En outre, tous les états de norme négative trouvés jusqu'à présent sont colorés et, en raison du confinement, devraient être exclus de l'espace physique. De plus, la solution de mise à l'échelle et la solution de découplage du propagateur du gluon présentent toutes deux des violations de positivité [15], qui ont également été trouvées dans des études sur le réseau [32, 48–52]. Ce sont des indications supplémentaires qu'une nouvelle définition de l'espace physique, qui reste à construire, est nécessaire et que le modèle ne peut donc pas être écarté sur la base des arguments utilisés au départ.

L'un des avantages de l'utilisation du modèle CF est qu'il présente certaines trajectoires du groupe de renormalisation dans lesquelles le couplage de jauge admet un traitement perturbatif [53, 54]. De plus, ceci est en accord avec les simulations sur le réseau de la version de jauge pure de la QCD, également appelée théorie de Yang-Mills (YM) pure, qui montrent un couplage faible pour les grands moments, augmentant modérément vers l'infrarouge, pour redevenir faible dans l'infrarouge profond, ce qui est compatible avec l'approximation perturbative sur toute la gamme de moments [29, 32, 55, 56]. Par conséquent, afin de tester le modèle, plusieurs fonctions de corrélation à deux et trois points pour une configuration cinématique arbitraire ont été évaluées de manière perturbative à une boucle. De manière générale, dans le cas de la théorie de YM pure, ces résultats sont en bon accord avec les données du réseau, avec une erreur estimée d'entre 10 % et 20 %. Récemment, les fonctions à deux points ont été évaluées à deux boucles, améliorant l'accord avec les données du réseau par rapport à l'évaluation à une boucle [54]. En présence de quarks, nous sommes convaincus que certains phénomènes, tels que le χSB, dépassent le cadre d'une approche purement perturbative. Pourtant, les résultats à une boucle semblent indiquer que certaines quantités peuvent être décrites avec précision par la théorie des perturbations. Plus précisément, les fonctions à deux points qui ne sont pas directement affectées par le χSB, semblent admettre un traitement perturbatif, à l'exception de la fonction d'habillage du quark. Cependant, il y a des raisons de croire que même cette quantité peut être capturée par le modèle de CF perturbatif lorsque les corrections à deux boucles sont incluses [58].

L'objectif de cette thèse est d'étendre plusieurs des évaluations à une boucle à l'ordre de deux boucles dans le modèle de CF dans la jauge de Landau, en poursuivant le travail commencé dans [54]. L'objectif principal est de tester plus rigoureusement l'utilisation perturbative du modèle pour décrire l'infrarouge de la théorie de YM pure et de la QCD et d'avoir un aperçu de la façon dont l'expansion perturbative est contrôlée.

Nous évaluons d'abord le vertex fantôme-antifantôme-gluon dans la théorie de YM pure, basée sur les groupes SU(3) et SU(2), et nous comparons ces résultats avec les données du réseau disponibles. Ce calcul est une extension de l'évaluation

à une boucle effectuée dans [57]. Afin de rendre le calcul réalisable, nous avons utilisé une configuration cinématique particulière dans laquelle le momentum du gluon s'annule. Cette évaluation est une prédiction pure du modèle de CF, puisque les paramètres du modèle, le couplage et la masse du gluon, ont déjà été déterminés dans [54], en ajustant des fonctions à deux points aux données du réseau. Dans le cas du groupe de jauge SU(3), les graphiques montrent que les corrections à une et deux boucles concordent très bien avec les données du réseau. Quant à SU(2), la qualité de la prédiction se détériore clairement par rapport à SU(3). Une façon complémentaire de vérifier le contrôle de l'expansion perturbative est d'estimer la dépendance du résultat sur le schéma de renormalisation. Conformément aux graphiques, alors que pour le groupe de jauge SU(3), la dépendance vis-à-vis du schéma diminue d'une à deux boucles. Il n'en va pas de même pour SU(2). Nous pensons que les différences entre les groupes sont directement liées au couplage de jauge, qui est plus élevé pour le groupe SU(2). En fait, ces différences sont déjà perceptibles pour les ajustements de la fonction à deux points, qui présentent des erreurs plus importantes pour le groupe SU(2). Par conséquent, afin d'éviter la propagation possible des erreurs des ajustements de la fonction à deux points à la prédiction du vertex fantôme-antifantôme-gluon dans le cas SU(2), nous avons choisi d'ajuster les fonctions à deux points et le vertex simultanément, obtenant des résultats raisonnables. De plus, les corrections à deux boucles présentent un meilleur accord avec les simulations que les corrections à une boucle. En résumé, nos résultats indiquent que le modèle perturbatif de CF est capable de reproduire dans une très bonne mesure les données du réseau du vertex fantôme-antifantôme-gluon dans la théorie de jauge pure, basée sur le groupe SU(3). En ce qui concerne SU(2), le modèle perturbatif de CF donne des résultats raisonnables. Toutefois, dans ce cas, il faut être prudent, car les erreurs devraient être plus importantes. En guise de remarque finale, nous mentionnons que les barres d'erreur des simulations du réseau sont assez grandes dans la configuration cinématique particulière que nous analysons. Par conséquent, il se pourrait qu'une partie des divergences que nous observons dans le cas du SU(2) trouve son origine dans les simulations et non dans le modèle. Ces résultats ont été publiés dans [59].

Nous évaluons ensuite le vertex à trois gluons dans la théorie de YM pure, basée sur les groupes SU(3) et SU(2), dans la configuration cinématique particulière où le momentum d'un des gluons extérieurs s'annule. Ce calcul est une extension de l'évaluation à une boucle effectuée dans [57], et, comme dans le cas précédent, est aussi une prédiction pure du modèle (moins un facteur de normalisation global). Pour les deux groupes de jauges, nous observons un très bon accord avec les données du réseau. De plus, l'évaluation à deux boucles décrit les simulations sur le réseau avec plus de précision que l'évaluation à une boucle, ce qui renforce l'idée que le modèle de CF est capable de décrire de manière perturbative l'infrarouge de la théorie de YM pure. Ceci est confirmé par l'analyse de la dépendance avec le schéma de renormalisation, qui diminue de une à deux boucles dans SU(3) et SU(2). En accord avec les calculs perturbatifs précédents dans le cadre du modèle de CF, nous observons que le cas SU(3) conduit à de plus petites erreurs et est moins dépendant du schéma que le cas SU(2). Enfin, nous étudions le passage à zéro de la fonction d'habillage du vertex des trois gluons. Nous montrons que cela se produit pour tous les ordres de la théorie des perturbations. De plus, nous trouvons une expression exacte pour la contribution dominante dans l'infrarouge.

Nous constatons qu'il coïncide avec le terme dominant de l'expansion infrarouge à deux boucles. Nous notons cependant que l'échelle à laquelle le passage à zéro se produit est significativement réduite de une à deux boucles, ce qui semble être cohérent avec les données du réseau de [230]. La préimpression de ce travail, qui a récemment été acceptée pour publication dans Physical Review D, peut être consultée à [60].

Dans la dernière partie de la thèse, nous effectuons l'évaluation à deux boucles de toutes les fonctions à deux points en présence de deux saveurs dégénérées de quarks avec les ajustements correspondants aux données du réseau de [11, 163]. Étant donné qu'en présence de quarks, le couplage régissant l'expansion perturbative est plus important que dans la théorie de YM pure, les informations fournies par ce calcul sont cruciales pour vérifier la validité du modèle de CF perturbatif. De plus, il faut tenir compte du fait que, comme on le sait, la χSB n'admet aucun type de description perturbative. Ainsi, pour étudier l'impact de χSB, nous comparons nos résultats avec deux ensembles de données du réseau, l'un proche de la limite chirale et l'autre éloigné de celle-ci. Nous calculons les fonctions d'habillage du gluon et du fantôme, liées à leurs propagateurs respectifs, ainsi que les fonctions d'habillage et de masse du quark, toutes deux liées au propagateur du quark. Nos résultats montrent que les quantités qui ne sont pas directement affectées par χSB, c'est-à-dire les fonctions de habillage du gluon, du fantôme et du quark, admettent une description perturbative dans le cadre du modèle CF. Ceci est confirmé par le fait que les résultats à deux boucles améliorent systématiquement l'accord avec les données du réseau par rapport aux résultats à une boucle. Dans le cas des fonctions d'habillage du fantôme et du gluon, la validité du modèle a déjà été confirmé dans la Réf. [58], à une boucle. Quant à la fonction d'habillage des quark, le résultat à une boucle est incapable de reproduire les données du réseau, même au niveau qualitatif, où il présente une monotonicité erronée. Cependant, ceci est corrigé à deux boucles, et les données du réseau sont reproduites avec une grande précision, comme prévu dans la Réf. [58]. Dans le cas de la fonction de masse du quark, nos résultats confirment que l'approximation perturbative est incapable de décrire les données du réseau à proximité de la limite chirale. Cependant, dans le cas éloigné de cette limite, le modèle est à nouveau utile, donnant des résultats raisonnables même dans le cas de la fonction de masse du quark. Nous avons également étudié l'impact de la masse non-perturbative, fournie par les simulations, sur les ajustements des fonctions d'habillage et avons constaté qu'il était minime. Il s'agit d'une autre confirmation de la nature perturbative des fonctions fantôme, gluon et quark dans le modèle de CF. Ces résultats ont été publiés dans [61].

Tous les résultats ci-dessus, en plus d'autres travaux pour des température et densité [193–199] ainsi que du potentiel chimique finis [200], soutiennent l'idée que la théorie de YM pure peut être bien décrite par le modèle de CF perturbatif. Ceci s'étend à la QCD dans la mesure où nous nous référons à des quantités qui ne sont pas directement affectées par le χSB. Mais même dans le cas de la fonction de masse du quark, cela reste vrai tant que l'on s'éloigne de la limite chirale. Pour tester cette affirmation de manière plus stricte, nous prévoyons d'évaluer le vertex quark-antiquark-gluon à deux boucles dans un avenir proche. Après ce calcul, un dernier test intéressant sur le modèle que nous prévoyons d'effectuer est l'évaluation à deux boucles de toutes les fonctions à deux et trois points de la

théorie de YM pure en trois dimensions.

Pour les situations physiques proches de la limite chirale, on peut toujours faire appel au modèle de CF mais en utilisant une approximation qui va au-delà de la théorie des perturbations, comme celle décrite dans [192, 250]. Dans ces travaux, le secteur de pure jauge est traité dans une approximation purement perturbative alors que dans le secteur des quark, tous les ordres sont conservés dans le couplage au prix d'une autre expansion dans l'inverse du nombre de couleur. Cela ouvre la porte à l'extension de l'utilisation du modèle CF pour calculer des observables physiques, tels que le spectre de masse des hadrons.

Contents

Introduction **1**

1 Basics of QCD **5**
1.1 The building blocks . . . 5
1.1.1 The classical theory . . . 5
1.1.2 The quantum theory . . . 7
1.2 The Faddeev-Popov procedure . . . 10
1.2.1 Too many degrees of freedom . . . 10
1.2.2 Gauge fixing for non-abelian gauge theories . . . 11
1.2.3 The gauge-fixed Lagrangian . . . 13
1.3 BRST symmetry . . . 16
1.3.1 Space of physical states . . . 17
1.4 Perturbation theory . . . 18
1.4.1 Feynman diagrams . . . 19
1.4.2 Feynman rules . . . 22
1.5 Regularization and renormalization . . . 28
1.5.1 Superficial degree of divergence . . . 30
1.5.2 Determination of the Z-factors . . . 31
1.5.3 Renormalization group equations . . . 32
1.5.4 Asymptotic freedom . . . 33

2 The various paths to infrared QCD **35**
2.1 The Gribov ambiguity . . . 35
2.1.1 Gribov copies and the perturbative regime . . . 36
2.1.2 The Gribov region . . . 37
2.1.3 The fundamental modular region . . . 37
2.1.4 The Gribov-Zwanziger action . . . 38
2.2 Functional methods . . . 39
2.2.1 Dyson-Schwinger equations . . . 39
2.3 Lattice QCD . . . 42
2.3.1 Basic concepts . . . 43
2.3.2 Some results: two- and three-point functions . . . 46

3 The Curci-Ferrari model **49**
3.1 The Curci-Ferrari Lagrangian . . . 49
3.1.1 Symmetries and renormalizability . . . 50
3.2 Perturbation theory . . . 51
3.3 Two-loop calculation of YM propagators . . . 53

3.3.1 Infrared safe renormalization scheme . . . 54
3.3.2 Renormalization group . . . 55
3.3.3 Fitting procedure . . . 56
3.3.4 Results . . . 57
3.3.5 Scheme dependence . . . 58

4 Ghost-antighost-gluon vertex 61
4.1 Generalities . . . 61
4.2 Two-loop evaluation . . . 63
4.2.1 Diagrams . . . 63
4.2.2 Reduction to master integrals . . . 65
4.2.3 UV divergences . . . 68
4.2.4 Finite parts . . . 70
4.3 Crosschecks . . . 70
4.3.1 UV behavior . . . 71
4.3.2 IR behavior . . . 72
4.3.3 Regularity at $k^2 = m^2$ . . . 73
4.3.4 Zero mass limit . . . 74
4.4 Results . . . 75
4.4.1 Prediction . . . 75
4.4.2 Independent fit of the various vertex functions . . . 77
4.4.3 Scheme dependence . . . 77

5 Three-gluon vertex 81
5.1 Generalities . . . 82
5.1.1 IR and zero-crossing . . . 82
5.2 Two-loop evaluation . . . 84
5.2.1 Diagrams . . . 84
5.2.2 Reduction to master integrals . . . 85
5.2.3 Renormalization . . . 85
5.2.4 Finite parts . . . 87
5.3 Crosschecks . . . 87
5.3.1 UV asymptotic behavior . . . 88
5.3.2 IR asymptotic behavior . . . 88
5.3.3 Regularity at $p^2 = m^2$ . . . 89
5.3.4 Zero mass limit . . . 89
5.4 Renormalization group . . . 90
5.5 Results . . . 90
5.5.1 SU(3) . . . 91
5.5.2 SU(2) . . . 93
5.5.3 Scheme dependence . . . 94

6 QCD two-point functions 97
6.1 Some preliminary remarks . . . 97
6.2 Generalities . . . 98
6.2.1 Notation . . . 99
6.2.2 Infrared safe scheme . . . 99
6.3 Two-loop evaluation . . . 100
6.3.1 Diagrams . . . 100

6.3.2 Renormalization . . . 101
6.3.3 Finite parts . . . 102
6.4 Crosschecks . . . 102
6.4.1 MS scheme and quenched limit . . . 102
6.4.2 Ultraviolet behavior . . . 103
6.4.3 Infrared behavior . . . 104
6.4.4 Spurious singularities . . . 105
6.4.5 Zero mass limit . . . 106
6.5 Renormalization group . . . 106
6.5.1 Asymptotic behaviors . . . 107
6.6 Results . . . 108
6.6.1 Dressing functions . . . 108
6.6.2 The quark mass function . . . 111
6.6.3 Impact of the non-perturbative quark mass on the dressing functions . . . 115

7 Conclusions and outlook 119

A Ghost-antighost-gluon vertex Feynman diagrams 123

B Three-gluon vertex Feynman diagrams 127
B.1 One-loop diagrams . . . 127
B.2 Two-loop diagrams . . . 128

C QCD two-point functions Feynman diagrams 131
C.1 Gluon two-point function . . . 131
C.1.1 One-loop diagrams . . . 131
C.1.2 Two-loop diagrams . . . 132
C.2 Ghost two-point function . . . 132
C.2.1 One-loop diagram . . . 133
C.2.2 Two-loop diagrams . . . 133
C.3 Quark two-point function . . . 134
C.3.1 One-loop diagram . . . 134
C.3.2 Two-loop diagrams . . . 134

D Reduction of integrals with one inverted propagator 135

E Master integrals to order ϵ 137

F Small momentum expansion 143
F.0.1 Small k^2 expansion of $U_{0m00}(k^2)$ . . . 143
F.0.2 Small k^2 expansion of $U_{00m0}(k^2)$ . . . 146
F.0.3 Small k^2 expansion of $U_{0mm0}(k^2)$ . . . 149
F.0.4 Small k^2 expansion of $S_{m00}(k^2)$ . . . 150
F.0.5 Small k^2 expansion of $S_{mm0}(k^2)$ . . . 151

G Small mass expansion 155

H IR structure of the CF model **159**
H.1 IR expansion of Feynman graphs 159
H.1.1 Asymptotic irreducible graphs 159
H.1.2 Taylor and asymptotic power mass 160
H.2 Asymptotic expansion in the CF model 160
H.2.1 AI subgraphs 160
H.2.2 Taylor mass power of an AI subgraph 161
H.2.3 Highest asymptotic mass power 162
H.2.4 Next-to-highest asymptotic mass power 162
H.2.5 Structure of leading logs 163

I Asymptotic $\gamma-$functions **165**
I.1 UV asymptotic behaviour 165
I.2 IR asymptotic behaviour 167

Bibliography **173**

Introduction

Quantum Chromodynamics (QCD) is the quantized non-abelian gauge theory, based on the group SU(3), describing the strong interaction. This theory dictates the physics of *hadrons*, a large set of particles among which we can find, for instance, the neutrons and protons. However, the fundamental entities of QCD are not the hadrons themselves but its constituents, the *quarks* and *gluons*. The former are spin 1/2 fermions with fractional electric charge and come in six different types or *flavors*. Gluons are spin 1 gauge bosons with no electric charge. The charge associated with the strong interaction is the *color*. Both quarks and gluons carry color charge, which implies that the latter can interact with quarks but also among themselves.

The investigation of non-abelian gauge theories based on the group SU(N) started years before the emergence of QCD as such, with the work of C.N. Yang and R.L. Mills in 1954 [1]. In 1967, L. Faddeev and V. Popov published their famous procedure for the gauge fixing of such theories [2], whose renormalizabilty was demonstrated by G. t'Hooft in 1971 [3]. Two years later, D. Gross and F. Wilczek and independently D. Politzer found that QCD is *asymptotically free* [4, 5], which means that, at high energies, the value of the gauge coupling is a decreasing function of the energy. The non-abelian nature of QCD is essential for this property to be fulfilled in four dimensions, as demonstrated by S. Coleman and D. Gross [6].

A remarkable consequence of asymptotic freedom is that, for sufficiently high momenta, the gauge coupling becomes as small as to be compatible with a perturbative treatment. Within this approach, quarks and gluons are considered as effective free fields at leading order. The corrections come from the interactions and are incorporated by means of a perturbative expansion. The use of this technique in combination with the Faddeev-Popov (FP) gauge fixed theory has been proven to be quite fruitful, for instance, to deal with cross sections. The validity of QCD in the perturbative regime has been corroborated in various experimental instances, such as the energy dependence of the gauge coupling and in the rates of the electron-proton annihilation.

In contrast, QCD gives us a quite different picture for processes characterized by a momentum scale of 1 GeV or smaller, in what is referred to as the low momentum or infrared region of QCD. In the first place, the coupling becomes increasingly larger towards the low momentum region, ceasing to be, beyond a certain scale, in the domain of validity of the perturbative approach. This claim, however, needs to be taken with a grain of salt, since the coupling dependence on the momentum is evaluated by means of the FP gauge fixed theory, which leads to our second observation. The FP gauge fixed theory is not fully justified

in the infrared, owing to the existence of Gribov copies. These were first noticed by V. Gribov in his seminal work from 1977 [7], being the result of a gauge fixing condition which selects more than one representative of the gauge field. As I. Singer showed [8], all the continuous gauge fixing conditions fall into this category. At high momentum the effect of Gribov copies is minimal in regard to the FP procedure, as opposed to the low momentum regime, where such copies seriously question one of the underlying hypothesis of the procedure.

The fact that the analytical tools employed to describe the high momentum regime of QCD cannot be uncritically extrapolated to the infrared regime do not imply in any sense a conflict with the content of the theory but rather that we need a different approach to access it. Moreover, two important phenomena, not fully understood to date, are thought to be explained by low momentum QCD. Firstly, there is the confinement, *i.e.* quarks and gluons are never observed freely but forming colorless bound states. Secondly, there is the spontaneous breaking of chiral symmetry (χSB). Actually, this is a symmetry of a QCD-like theory with massless quarks. As for QCD, quarks are massive, so it does not hold exactly. However, it is a good approximation as far as light quarks are concerned. A consequence of the χSB is that in the broken phase, the hadrons acquire a much larger mass than the simple sum of its constituent quark masses. An astonishing result of this is that χSB accounts for 98% of the mass of the visible matter.

Over the last decades, several strategies have been developed in order to gain insight into the infrared of QCD, and consequently, to be able of explaining the intriguing questions described above. Lattice QCD is certainly the most prominent among them. It is a fully non-perturbative, first-principles and manifestly gauge invariant approach, based on Monte-Carlo simulations. This technique has been employed to compute many hadronic properties, such as the hadron spectrum [9], with a very good agreement with empirical measurements. Moreover, it is consistent with confinement [10] and the χSB [11]. However, despite its success, lattice QCD functions as a sort of black box, hiding potential interplays among the various elements of the theory and not providing information on the relative importance of each contribution to the final outcome. Furthermore, it is limited by the enormous computational resources it requires and its results are always affected by uncertainties when extrapolating to the continuum limit.

These reasons have motivated the search for continuum approaches to access the infrared of QCD. Unlike the lattice approach, in the continuum one is forced to fix the gauge in order to evaluate physical observables. Depending on how this issue is addressed, the continuum strategies can be broadly divided into two classes.

Within one of these classes we can include the functional methods, which promote the gauge fixed theory *à la* FP to the non-perturbative level, such as the Dyson-Schwinger equations (DSE) [12–19] and the functional renormalization group [20–23]. This typically leads to an infinite set of equations relating all the possible correlation functions of QCD. Once this system is solved, one can reconstruct any physical observable from the correlation functions. In practice, however, it is necessary to introduce some sort of truncation on the infinite tower of equations in order to be able to solve it. Unfortunately, the choice of the truncation impacts on the final outcome of these methods. This has motivated the lattice community to evaluate gauge fixed two- and three-point functions,

the fundamental quantities of the functional methods, so as to provide guidance for the continuum approaches. Such simulations are generally implemented in Landau gauge, due to the various symmetries this gauge benefits from, and because it possesses a well established non-perturbative definition which can easily be performed on the lattice. A paradigmatic example of the rich interplay between lattice studies and continuum approaches can be found in the investigation of the gluon propagator. Before disposing of conclusive lattice simulations, it was not clear within DSE studies the precise behavior of this quantity in the infrared. Early calculations led to a propagator approaching zero as the momentum vanishes, in what is called as the scaling solution, see *e.g.* [24, 25]. In addition to these investigations, later, some studies came to the conclusion that a different type of behavior was also possible, the *decoupling or massive* solution, see *e.g.* [26, 27]. This solution is characterized by a gluon propagator saturating to a finite value at vanishing momentum. Eventually, lattice data clearly favored the latter scenario [28–37], thus allowing DSE studies to be formulated on more solid ground.

A second class of strategies opt, instead, for abandoning the standard FP gauge fixed action in the infrared in favor of an alternative action which either intends to incorporate the effects of the Gribov copies or is phenomenologically motivated by experimental or lattice data.

The main representative of the approaches which deal with the Gribov copies was first devised by V. Gribov and continued by D. Zwanziger. Its ultimate goal is to restrict the functional integrals appearing in the computation of correlation functions to a region of the configuration space free of copies. The region they originally proposed [7] is referred to as the first Gribov region and it has been proven that, even reducing significantly the number of copies, it still contains some of them [38]. However, following the conjecture that these extra copies can be safely ignored [39], several evaluations within the first Gribov region have been carried out and compared to lattice data. The restriction has been implemented by introducing auxiliary fields, leading to the so called Gribov-Zwanziger (GZ) action [39]. The propagators derived from this action shown to be inconsistent with the lattice simulations. Nonetheless, a generalization of the GZ action, the so called refined GZ action [40], corrected this, featuring good agreement with the lattice simulations.

The main representative of the phenomenologically motivated models is a particular case of the Curci-Ferrari Lagrangians in Landau gauge [41]. It is motivated by the behavior of the gluon propagator on the lattice, consistent with a massive field. The simplest way to incorporate this phenomenon and investigate its consequences is by considering an effective model whose action is a gluon mass extension of the standard FP gauge-fixed action [42, 43]. We will denote the model so defined simply as the Curci-Ferrari (CF) model in Landau gauge. The model has proven to be renormalizable [41, 44–46] and it is equivalent to the FP gauge fixed action at high momenta. Proposed originally in the mid-seventies, it was discarded because the standard construction of the physical space of the theory contains negative norm states [45, 47]. However, one could also blame the standard construction for the emergence of these states, since it could be the case that an alternative construction could get rid of such states. In addition, all the negative norm states found to date are colored and, due to confinement, they should be excluded from the physical space. Furthermore, both the scaling and decoupling solution of the

gluon propagator present positivity violations [15], which have also been found in lattice studies [32, 48–52]. These are further indications that a new definition of physical space, yet to be constructed, is needed.

One of the advantages of using the CF model is that it features certain renormalization group trajectories in which the gauge coupling admits a perturbative treatment [53, 54]. Moreover, this is in line with lattice simulations of the pure gauge version of QCD, also denoted as pure Yang-Mills (YM) theory, which show a small coupling at high momenta, growing mildly towards the infrared, to become small again in the deep infrared, being compatible with a perturbative approach for the whole range of momenta [29, 32, 55, 56]. Therefore, with the purpose of testing the model, several two- and three-point correlation functions have been perturbatively evaluated at one-loop order for an arbitrary kinematic configuration. In general terms, as for the YM theory, these results are in good agreement with the lattice data, with an estimated error between 10% and 20% [42, 43, 57]. Recently, the two-point functions were evaluated at two-loop order, improving the agreement with the lattice data with respect to the one-loop evaluation [54]. In the presence of quarks, we are certain that some phenomena, such as the χSB, are out of reach of a purely perturbative approach. Anyway, one-loop results seem to indicate that there is room for some quantities to be accurately described by plain perturbation theory [58]. More precisely, the two-point functions not directly affected by the χSB, seem to admit a perturbative treatment, with the exception of the quark dressing function. Nevertheless, there are reasons to believe that even this quantity can be captured by the perturbative CF model when including two-loop corrections [58].

The aim of this thesis is to extend various of the one-loop evaluations to two-loop order within the CF model, continuing the work initiated in [54]. The main objective is to further test the perturbative use of the model to describe the infrared of pure YM theory and QCD and to gain insight into how controlled the pertubative expansion actually is.

The thesis is organized as follows. In Chapter 1 we introduce the general elements of QCD and fix the notation we will use throughout this manuscript. In Chapter 2, we dive further into the infrared of QCD. We present the problems which are typically encountered when attempting to access it and review various relevant strategies to tackle them. In Chapter 3 we introduce the Curci-Ferrari model in Landau gauge and present its main properties and relevant results. In Chapters 4 and 5 we present the evaluation of the ghost-antighost-gluon vertex and the three-gluon vertex at two-loop order in the pure gauge theory, respectively. Both quantities show a very good agreement with the lattice data. Such agreement is systematically improved as two-loop corrections are included [59]. As for the three-gluon dressing function, we also discuss the zero-crossing. Moreover, we find its exact leading behavior in the infrared and verified that it is consistent with the infrared behavior of the three-gluon dressing function at two-loop order [60]. In Chapter 6 we show our results for the two-point functions at two-loop order in the presence of quarks. In this case, the analysis is more subtle since the quark mass function does not admit a purely perturbative treatment. For the other quantities, we show that, to a great extent, their infrared behavior is captured by the perturbative CF approach [61]. We end this manuscript in Chapter 7, by presenting the conclusions and outlook of this thesis.

Chapter 1

Basics of QCD

Quantum Chromodynamics (QCD) is the theory that describes the physics of quarks and gluons, the fundamental constituents of hadrons. In the language of quantum field theory, QCD is a non-abelian gauge theory with gauge group SU(3). In this chapter we introduce the elements of non-abelian gauge theories, both at the classical and quantum level. The techniques of perturbation theory, regularization and renormalization are also addressed. The topics covered in this chapter are generally found in any quantum field theory textbook, see *e.g.* [62–66].

1.1 The building blocks of non-abelian gauge theories

Field theories with a non-commutative gauge group are termed as *non-abelian* gauge theories. In this section we introduce the fields and main features of a particular class of such theories, those with a SU(N) symmetry group.

1.1.1 The classical theory

The Lagrangian density associated with a theory invariant under the SU(N) group can be split into two components:

$$\mathcal{L} = \mathcal{L}_{\mathrm{YM}} + \mathcal{L}_{\mathrm{M}}. \tag{1.1}$$

To begin with, let us focus on the term

$$\mathcal{L}_{\mathrm{YM}} = \frac{1}{2}\,\mathrm{Tr}\left(F_{\mu\nu}F_{\mu\nu}\right), \tag{1.2}$$

where the trace is taken over the color indices, to be introduced below. This is the Yang-Mills (YM) Lagrangian density [1]. Unless otherwise specified, we will assume Einstein notation from now on. Greek indices denote space-time coordinates. Throughout this manuscript these will be Euclidean, since we are interested in comparing our results with numerical simulations. We can retrieve Minkowski from Euclidean space-time via a Wick's rotation, as we explain in Section 1.1.2. The tensor

$$F_{\mu\nu} = \partial_\mu A_\nu - \partial_\nu A_\mu - ig[A_\mu, A_\nu]. \tag{1.3}$$

is the non-abelian generalization of the Quantum Electrodynamics (QED) field-strength tensor. The field A_μ is known as the *gauge* or *gluon field* and belongs to

the adjoint representation of the SU(N) group, which means

$$A_\mu(x) = A^a_\mu(x) t^a, \tag{1.4}$$

where t^a designates the generators of the Lie algebra $\mathfrak{su}(n)$. The index "a" is called the color index and can take natural values between 1 and $\mathrm{N}^2 - 1$. We can choose the generators of the Lie algebra to be hermitian, *i.e.* $(t^a)^\dagger = t^a$, and to be normalized as

$$\mathrm{Tr}\left(t^a t^b\right) = \frac{\delta^{ab}}{2}. \tag{1.5}$$

Besides, the generators satisfy the commutation relation

$$[t^a, t^b] = i f^{abc} t^c, \tag{1.6}$$

where f^{abc} are the *structure constants* of the gauge group. These objects are completely antisymmetric in the color indices. Likewise, the field-strength tensor reads

$$F_{\mu\nu} = F^a_{\mu\nu} t^a, \tag{1.7}$$

and consequently

$$F^a_{\mu\nu} = \partial_\mu A^a_\nu - \partial_\nu A^a_\mu + g f^{abc} A^b_\mu A^c_\nu. \tag{1.8}$$

In terms of these components, the Lagrangian (1.2) takes the form

$$\mathcal{L}_{\mathrm{YM}} = \frac{1}{4} F^a_{\mu\nu} F^a_{\mu\nu}. \tag{1.9}$$

Under a gauge transformation, A_μ transforms as

$$A_\mu \to A^U \equiv U A_\mu U^\dagger + \frac{i}{g} U \partial_\mu U^\dagger, \tag{1.10}$$

where $U(x)$ is an element of the SU(N) gauge group,

$$U(x) = e^{-ig\theta^a(x) t^a}, \tag{1.11}$$

$\theta^a(x)$ is an arbitrary real function and g is referred to as the *coupling constant*. Then, from Eqs. (1.3) and (1.10) , we can infer that

$$F_{\mu\nu} \to F^U_{\mu\nu} = U F^{\mu\nu} U^\dagger. \tag{1.12}$$

Hence, $\mathcal{L}_{\mathrm{YM}}$ is invariant under the SU(N) group.

For future convenience, we write the gauge transformation on A^a_μ at the infinitesimal level,

$$A^a_\mu \to (A^U)^a_\mu \equiv A^a_\mu - D^{ab}_\mu \theta^b, \tag{1.13}$$

where we have introduced the covariant derivative in the adjoint representation

$$D^{ab}_\mu \equiv \partial_\mu \delta^{ab} - g f^{abc} A^c_\mu. \tag{1.14}$$

The matter content of the theory is captured by the second term of the right hand side of Eq. (1.1),

$$\mathcal{L}_{\mathrm{M}} = \sum_{i=1}^{N_f} \bar{\psi}_i (D_\mu \gamma_\mu + M_i) \psi_i. \tag{1.15}$$

The fields ψ_i and $\bar{\psi}_i \equiv \gamma^0 \psi_i^\dagger$ are the quark and antiquark fields of the theory, respectively. We have used the condensed notation:

$$\psi_i(x) \equiv \psi_i(x)^{\alpha,l}, \tag{1.16}$$

where the color, "l", and the spinor index, "α", can take natural values between 1 and the number of colors N, and between 1 and 4, respectively. The sum from (1.15) runs over the number of different types or *flavors* of fermions and M_i is the *mass* of the fermion ψ_i. The fields ψ and $\bar{\psi}$ belong to the fundamental representation of SU(N), so they transform according to

$$\psi \to \psi^U = U\ \psi, \tag{1.17}$$

$$\bar{\psi} \to \bar{\psi}^U = \bar{\psi}\ U^\dagger, \tag{1.18}$$

which correspond to the following infinitesimal transformations

$$\psi \to \psi^U = -ig\theta^a(x)t^a\psi, \tag{1.19}$$

$$\bar{\psi} \to \bar{\psi}^U = ig\theta^a(x)\bar{\psi}t^a. \tag{1.20}$$

Another element we have introduced in Eq. (1.15) is the covariant derivative in the fundamental representation

$$D_\mu = \partial_\mu - igA_\mu^a t^a. \tag{1.21}$$

Lastly, we have to mention the Euclidean Dirac matrices γ_μ, whose anticommutator reads

$$\{\gamma_\mu, \gamma_\nu\} = \mathbb{1}(2\delta_{\mu\nu}). \tag{1.22}$$

These matrices act upon the spinor indices.

From these definitions it is easy to check that the matter Lagrangian (1.15) is invariant under a SU(N) transformation as well. Hence, this confirms that SU(N) is a symmetry group of the Lagrangian (1.1). The action, defined as the Euclidean space-time integration of the Lagrangian, *i.e.*

$$S = \int d^4x\ \mathcal{L}, \tag{1.23}$$

is of fundamental importance in order to proceed with the quantization.

1.1.2 The quantum theory

The theory we have been working on is a classical field theory. The quantization may be carried out by means of three well known methods: the *canonical operator formalism* [67], the *stochastic formalism* [68] and the *functional-integral formalism* [69].

We begin by analyzing the n-point correlation functions or Green's functions, since the infinite set of them completely determines the quantum field theory. Even though the three methods differ in the way they compute these objects, all of them yield the same physics.

In the stochastic formalism the fields are regarded as stochastic variables and the Green's functions are calculated as the statistical average of the product of fields in equilibrium. In the canonical operator formalism, the fields are promoted

to operators that fulfill certain commutation relations. Within this framework, the Green's functions are computed as vacuum expectation values of time-ordered products of these operators, *i.e.*

$$\langle \Phi_{i_1} \dots \Phi_{i_n} \rangle \equiv \langle \Omega | \, T[\hat{\Phi}_{i_1} \dots \hat{\Phi}_{i_n}] \, | \Omega \rangle \,, \tag{1.24}$$

where, to avoid a cumbersome notation, a classical superfield Φ_{i_j} was introduced. The index i_j accounts for the field-type and all of its indices as well as position or momentum. The quantity $\hat{\Phi}_{i_j}$ indicates its respective operator in Heisenberg picture, T designates the time-ordered product and $|\Omega\rangle$ refers to the vacuum of the theory. It can be shown, see for example [62, 65, 70], that this quantity is exactly the same than the one deduced through the functional integral formalism. This technique, introduced by R. Feynman, regards the fields as c-numbers and the Lagrangian in its classical form. The Green's functions are obtained by integrating the product of fields over all possible paths with the weight e^{iS_M}:

$$\langle \Phi_{i_1} \dots \Phi_{i_n} \rangle = \frac{\int \mathcal{D}\Phi \; \Phi_{i_1} \dots \Phi_{i_n} e^{iS_M}}{\int \mathcal{D}\Phi \; e^{iS_M}} \tag{1.25}$$

where S_M is the classical action in Minkowski space-time. As was stated above, to go from Minkowski to Euclidean space we must perform a Wick's rotation. This consists in rotating the temporal coordinate from the real to the imaginary axis by means of the transformation $x^0_M \to ix^E$, after which we arrive at the Euclidean Green's function

$$\frac{\int \mathcal{D}[\Phi] \; \Phi_{i_1} \dots \Phi_{i_n} e^{-S_E}}{\int \mathcal{D}\Phi \; e^{-S_E}}, \tag{1.26}$$

with S_E the classical action in Euclidean space-time. From now on, unless otherwise stated, whenever we mention the action we will be referring to the Euclidean one and we will designate it simply by S.

Generating functionals from the functional-integral approach

Due to the fact that the classical Lagrangian is involved in the integrand, the functional integral quantization method preserves the symmetries of the theory explicitly, which makes it particularly useful when these have to be taken into account. Furthermore, this formalism allows us to easily introduce and manipulate the generating functionals Z, W and Γ.

The functional $Z[J]$ is defined as

$$Z[J] \equiv \int \mathcal{D}\Phi e^{-S + \int_i J_i \Phi_i}, \tag{1.27}$$

where an implicit sum over all the fields Φ_i of the theory is assumed. The quantity J_i is the *source* associated to the field Φ_i. The symbol $\int_i$ represents the integral over space-time. As we can obtain any correlation function by functional differentiating Z with respect to the sources,

$$\langle \Phi_{i_1} \dots \Phi_{i_n} \rangle = \frac{1}{Z[J]} \frac{\delta^n Z[J]}{\delta J_{i_n} \dots \delta J_{i_1}} \bigg|_{J=0}, \tag{1.28}$$

we call Z the generating functional of correlation functions.

The functional $W[J]$ is defined as

$$W[J] \equiv \log[Z[J]], \tag{1.29}$$

and, because we can get any *connected* Green's function from it,

$$\langle \Phi_{i_1} \dots \Phi_{i_n} \rangle_c = \frac{1}{W[J]} \frac{\delta^n W[J]}{\delta J_{i_n} \dots \delta J_{i_1}} \bigg|_{J=0}, \tag{1.30}$$

$W[J]$ is denoted as the generating functional of connected correlation functions. Green's connected functions are related to full ones by means of the following recursion relation:

$$\begin{aligned} \langle \Phi_i(x) \rangle_c &= \langle \Phi_i(x) \rangle, \\ \langle \Phi_i(x) \Phi_j(y) \rangle_c &= \langle \Phi_i(x) \Phi_j(y) \rangle - \langle \Phi_1(x) \rangle_c \langle \Phi_j(y) \rangle_c, \\ \langle \Phi_i(x) \Phi_j(y) \Phi_k(z) \rangle_c &= \langle \Phi_i(x) \Phi_j(y) \Phi_k(z) \rangle - \langle \Phi_i(x) \Phi_j(y) \rangle_c \langle \Phi_k(z) \rangle_c + \text{perm.}, \end{aligned} \tag{1.31}$$

and so on.

Finally, the *effective action*, $\Gamma[\phi]$, is the result of taking the Legendre transformation of $W[J]$:

$$\Gamma[\phi] = W[J] - \int_i J_i \phi_i. \tag{1.32}$$

$\Gamma[\phi]$ is a functional of the so-called *classical* field, $\phi(x)$, which is the vacuum expectation value of the corresponding Heisenberg field $\hat{\Phi}(x)$ in the presence of the currents:

$$\phi_i = \langle \Omega | \hat{\Phi}_i(x) | \Omega \rangle_J = \frac{\delta W[J]}{\delta J_i(x)}. \tag{1.33}$$

Additionally, the effective action satisfies

$$J_i(x) = -\frac{\delta \Gamma[\phi_i]}{\delta \phi_i}. \tag{1.34}$$

This equation actually justifies the name of $\Gamma[\phi]$. In the absence of an external current, $J_i(x) = 0$, the effective action has an extremum on the physical field expectation value. Therefore, $\Gamma[\phi]$ is the analogous of the classical action for the quantum theory.

Two-point connected Green's functions and the second derivative of the effective action are related through the identity

$$\langle \Phi_i(x) \Phi_j(y) \rangle_c = \left(\frac{\delta^2 \Gamma[\phi]}{\delta \phi_i(x) \phi_j(y)} \right)^{-1} \bigg|_{J=0}. \tag{1.35}$$

For $n \geq 3$, the effective action is the functional generator of the so-called *proper* or *one-particle irreducible* Green's functions[1]

$$\langle \Phi_{i_1} \dots \Phi_{i_n} \rangle_{1\text{PI}} = \frac{\delta^n \Gamma[\phi]}{\delta \phi_{i_n} \dots \delta \phi_{i_1}} \bigg|_{J=0}. \tag{1.36}$$

[1] Another current name for this quantity is proper or one-particle irreducible *vertex*.

One-particle irreducible correlation functions are better understood in the context of Feynman diagrams, so we will introduce them properly in Section 1.4.1. Three-point connected and proper correlation functions are related through

$$\begin{aligned}
&\langle \Phi_k(z)\Phi_i(x)\Phi_j(y)\rangle_c \\
&= -\int_{wuv} \langle \phi_l(w)\phi_k(z)\rangle_c \langle \phi_i(x)\phi_m(u)\rangle_c \langle \phi_j(y)\phi_n(v)\rangle_c \left(\frac{\delta^3\Gamma[\phi]}{\delta\phi_l(w)\delta\phi_m(u)\delta\phi_n(v)} \right) \\
&= -\int_{wuv} \langle \phi_l(w)\phi_k(z)\rangle_c \langle \phi_i(x)\phi_m(u)\rangle_c \langle \phi_j(y)\phi_n(v)\rangle_c \langle \phi_l(w)\phi_m(u)\phi_n(v)\rangle_{1\mathrm{PI}},
\end{aligned} \tag{1.37}$$

where we have introduced the shorthand notation

$$\int_{x_1\ldots x_n} \equiv \int d^4x_1 \ldots d^4x_n. \tag{1.38}$$

Expressions analogous to Eq. (1.37) can be obtained for higher correlation functions, see *e.g.* [62].

Let us end this section by referring to the calculation of observables within the functional-integral formalism. A *physical observable* or simply observable is an operator, *i.e.* a functional of the fields of the theory, which is invariant under a gauge transformation. If we denote it by the symbol $\mathcal{O}$, its expectation value is computed as

$$\langle \mathcal{O} \rangle = \frac{\int \mathcal{D}[\Phi]\ \mathcal{O}[\Phi] e^{-S}}{\int \mathcal{D}[\Phi] e^{-S}}, \tag{1.39}$$

where $\mathcal{D}[\Phi]$ is a gauge-invariant integral measure.

1.2 The Faddeev-Popov procedure

1.2.1 Too many degrees of freedom

A naive calculation of the functional-integrals from (1.39) would lead us to an undetermined result of the type $\frac{\infty}{\infty}$. The reason for this stems from the fact that any gauge field configuration, $\tilde{A}_\mu(x)$, comes associated with infinitely many gauge-transformed fields $\tilde{A}^U_\mu(x)$ via (1.10). The set composed by the totality of such physically equivalent fields constitute the so called *gauge orbit* of $\tilde{A}_\mu(x)$. Since the action and the measure of the integral are gauge invariant, the integral over the gauge field may be schematically written as

$$\int \mathcal{D}A\ e^{-S} = \int \mathcal{D}\tilde{A}\ e^{-S} \int \mathcal{D}U, \tag{1.40}$$

which is divergent. From this, it is clear that the divergence is the result of not properly separating the redundant degrees of freedom of the theory, related to gauge invariance, from the physical ones.

One possible way of getting rid of these extra degrees of freedom is to restrict the functional integration to a region of the configuration space where there is one and only one representative of the gauge field per gauge orbit. This region receives the name of fundamental modular region and will be described in more detail in Section 2.1.3.

Another method rests on factorizing out in Eq. (1.39) the divergent term from both the numerator and denominator. Since these divergences have a common origin, they should mutually cancel out, leading to well defined calculations. In continuum methods[2] this can be achieved by fixing the gauge, which consists in imposing a *gauge condition*. This condition takes the form of a functional of the gluon field which vanishes at each point of the space-time:

$$\mathcal{F}[A] = 0. \tag{1.41}$$

In practice, an *ideal gauge condition*, *i.e.* a gauge condition which selects only one representative of the gauge field from each gauge orbit, is very hard to find. In general, the gauge condition $\mathcal{F}[A] = 0$ picks up many (often infinitely many) representatives of the gauge field. This means that for each gluon field satisfying $\mathcal{F}[A] = 0$ there are gauge-transformed fields A^U satisfying the same condition. These fields are referred to as *Gribov copies* [7] and are named after Vladimir Gribov, who was the first one to point out their existence. We will come back to this issue in Section 2.1.1.

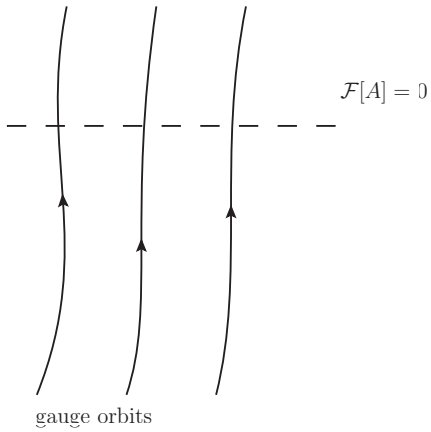

Figure 1.1: Pictorial representation of a gauge fixing functional. Solid lines correspond to gauge transformed trajectories. The dotted line refers to a gauge fixing condition.

1.2.2 Gauge fixing for non-abelian gauge theories

The standard method to fix the gauge in non-abelian gauge theories was first introduced by Ludvig Faddeev and Victor Popov [2] in 1967. A nice pedagogical description of the method, on which we base this section, can be found in Ref. [71]. We will explain it in detail since it will be of importance when introducing the Curci-Ferrari model in Chapter 3. For simplicity, throughout this section we will work with pure YM theory.[3]

To begin with, let us remind a well known result from calculus:

$$\frac{1}{\sum_i \frac{1}{|f'(x_i)|}\big|_{f(x_i)=0}} \int dx\ \delta(f(x)) = 1, \tag{1.42}$$

[2]We speak about continuum methods as opposed to methods in which the space-time is discretized, such as numerical simulations. See Section 2.3.

[3]The extension to the quark sector is trivial.

where f is real function and the sum is performed over the roots of this function. Under the assumption that the function f posses only one root, this identity can be easily inferred from the following relation

$$1 = \int df \delta(f) = \int dx\ \delta(f(x)) \left| \frac{df}{dx} \right|_{f(x)=0}, \tag{1.43}$$

whose generalization to n dimensions reads

$$1 = \int \prod_i^n df_i\ \delta^n(f) = \int \prod_i^n d\theta_i\ \delta^n(f(\theta)) \left| \det \frac{\partial f_i}{\partial \theta_j} \right|, \tag{1.44}$$

where f and θ are n-dimensional vectors with components f_i and θ_i, respectively. The determinant is the Jacobian, associated to the change of variables $f \to \theta$.

As for functional integrals, *under the assumption of an ideal gauge condition*[4] of the form $\mathcal{F}[A] = 0$, the analogous to Eq. (1.44) takes the form [71]

$$\mathbb{1} = \int \mathcal{D}U\ \delta(\mathcal{F}[A^U]) \Delta_{\text{FP}}[A], \tag{1.45}$$

where we have used the shorthand notation

$$\begin{aligned} \delta(\mathcal{F}[A^U]) &= \Pi_x \Pi_a \delta(\mathcal{F}^a[A^U_\mu(x)]), \\ \mathcal{D}U &\sim \Pi_x \Pi_a d\theta^a(x). \end{aligned} \tag{1.46}$$

We have also introduced the *Faddeev-Popov determinant*[5]:

$$\Delta_{\text{FP}} \equiv \det M^{ab}_{xy}[A], \tag{1.47}$$

with $M^{ab}_{xy}[A]$ the *Faddeev-Popov operator*, defined as

$$M^{ab}_{xy}[A] \equiv \left. \frac{\delta \mathcal{F}^a[A^U_\mu(x)]}{\delta \theta^b(y)} \right|_{\mathcal{F}[A^U]=0}. \tag{1.48}$$

We recall here that $A^U_\mu(x)$ is by definition

$$A^U_\mu \equiv U A_\mu U^\dagger + \frac{i}{g} U \partial_\mu U^\dagger \tag{1.49}$$

where $U(x)$ is an element of the SU(N) gauge group,

$$U(x) = e^{-ig\theta^a(x)t^a}. \tag{1.50}$$

Inserting the identity from Eq. (1.45) into Eq. (1.39) leads to

$$\langle \mathcal{O} \rangle = \frac{\int \mathcal{D}U \int \mathcal{D}A^U\ \delta(\mathcal{F}[A^U]) \Delta_{\text{FP}}[A^U] \mathcal{O}[A^U] e^{-S_{\text{YM}}}}{\int \mathcal{D}U \int \mathcal{D}A^U\ \delta(\mathcal{F}[A^U]) \Delta_{\text{FP}}[A^U] e^{-S_{\text{YM}}}}. \tag{1.51}$$

[4] To fix the gauge with an ideal gauge condition is actually equivalent to restrict the functional integrals to the fundamental modular region.

[5] To be rigorous, we should use the definition $\Delta_{\text{FP}} \equiv |\det M^{ab}_{xy}[A]|$. However, under the assumption that the gauge condition is ideal and that the solution $\mathcal{F}[A] = 0$ changes continuously as we move continuously between gauge orbits, the sign of $\det M^{ab}_{xy}[A]$ does not switch and therefore is irrelevant for the subsequent discussion.

In Eq. (1.51) we have performed a change of variables from A to A^U. We have also used that the measure $\mathcal{D}A$, the observable $\mathcal{O}[A]$ and the action $S_{\rm YM}$ are gauge independent and that the Faddeev-Popov determinant $\Delta_{\rm FP}[A]$ does not depend independently on A and U[6]. As in Eq. (1.51) A^U acts only as an integration label, nothing prevents us from making $A^U \to A$, which allows us to factorize out the volume of the gauge group $\int \mathcal{D}U$. Since this infinite volume is the same in the numerator and denominator, it cancels out, giving as a result

$$\langle \mathcal{O} \rangle = \frac{\int \mathcal{D}A\ \delta(\mathcal{F}[A])\Delta_{\rm FP}[A]\mathcal{O}[A]e^{-S_{\rm YM}}}{\int \mathcal{D}A\ \delta(\mathcal{F}[A])\Delta_{\rm FP}[A]e^{-S_{\rm YM}}}. \tag{1.52}$$

1.2.3 The gauge-fixed Lagrangian

The expression (1.52) does not allow us to make analytic computations yet. This can be done by rewriting the terms $\Delta_{\rm FP}[A]$ and $\delta(\mathcal{F}[A])$ as a local modification of the action from Eq. (1.23). Accordingly, after this rewritten is carried out, we will work with an effective action of the form $S_{\rm inv.} + S_{\rm FP} + S_{\rm GC}$, where the former term of the sum is the gauge-invariant action from Eq. (1.23) and the latter ones are related to the modification that comes from $\Delta_{\rm FP}[A]$ and $\delta(\mathcal{F}[A])$, respectively.

Firstly, let us concentrate on the Faddeev-Popov determinant. This quantity is independent of θ^a and, thus, we have the freedom to impose

$$M^{ab}_{xy}[A] = \left.\frac{\delta \mathcal{F}[A^U_\mu(x)]}{\delta \theta^b(y)}\right|_{\theta=0;\ \mathcal{F}[A]=0}. \tag{1.53}$$

By applying the chain rule, we get

$$M^{ab}_{xy}[A] = \int d^4z \frac{\delta \mathcal{F}^a[A_\mu(x)]}{\delta A^c_\mu(z)} \frac{\delta A^{c,U}(z)}{\delta \theta^b(y)}\bigg|_{\theta=0;\ \mathcal{F}[A]=0}, \tag{1.54}$$

and by taking into consideration that an infinitesimal gauge transformation for the gluon field reads

$$A^U_\mu = A_\mu - (D_\mu \theta)^a t^a + \mathcal{O}(\theta^2), \tag{1.55}$$

we arrive at

$$M^{ab}_{xy}[A] = \int dz\ \frac{\delta \mathcal{F}^a[A_\mu(x)]}{\delta A^c_\mu(z)} \left(-D^{bc}_\mu \delta(y-z)\right)\bigg|_{\mathcal{F}(A)=0}. \tag{1.56}$$

This is the most general expression we can deduce without actually opting for a particular gauge condition. In practical calculations it is generally useful to remain within the family of linear covariant gauges[7], given by

$$\mathcal{F}^a[A_\mu(x)] = \partial_\mu A^{\mu,a}(x) - B^a(x), \tag{1.57}$$

where $B^a(x)$ is an arbitrary scalar field. Plugging this condition into Eq. (1.56), we obtain

$$M^{ab}_{xy}[A] = -\partial_\mu D^{ab}_\mu \delta(y-x). \tag{1.58}$$

[6]This follows from the identity $A^{VU} = (A^U)^V$, which yields $F[A^{\delta VU}] = F[(A^U)^{\delta V}]$.
[7]This is known as the Lorentz gauge condition.

Finally, by exploiting the fact that the determinant of a matrix can be written in terms of a Gaussian integral of Grassmannian fields[8], we get

$$\begin{aligned}\Delta_{\mathrm{FP}}[A] &= \int \mathcal{D}[\bar{c},c] \exp\left\{-\int d^4x\ d^4y\ \bar{c}^a(x) M^{ab}_{xy}[A] c^b(y)\right\} \\ &= \int \mathcal{D}[\bar{c},c] \exp\left\{\int d^4x\ d^4y\ \bar{c}^a(x) \partial_\mu D^{ab}_\mu \delta(y-x) c^b(y)\right\} \\ &= \int \mathcal{D}[\bar{c},c] \exp\left\{-\int d^4x\ \partial_\mu \bar{c}^a(x) D_\mu c^a(x)\right\}, \end{aligned} \tag{1.59}$$

where in the last line we have integrated by parts. Additionally, we have introduced the *ghost*, c, and *antighost*, $\bar{c}$, fields. These are anticommuting complex scalar fields and, therefore, they violate the spin-statistics theorem. This is a consequence of their nature: these fields are nothing but pure artifacts of the theory, necessary in order to carry out certain calculations, but of which physical observables are independent. As anticipated, Eq. (1.59) permits to express the Faddeev-Popov determinant as an added term to the invariant action. Nevertheless, this is achieved only at the price of introducing auxiliary fields in the calculations.

Secondly, we have to focus on the Dirac delta term associated to a gauge condition of the form of Eq. (1.57). By taking advantage of the arbitrariness of $B^a(x)$, we can integrate over this field with an appropriate weight, having as a result

$$\begin{aligned}\int \mathcal{D}B^a \exp\left\{-\frac{1}{2\xi}\int d^4x (B^a(x))^2\right\} \delta(\partial_\mu A^a_\mu(x) - B^a(x)) \\ = \exp\left\{-\frac{1}{2\xi}\int d^4x\ (\partial_\mu A^a_\mu)^2\right\}. \end{aligned} \tag{1.60}$$

A specific value of ξ determines a particular gauge condition. Owing to this, ξ is known as the *gauge parameter*. Two important instances are $\xi = 0$ and $\xi = 1$, termed *Landau* and *Feynman gauge*, respectively.

Lastly, combining Eq. (1.59) and Eq. (1.60) with Eq. (1.52), we get

$$\langle \mathcal{O} \rangle = \frac{\int \mathcal{D}[A,\bar{c},c]\ \mathcal{O} e^{-(S_{\mathrm{YM}}+S_{\mathrm{GC}}+S_{\mathrm{FP}})}}{\int \mathcal{D}[A,\bar{c},c]\ e^{-(S_{\mathrm{YM}}+S_{\mathrm{GC}}+S_{\mathrm{FP}})}}. \tag{1.61}$$

The terms Δ_{FP} and $\delta(\mathcal{F}[A])$ have been absorbed into the term $S_{\mathrm{YM}} + S_{\mathrm{GC}} + S_{\mathrm{FP}}$, where S_{GC} and S_{FP} are given by the integration over the Euclidean space-time of their respective Lagrangian densities, defined as

$$\mathcal{L}^{\xi}_{\mathrm{GC}} \equiv \frac{1}{2\xi}\left(\partial_\mu A^a_\mu(x)\right)^2 \quad \text{and} \tag{1.62}$$

$$\mathcal{L}_{\mathrm{FP}} \equiv \partial_\mu \bar{c}^a(x) D_\mu c^a(x). \tag{1.63}$$

[8]For any natural number N, the determinant of a matrix reads

$$\det M = \left[\prod_{i=1}^{N} \int d\bar{c}_i dc_i\right] e^{-\bar{c}_j M_{ji} c_i},$$

where $\bar{c}$ and c are anti-commuting Grassmann variables.

Let us end this section by making two important remarks concerning the Faddeev-Popov derivation. Firstly, we have neglected the absolute value of the Faddeev-Popov determinant in order to introduce the ghosts. By doing so, we have assumed that the sign of the determinant does not change. As we will see in the next chapter, this is far from being the generality. Secondly, we have used an ideal gauge condition. This is a necessary hypothesis if Eq. (1.45) is to be valid. In the non-ideal case, this equation must be replaced by one of the type of Eq. (1.42).

In Section 2.1.1 we will see that the condition from Eq. (1.57) is not ideal and, as a consequence, the Faddeev-Popov method is not fully right. For the moment we will leave this intriguing issue aside to analyze more deeply the gauge-fixed Lagrangian we have just deduced.

QCD gauge-fixed action in Landau gauge

QCD and pure YM correlation functions can be computed by means of numerical simulations, which are introduced in some detail in Section 2.3. The Landau gauge condition is by far the most widely used gauge for such computations. As the results of this thesis are compared with these simulations, we will work in Landau gauge, whose gauge condition is given by

$$\mathcal{F}[A] = \partial_\mu A^a_\mu = 0. \tag{1.64}$$

This is equivalent to set $\xi = 0$ in 1.62, which yields a divergent term in the Lagrangian. A more convenient way of expressing the same condition is obtained by introducing a bosonic field, h^a, such that

$$\int \mathcal{D}h^a \exp\left\{-\int d^4x \left(\frac{\xi}{2}(h^a)^2 + ih^a\partial_\mu A^a_\mu\right)\right\} = \exp\left\{-\frac{(\partial_\mu A_\mu)^2}{2\xi}\right\}\sqrt{\frac{2\pi}{\xi}}. \tag{1.65}$$

The field h^a is referred to as the Nakanishi-Lautrup field [72]. Due to this identity, we may rewrite the Landau gauge condition by adding the auxiliary field h^a in the functional integration and replacing $\frac{1}{2\xi}\left(\partial_\mu A^a_\mu(x)\right)^2$ by $ih^a\partial_\mu A^a_\mu$ in Eq. (1.62).

To conclude, we arrive at the QCD gauge fixed action in Landau gauge

$$S_{\rm GF} \equiv \int d^4x\ \mathcal{L}_{\rm GF}, \tag{1.66}$$

with

$$\mathcal{L}_{\rm GF} \equiv \mathcal{L}_{\rm inv.} + \mathcal{L}_{\rm GC} + \mathcal{L}_{\rm FP}, \tag{1.67}$$

where $\mathcal{L}_{\rm inv.}$ corresponds to the gauge invariant part of the Lagrangian

$$\mathcal{L}_{\rm inv.} = \frac{1}{4}F^a_{\mu\nu}F^a_{\mu\nu} + \sum_{i=1}^{N_f}\bar{\psi}_i(-\gamma_\mu D_\mu + M_i)\psi_i, \tag{1.68}$$

$$\mathcal{L}_{\rm GC} = ih^a\partial_\mu A^a_\mu \tag{1.69}$$

and $\mathcal{L}_{\rm FP}$ is given by Eq. (1.63). In the remainder of this thesis, whenever we talk about the Faddeev-Popov action, we will be referring to the theory described by the action (1.66). As it will be explained in detail in Chapter 2, the gauge fixation procedure described above is only valid at high energies and strictly speaking the action (1.66) does not describe QCD in Landau gauge out of that region of energy.

Other gauges

Even though we will not use them in this manuscript, it is worth mentioning that many gauges are possible in addition to the linear covariant ones. A first class of those is composed by the non-linear covariant gauges, such as the t'Hooft gauge [73]. A second class of gauges are the non-covariant gauges, which break Lorentz invariance. Among these we can find the Coulomb gauge, whose gauge condition is given by $\mathcal{F}^a[A] = \partial_i A_i^a$ [9], the axial and the temporal gauge. A review on non-covariant gauges can be found in Ref. [74]. A third class of gauges are the ones which break color symmetry, *e.g.* the maximal abelian gauge [75].

1.3 BRST symmetry

Of course, because of gauge fixation, the action in Eq. (1.66) is no longer gauge invariant. However, it still preserves a symmetry: the Becchi-Rouet-Stora-Tyutin (BRST) symmetry. It was introduced by Carlo Becchi, Alain Rouet and Raymond Stora [76, 77] and independently by Igor Tyutin [78] in 1975.

For the purpose of introducing this symmetry it is useful to consider a superfield $\Phi \in \{A, c, \bar{c}, \psi, \bar{\psi}, h^a\}$. A BRST transformation acts on Φ in the following manner:

$$\Phi \to \Phi + \delta_{\mathtt{s}}\Phi \tag{1.70}$$

where

$$\delta_{\mathtt{s}}\Phi = \eta\ \mathtt{s}\Phi \tag{1.71}$$

and η is a space-time independent Grassmann number. We have also introduced the BRST operator: $\mathtt{s}$. It transforms the fields according to

$$\mathtt{s}A_\mu^a = (D_\mu c)^a,\ \mathtt{s}\psi = igt^a c^a \psi,\ \mathtt{s}c^a = -\frac{g}{2} f^{abc} c^b c^c,\ \mathtt{s}\bar{c}^a = ih^a \text{ and } \mathtt{s}h^a = 0. \tag{1.72}$$

Over the product of two fields Φ_1 and Φ_2, the operator $\mathtt{s}$ acts as

$$\mathtt{s}\,(\Phi_1\Phi_2) = (\mathtt{s}\Phi_1)\Phi_2 \pm \Phi_1(\mathtt{s}\Phi_2). \tag{1.73}$$

The $\pm$ sign is determined by the nature of the field Φ_1. A bosonic field carries a plus sign while a fermionic field is associated with a minus sign.

From the above definitions it is not difficult to prove (see for instance [63]) that every BRST transformation is *nilpotent*, *i.e.* if F is any functional of Φ, then

$$\mathtt{s}^2 F[\Phi] = 0. \tag{1.74}$$

This is commonly written just as $\mathtt{s}^2 = 0$. Since a BRST transformation over A and ψ can be interpreted as an infinitesimal gauge transformation with parameter $\theta^a(x) = -\eta c^a(x)$ (see Eqs. (1.13) and (1.19)) it is evident that the gauge invariant part of the gauge-fixed action is invariant under a BRST transformation. Therefore, in order to demonstrate that BRST is an actual symmetry of the action,

[9] This condition has the same form that Landau's but it applies to spatial dimensions only.

it is enough to prove it for the gauge-dependent part of it. In the case of linear covariant gauges this is

$$S_{\mathrm{GD}} = \int d^4x \; \frac{\xi}{2}(h^a)^2 + ih^a\partial_\mu A^a_\mu + \partial_\mu \bar{c}^a D_\mu c^a. \tag{1.75}$$

Because this quantity may be written as

$$S_{\mathrm{GD}} = \mathtt{s}\Psi, \tag{1.76}$$

where

$$\Psi = \int d^4x \; \left(\bar{c}^a\partial_\mu A^a_\mu - i\frac{\xi}{2}\bar{c}^a h^a\right), \tag{1.77}$$

and owing to the nilpotency of BRST, we get

$$\mathtt{s}S_{\mathrm{GD}} = 0. \tag{1.78}$$

Which proves that BRST is a symmetry of the gauge-fixed action.

1.3.1 Space of physical states

We can exploit BRST symmetry to determine the space of physical states, see *e.g.* [63]. In order to do so, let us start by reminding that the scalar product of two physical states $\langle\alpha|\beta\rangle$ is a gauge-independent quantity. In other words, $\langle\alpha|\beta\rangle$ is independent of Ψ. Then, if we arbitrarily modify Ψ by an amount $\tilde{\delta}\Psi$, the change in the matrix element $\langle\alpha|\beta\rangle$,

$$\tilde{\delta}\langle\alpha|\beta\rangle = -\langle\alpha|\mathtt{s}\tilde{\delta}\Psi|\beta\rangle, \tag{1.79}$$

must vanish for physical states. On the other hand, since BRST is a global symmetry, there is an associated conserved Noether current, whose charge Q is the generator of the symmetry, hence

$$i\mathtt{s}\Phi = i[Q,\Phi]_{\mp}, \tag{1.80}$$

the sign is $-$ or $+$ depending on whether Φ is bosonic or fermionic, respectively. Inserting Eq. (1.80) into Eq. (1.79) we get

$$\tilde{\delta}\langle\alpha|\beta\rangle = \langle\alpha|[Q,\tilde{\delta}\Psi]|\beta\rangle = 0, \tag{1.81}$$

but, as this is true for any $\tilde{\delta}\Psi$, the only possible option is

$$\langle\alpha|Q = Q|\beta\rangle = 0. \tag{1.82}$$

Thus, physical states are in the kernel of Q. In addition, because of the nilpotency of BRST transformations, we have

$$[Q^2,\Phi] = 0. \tag{1.83}$$

For this condition to be fulfilled for an arbitrary operator Φ, Q^2 must either vanish or be proportional to the identity. But the last option is not possible since Q^2 has a non-vanishing ghost number. Then, Q is a nilpotent operator. As a consequence, two physical states that differ only by a state in the image of Q will have exactly

the same scalar product with respect to any other physical state. This implies that independent physical states correspond to states in the kernel of Q modulo the image of Q. This is known as the cohomology of Q. Therefore, physical states belong to the cohomology of Q.

Moreover, BRST is used to prove the unitarity of the gauge-fixed action in perturbation theory, see *e.g.* [79]. This means that:

1. States that are the result of interactions of physical states are physical states.

2. All physical states have positive norm.

Furthermore, BRST also allows one to prove that ghost particles are excluded from the physical space, which of course must be the case since the ghost field is non-physical.

In addition, BRST is useful to prove the renormalizability (see Section 1.5) of the gauge-fixed QCD action.

To end this section, let us mention that there is also a different approach to BRST symmetry, the so called BRST formalism. Within such approach, BRST symmetry is elevated to a first principle and it is postulated that the effective Lagrangian for non-abelian gauge theories must be BRST invariant so as to lead to a renormalizable theory which yields a unitary S-matrix. Likewise, BRST symmetry is the basis for the canonical operator formalism [80].

1.4 Perturbation theory

Even after gauge fixing, the analytic computation of correlation functions for a non-abelian gauge theory remains as something extremely hard to accomplish. Actually, all the approaches we know calculate them only approximately. Among these, perturbation theory stands as one of the most prominent and widely used methods. This technique exploits the fact that the free theory, *i.e.* the theory where all couplings vanish, is completely solvable analytically. As a result, if the couplings are small enough, by performing a Taylor expansion around the free theory, we may have a good approximation of the interacting theory. Equally important, the approximation is under control. A detailed development of the application of this idea to QCD can be found in any textbook of the subject (see *e.g.* [62, 70, 81]). Here we will just mention some basic features and introduce the main tool to make calculations within a perturbation approach: the Feynman diagrams.

We aim at computing any correlation function from the gauge fixed action. In general terms, an n-point correlation function reads

$$\langle \Phi_1(x_1)\cdots\Phi_n(x_n)\rangle = \frac{\int \mathcal{D}[A,h,c,\bar{c},\bar{\psi},\psi]\Phi_1(x_1)\cdots\Phi_n(x_n)e^{-\int d^4x\ \mathcal{L}}}{\int \mathcal{D}[A,h,c,\bar{c},\bar{\psi},\psi]e^{-\int d^4x\ \mathcal{L}}}, \tag{1.84}$$

where $\Phi_i \in \{A,h,c,\bar{c},\bar{\psi},\psi\}$. In order to be able to carry out the expansion around the free theory, it is convenient to split the Lagrangian as

$$\mathcal{L} = \mathcal{L}_0 + \mathcal{L}_{\text{int}}, \tag{1.85}$$

where $\mathcal{L}_0$ is the Lagrangian of the free theory and $\mathcal{L}_{\text{int}}$ is the Lagrangian associated with the interactions of the theory. In the case of QCD, this is

$$\mathcal{L}_0 = \frac{1}{4}(\partial_\mu A^a_\nu - \partial_\nu A^a_\mu)^2 + \sum_{i=1}^{N_f} \bar{\psi}_i(-\gamma_\mu \partial_\mu + M_i)\psi_i + \partial_\mu \bar{c}^a \partial_\mu c^a + ih^a \partial_\mu A^a_\mu, \quad (1.86)$$

$$\begin{aligned}\mathcal{L}_{\text{int}} = \frac{g}{2} f^{abc}(\partial_\mu A^a_\nu - \partial_\nu A^a_\mu) A^b_\mu A^c_\nu + \frac{g^2}{4}(f^{abc} A^b_\mu A^c_\nu)^2 \\ + ig \sum_{i=1}^{N_f} \bar{\psi}_i \gamma_\mu A^a_\mu t^a \psi_i + g f^{abc} \partial_\mu \bar{c}^a A^b_\mu c^c.\end{aligned} \quad (1.87)$$

Assuming that the coupling constant g is small enough, we can make the approximation

$$\begin{aligned}e^{-\int d^4x\ \mathcal{L}} \sim e^{-\int d^4x\ \mathcal{L}_0} \Bigg(1 - \int d^4x\ \mathcal{L}_{\text{int}} + \frac{1}{2}\left(\int d^4x\ \mathcal{L}_{\text{int}}\right)^2 \\ - \frac{1}{3!}\left(\int d^4x\ \mathcal{L}_{\text{int}}\right)^3 + \cdots\Bigg),\end{aligned} \quad (1.88)$$

which can be inserted into Eq. (1.84). This allows us to approximate the correlation function from the left hand side of the equation in terms of correlation functions of the free theory, which can be calculated exactly:

$$\langle \Phi_1(x_1) \cdots \Phi_n(x_n) \rangle = \frac{\int \mathcal{D}\Phi\ \Phi_1(x_1) \cdots \Phi_n(x_n) e^{-\int d^4x\ \mathcal{L}_0} \left(1 - \int d^4x\ \mathcal{L}_{\text{int}} + \cdots\right)}{\int \mathcal{D}\Phi\ e^{-\int d^4x\ \mathcal{L}_0} \left(1 - \int d^4x\ \mathcal{L}_{\text{int}} + \cdots\right)}. \quad (1.89)$$

Furthermore, this expansion benefits from the fact that the error between the approximation and the exact quantity is under control and can be estimated up to certain extent[10]. In principle, the Green's functions of the free theory may be computed by simply decomposing the fields in terms of ladder operators. Albeit, a much easier way rests on the Wick's theorem. Mathematically it can be stated as:

$$\begin{aligned}\langle \Phi_1(x_1) \cdots \Phi_n(x_n) \rangle_0 = &\langle \Phi_1(x_1)\Phi_2(x_2)\rangle_0 \cdots \langle \Phi_{n-1}(x_{n-1})\Phi_n(x_n)\rangle_0 \\ &+ \langle \Phi_1(x_1)\Phi_3(x_3)\rangle_0 \cdots \langle \Phi_{n-1}(x_{n-1})\Phi_n(x_n)\rangle_0 \\ &+ \text{all permutations within two-point functions.}\end{aligned} \quad (1.90)$$

The terms $\langle \Phi_i(x_i)\Phi_j(x_j)\rangle_0$ correspond to two-point functions from the free theory. As these quantities are easy to compute, Wick's theorem greatly simplifies the calculations from Eq. (1.89).

1.4.1 Feynman diagrams

Due to the permutations in Eq. (1.90), generally there is a large amount of terms to consider when making the calculations from Eq. (1.89). *Feynman diagrams* or *graphs* [82], named after Richard Feynman, who introduced them in 1949, constitute a pretty valuable tool so as to carry out an ordered and systematized perturbative computation. Furthermore, as the various terms are represented

[10] This series is not convergent.

by drawings, Feynman graphs are helpful to illustrate different aspects of the calculation.

The diagrams are built on three type of objects:

a) Vertices: represented by a dot with some lines (also called legs) coming in or out from it. Each type of vertex represents an interaction term from $\mathcal{L}_{\text{int}}$ and the number of lines corresponds to the number of fields that participate in the interaction.

b) Internal lines: corresponding to lines between two vertices. Each line represents a *propagator*, *i.e.* a two-point Green's function.

c) External legs: represented by lines with at least one of its ends not connected to any other internal line or vertex of the diagram. Such unconnected border is associated with a coordinate variable that is not integrated in the perturbative series.

It can be shown [62, 83] that $\langle \Phi_1(x_1) \cdots \Phi_n(x_n) \rangle$ is given by the sum of all Feynman diagrams with n external legs terminating at $x_1, \ldots, x_n$, excluding *vacuum bubbles*[11]. *i.e.* excluding diagrams which are disconnected from all the external legs.

Full, connected and one-particle irreducible diagrams

The quantity we have been working on throughout this section is the n-point Green's function $\langle \Phi_1(x_1) \cdots \Phi_n(x_n) \rangle$. It is also commonly known as the *full* n-point Green's function.

In Section 1.1.2 we introduced $W[J]$, the generating functional of connected correlation functions. It turns out, see *e.g.* [62, 65, 83], that $\langle \Phi_1(x_1) \cdots \Phi_n(x_n) \rangle_c$ is given by the sum of the connected Feynman graphs with external legs terminating at $x_1, \ldots, x_n$. A connected Feynman diagram is characterized by the following property: for every two elements of the graph, *i.e.* vertices, propagators or lines, there is a continuous path from one to the other[12]. We can say that connected diagrams are more fundamental that non-connected ones since the latter can be made up from the former.

One-particle irreducible (1-PI) or proper diagrams form a third class of Feynman graphs. This kind of diagram cannot be disconnected into two pieces by cutting a single internal line. An example is provided in Fig. 1.2.

The proper n-point Green's functions,

$$\langle \Phi_1(x_1) \cdots \Phi_n(x_n) \rangle_{\text{1-PI}}, \tag{1.91}$$

introduced in Section 1.1.2, are given by the sum of 1-PI diagrams with external legs terminating at $x_1, \ldots, x_n$. As we stated before, 1-PI Green's functions are generated by taking functional derivatives on the effective action $\Gamma[\phi]$ and setting the sources to zero.

[11] In principle, vacuum bubbles are included in the calculation, but the ones from the numerator are canceled with the ones coming from the denominator in Eq. (1.89)

[12] In this context, in order to define a path we must ignore the nature of the lines and eventual arrows on them.

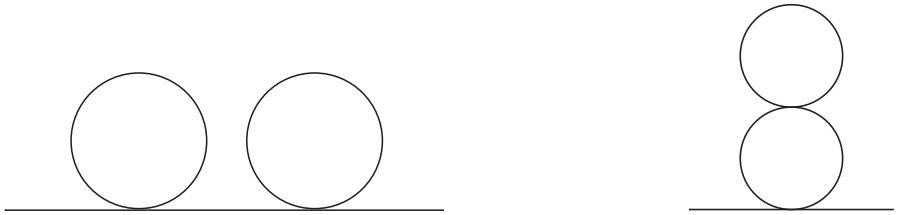

Figure 1.2: A one-particle reducible diagram (left) vs a one-particle irreducible diagram (right). The diagram from the left can be disconnected into two pieces by cutting the line connecting the loops. All Feynman diagrams presented in this thesis were drawn with JAXODRAW [84].

One-particle irreducible Green's functions are more fundamental than connected Green's functions. This is because the latter can always be built as a sum of *tree* diagrams, *i.e.* graphs that become disconnected by cutting any internal line, where the vertices are given by proper vertices and the internal lines are full connected propagators [62, 83]. In other words, connected correlation functions can be obtained from a functional integral in which we use $\Gamma[\phi]$ instead of the classical action $S[\phi]$ and diagrams are restricted to tree level topologies.

Loop counting

In Feynman diagrams the order of the perturbative expansion is determined by the number of loops of the considered graphs. Larger amount of loops correspond to higher orders in the perturbative series. Then, the lowest order in the expansion corresponds to tree diagrams, in which no loops are present.

It can be shown that if we make the replacements $S \to \frac{1}{\lambda}S$ and $J \to \frac{1}{\lambda}J$ in the functional integral (1.27), the parameter λ acts as loop counting parameter [83]. This is to say that the generating functional of connected Green's functions reads

$$W[J] = \sum_{L=0}^{\infty} \lambda^{L-1} W_L[J], \tag{1.92}$$

where $W_L[J]$ is the L-loop contribution to $W[J]$. By restoring $\hbar$[13] in the exponent of the functional integral, it changes as $-(S+\int_i J_i\Phi_i) \to -\frac{1}{\hbar}(S+\int_i J_i\Phi_i)$, so $\hbar$ acts as a loop-counting parameter. Then, we can take $\lambda = \hbar$. As a result, the limit $\hbar \to 0$ allows us to isolate the contributions coming from tree-diagrams. Therefore, tree diagrams are associated to classical approximations, while quantum corrections come from loop diagrams. Since we take $\phi_{\rm cl} \equiv \langle\Omega|\hat{\Phi}_i(x)|\Omega\rangle_{J=0} = 0$, perturbative corrections are taken around $\Phi_{\rm cl} = 0$.

In the $\hbar \to 0$ limit we can evaluate the functional integral (1.27) in a saddle-point approximation, which give us an integral dominated by fields ϕ such that $\frac{\delta S}{\delta \phi_i} + J_i = 0$. A direct derivation of this result is

$$W_0[J] = S[\phi] + \int d^4x \; J_i(x)\phi_(x). \tag{1.93}$$

This means that the tree level contribution to $W[J]$, $W_0[J]$, is the inverse Legendre transform of the classical action. On top of this, as $\Gamma[\phi]$ is the Legendre transform

[13] For convenience we have set $\hbar = 1$.

of $W[J]$, then, in the classical limit, $\Gamma[\phi]$ is just the classical action. In other words, $\Gamma[\phi]$ can be thought of as the classical action $S[\phi]$ plus quantum corrections.

1.4.2 Feynman rules

To make calculations from a Feynman graph it is necessary to follow the so called *Feynman rules*. These rules operate as a sort of dictionary which dictate the mathematical expressions associated to each propagator or vertex and how these elements can be combined to construct a specific diagram. In this section we illustrate how to derive Feynman rules from a given action by using the example of the Faddeev-Popov theory in Landau gauge, hereafter denoted simply by S:

$$S = \int d^4x \ \left(\frac{1}{4} F^a_{\mu\nu} F^a_{\mu\nu} + i h^a \partial_\mu A^a_\mu + \partial_\mu \bar{c}^a \partial_\mu c^a + g f^{abc} \partial_\mu \bar{c}^a A^b_\mu c^c \right. \\ \left. + \sum_{i=1}^{N_f} \bar{\psi}_i (-\gamma_\mu D_\mu + M_i) \psi_i \right). \tag{1.94}$$

In first place, let us deduce expressions for propagators and vertices at tree level. As explained in the preceding section

$$\Gamma_{\text{tree}}[\langle \Phi \rangle] = S[\langle \Phi \rangle]. \tag{1.95}$$

Moreover, owing to $\phi_{\text{phys}} = \langle \Phi \rangle = 0$, full and connected two-point functions are equivalent (see Eq. (1.31)). Thus, we can compute tree level propagators as

$$\langle \Phi(x) \Phi(y) \rangle_{\text{tree}} = \left(\frac{\delta^2 S[\phi]}{\delta \phi(x) \delta \phi(y)} \right)^{-1}. \tag{1.96}$$

The tree level proper vertices are obtained by taking functional derivatives on the classical action. The number and type of derivative is determined by the number and type of external legs of the vertex we want to deduce.

We are interested in computing these quantities in the momentum space. As a result, we will have to work with Fourier transformations. We choose the following convention:

$$f(p) = \int d^4x \ e^{ipx} f(x). \tag{1.97}$$

Propagators

In this section we will provide two examples, concerning the ghost and gluon field, on how to obtain mathematical expressions for tree level propagators.

The tree level ghost propagator is given by

$$\langle c^a(x) \bar{c}^b(y) \rangle_{\text{tree}} = \left(\frac{\delta^2 S[A_\mu, c, \bar{c}, \psi, \bar{\psi}, h^a]}{\delta c^a(x) \delta \bar{c}^b(y)} \right)^{-1}, \tag{1.98}$$

where the first derivative is taken with respect to the antighost and the second one with respect to ghost field. Since these fields are Grassmannian, switching the order leads to a change of sign. The functional derivative of the action is

$$\begin{aligned}\frac{\delta^2 S[A_\mu, c, \bar{c}, \psi, \bar{\psi}, h^a]}{\delta c^a(x)\delta\bar{c}^b(y)} &= \frac{\delta}{\delta c^a}\int d^4z\ \partial_\mu(\delta(y-z))\partial_\mu c^b(z) \\ &= \delta^{ab}\int d^4z\ \partial_\mu(\delta(y-z))\partial_\mu(\delta(x-z)) \\ &= -\delta^{ab}\partial_y^2(\delta(x-y)),\end{aligned} \tag{1.99}$$

where in the last line we integrated by parts. By taking the Fourier transform we can get the ghost propagator in momentum space. If we make $(x-y)\to u$ in the last line of Eq. (1.99), its corresponding Fourier transform reads

$$\begin{aligned}(G^{ab}_{\text{tree}}(p))^{-1} &= -\int d^4u\ e^{ipu}\partial_u^2(\delta(u)) \\ &= -\delta^{ab}\int d^4u\ \partial_u^2(e^{-ipu})\delta(u) \\ &= \delta^{ab}p^2,\end{aligned} \tag{1.100}$$

where we integrated by parts twice in the last line. From this, we can extract the ghost propagator at tree level:

$$G^{ab}_{\text{tree}}(p) = \frac{\delta^{ab}}{p^2}. \tag{1.101}$$

Further in this thesis we will talk about the *ghost dressing function*, which is related to the ghost propagator through

$$G^{ab}(p) = \delta^{ab}\frac{F(p)}{p^2}. \tag{1.102}$$

Obviously, at tree level $F(p) = 1$, but this is no longer the case after we include loop corrections. In this manuscript, tree level ghost propagators will be represented by a dotted line, as is shown in Fig. 1.3.

Let us look now at the gluon propagator. We have to take into account two different derivatives of the action in order to compute it:

$$\frac{\delta^2 S[A_\mu, c, \bar{c}, \psi, \bar{\psi}, h]}{\delta A^b_\nu(y)\delta A^a_\mu(x)} \quad \text{and} \quad \frac{\delta^2 S[A_\mu, c, \bar{c}, \psi, \bar{\psi}, h]}{\delta h^b(y)\delta A^a_\mu(x)}. \tag{1.103}$$

Both derivatives must be evaluated in the absence of sources, $J = 0$. Since we have taken $\langle\Phi\rangle_{J=0} = 0$, this is equivalent to evaluate the derivatives of the action at zero fields. Therefore, in order to calculate such derivatives, it is enough to consider only quadratic terms in A^a_μ in the action, *i.e.*

$$S_{AA} = \frac{1}{4}\int d^4x\ \left(\partial_\mu A^a_\nu\partial A^a_\nu + \partial_\nu A^a_\mu\partial_\nu A^a_\mu - \partial_\mu A^a_\nu\partial_\nu A^a_\mu - \partial_\nu A^a_\mu\partial_\mu A^a_\nu\right), \tag{1.104}$$

so as to evaluate the former derivative in Eq. (1.103) we have

$$\begin{aligned}
\frac{\delta^2 S[A_\mu, c, \bar{c}, \psi, \bar{\psi}, h]}{\delta A^b_\nu(y)\delta A^a_\mu(x)} &= \frac{\delta^2 S_{AA}[A_\mu]}{\delta A^b_\nu(y)\delta A^a_\mu(x)} \\
&= \frac{\delta}{\delta A^b_\nu(y)}\left\{\frac{1}{4}\int d^4z\ \left(4\partial_\lambda(\delta(z-x))\partial_\lambda A^a_\mu - 4\partial_\mu A^a_\lambda \partial_\lambda(\delta(z-x))\right)\right\} \\
&= \frac{\delta}{\delta A^b_\nu(y)}\left\{\int d^4z\ \partial_\lambda(\delta(z-x))\left(\partial_\lambda A^a_\mu - \partial_\mu A^a_\lambda\right)\right\} \\
&= \int d^4z\ \partial_\lambda(\delta(z-x))\left(\delta^{ab}\delta_{\mu\nu}\partial_\lambda(\delta(z-y)) - \delta^{ab}\delta_{\lambda\nu}\partial_\mu(\delta(z-y))\right) \\
&= -\delta^{ab}\int d^4z\ \delta(z-x)\left(\delta_{\mu\nu}\partial^2(\delta(z-y)) - \partial_\mu\partial_\nu(\delta(z-y))\right) \\
&= -\delta^{ab}\left(\delta_{\mu\nu}\partial^2_x(\delta(x-y)) - \partial_{\mu,x}\partial_{\nu,x}(\delta(x-y))\right). \qquad (1.105)
\end{aligned}$$

The Fourier transform of the last line of Eq. (1.105) is

$$\begin{aligned}
&-\delta^{ab}\int d^4u\ e^{ipu}\left(\delta_{\mu\nu}\partial^2_u(\delta(u)) - \partial_{\mu,u}\partial_{\nu,u}(\delta(u))\right) \\
&= \delta^{ab}\left(p^2\delta_{\mu\nu} - p_\mu p_\nu\right) = \delta^{ab}p^2 P^\perp_{\mu\nu}(p), \qquad (1.106)
\end{aligned}$$

where we have made the change of variables $(x-y) \to u$ and we have integrated by parts. Besides, we have introduced the transverse projector, defined as

$$P^\perp_{\mu\nu}(p) \equiv \delta_{\mu\nu} - \frac{p_\mu p_\nu}{p^2}. \qquad (1.107)$$

The second term in (1.103) is

$$\frac{\delta S[A_\mu, c, \bar{c}, \psi, \bar{\psi}, h]}{\delta h^b(y)\delta A^a_\mu(x)} = i\delta^{ab}\partial_{\mu,y}(\delta(x-y)), \qquad (1.108)$$

whose Fourier transform is given by

$$i\delta^{ab}\int d^4u\ e^{ipu}(-\partial_{\mu,u}(\delta(u)) = -\delta^{ab}p_\mu. \qquad (1.109)$$

Then, the matrix for the second derivative of the action is

$$\Gamma^{(2)} = \delta^{ab}\begin{pmatrix} p^2 P^\perp_{\mu\nu}(p) & -p_\mu \\ p_\nu & 0 \end{pmatrix} \qquad (1.110)$$

The inverse of this matrix can be found by choosing the following ansatz

$$\left(\Gamma^{(2)}\right)^{-1} = \delta^{ab}\begin{pmatrix} MP^\perp_{\sigma\mu}(p) + NP^\parallel_{\sigma\mu}(p) & Bp_\sigma \\ Cp_\mu & D \end{pmatrix}, \qquad (1.111)$$

where we have introduced the longitudinal projector

$$P^\parallel_{\mu\nu} \equiv \frac{p_\mu p_\nu}{p^2}. \qquad (1.112)$$

The coefficients are determined by imposing that the product of $\Gamma^{(2)}$ and its inverse is the identity matrix, *i.e.*

$$\delta^{ab}\begin{pmatrix} Mp^2 P^\perp_{\sigma\nu}(p) + Bp_\sigma p_\nu & -Np_\sigma \\ Dp_\nu & -Cp^2 \end{pmatrix} = \delta^{ab}\delta_{\sigma\nu}, \qquad (1.113)$$

whose solution is $M = \frac{1}{p^2}$, $N = 0$, $B = \frac{1}{p^2}$, $C = -\frac{1}{p^2}$ and $D = 0$. Then,

$$\left(\Gamma^{(2)}\right)^{-1} = \delta^{ab} \begin{pmatrix} \frac{P^{\perp}_{\sigma\mu}(p)}{p^2} & \frac{p_\sigma}{p^2} \\ -\frac{p_\mu}{p^2} & 0 \end{pmatrix}. \tag{1.114}$$

In brief, the tree level gluon propagator is

$$G^{ab}_{\mu\nu,\,\text{tree}} = \delta^{ab} \frac{P^{\perp}_{\mu\nu}(p)}{p^2}. \tag{1.115}$$

It is customary to work with the *gluon dressing function*, related to the gluon propagator via the identity

$$G^{ab}_{\mu\nu}(p) = \delta^{ab} \frac{P^{\perp}_{\mu\nu}(p)}{p^2} D(p). \tag{1.116}$$

As occurred with the ghost dressing function, at tree level $D(p) = 1$, but this changes as soon as we consider quantum corrections.

The term gluon propagator is also often used for the quantity, $G(p)$, defined as

$$G(p) \equiv p^2 D(p). \tag{1.117}$$

Depending on the context it should be clear to which object $G(p)$ or $G^{ab}_{\mu\nu}$ we are referring to.

From Section 1.4.2 it is clear that $\langle h^a(x) A^b_\mu(y) \rangle$ is nonzero. However, since no vertices involve the field $h^a(x)$ (see Fig. 1.6), this correlation function plays no role in Feynman diagrams. In this thesis, tree level gluon propagators will be represented by a wiggled line, as shown in Fig. 1.3.

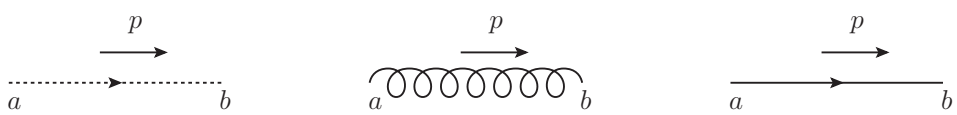

Figure 1.3: Pictorial representation of the ghost (left), gluon (middle) and quark (right) propagator. The arrow above each line indicates the momentum carried by the propagator. In the case of the ghost and quark propagator, the arrow over the line is known as the particle flow arrow and is useful to distinguish particles from antiparticles.

The tree level quark propagator can be derived similarly to the previous cases, see for instance [85], having as a result:

$$S^{ab}_{\text{tree}}(p) = \delta^{ab} \frac{i\not{p} + M}{p^2 + M^2}. \tag{1.118}$$

In Feynman diagrams these propagators will be represented by a solid line, as can be seen in Fig. 1.3. Beyond tree level order the quark propagator is normally written as

$$S^{ab}(p) = \delta^{ab} Z(p) \frac{i\not{p} + M(p)}{p^2 + M(p)^2}, \tag{1.119}$$

where $M(p)$ and $Z(p)$ are called the *quark mass function* and the *quark dressing function*, respectively. Both quantities depend on the momentum.

Vertices

As we did with the propagators, we can obtain the tree level vertices of the theory by appropriately differentiating the action. From the Lagrangian of interactions, vertices can be extracted in the following manner:

$$\begin{aligned}\int d^4x\mathcal{L}_{\text{int}} &= \int d^4x \left\{\frac{g}{2}f^{abc}(\partial_\mu A^a_\nu - \partial_\nu A^a_\mu)A^b_\mu A^c_\nu + \frac{g^2}{4}(f^{abc}A^b_\mu A^c_\nu)^2 + gf^{abc}\partial_\mu \bar{c}^a c^b A^c_\mu\right\} \\ &= \int_{xyz} A^a_\mu(x)A^b_\nu(y)A^c_\rho(z)\Gamma^{abc}_{\mu\nu\rho,\ \text{tree}}(x,y,z) \\ &+ \int_{xyzw} A^a_\mu(x)A^b_\nu(y)A^c_\rho(z)A^d_\sigma(w)\Gamma^{abcd}_{\mu\nu\rho\sigma,\ \text{tree}}(x,y,z,w) \\ &+ \int_{xyz} A^a_\mu(x)\bar{c}^c(z)c^b(y)\Gamma^{abc}_{\mu,\ \text{tree}}(x,y,z) \\ &+ \int_{xyz} A^c_\mu(z)\bar{\psi}^b(y)\Gamma^{abc}_{\mu,\psi,\ \text{tree}}(x,y,z)\psi^a(x),\end{aligned} \tag{1.120}$$

where $\Gamma^{abc,\ \text{tree}}_{\mu\nu\rho}(x,y,z)$, $\Gamma^{abcd}_{\mu\nu\rho\sigma,\ \text{tree}}(x,y,z,w)$, $\Gamma^{abc}_{\mu,\ \text{tree}}(x,y,z)$ and $\Gamma^{abc}_{\mu,\psi,\ \text{tree}}(x,y,z)$ are the triple gluon, the four gluon, the ghost-gluon and the quark gluon tree level vertex, respectively. We can compute these quantities as

$$\Gamma^{abc}_{\mu\nu\rho,\ \text{tree}}(x,y,z) = \left.\frac{\delta^3 S[A_\mu, c, \bar{c}, \psi, \bar{\psi}, h]}{\delta A^a_\mu(x)\delta A^b_\nu(y)\delta A^c_\rho(z)}\right|_{A,c,\bar{c}=0}, \tag{1.121}$$

$$\Gamma^{abcd}_{\mu\nu\rho\sigma,\ \text{tree}}(x,y,z,w) = \left.\frac{\delta^4 S[A_\mu, c, \bar{c}, \psi, \bar{\psi}, h]}{\delta A^a_\mu(x)\delta A^b_\nu(y)\delta A^c_\rho(z)\delta A^d_\sigma(w)}\right|_{A,c,\bar{c}=0}, \tag{1.122}$$

$$\Gamma^{abc}_{\mu,\ \text{tree}}(x,y,z) = \left.\frac{\delta^3 S[A_\mu, c, \bar{c}, \psi, \bar{\psi}, h]}{\delta c^b(y)\delta \bar{c}^c(z)\delta A^a_\mu(x)}\right|_{A,c,\bar{c}=0}, \tag{1.123}$$

$$\Gamma^{abc}_{\mu,\psi,\ \text{tree}}(x,y,z) = \left.\frac{\delta^3 S[A_\mu, c, \bar{c}, \psi, \bar{\psi}, h]}{\delta \psi^a(x)\delta \bar{\psi}(y)\delta A^c_\mu(z)}\right|_{A,\psi,\bar{\psi}=0}. \tag{1.124}$$

As it was the case for the propagators, we are interested in the vertices in momentum space. This implies that after we have computed them via Eqs. (1.121) to (1.124) we must calculate their corresponding Fourier transform.

As an example, let us compute the ghost-gluon vertex at tree level. The remaining vertices can be computed similarly. A detailed calculation of them can be found in [85]. The only term we need to focus on for this calculation is

$$S_{\bar{c}cA}[A_\mu, c, \bar{c}] = g\int d^4u\ f^{a'b'c'}\partial_\rho \bar{c}^{a'}c^{b'}A^{c'}_\rho. \tag{1.125}$$

In order to compute the tree level ghost-gluon vertex we must differentiate $S_{\bar{c}cA}[A_\mu, c, \bar{c}]$ according to Eq. (1.123), whose result is

$$\frac{\delta^3 S_{\bar{c}cA}[A_\mu, c, \bar{c}]}{\delta c^b(z)\delta \bar{c}^c(y)\delta A^a_\mu(x)} = -gf^{abc}\partial_{\mu,x}(\delta(x-y))\delta(z-x). \tag{1.126}$$

Its corresponding Fourier transform can be calculated as

$$\begin{aligned}\Gamma^{abc}_{\mu,\,\mathrm{tree}}(k,p,r) &= \int_{xyz} e^{ikx}e^{ipy}e^{irz}\partial_{\mu,x}(\delta(x-y))\delta(z-x)\\ &= gf^{abc}\int_{xy}\partial_{\mu,x}e^{i(k+r)x}e^{ipy}\delta(x-y)\\ &= igf^{abc}(k+r)_\mu\int d^4x e^{i(k+r+p)x}\\ &= igf^{abc}(k+r)_\mu(2\pi)^4\delta(p+k+r). \end{aligned} \tag{1.127}$$

The term $(2\pi)^4\delta(p+k+r)$ is simply a consequence of the momentum conservation at the vertex. In Feynman rules we can omit this term by just adding a rule imposing momentum conservation at each vertex in a given diagram. Thus, the expression we will use for the tree level ghost-gluon vertex when computing Feynman diagrams is

$$\Gamma^{abc}_{\mu,\mathrm{tree}}(k,p,r) = -igf^{abc}p_\mu, \tag{1.128}$$

where p_μ is the antighost momentum. The typical pictorial representation of this vertex is in Fig. 1.4.

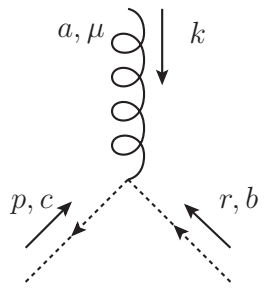

Figure 1.4: Pictorial representation of the ghost-gluon vertex. The antighost is represented by the line in which the particle flow arrow is opposed to the momentum one. This is the custom representation of antiparticles.

Nonetheless, for convenience, we will use a different convention for the antighost field. We can just make $p \to -p$ in Eq. (1.128) and impose that, in the pictorial representation of the vertex, the particle flow arrow of the antighost field points towards the same direction as the momentum, as it is drawn in Fig. 1.5.

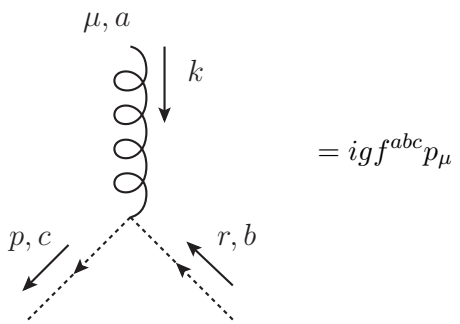

Figure 1.5: The pictorial representation of the ghost-gluon vertex we will use in this manuscript.

QCD Feynman rules

From the previous analysis, the Feynman rules for QCD in Landau gauge are:

1. Associate to each vertex and propagator its corresponding mathematical expression from Fig. 1.6.

2. Impose momentum conservation at each vertex.

3. Integrate over each undetermined loop momentum: $\int \frac{d^4 l}{(2\pi)^4}$.

   Since the vertices in a given Feynman graph come from the terms $-\frac{1}{n!}(\mathcal{L}_{\text{int}})^n$ in the expansion from Eq. (1.88), the diagram will be always accompanied with a sign $(-1)^{V_{c\bar{c}A}+V_{\psi\bar{\psi}A}+V_{AAA}+V_{AAAA}}$, where $V_{\Phi_1\ldots\Phi_n}$ is the total number of vertices corresponding to the interaction of the fields $\Phi_1, \ldots, \Phi_n$. We can forget of this sign by just adding an extra (-1) factor to the mathematical expression associated to each vertex. This is actually what we did in the rules provided in Fig. 1.6. The term $\frac{1}{n!}$ will be included in the symmetry factor of the diagram.

4. Calculate the symmetry factor according to the rules displayed below:

   (a) Each fermion loop contributes with an overall minus sign.

   (b) Each diagram comes with a factor $\frac{1}{V_{c\bar{c}A}!V_{\psi\bar{\psi}A}!V_{AAA}!V_{AAAA}!}$, which stems from the expansion (1.88) [14].

   (c) Compute the usual combinatorial factor due to contractions from Wick's theorem.

1.5 Regularization and renormalization

In the preceding section we presented a strategy quite fruitful to compute correlation functions as long as the coupling remains small. But this is not the end of the story. Beyond tree level, perturbative computations are plagued with ultraviolet (UV) divergent integrals. This is not a particularity of QCD but a general feature

[14] The term $\frac{1}{n!}$ has been absorbed into this factor.

ghost propagator: 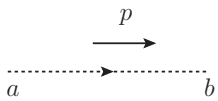

$$= \frac{\delta^{ab}}{p^2}$$

gluon propagator: 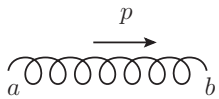

$$= \delta^{ab} \frac{P^{\perp}_{\mu\nu}(p)}{p^2}$$

quark propagator: 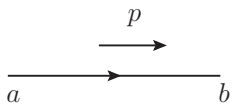

$$= \delta^{ab} \frac{i\not{p} + M}{p^2 + M^2}$$

ghost-gluon vertex: 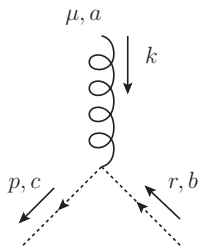

$$= -igf^{abc}p_\mu$$

quark-gluon vertex: 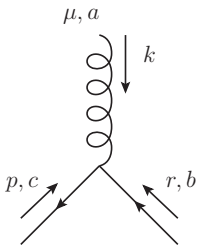

$$= -igt^a\gamma_\mu$$

three-gluon vertex: 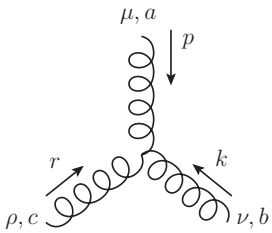

$$= -\frac{ig}{3!} f^{abc} \left[(k-r)_\mu \delta_{\nu\rho} + (r-p)_\nu \delta_{\mu\rho} + (p-k)_\rho \delta_{\mu\nu} \right]$$

four-gluon vertex: 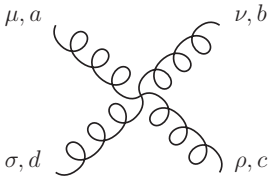

$$= -\frac{g^2}{4!} [f^{eab} f^{ecd} (\delta_{\mu\rho}\delta_{\nu\sigma} - \delta_{\mu\sigma}\delta_{\nu\rho}) + f^{eac} f^{ebd} (\delta_{\mu\nu}\delta_{\rho\sigma} - \delta_{\mu\sigma}\delta_{\nu\rho}) + f^{ead} f^{ecb} (\delta_{\mu\rho}\delta_{\nu\sigma} - \delta_{\mu\nu}\delta_{\sigma\rho})]$$

Figure 1.6: Feynman rules for propagators and vertices corresponding to QCD in Landau gauge.

of quantum field theories (QFTs). Nowadays, the emergence of these infinities is interpreted as the manifestation of some unknown physics beyond certain scale Λ. QCD, and in general QFTs with UV divergences, may be interpreted as low-energy

effective theories valid only up to the scale Λ[15].

In the *regularization* process we render the divergent integrals finite by introducing a *regulator*, which allows us to keep track of the infinities. The most well known techniques to regularize the integrals are: the inclusion of a UV cut-off, the Pauli-Villars, the dimensional and the lattice regularizations [65]. In this thesis we will exclusively use dimensional regularization, however, in the context of this introduction, an ultraviolet cut-off makes easier to understand how to deal with UV divergent integrals. Within this regularization approach, a UV-divergent integral is substituted by a UV finite one in the following manner:

$$\int^{\infty} dq \to \int^{\Lambda} dq. \tag{1.129}$$

Physically, the Λ parameter may be understood precisely as the scale beyond which our field theory is no longer valid. Since we have replaced the upper infinity with a finite value, the divergences are no longer present. At the end, we should make $\Lambda \to \infty$, but, if the renormalization was properly done, this would have no impact on the calculation of Green's functions.

In the *renormalization* process we aim at absorbing the dependence on Λ by means of an appropriate redefinition of the fields and the parameters in the Lagrangian, *i.e.*

$$\Phi_B = \sqrt{Z_\Phi}\Phi, \quad X_B = Z_X X. \tag{1.130}$$

There will be one of such identities for each field Φ, mass and coupling X of the theory. As for QCD in Landau gauge this is $\Phi \in \{A^a_\mu, c^a, \psi\}$ and $X \in \{g, M\}$. The subscript "B" refers to *bare* quantities, *i.e.* objects that are present in the Lagrangian prior to renormalization. Hereafter, quantities without this subscript will be the *renormalized or physical* ones. The Z factors are named *renormalization factors*. A theory is said to be *renormalizable* if this procedure can be carried out by introducing only a finite number of Z-factors.

1.5.1 Superficial degree of divergence

In order to study the renormalizability of a theory it is convenient to introduce the notion of *superficial degree of divergence*. Typically, the expression associated to a Feynman diagram has the following form

$$\int \frac{d^4 l_1}{(2\pi)^4} \cdots \frac{d^4 l_n}{(2\pi)^4} \frac{i\not{l}_1 + M}{(l_1 + M) \cdots l_n^2}. \tag{1.131}$$

For each loop of the diagram there is a potentially divergent integral, where each propagator contributes to the convergence of the integral by adding one or two powers of momentum in the denominator. Naively, one could expect that a Feynman diagram diverges as Λ^D if $D > 0$ and as $\log[\Lambda]$ if $D = 0$, where D is given by

$$\begin{aligned} D \equiv &(\text{powers of momentum in the numerator}) \\ &- (\text{powers of momentum in the denominator}). \end{aligned} \tag{1.132}$$

[15] One could argue that QCD might be valid for arbitrarily high energies due to asymptotic freedom. However, we cannot ensure that this property remains unchanged as we go up in the energy scale, specifically to regions where no experimental access is currently available.

D is referred to as the *superficial degree of divergence*. This quantity can be rewritten in terms of the elements of a diagram, such as the number of vertices, external legs and internal lines. As its name suggests, often D does not coincide with the actual divergence of the diagram. This one can be smaller or larger than D. The former case occurs because of the existence of symmetries, which can make some terms to cancel. The latter is due to the existence of subdiagrams[16] with superficial degree of divergence larger than the one corresponding to the whole diagram. This information is captured by the power-counting theorem. It states that a diagram G is absolutely convergent if the superficial degree of divergence D_H for a subdiagram $H \in G$ is negative for all possible H, including $H = G$, see [65] and references therein.

As a result of this theorem, in order to study the renormalizability of a theory, it is enough to solely consider diagrams with an overall divergence, *i.e.* diagrams whose divergence is coming from the whole diagram.

In the case of QCD in Landau gauge, it can be shown that [65]

$$D = 4 - N_A - \frac{3}{2}\left(N_c + N_\psi\right), \tag{1.133}$$

where N_A, N_c and N_ψ correspond to the number of gluon, ghost and quark external legs, respectively. Thus we have only seven cases in which
$D \geq 0$: the gluon, ghost and quark inverse propagators, and the three-gluon, ghost-gluon, quark-gluon and four-gluon vertices. However, we have only five Z-factors to remove these divergences. Thankfully, owing to the BRST symmetry, some identities among the divergent Green's functions, termed Slavnov-Taylor identities [86, 87], may be established, leaving only five independent UV-divergent Green's functions, which proves the renormalizability of QCD [3, 73, 88–90].

1.5.2 Determination of the Z-factors

Renormalized Green's functions (G_R), computed in terms of renormalized fields, couplings and masses, are related to bare Green's functions (G_B) through

$$G_B(p_1, \cdots, p_n; g_B, M_B) = \left[\prod_{i=1}^{n} \sqrt{Z_i}\right] G_R(p_1, \cdots, p_n; g, M), \tag{1.134}$$

where each $\sqrt{Z_i}$ corresponds to a field in the correlation function. Most of the time we will be interested in *amputated* correlation functions, *i.e.* correlation functions where full propagators have been removed from external propagators. Since each propagator comes with a Z factor we get

$$G_R^{\text{amp}}(p_1, \cdots, p_n; g, M) = \left[\prod_{i=1}^{n} \sqrt{Z_i}\right] G_B^{\text{amp}}(p_1, \cdots, p_n; g_B, M_B). \tag{1.135}$$

For the purpose of determining the renormalization factors, we choose *renormalization conditions*, *i.e.* we impose the values of various Green's functions at the so called *renormalization scale* μ. As a consequence, we introduce a double arbitrariness in the calculation. On the one hand, the value of the Green's functions,

[16] By subdiagram we mean a part of the total diagram corresponding to a certain connected Feynman diagram.

on the other hand the renormalization scale. The choice of the former defines the *renormalization scheme*. In every renormalization scheme the Z-factors must remove all the divergences coming from correlation functions. Regardless of this, they may differ in how much they modify the finite part of the Green's functions. Moreover, two different renormalization schemes are always connected by a finite renormalization [65].

In order to illustrate this procedure with an example, let us introduce the momentum-space substraction scheme (MOM). Within this scheme the Z-factors are defined in such a way that the fundamental two- and three-point correlation functions equal their corresponding tree level expressions at the renormalization scale μ. Following this idea, the renormalized ghost propagator can be expressed in terms of the bare ghost propagator, of the form (1.102), as

$$D^{ab}(p) = \delta^{ab} Z_c^{-1} \frac{F_B(p)}{p^2} = \delta^{ab} \frac{F(p)}{p^2}. \tag{1.136}$$

Therefore, in the MOM scheme we determine Z_c by choosing

$$D^{ab}(p = \mu) = \delta^{ab} \frac{1}{\mu^2}. \tag{1.137}$$

1.5.3 Renormalization group equations

The couplings, masses and Green's functions depend on the renormalization scale μ, at which the renormalization conditions are imposed. The renormalization group equations [91–94] allow us to determine this dependence. These equations can be derived by noticing that bare Green's functions do not depend on the renormalization scale μ as far as the bare parameters are fixed, *i.e.*

$$\mu \frac{d}{d\mu} G_B(p, g_B, \{M_{i,B}\})\Big|_{g_B, \{M_{i,B}\}} = 0, \tag{1.138}$$

when regarding a theory with just one coupling. This expression can be rewritten in terms of the renormalized fields, coupling and masses by means of the redefinitions from Eq. (1.130), yielding to the Callan-Symanzik equation [92, 93]:

$$\left(\mu \frac{\partial}{\partial \mu} + \frac{1}{2} \sum_{\text{fields}} n_\Phi \gamma_\Phi + \beta_g \frac{\partial}{\partial g} + \sum_i^{N_f} \beta_{M_i} \frac{\partial}{\partial M_i} \right) G(p, \mu, g(\mu), \{M_i(\mu)\}) = 0, \tag{1.139}$$

where n_Φ is the number of fields Φ involved in the correlation function G. Besides, we have introduced the β-function and the so called anomalous dimension γ, defined as

$$\beta_X(g, \{M_i\}) = \mu \frac{dX}{d\mu}\Big|_{g_B, \{M_{i,B}\}} \quad \text{and} \quad \gamma_\Phi(g, \{M_i\}) = \mu \frac{d \log Z_\Phi}{d\mu}\Big|_{g_B, \{M_{i,B}\}}. \tag{1.140}$$

For QCD, $\Phi \in \{A^a_\mu, c^a, \bar{c}^a, \psi, \bar{\psi}\}$ and $X \in \{g, M_i\}$.

It will be useful for subsequent chapters to write Eq. (1.139) in terms of a vertex function with n_A gluon legs, n_c ghost legs and n_ψ quark legs:

$$\begin{aligned}&\Bigg(\mu\partial_\mu - \frac{1}{2}(n_A\gamma_A + n_c\gamma_c + n_\psi\gamma_\psi)\\&+\beta_g\frac{\partial}{\partial g} + \sum_i^{N_f}\beta_{M_i}\frac{\partial}{\partial M_i}\Bigg)\Gamma^{(n_A,n_c,n_\psi)}(p,\mu,g(\mu),\{M_i(\mu)\}) = 0.\end{aligned} \tag{1.141}$$

The solution to this equation enable us to relate the vertex function at two different renormalization scales, μ and μ_0, in the following way

$$\begin{aligned}&\Gamma^{(n_A,n_c,n_\psi)}(p,\mu,g(\mu),\{M_i(\mu)\})\\&= z_A(\mu,\mu_0)^{n_A/2}z_c(\mu,\mu_0)^{n_c/2}z_\psi(\mu,\mu_0)^{n_\psi/2}\Gamma^{(n_A,n_c,n_\psi)}(p,\mu_0,g(\mu_0),\{M_i(\mu_0)\}),\end{aligned} \tag{1.142}$$

where

$$\log z_\Phi(\mu,\mu_0) = \int_{\mu_0}^{\mu}\frac{d\mu'}{\mu'}\gamma_\Phi(g(\mu'),\{M_i(\mu')\}), \tag{1.143}$$

with $\Phi \in \{A^a_\mu, c^a, \psi\}$.

The Callan-Symanzik equations are of paramount importance when it comes to perturbative calculations. This is because typically there are corrections of the form $g^2\log\left(\frac{p^2}{\mu^2}\right)$. As perturbative expansions remain valid only if successive corrections are increasingly smaller, these terms are hazardous since they could spoil the perturbative series in the momentum region where $p \gg \mu$. A solution to this problem consists in computing the renormalized Green's function by choosing a varying renormalization scale, such that $\mu \approx p$. Only after we posses this information, we are in condition of safely determining the vertex function at a fixed renormalization scale μ_0, thanks to Eq. (1.142).

1.5.4 Asymptotic freedom

As we have stated before, the validity of perturbation theory depends on a small expansion parameter. For a quantum field theory, typically this parameter is not g but λ [70], which in four space-time dimensions is

$$\lambda = \frac{Ng^2}{16\pi^2}, \tag{1.144}$$

where N is the number of colors. Just as the coupling, the expansion parameter does depend on the renormalization scale. This dependence is encoded in β_g. We can compute it by using perturbation theory and, as a result, we are able to determine the dependence $\lambda(\mu)$. This determination is trustful only in the momentum region where $\lambda(\mu)$ is small, since only there it is legitimate to carry out perturbative calculations.

In the case of QCD, the β_g-function was first computed by David Gross and Frank Wilczek and independently by David Politzer in 1973 [4, 5]. It can be derived from the four vertices which define g, which are, the ghost-gluon, the quark-gluon, the three-gluon and the four-gluon vertex. The four derivations are equivalent due to Slavnov-Taylor identities.

There is an additional restriction on the renormalization factors Z_g, Z_A and Z_c. It stems from the observation that, due to both the transversality of the gluon propagator and the particular form of the tree level ghost-gluon interaction, there are no loop corrections to the ghost-gluon vertex in the limit of vanishing ghost momentum. This is:

$$\Gamma^{abc}_{\mu,B}(r=0,p) = -ig_B f^{abc} p_\mu, \tag{1.145}$$

at all orders of perturbation theory. The renormalized ghost-gluon vertex satisfies

$$\Gamma^{abc}_{\mu,R}(r=0,p) = -i\sqrt{Z_A} Z_c Z_g g f^{abc} p_\mu. \tag{1.146}$$

Therefore $\sqrt{Z_A} Z_c Z_g$ is finite [86]. The so called Taylor renormalization scheme extends this result to the finite parts as well

$$\sqrt{Z_A} Z_c Z_g = 1. \tag{1.147}$$

Consequently, Z_g can be computed in terms of Z_A and Z_c, which can be determined by calculating perturbatively the ghost and gluon propagators. Finally, the β_g-function can be found by means of

$$\mu \frac{d}{d\mu} g_B = \mu \frac{d}{d\mu}(Z_g g) = 0. \tag{1.148}$$

At two-loops, for energy scales much larger than the quark masses, $\mu \gg M$, the result is [95, 96]:

$$\beta_g(g(\mu)) = -\beta_0 \frac{g(\mu)^3}{16\pi^2} - \beta_1 \frac{g(\mu)^5}{256\pi^4} + \mathcal{O}(g^7), \tag{1.149}$$

where the coefficients β_0 and β_1 are renormalization scheme independent [65] and take the values:

$$\beta_0 = \frac{11}{3} C_a - \frac{4}{3} T_f N_f, \tag{1.150}$$

$$\beta_1 = \frac{34}{3} C_a^2 - 4 C_f T_f N_f - \frac{20}{3} C_a T_f N_f. \tag{1.151}$$

For a general SU(N) gauge group the parameters are $C_a = N$, $C_f = \frac{N^2-1}{2N}$ and $T_f = 1/2$.

As for QCD, $N_f = 6$, which leads to a negative β_g-function. This result shows that, as the energy value tends to increment, the coupling tends to be increasingly small. This phenomenon receives the name of *asymptotic freedom*, and permits the utilization of perturbation theory to compute Green's functions in QCD at very high energies. In contrast, this is no longer the case as we consider lower energies. Actually, the perturbative calculation of the running coupling displays a *Landau pole*, *i.e.* a finite energy scale at which the coupling diverges. This should not be interpreted as a genuine infinity of the theory, rather as a manifestation of the breakdown of perturbation theory.

Chapter 2

The various paths to infrared QCD

As we stated at the end of the previous chapter, at sufficiently large momentum the coupling becomes small, making of perturbation theory a suitable tool to compute correlation functions. On the contrary, in the low-momentum region the coupling encounters a Landau pole[1]. Typically this is interpreted as a failure of the perturbative paradigm. However, this could be attributed to extending the use of the FP theory beyond its range of validity, as we will discuss in this chapter. Moreover, in this thesis we will show that certain aspects of YM theory and QCD seem to admit a perturbative treatment.

The IR of QCD is of great relevance so as to comprehend the phenomenon of *confinement*, *i.e.* the nonexistence of colored asymptotic particle states[2][99–102]. In spite of some progress , see for example [103, 104], a fully analytic explanation of this phenomenon remains elusive, making of confinement one of the most intriguing and important problems of theoretical physics nowadays. Even though we will not tackle this problem in this manuscript, the model we will analyze in the subsequent chapters opens the door to address this tough topic in a new framework.

As the perturbative analysis is no longer valid to understand the IR of QCD, several alternative methods have been developed in order to grasp that regime. This chapter is devoted to the introduction of several of these approaches.

2.1 The Gribov ambiguity

As we pointed out in section 1.2.2, in the Faddeev-Popov method the gauge-fixing functional must pick up only one representative of the gauge field from each gauge orbit, if the procedure is to be rigorously valid. Unfortunately, generally this is not the case. In his famous work from 1977 [7], Vladimir Gribov was the first one to notice this problem. One year later, Singer [8] showed that, because of a topological obstruction, there is no continuous gauge-fixing condition, $\mathcal{F}[A] = 0$, free of Gribov copies on the whole configuration space. Gauges free of Gribov

[1]Note that the definition of the coupling depends on the renormalization scheme chosen and hence it is not unique. [97]

[2]For a detailed analysis on confinement see, for instance, [98].

copies do exist, see *e.g.* [105], but they are singular and, therefore, very hard to manipulate in calculations.

2.1.1 Gribov copies and the perturbative regime

As we will show in this section, Gribov copies do not pose any problem in the high-energy region, and, as a consequence, the Faddeev-Popov procedure is a fully justified method in order to fix the gauge at such energy scales.

To begin with, let us consider two equivalent Gribov copies, A_μ and A'_μ, connected by a gauge transformation (1.10) in Landau gauge. They satisfy:

$$A'_\mu = UA_\mu U^\dagger + \frac{i}{g}U\partial_\mu U^\dagger, \quad \partial_\mu A_\mu = 0 \text{ and } \partial_\mu A'_\mu = 0, \tag{2.1}$$

which is equivalent to

$$(\partial_\mu U)A_\mu U^\dagger + U(\partial_\mu A_\mu)U^\dagger + UA_\mu(\partial_\mu U^\dagger) + \frac{i}{g}(\partial_\mu U)(\partial_\mu U^\dagger) + \frac{i}{g}U\partial^2 U^\dagger = 0 \tag{2.2}$$

If U is an infinitesimal transformation of the type $U = 1 + \alpha$, with $\alpha = \alpha^a t^a$, expanding up to first order in α^a we arrive at

$$-\partial_\mu(\partial_\mu\alpha + ig[\alpha, A_\mu]) = 0, \tag{2.3}$$

where we used $U^\dagger = 1 - \alpha$.

By means of Eq. (1.6) and Eq. (1.14), we can rewrite this expression as

$$-\partial_\mu D_\mu \alpha = 0. \tag{2.4}$$

As a consequence, this equation expresses the condition for infinitesimal Gribov copies to exist in Landau gauge. The term $-\partial_\mu D_\mu$ is the Faddeev-Popov operator in linear covariant gauges, see Eq. (1.58). For transverse gluons, $\partial_\mu A_\mu = 0$, this operator is hermitian

$$-\partial_\mu D_\mu = -D_\mu \partial_\mu. \tag{2.5}$$

As a result, Eq. (2.4) has trivial solutions, consisting in constant eigenvectors, $\partial_\mu \alpha = 0$, which generate non-local gauge transformations. Such solutions are of no interest for our study.

In the perturbative regime, *i.e.* $A_\mu \sim 0$, the Eq. (2.4) reads $-\partial_\mu^2 \alpha = 0$. In addition, it is clear that the eigenvalue equation

$$-\partial_\mu^2 \alpha = \epsilon\alpha, \tag{2.6}$$

only admits positive eigenvalues $\epsilon = p^2$[3]. Hence, there are no infinitesimal Gribov copies in the perturbative region. Moreover, the Faddeev-Popov operator is definite positive. These two features guarantee that the Faddeev-Popov procedure is fully justified in the ultraviolet region. For larger values of A_μ, Eq. (2.4) has non-trivial solution for SU(N) gauge theories, and, as a result, there are Gribov copies[4]. For explicit constructions of zero modes of the Faddeev-Popov operator see Refs. [106–108].

[3] p^2 denotes the modulus of the Euclidean momentum squared. It is related to the Minkowskian momentum through $p^2 = -p_M^2$.

[4] It is worth mentioning that QED [gauge group U(1)] is free of Gribov copies in Landau gauge. See, for example, [71].

2.1.2 The Gribov region

As was first devised by Gribov, the solution to this problem should come out from restricting the generating functionals to a region of the gluon configuration space where no Gribov copies are present. A first attempt to determine this zone was proposed in [7], in what nowadays is called the *Gribov region*, denoted by the symbol Ω. It is defined as

$$\Omega = \{A^a_\mu, \partial_\mu A^a_\mu = 0, -\partial_\mu D_\mu[A] > 0\}, \tag{2.7}$$

i.e. the space of transverse gluons in which the Faddeev-Popov operator is positive definite. The boundary of this region is called the first Gribov horizon and, on it, the determinant of the Faddeev-Popov operator vanishes.

An alternative definition of the Gribov region is given by the set of gluon fields which are *relative* minima of the functional

$$F_A[U] = ||A^U||^2 = \mathrm{Tr}\int d^4x\ A^U_\mu(x)A^U_\mu(x) = \frac{1}{2}\int d^4x\ A^{Ua}_\mu(x)A^{Ua}_\mu(x). \tag{2.8}$$

For the purpose of demonstrating that the space so defined is exactly Ω, let us consider a gauge field A^a_μ such that it is a local minimum of $F_A[U]$ at $U = 1$. As A^a_μ is a relative minimum of $F_A[U]$, an infinitesimal gauge transformation of A^a_μ should vanish,

$$\delta||A||^2 = \delta\left(\frac{1}{2}\int d^4x\ A^a_\mu(x)A^a_\mu(x)\right) = \int d^4x\ \delta(A^a_\mu(x))A^a_\mu(x) \tag{2.9}$$

$$= -\int d^4x\ D^{ab}_\mu\theta^b(x)A^a_\mu(x) = -\int d^4x\ \partial_\mu\theta^a(x)A^a_\mu(x) \tag{2.10}$$

$$= \int d^4x\ \theta^a(x)\partial_\mu A^a_\mu(x) = 0.$$

Since this equation is valid for an arbitrary function $\theta^a(x)$, then $\partial_\mu A_\mu = 0$. Furthermore, for A^a_μ to be a local minimum it must satisfy

$$\delta(\delta||A||^2) = \int d^4x\ \theta^a(x)(-\partial_\mu(D_\mu\theta)^a) > 0, \tag{2.11}$$

and, as a consequence, the operator $-\partial_\mu D_\mu$ is positive definite.

The Gribov region is convex, bounded in every direction and contains $A_\mu = 0$. This last property ensures that the perturbative domain is included in the Gribov region. In addition, it can be shown that every gauge orbit intersects the Gribov region at least once. Detailed proofs of these properties are in [71] and references therein. Unfortunately, the Gribov region contains Gribov copies. This is quite natural to think from the second definition of Ω we provided: the functional $F_A[U]$ has multiple relative minima for each gauge orbit. A general argument showing the existence of Gribov copies inside the Gribov region is given in [71]. Explicit examples are provided in [38] and references therein. Moreover, numerical studies have also detected Gribov copies in Ω, see *e.g.* [109].

2.1.3 The fundamental modular region

Continuing with the previous reasoning, a logic step towards the elimination of these remnant Gribov copies, consists in taking a more restricted region: the

space of gauge fields which are an *absolute* minimum of the functional $F_A[U]$ from Eq. (2.8). This region is known as the *fundamental modular region* and it is symbolized by Λ[5]. This procedure would guarantee that, for each gauge orbit, the minimum condition would select one and only one representative of the gauge field if the absolute minimum of $F_A[U]$ is non-degenerate. Despite it has been proven that this is not the case, luckily enough, all of these degenerated minima are located on the boundary of the fundamental modular region, $\delta\Lambda$ [107]. Thus, they constitute a zero measure set and do not contribute to functional integrals on Λ.

It is obvious that Λ is included in Ω. Besides, it can be shown that the fundamental modular region is convex, bounded in every direction and that $A_\mu = 0$ belongs to Λ, see [71] and references therein.

As a conclusion, in order to properly quantize QCD, it is necessary to restrict the domain of integration of the functional integrals from (1.61) to the fundamental modular region. Unfortunately, it is unknown how to implement this restriction in the continuum so far [110].

It has been conjectured that relevant configurations of the gauge field are located on the intersection between the boundaries from the Gribov region and the fundamental modular region, $\delta\Omega \cap \delta\Lambda$ [39, 111, 112]. Accordingly, the remaining Gribov copies in Ω could safely be ignored, allowing a rigorous gauge fixing by just restrict the integrals to Ω instead of Λ. In practice this would represent an enormous advantage, since calculations inside the Gribov region can be carried out. Nonetheless, it is important to keep in mind that these ideas are not supported by any kind of demonstration yet.

2.1.4 The Gribov-Zwanziger action

The restriction of the functional integrals to the Gribov region can be performed by introducing a new effective action, which encodes the information of the Gribov region, and integrating over the whole configuration space, similarly to what is done with the gauge fixation in the Faddeev-Popov procedure, see Section 1.2.

One of the theories derived from such procedure is the so-called Gribov-Zwanziger (GZ) action [39]. This action leads to a vanishing gluon propagator at zero momentum [113] and an enhanced ghost propagator[6] at tree-level [39], which is not the behavior found in numerical simulations, see Section 2.3. Various studies have been carried out within the GZ approach. Among other topics, the breaking of the standard BRST symmetry [114], the definition of a non-perturbative BRST transformation [115] and the construction of physical operators [116, 117] have been addressed.

In order to have an action capable of eliminating the discrepancies with the propagators from numerical simulations, a generalization of the GZ action, which takes into account the existence of various condensates, was introduced. This is referred to as the refined Gribov-Zwanziger (RGZ) action [40, 118]. Even though the specific form of the action depends on the particularities of the condensates, it is always chosen such that its infrared behavior corresponds to the one from

[5] Restriction to this zone is also referred to as the minimal Landau gauge.

[6] An enhanced ghost propagator can be approximated by $D(k^2) \sim \frac{1}{k^{2+\kappa}}$, with $\kappa > 0$, for small momentum k.

numerical studies.

In both, GZ and RGZ actions, BRST symmetry is softly broken [40]. This is enough to prove the renormalizabilty of these models but impedes to define the physical Hilbert space as the cohomology of the BRST transformation, as was done in section 1.3.1. Therefore, the unitarity problem remains unsolved. Since these models introduce additional fields in the action, the computations are cumbersome. Nevertheless progress has been made regarding, for instance, propagators [119–121], the glueball spectrum [122, 123] and the ghost-antighost-gluon vertex [124].

2.2 Functional methods

In general terms, functional methods relate various Green's functions through integral, differential or integro-differential equations. They have various origins, such as being equations of motion of correlation functions or equations derived from underlying symmetries of a given theory. As for QCD, functional methods are directly applied on the gauge-fixed action. Additionally, some modeling, which typically substitute missing information, usually must be introduced in order to carry out practical computations.

Functional methods are employed to tackle a diverse range of problems in physics, such as condensed matter, gravity or quantum field theory. A complete review regarding applications of functional equations to QCD can be found in Ref. [110].

In the field of QCD and YM-theory, two-, three- and four-point correlation functions have been computed within these approaches, see *e.g.* [16–19, 125, 126]. Recently, the glueball spectrum was computed without the need of extra modeling [127]. With the aid of effective models, phenomenological implications of functional methods have also been addressed, see for instance [15, 128, 129].

As an example of these methods we will briefly present the Dyson-Schwinger approach. The remaining functional methods are: the functional renormalization group equations [20–23], the equations of motion from nPI effective actions [130–133] and the Hamiltonian approach [134–138].

2.2.1 Dyson-Schwinger equations

Dyson-Schwinger equations (DSE) are named after Julian Schwinger and Freeman Dyson, who were the first ones to introduce the use of this formalism [12–14]. Here we will sketch the main ideas and problems found when using these equations. Overviews on DSE and its applications to QCD can be seen in Refs. [15, 139].

With appropriate boundary conditions, the integral of a total derivative vanishes. DSE are a consequence of this. In the context of the generating functional of correlation functions, $Z[J]$, this idea translates into

$$\int \mathcal{D}[\Phi]\; e^{-S[\Phi]+\int d^4x \Phi_j J_j} \left(-\frac{\partial S}{\partial \Phi_i} + J_i \right) = 0, \tag{2.12}$$

which is equivalent to

$$\left\langle \frac{\partial S}{\partial \Phi} - J \right\rangle_J = 0. \tag{2.13}$$

As in Chapter 1, Φ is a superfield such that $\Phi \in \{A, c, \bar{c}, \psi, \bar{\psi}, h^a\}$ and $\mathcal{D}[\Phi]$ denotes an appropriate integral measure. The sources are given by Eq. (1.34).

DSE arise as a result of taking successive derivatives on Eq. (2.13), where the number and type of derivative depend on the specific Green's function one wants to calculate, and setting the sources to zero. In order to clarify how these ideas are implemented, we introduce a concrete example.

Consider QCD in Landau gauge, whose action is given by Eq. (1.66), in the *quenched approximation*, *i.e.* with infinitely heavy quarks [7]:

$$S = \int d^4x \left\{ \frac{1}{4} F^a_{\mu\nu} F^a_{\mu\nu} - \bar{c}^a \partial_\mu (\partial_\mu + g f^{abc} A^b_\mu c^c) + i h^a \partial_\mu A^a_\mu \right\}. \tag{2.14}$$

Since the expectation value from (2.13) takes into account the sources it is necessary to introduce

$$S_{\text{sources}} = \int d^4x \{ J^a_\mu A^a_\mu + \bar{\chi}^a c^a + \bar{c}^a \chi^a + R^a h^a \}. \tag{2.15}$$

Then, we can take $\Phi = \bar{c}^a$ in (2.13) which yields

$$\left\langle \frac{\partial S}{\partial \bar{c}^a(x)} - \chi^a(x) \right\rangle_J = 0. \tag{2.16}$$

If we take the derivative with respect to $\chi^b(y)$ we arrive at

$$\left\langle \frac{\partial S}{\partial \bar{c}^a(x)} \bar{c}^b(y) \right\rangle = \delta^{ab} \delta(x-y). \tag{2.17}$$

Furthermore, the derivative of the action with respect to the antighost can be computed explicitly

$$\frac{\partial S}{\partial \bar{c}^a(x)} = -\partial_\mu D_\mu c^a. \tag{2.18}$$

As a consequence, we have

$$\begin{aligned}
&\left\langle \frac{\partial S}{\partial \bar{c}^a(x)} \bar{c}^b(y) \right\rangle \\
&= -\partial^2_x \langle c^a(x) \bar{c}^b(y) \rangle - \left\langle g f^{adc} \partial_{\mu,x} \int_{zz'} A^d_\mu(z) c^c(z') \delta(z-x) \delta(z-z') \bar{c}^b(y) \right\rangle \\
&= -\partial^2 D^{ab}(x-y) + \int_{zz'} (-g f^{adc} \partial_{\mu,x} \delta(z-x) \delta(z-z') \langle c^c(z') \bar{c}^b(y) A^d_\mu(z) \rangle) \\
&= \delta^{ab} \delta(x-y)
\end{aligned} \tag{2.19}$$

where in the last line we have inserted the ghost propagator via the identification $D^{ab}(x-y) = \langle c^a(x) \bar{c}^b(y) \rangle$. In Eq. (2.19) there are also the tree-level inverse of the ghost propagator and the tree level ghost-gluon vertex (see Eqs. (1.99) and (1.126)) in coordinate space, *i.e.*

$$-\partial^2 \quad \text{and} \quad -g f^{adc} (\partial_{\mu,z} \delta(z-x)) \delta(z-z'), \tag{2.20}$$

respectively.

[7] To practical effects, this means that quarks can be completed neglected.

Green's functions in (2.19) are full correlation functions since they are derived from $Z[j]$. According to Eq. (1.31) and because we have set $\langle\Phi\rangle = 0$, full and connected three-point functions coincide. Moreover, thanks to Eq. (1.37), it is legitimate to write

$$\langle c^c(z)\bar{c}^b(y)A^a_\mu(x)\rangle = \langle c^c(z)\bar{c}^b(y)A^a_\mu(x)\rangle_{\text{conn.}} \tag{2.21}$$

$$= -\int_{uvw} D^{ad}_{\mu\nu}(x-u)D^{ce}(z-v)\Gamma^{def}_\nu(u,v,w)D^{fb}(w-y), \tag{2.22}$$

where Γ^{def}_ν is the proper ghost-gluon vertex. Plugging this identity into (2.19) we obtain

$$\begin{aligned}
&-\partial^2_x D^{ab}(x-y) + gf^{adc}\int_{uvwzz'}(\partial_{\mu,x}\delta(z-x))\delta(z-z')D^{de}_{\mu\nu}(z-u)\times \\
&\times D^{cf}(z'-v)\Gamma^{efh}_\nu(u,v,w)D^{hb}(w-y) \\
&= \Bigg[\int_w \delta(x-w)\delta^{ah}(-\partial^2) + gf^{adc}\int_{uvwzz'}(\partial_{\mu,x}\delta(z-x))\delta(z-z') \\
&D^{de}_{\mu\nu}(z-u)D^{cf}(z'-v)\Gamma^{efh}_\nu(u,v,w)\Bigg]D^{hb}(w-y) = \delta^{ab}\delta(x-y),
\end{aligned} \tag{2.23}$$

which is represented diagrammatically in Fig. 2.1. Proceeding in an analog manner we can obtain a DSE for the gluon propagator. The pictorial representation of it is in Fig. 2.2.

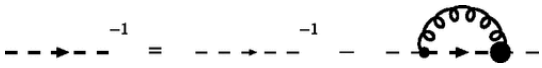

Figure 2.1: The ghost DSE. Bold propagators are dressed. The thick dot denotes a full ghost-gluon vertex. Original figure from [140].

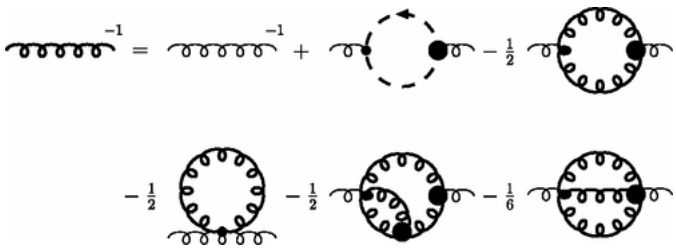

Figure 2.2: The gluon DSE. Bold propagators are dressed. Thick dots denote full vertices. Original figure from [140].

It is clear from Figs. 2.1 and 2.2 that in order to solve the two-point functions we need information about higher order correlation functions, yielding to an infinite tower of coupled non-linear equations. DSE are characterized by leading to this kind of systems of equations. By solving these equations we would be in position to reconstruct the whole generating functional, solving completely the gauge-fixed theory. In practice, however, this is not possible and it is necessary to specify a truncation scheme, this is to say, a specification of the maximum number of legs which will be treated self-consistently in the DSE. Generally, truncation

schemes are chosen so as to fulfill certain properties of the theory, such as global and local symmetries, renormalizability and analyticity [129].

Gluon and ghost two-point functions from DSE

The first works which solved the DSE for both the gluon and ghost propagators [24, 25] found a solution where the gluon propagator (1.117) is IR vanishing and the ghost dressing function (1.102) is IR enhanced. This is in qualitative agreement with the confinement scenario by Kugo and Ojima [141] and the GZ approach. This solution is named the *scaling* solution and the dressing functions are characterized by the behavior

$$D(p) \propto (p^2)^{\delta_A}, \quad F(p) \propto (p^2)^{\delta_c}, \tag{2.24}$$

where the coefficients satisfy the relation

$$\kappa = -\delta_c = \frac{\delta_A}{2}, \tag{2.25}$$

where $\kappa = 0.595353$ (see [110] and references therein). More recent numerical simulation clearly contradict this behavior, see *e.g.* [11, 32, 50, 142, 143], by displaying an IR finite gluon propagator along with an IR finite ghost dressing function, see Fig. 2.3. This kind of solution receives the name of massive or *decoupling* solution. In the framework of functional equations, it is possible to obtain an infinite number of decoupling solutions, where the scaling solution is just a particular case with an infinite gluon mass [125]. As a final comment, let us mention that only the scaling solution posses an intact BRST symmetry [141]. Consequently, this symmetry is not realized in numerical computations, see *e.g.* Ref. [144].

2.3 Lattice QCD

Every semi-analytical approach which intends to describe the infrared region of QCD and YM theories must test its results. Typically, this is carried out by comparison with Monte-Carlo simulations on a lattice.

Lattice simulations, first introduced by Kenneth G. Wilson [145], constitute the only first principles, manifestly gauge invariant, fully nonperturbative approach to study QCD to date [55, 146]. Because of these relevant features, it is the most reliable and powerful technique to access to the low-energy regime of QCD. Pedagogical introductions to the subject can be found in Refs. [55, 146–149], to name a few.

Lattice simulations have been extensively used to analyze QCD. For instance, they have been used to reproduce with great precision the hadron spectrum, by using as input parameters solely the coupling constant and the quarks masses[9]. In addition, lattice studies have also been widely utilized to explore the phase structure of QCD under extreme conditions of temperature [150, 151] and density [152–155]. Such results are of importance for a variety of phenomena, such as high energy nuclear collisions and astrophysics of ultra-compact stars [156]. More relevant for this thesis, various two- and three- point correlation functions have

been calculated in pure YM theory, *e.g.* [28, 32–34, 36, 55, 142, 157–159] and QCD *e.g.* [160–164].

In general terms, lattice simulations are generated in three steps [9]. Firstly, the Euclidean space-time, on which the theory is defined, is transformed into a lattice of points. The theory, now restricted to a discretized space-time, is automatically UV-finite since the lattice spacing acts as a natural UV-regulator. This is the only known regularization of QCD beyond perturbation theory [55]. A second step consists in computing the Green's functions in the discrete theory by means of stochastic integration of the path integrals. In the final step, the continuum limit is taking by removing the regulator introduced in the first step. This is achievable as long as the coupling is not UV-divergent. Fortunately, thanks to asymptotic freedom, this is the case for QCD.

2.3.1 Basic concepts

After discretization, integrals on space-time are replaced by sums over lattice sites, this is

$$\int d^4x \to a^4 \sum_{\text{sites}} \quad , \tag{2.26}$$

where we are assuming that the lattice spacing, a, is the same in every space-time direction [8]. Let us denote by x the position of a lattice site and by $\hat{\mu}$ a unit vector in the x_μ direction of space-time. Fermion and antifermion fields are evaluated on lattice sites, while gluon fields are associated with links between adjacent points of the lattice. This is because in lattice gauge theory we do not work directly with the gauge field itself $A_\mu(x)$. Rather, we use the so called *link variables*, symbolized by $U_{x,\mu}$ and defined as

$$U_{x,\mu} \equiv \mathtt{P} e^{ig_0 \int_0^1 dt A_\mu(x+ta\hat{\mu})}. \tag{2.27}$$

where $\mathtt{P}$ is the path ordering operator[9] and g_0 is the bare coupling constant. Link variables must be introduced in order to keep the gauge invariance of the action explicit [9, 165].

For the purpose of defining the QCD action on the lattice it is convenient to concentrate on the gluonic and matter content separately[10]in such a way that

$$S_{\text{QCD}} = S_{\text{YM}}[U] + S_{\text{M}}[U, \bar{\psi}, \psi], \tag{2.28}$$

where we have indicated explicitly the dependence on the fermion and antifermion fields as well as on the link variable. Both parts depend on the gauge field $U \equiv \{U_{x,\mu}\}$.

[8]Studies on anisotropic lattices have also been performed [9].

[9]The path ordering operator orders the gauge field along the integration path in such a way that $A_\mu(x + t_1 a\hat{\mu})$ is located to the left of $A_\mu(x + t_2 a\hat{\mu})$ if $t_1 > t_2$.

[10]Recall that in the continuum, $S_{\text{QCD}} = S_{\text{YM}} + S_{\text{M}}$, with

$$S_{\text{YM}} = \frac{1}{4} \int d^4x \; F^a_{\mu\nu} F^a_{\mu\nu},$$

$$S_{\text{M}} = \int d^4x \; \bar{\psi}(-\gamma_\mu \partial_\mu + M)\psi.$$

Gluonic sector

To build the term associated to $S_{\rm YM}$ on the lattice, we begin by defining the *plaquette*:

$$\Box_{x,\mu\nu} = U_{x,\mu} U_{x+\hat{\mu},\nu} U^{\dagger}_{x+\hat{\nu},\mu} U^{\dagger}_{x,\nu}, \tag{2.29}$$

whose trace is a gauge invariant quantity[11]. Since

$$\Box_{x,\mu\nu} = 1 + i g_0 a^2 F_{\mu\nu} - \frac{1}{2} g_0^2 a^4 F_{\mu\nu}^2 + \mathcal{O}(a^6), \tag{2.30}$$

the simplest discretization of the continuum YM action, the so-called Wilson action, reads [145]

$$S_{\rm W} = \beta \sum_x \sum_{1\leq\mu\leq\nu\leq 4} \left(1 - \frac{1}{N} {\rm Re}\{{\rm Tr}\Box_{x,\mu\nu}\}\right), \tag{2.31}$$

where N is the number of colors, for QCD $N = 3$. The parameter β is defined in such a way that the YM action is retrieved from Wilson action in the continuum limit $a \to 0$,

$$\beta \equiv \frac{2N}{g_0^2}, \tag{2.32}$$

which means that

$$S_{\rm W} \underset{a\to 0}{\to} \frac{1}{4} \int d^4x {\rm Tr}(F_{\mu\nu}(x)^2) + \mathcal{O}(a^2). \tag{2.33}$$

The error associated to the Wilson action is of order $\mathcal{O}(a^2)$. It is worth mentioning that the non-uniqueness of the discretization may be exploited to find discretized versions of the YM action with higher order errors.

Matter sector

A naive discretization of $S_{\rm M}$ is given by

$$S_{\rm M,\ latt.} = a^4 \sum_x \bar{\psi}_x \left(\sum_{\mu=1}^{4} \gamma_\mu \frac{\psi_{x+\hat{\mu}} - \psi_{x-\hat{\mu}}}{2a} + M \right), \tag{2.34}$$

which leads to a ill-defined expression for the quark propagator, in what is known as the doubling problem. There are various strategies to deal with this issue, such as the Wilson [145], staggered [166–168] or twisted mass fermions [169] for example.

In general terms, such strategies rest on writing the fermionic part of the action as

$$S_{\rm M} = a^4 \sum_x \psi_x Q_{xy} \psi_y, \tag{2.35}$$

where Q_{xy} depends on the link variable. By using the rules of Grassmanian integration we get

$$\int \mathcal{D}[\psi, \bar{\psi}] e^{-S_{\rm M}} = \det(Q). \tag{2.36}$$

[11] This is because we are taking a closed loop of parallel transports. The plaquette is the simplest of those loops. More complex combination give place to gauge invariant quantities as well.

This identity allows us to write the QCD action on the lattice as

$$S_{\text{QCD,latt.}} = S_{\text{W}} - \log[\det(Q)]. \tag{2.37}$$

The role of quarks is now completely captured by the fermion determinant, $\det(Q)$. In the quenched approximation of QCD this determinant is set equal to one.

Numerical evaluation of an observable

The expected value of an observable in terms of the link variables, the fermion and antifermion fields reads

$$\langle O \rangle = \frac{1}{Z} \int \mathcal{D}U_\mu \int \mathcal{D}[\psi, \bar{\psi}]\ O e^{-(\bar{\psi} Q[U] \psi + S_{\text{YM}}[U])}. \tag{2.38}$$

By using (2.36) this equation can be rewritten as

$$\langle O \rangle = \frac{1}{Z} \int \prod_{x,\mu} dU_\mu(x) \det(Q)[U]\ O e^{-S_{\text{YM}}[U]}. \tag{2.39}$$

From a numerical point of view, the only category of numerical approaches suitable to compute this sort of integrals is the one based on Monte Carlo simulations. In these calculations observables are averaged on randomly produced gauge field configurations, U_μ[12]. Nevertheless, such way of carrying out computations turns out to be extremely inefficient. Rather, a significant improvement is realized when gauge field configurations are generated with a probability proportional to $\det(Q) \times e^{-S_W(U)}$. As a result, the expectation value of an observable is calculated as an unweighted average over the gauge configurations produced with the latter approach.

$$\langle O \rangle = \frac{1}{N_{\text{conf.}}} \sum_{\alpha}^{N_{\text{conf.}}} O[U_\alpha], \tag{2.40}$$

where $N_{\text{conf.}}$ is the number of configurations generated.

Landau gauge

Lattice simulations do not need of a gauge fixation procedure in order to compute physical observables. This is because only a finite number of configurations are taken into account when computing path integrals on a lattice. On the contrary, semi-analytical methods can only be developed after gauge fixation. Within these frameworks, typically it is easier to compute gauge-dependent quantities. Moreover, the study of observables relies on good descriptions of fundamental gauge dependent Green's functions. So, to provide data which serves as a guide to semi-analytical studies, gauge dependent objects have been calculated on the lattice as well.

The configurations $\{U_\alpha\}$ generated according to the method described above do not satisfy any gauge condition in particular. In order to fix the gauge on the lattice we simply have to apply successive gauge transformations to each of the

[12] Due to the stochastic nature of the computation there are always statistical errors associated with it. Estimations of such errors are carried out via the so called jackknife or bootstrap methods, see *e.g.* [170].

link variables generated [13] until it fulfills the gauge condition we want. Let us denote this specific configuration by $U_\mu^\theta(x)$. Proceeding in this way we arrive at a set of link variables, all of which satisfy the gauge condition $\{U_\mu^\theta\}$. Once this is achieved, we must compute any operator R [14], which of course can be gauge dependent, as

$$\langle R \rangle = \frac{1}{N_{\text{conf.}}} \sum_{\alpha}^{N_{\text{conf.}}} R[U_\alpha^\theta]. \tag{2.42}$$

In subsequent chapters we will be particularly interested in lattice data results in Landau gauge. In order to find a link variable $\{U_\mu^\theta\}$ on the lattice satisfying the Landau gauge condition it is enough to consider the quantity

$$F_U[\theta] \equiv \frac{1}{4} \sum_x \sum_{\mu=1}^{4} \text{ReTr}(U_\mu^\theta(x)). \tag{2.43}$$

This is the lattice equivalent of Eq. (2.8) and as a result, all the minima of the functional $F_U[\theta]$ fulfill the Landau gauge condition. Contrary to what occurs in the continuum, on the lattice it is possible to pick up one and only of these minima without much difficulty by using standard algorithms. Due to this, the Gribov problem can be circumvented on the lattice. Unfortunately, this procedure has not an analytical equivalent.

2.3.2 Some results: two- and three-point functions

Simulations of the ghost and gluon propagators have become very precise in the last years [11, 32, 34–37, 142]. As for the gluon two-point function, they indicate, without any reasonable doubt, a decoupling solution in $d = 3$ and $d = 4$ both for YM theory and QCD. As for the ghost dressing function, lattice data shows that this quantity remains finite in the deep IR, and therefore, no enhancement of the ghost propagator is found, see Fig. 2.3. In $d = 2$ dimensions lattice result display a scaling solution along with an enhanced ghost propagator [36, 50]. Regarding three-point functions in pure YM-theory, the coupling constant, which can be extracted from them, takes moderate values for the whole range of momenta, including the deep IR, where typically its value slowly decreases towards zero [29, 32, 55, 56]. This may be observed in Fig. 2.4. In that plot we see $\alpha_S(q^2)$, which normally is referred to as the coupling as well, as a function of momentum. This quantity is related to the expansion parameter of a perturbative series, presented in Section 1.5.4, in the following way

$$\lambda(q^2) = \frac{N g^2(q^2)}{16\pi^2} = \frac{N \alpha_S(q^2)}{4\pi}. \tag{2.44}$$

In Fig. 2.4 the Taylor scheme was the one used to define $\alpha_S(q^2)$. In this renormalization scheme, this quantity ends up being expressed simply in terms of the

[13] A gauge transformation on the link variables reads

$$U_\mu(x) \to U_\mu^U(x) = U(x) U_\mu(x) U^\dagger(x + a\hat{\mu}), \tag{2.41}$$

where $U(x) \in SU(N)$.

[14] With operator we simply refer to a functional of fields.

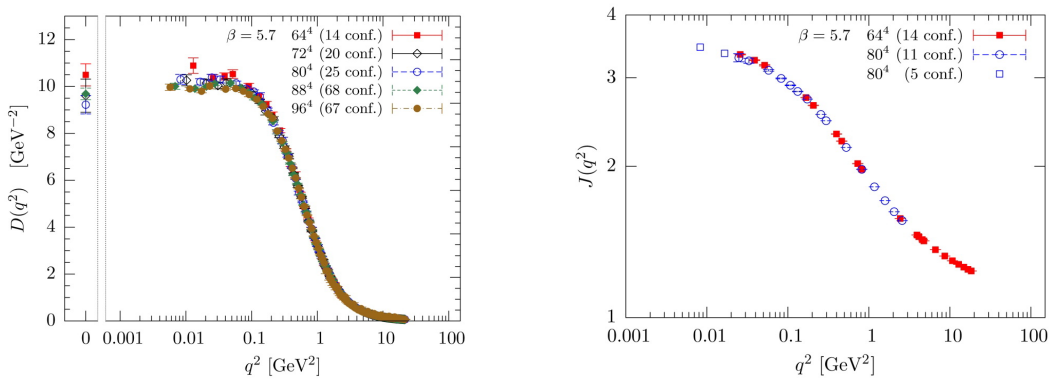

Figure 2.3: Lattice gluon propagator (left) and ghost dressing function (right) for SU(3) pure YM theory in Landau gauge. Figures extracted from [32]. In that reference $J(q^2)$ refers to the ghost dressing function. In this manuscript, such a quantity will be designated by $F(q^2)$.

gluon and ghost dressing functions as

$$\alpha_S(q^2) = \frac{g_0^2}{4\pi} D(q^2) F^2(q^2), \tag{2.45}$$

where g_0 is the renormalized coupling evaluated at the renormalization scale μ_0. D and F refer to the gluon and ghost dressing functions, respectively. It is clear

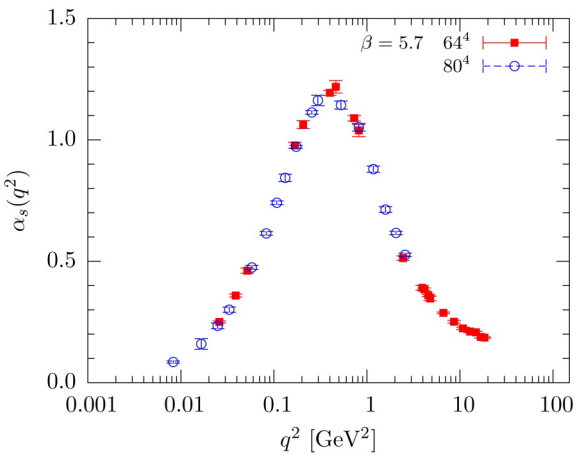

Figure 2.4: Lattice running coupling constant for SU(3) pure YM theory in Landau gauge. Figure extracted from [32]. The configuration of momenta corresponds to the Taylor scheme.

from Fig. 2.4 that, since $\alpha_S(q^2)$ never exceeds 1.3, $\lambda(q^2)$ does not take values larger than 0.3. This behavior was completely unexpected and it is quite remarkable, since, in the absence of any prejudice, it should be taken as an indication of the validity of some sort of perturbative analysis for the whole range of momenta and not for the UV region solely. As was explained at the beginning of this chapter, this not the traditional view on the IR regime YM theory.

As for the quark propagator, see *e.g.* [11, 160, 161], it shows a significant dynamical mass generation [15], *i.e.* even in the cases where the running mass is

[15] This phenomenon can be interpreted as a signature of the spontaneous breaking of chiral

very small at high momentum (of the order of a few MeV), its zero momentum limit is of the order of several hundreds MeV, as can be seen in Fig. 2.5.

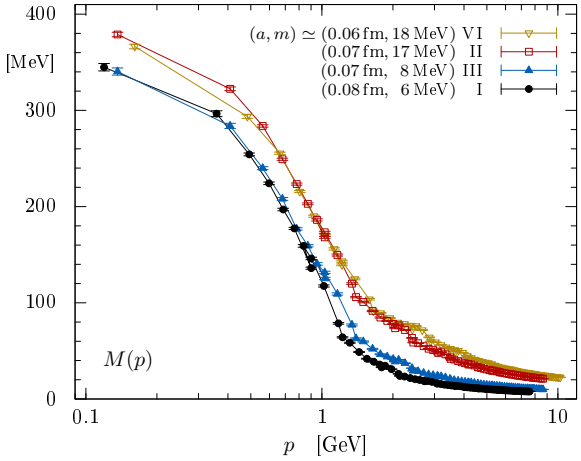

Figure 2.5: Lattice quark mass running for QCD with two degenerate quark flavors $N_f = 2$. The parameter a denotes the lattice spacing and m the bare quark mass. Figure extracted from [11].

The quark-gluon vertex has also been simulated in Refs. [164, 171–173], for instance. From this quantity we can derive the coupling constant associated to the quark sector. Lattice simulations display a coupling which is up to three times larger than in pure YM theory. This difference confirms that, contrary to pure gluodynamics, light quark dynamics is strongly coupled. This was early anticipated in [174], where it was pointed out that in order to have spontaneous chiral symmetry breaking it is necessary to have a sufficiently large quark-gluon coupling in the IR.

symmetry.

Chapter 3

The Curci-Ferrari model

FThe route we will actually take to access the IR of YM theory and QCD is different from the ones described in the preceding chapter. It is motivated by the striking behavior of the lattice gluon propagator, which clearly saturates to a finite value at zero momentum [28–37], as can be seen in Fig. 2.3, which means that the gluon behaves as if it were massive in the infrared. The precise origin for such a mass is a matter of debate. It could be the result of some sort of non-perturbative effect (deriving from DSE or FRG for instance [175, 176]), it could derive from the generation of condensates, see for example [40, 177–179] or could be a consequence of the Gribov ambiguity, see *e.g.* [180–182]. Leaving aside this intriguing issue, the simplest way of incorporating this phenomenon and exploring its consequences is by means of an effective model, whose Lagrangian is given by a gluon mass extension of the standard FP Lagrangian. This is a particular case of the so called Curci-Ferrari (CF) Lagrangians [41].

In this chapter we will introduce the CF Lagrangian in Landau gauge. More precisely, we will present its main properties and will review some important results concerning the IR of YM theory and QCD. In particular, we will address the study of the two-point Green's functions from the CF model in pure YM theory at two-loop order. These results will be extensively used in Chapters 4 and 5.

3.1 The Curci-Ferrari Lagrangian

The Curci-Ferrari model is characterized by the following Lagrangian density in Landau gauge

$$\mathcal{L} = \frac{1}{4}F^a_{\mu\nu}F^a_{\mu\nu} + \partial_\mu \bar{c}^a (D_\mu c)^a + ih^a \partial_\mu A^a_\mu + \frac{m^2}{2} A^a_\mu A^a_\mu + \sum_{i=1}^{N_f} \bar{\psi}_i (D_\mu \gamma_\mu + M_i)\psi_i, \quad (3.1)$$

where the notation is the same as the one used in Section 1.1.1. The masses and the gauge coupling are the bare ones. The only modification in the above Lagrangian with respect to the FP Lagrangian is the massive term for the gluon field. Hereafter, whenever we refer to the CF Lagrangian we will be making reference to the Lagrangian from Eq. (3.1).

The Lagrangian (3.1) is a particular case of a more involved model introduced in the mid-seventies by G. Curci and R. Ferrari as an alternative to the

Higgs mechanism, in order to consistently describe massive vector bosons [41]. The model was later abandoned due to arguments on the unitarity of the theory. However, as discussed in Section 3.1.1, these ideas are not strong enough as to rule out the CF model in the case of a confining theory, such as QCD or YM theory. Consequently, over the last decade the model has been reconsidered in order to access the infrared of YM/QCD [42, 43]. A recent review on the Curci-Ferrari model and its applications to QCD and YM theory can be found in Ref. [156].

It is important to stress that the CF Lagrangian is introduced at the gauge fixed level, as a substitute for the FP Lagrangian, whose use is not fully justified in the infrared. We emphasize that the main motivation behind the inclusion of the gluon mass term comes from the decoupling behavior of the lattice gluon propagator. This term acts as an effective parameter which capture the main features that the FP procedure misses in the infrared. The precise mechanism by which this occurs is still unclear, even though there have been some attempts to unveil it. For instance, in [180] the Gribov ambiguity is resolved by summing over all Gribov copies with a non-flat weight function[1], which lift the degeneracy between equivalent Gribov copies and compensates their multiple counting in the path integral. This procedure leads to a gluon mass term, however, the actual status of this mass is unclear since there is a subtle replica limit to be taken. See also [181].

We end this section by mentioning that a gluonic mass operator has been considered in a series of articles [183–187]. Nonetheless, in contrast to the CF approach, the underlying hypothesis in this case is that the FP action remains unchanged in the IR. The gluonic operator enters into the calculations by being formally added and subtracted to the FP action. This operations allows for a reorganization of standard perturbation theory, avoiding its problematic features in the IR.

3.1.1 Symmetries and renormalizability

The gluon mass term breaks BRST invariance. However, the CF model still enjoys of a modified BRST symmetry given by the transformations

$$\Phi \to \Phi + \delta_{\mathtt{r}}\Phi \tag{3.2}$$

where $\Phi \in \{A, c, \bar{c}, \psi, \bar{\psi}, h\}$ and $\delta_{\mathtt{r}}\Phi = \eta \mathtt{r}\Phi$, with η a space-time independent Grassmann number and

$$\mathtt{r}A^a_\mu = (D_\mu c)^a, \quad \mathtt{r}c^a = -\frac{g}{2} f^{abc} c^b c^c, \quad \mathtt{r}\bar{c}^a = ih^a, \quad \mathtt{r}(ih^a) = m^2 c^a. \tag{3.3}$$

In the massless gluon scenario, $m = 0$, the above symmetry is the standard BRST symmetry. For a non-vanishing gluon mass, the transformations described by Eq. (3.3) can be regarded as a deformation of the standard BRST symmetry. Such deformation modifies the behavior of the theory uniquely for momenta comparable to or smaller than the renormalized gluon mass. In other words, these deformations do not modify the behavior with respect to the FP theory in the UV. These sort of deformations are termed as *soft*. In Landau gauge, the only possible soft deformation of FP, without adding extra field content, is the gluon mass term [156].

[1] a flat weight function corresponds to the one from the Faddeev-Popov procedure

The renormalizability of the theory was proven by means of the symmetries of the theory, more specifically by using the modified BRST symmetry [41, 44–46]. The renormalization factors of the CF model are:

$$A^a_{\mu,B} = \sqrt{Z_A} A_\mu, \quad c^a = \sqrt{Z_c} c^a, \quad \bar{c}^a = \sqrt{Z_c} \bar{c}^a, \quad \psi_B = \sqrt{Z_\psi} \psi,$$
$$g_B = Z_g g, \quad m_B^2 = Z_{m^2} m^2. \tag{3.4}$$

A generalization of the Taylor non-renormalization theorem, introduced in Section 1.5, also applies to the CF model, leading to

$$\sqrt{Z_A} Z_c Z_g \text{ is finite.} \tag{3.5}$$

In addition, the CF model benefits from another non-renormalization theorem, which reads

$$Z_A Z_c Z_{m^2} \text{ is finite.} \tag{3.6}$$

This relation was first conjectured in Refs. [188, 189]. Both non-renormalization theorems were proven in [190] to all orders in perturbation theory.

Unitarity

The space of physical states of the CF model could be determined, in principle, by following a similar procedure to the one described in Section 1.3.1. In this case, however, the kernel of $\mathtt{r}$ is not nilpotent. Thankfully, in the subspace defined by the kernel of $\mathtt{r}^2$, which is also a symmetry of the CF action, the modified BRST symmetry is nilpotent and the construction developed for the FP theory, see Section 1.3.1, can be adapted to the CF model. Nonetheless, this subspace contains negative norm states, as shown in [45, 47]. Therefore, in the case where the gauge field is associated with an observable particle (in the context of weak interactions, for example), the CF model should be discarded as non-unitary. But this is not the case of QCD. Because of confinement, the actual physical space must be made up uniquely by colorless states, the only ones found in nature. It turns out that all the negative norm states found in Refs. [45, 47] are colored. Thus, one cannot discard a possible scenario consistent with both confinement *and* unitarity, where all negative norm states from the CF model are colored. We note as well that, precisely because it admits colored stated, the standard construction of the physical space of the FP theory, discussed in Section 1.3.1, is not yet completely satisfactory.

3.2 Perturbation theory

As a model driven by the decoupling behavior of the lattice gluon propagator, the most straightforward way of testing the validity of the CF model is to evaluate correlation functions and contrast the results with the corresponding lattice simulations. Over the last decade it has been proven that a simple one-loop calculation is enough to reproduce the lattice simulations of several correlation functions in pure YM theory and to some extent in QCD as well.

The use of a perturbative analysis for the whole range of momenta, even in the deep IR, is justified, firstly, by the behavior of the expansion parameter associated to the perturbative series on the lattice, see Fig. 2.4. As mentioned in Section 2.3.2,

Monte-Carlo simulations clearly indicate that this parameter increases towards the IR but only mildly, to become small again in the deep IR. Moreover, as for YM theory, the values of the parameter are compatible with a perturbative analysis for the whole range of momenta. As for QCD, the expansion parameter extracted from the lattice simulations is larger, which signals that the utilization of a perturbative approach is much more delicate than in the pure gauge sector. Part of the analysis to be presented in Chapter 6 intends to elucidate to which extent the perturbative approach, within the CF framework, can be extended to QCD.

Secondly, contrary to the case of the FP theory, the CF model benefits from certain renormalization group trajectories which are Landau pole free. More precisely, at one- and two-loop order of perturbation theory, the CF model, in the so called *infrared safe* (IRS) renormalization scheme, displays two classes of renormalization group trajectories in the space of the dimensionless parameters $(m^2/\mu^2, \lambda)$ [53, 54]. In one of these classes, the trajectories become singular at a finite scale, reaching a Landau pole. In the other class, the trajectories are well defined for the whole range of the renormalization scale and are characterized by a bounded coupling which approaches zero both in the UV and the IR, see Fig. 3.1. On top of this, the coupling corresponding to some of these trajectories remains small for the entirety range of momenta and therefore admits a perturbative treatment.

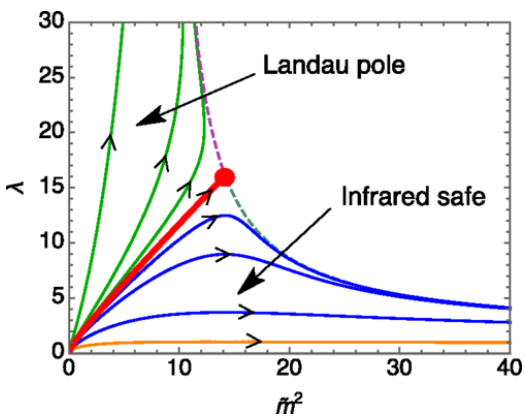

Figure 3.1: Various trajectories of the IRS-flow in the plane $(\tilde{m}^2 \equiv m^2/\mu^2, \lambda)$ in $d = 4$ at one-loop order. Green trajectories end at a Landau pole whereas the blue ones correspond to the infrared safe trajectories. The orange trajectory is the one which best describes the two-point functions for the SU(3) gauge group in the quenched approximation. Plot from Ref. [53]

The Feynman rules of the CF model are identical to the ones provided for the Faddeev-Popov action, with the exception of the gluon propagator, which in the CF model assumes the form shown in Fig. 3.2.

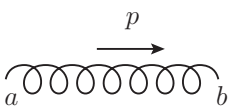

$$= \delta^{ab} \frac{P^{\perp}_{\mu\nu}(p)}{p^2 + m^2}$$

Figure 3.2: Feynman rule for the gluon propagator in the CF model.

As we mentioned above, various Green's functions have been evaluated at one-

loop order within the CF model. These are: the gluon and ghost dressing functions [42, 43], the ghost-antighost-gluon vertex and the three-gluon vertex in pure YM theory [57]. In all cases the agreement with lattice data is very good, with a maximal error between 10 and 20 %. In the presence of quarks, the two-point functions of the theory [58] as well as the quark-gluon vertex [85], the three-gluon and the ghost-antighost-gluon vertex [191] have been evaluated at one-loop order. In this case, the discrepancy with lattice simulations is larger compared to the pure gauge theory. One of the possible explanations for this behavior comes from the differences between the parameters controlling the perturbative series in each case. For example, the results from [192] show that the largest value taken by the expansion parameter of the gauge sector is $\lambda_g \approx 0.12$ for $N_c = 3$, while the expansion parameter associated to the quark-gluon sector reaches a maximum of $\lambda_q \approx 0.68$. These results are a clear indication that use of plain perturbation theory to the unquenched CF model must be done with care. Moreover, we know for certain that certain aspects of QCD, such as the spontaneous breaking of chiral symmetry, are out of reach of any perturbative description, regardless of the model in question. We address this matter in detail in Chapter 6.

The CF model has also been used to investigate the theory at finite temperature and density. As for YM theory and QCD with heavy quarks, the model successfully reproduces various features of the phase diagram. In particular, it can appropriately describe the confinement-deconfinement transition and its associated order parameter [193–199]. More recently, the case with finite chemical potential has also been tackled [200].

Recently, the two-loop evaluation of the two-point functions from pure YM theory was performed, by means of the CF model [54]. The parameters of the model were adjusted to fit the available lattice data, which could be done nicely (see below for a review of the results obtained). In this thesis we aim at extending such two-loop evaluations to other correlation functions, both in the pure gauge theory and in the presence of quarks. In the former case we will extensively use the parameters determined from the fits of the two-point functions. For this reason, we review in some detail the main concepts and results from Ref. [54].

3.3 Two-loop calculation of YM propagators

In the case of pure YM theory there are only two primary fields to which we can associate propagators: the gluon and the ghost fields. In order to compute any of these propagators we need to take into account that the full propagator, denoted in this section generically as $G^{(2)}(p)$, can be written in terms of full 1-PI propagators[2] as shown in Fig. 3.3.

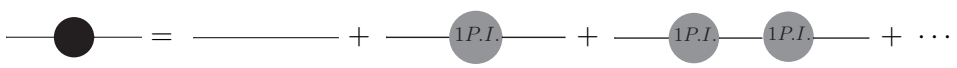

Figure 3.3: Full propagator expressed in terms of the tree-level propagator and 1-P.I. propagators.

By using the notation introduced in Fig. 3.4,

[2] By full 1-PI propagator we mean the sum of all amputated 1-PI contributions.

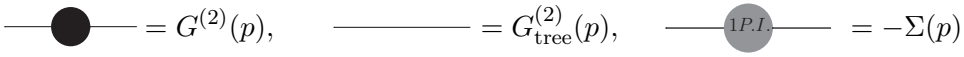

Figure 3.4: Full (left), tree-level (middle) and 1. P.I. propagator (right).

we can write

$$G^{(2)}(p) = G^{(2)}_{\text{tree}}(p) \sum_{n=0}^{\infty} \left(-\Sigma(p) G^{(2)}_{\text{tree}}(p) \right), \tag{3.7}$$

and therefore

$$(G^{(2)}(p))^{-1} = (G^{(2)}_{\text{tree}}(p))^{-1} + \Sigma(p). \tag{3.8}$$

As a consequence, in order to find the propagators we have to sum all 1-PI diagrams which make up $-\Sigma(p)$. In this section we will consider up to two-loop order contributions.

3.3.1 Infrared safe renormalization scheme

The Z-factors from the CF model are presented in Eq. (3.4). Instead of the gauge coupling, we will work with $\lambda = \frac{g^2 N}{16\pi^2}$, since this is the parameter governing the perturbative expansion[3], so we introduce

$$\lambda_B = Z_\lambda \lambda, \tag{3.9}$$

where $Z_\lambda = Z_g^2$. As we explained in Section 1.5, the renormalization factors are determined by imposing the values of two- and three-point functions at a certain scale μ. The renormalization scheme chosen in [54] satisfies

$$G^{-1}(p = \mu, \mu) = m^2 + \mu^2, \quad F(p = \mu, \mu) = 1, \tag{3.10}$$

where we recall that $G(p, \mu)$ and $F(p, \mu)$ refer to the gluon propagator and ghost dressing functions, respectively. The momentum p is external whereas μ refers to the renormalization scale. The two remaining renormalization conditions are given by the extension of the non-renormalization theorems (3.5), (3.6) to the finite parts, *i.e.*

$$\sqrt{Z_\lambda Z_A} Z_c = 1, \quad Z_{m^2} Z_A Z_c = 1. \tag{3.11}$$

These four conditions define the infrared safe scheme described in the preceding section. Once the renormalization factors have been found, the anomalous dimensions can be calculated as $\gamma = d \log Z / d\mu$. Afterwards, the β-functions corresponding to λ and m^2 can also been determined since they can be entirely expressed in terms of the anomalous dimensions γ_A and γ_c. This can be easily proven by introducing the quantities:

$$\gamma_\lambda \equiv \mu \partial_\mu \log(Z_\lambda); \quad \gamma_{m^2} \equiv \mu \partial_\mu \log(Z_{m^2}), \tag{3.12}$$

where we used the notation $\partial_\mu \equiv \frac{\partial}{\partial \mu}$.

[3]The actual expansion parameter is not exactly λ. We will discuss this issue later in this chapter.

Before continuing, we note that Feynman integrals are regularized by means of dimensional regularization [88, 201, 202], *i.e.* by working in $d = 4-2\epsilon$ dimensions, with $\epsilon > 0$. In the end we take $\epsilon \to 0$ and the poles in $1/\epsilon$ appearing in the two-point functions are absorbed into the renormalization factors. In this context, it is convenient to work with a dimensionless expansion parameter by explicitly writing the dimension as $\lambda\mu^{2\epsilon}$, where λ is now a dimensionless quantity. Taking into account that the bare gauge coupling is independent of the renormalization scale we are allowed to write

$$\mu\partial_\mu \log \lambda_B = \mu\partial_\mu \log\Big(Z_\lambda \lambda \mu^{2\epsilon}\Big) = \mu\partial_\mu \log Z_\lambda + \mu\partial_\mu \log\lambda + 2\epsilon = 0. \tag{3.13}$$

By using that $\beta_\lambda = \mu\frac{\partial\lambda}{\partial\mu}$ and $\epsilon \to 0$ we get

$$\gamma_\lambda = -\frac{\beta_\lambda}{\lambda}. \tag{3.14}$$

In addition, from $\mu\partial_\mu \log(\sqrt{Z_\lambda Z_A} Z_c) = 0$, we infer that

$$\gamma_\lambda = -\left(2\gamma_c + \gamma_A\right). \tag{3.15}$$

Finally, inserting this identity into Eq. (3.14) we obtain

$$\beta_\lambda = \lambda\left(2\gamma_c + \gamma_A\right). \tag{3.16}$$

In a similar manner, by using that $\mu\partial_\mu \log m_B^2 = 0$ and $\mu\partial_\mu \log(Z_{m^2} Z_A Z_c) = 0$ we arrive at

$$\beta_{m^2} = m^2\left(\gamma_A + \gamma_c\right). \tag{3.17}$$

3.3.2 Renormalization group

In the perturbative expansions it is common to find terms of the from $(\lambda(\mu))^n \ln(p^2/\mu^2)^n$, where n denotes the loop order. For values of p^2 large enough we can produce terms such that $\ln p^2/\mu^2 \sim 1/\lambda(\mu)$. Therefore, these terms are of the same order of magnitude to all orders in perturbation theory, which is inconsistent with the perturbative treatment. As we explained in Section 1.5.3, this problematic behavior can be avoided by choosing a renormalization scale such that $\mu(p) \sim p$. In particular, the authors of [54] used $\mu = p$. However, in order to compare the results with lattice simulations one needs to use a renormalization scale at a fixed value μ_0. The gluon propagator and the ghost dressing function evaluated at the fix scale μ_0 are related to the same quantities evaluated at $\mu = p$ via the Callan-Symanzik equation, whose solution is given by Eq. (1.142):

$$G(p,\mu_0) = z_A(p,\mu_0)G(p,p) = \frac{z_A(p)}{p^2 + m^2(p)}, \tag{3.18}$$

$$F(p,\mu_0) = z_c(p,\mu_0)F(p,p) = z_c(p,\mu_0), \tag{3.19}$$

where we used Eq. (3.10). In the IRS scheme, $z_A(\mu,\mu_0)$ and $z_c(\mu,\mu_0)$, defined via Eq. (1.143), acquire a very simple form, written exclusively in terms of $\lambda(\mu)$ and $m^2(\mu)$. To derive such expressions, let us start by noticing that another way of

writing the identities given by Eqs. (3.15) and (3.17), up to a term proportional to ϵ, is

$$\gamma_A = 2\frac{\beta_{m^2}}{m^2} - \frac{\beta_\lambda}{\lambda}, \quad \gamma_c = \frac{\beta_\lambda}{\lambda} - \frac{\beta_{m^2}}{m^2}. \tag{3.20}$$

From these equations we have

$$\log z_A(\mu,\mu_0) = \int_{\mu_0}^{\mu} \frac{d\mu'}{\mu'}\left(2\frac{\beta_{m^2}}{m^2} - \frac{\beta_\lambda}{\lambda}\right) = \log\left(\frac{m^4(\mu)\lambda(\mu_0)}{m^4(\mu_0)\lambda(\mu)}\right), \tag{3.21}$$

$$\log z_c(\mu,\mu_0) = \int_{\mu_0}^{\mu} \frac{d\mu'}{\mu'}\left(\frac{\beta_\lambda}{\lambda} - \frac{\beta_{m^2}}{m^2}\right) = \log\left(\frac{\lambda(\mu)m^2(\mu_0)}{\lambda(\mu_0)m^2(\mu)}\right). \tag{3.22}$$

Therefore,

$$z_A(\mu,\mu_0) = \frac{\lambda(\mu_0)}{\lambda(\mu)}\frac{m^4(\mu)}{m^4(\mu_0)}, \quad z_c(\mu,\mu_0) = \frac{\lambda(\mu)}{\lambda(\mu_0)}\frac{m^2(\mu_0)}{m^2(\mu)}. \tag{3.23}$$

Plugging these results into Eq. (3.18) we finally obtain

$$G(p,\mu_0) = \frac{\lambda(\mu_0)}{\lambda(p)}\frac{m^4(p)}{m^4(\mu_0)}\frac{1}{p^2+m^2(p)}, \tag{3.24}$$

$$F(p,\mu_0) = \frac{\lambda(p)}{\lambda(\mu_0)}\frac{m^2(\mu_0)}{m^2(p)}. \tag{3.25}$$

3.3.3 Fitting procedure

In [54], the ghost and gluon two-point functions were fitted to lattice data from Refs. [203, 204] for the SU(3) gauge group and from Ref. [29] in the SU(2) case.

With the $\beta-$functions determined from Eqs. (3.15) and (3.17), the running functions $\lambda(\mu)$ and $m(\mu)$ can be found, once the initial conditions $\lambda_0 = \lambda(\mu_0)$ and $m_0 = m(\mu_0))$ have been set. Accordingly, the gluon propagator and ghost dressing function can be fully determined through Eq. (3.24).

As a result, in order to carry out the fit, in [54], the authors explored the corresponding error for G and F, for a large set of values of the parameters λ_0 and m_0, with $\mu_0 = 1$ GeV. The error was defined in such a way that it averages the relative and absolute error:

$$\chi_X^2 = \sum_{i=1}^{N_{\text{latt.}}} \frac{X_{\text{latt.}}^{-2}(\mu_0) + X_{\text{latt.}}^{-2}(p_i)}{2N_{\text{latt.}}}\left(X_{\text{latt.}}(p_i) - \mathcal{N}_X X_{\text{CF}}(p_i)\right)^2, \tag{3.26}$$

where the sum runs over the lattice points and $X \in \{F, G\}$. The terms $X_{\text{latt.}}$ and X_{CF} refer to the quantity X on the lattice and the CF output, respectively. The normalization constant $\mathcal{N}_X$, between the CF evaluation and lattice data is fixed in such a way that it minimizes the error, *i.e.*

$$\mathcal{N}_X = \frac{\sum_{i=1}^{N_{\text{latt.}}}\left(X_{\text{latt.}}^{-2}(\mu_0) + X_{\text{latt.}}^{-2}(p_i)\right)X_{\text{latt.}}(p_i)X_{\text{CF}}(p_i)}{\sum_{i=1}^{N_{\text{latt.}}}\left(X_{\text{latt.}}^{-2}(\mu_0) + X_{\text{latt.}}^{-2}(p_i)\right)X_{\text{CF}}^2(p_i)}. \tag{3.27}$$

Finally, the values λ_0 and m_0 to perform the fit were chosen so as to minimize the joint error

$$\chi^2 = \frac{1}{2}\left(\chi_{AA}^2 + \chi_{\bar{c}c}^2\right) \tag{3.28}$$

3.3.4 Results

The results for the gluon propagator and ghost dressing function are shown in Figs. 3.5 and 3.6 for the SU(3) and SU(2) gauge groups,respectively. In both cases the CF model features a very good agreement with lattice data. Moreover, such agreement improves when two-loop corrections are included, which is coherent with the perturbative analysis we have implemented.

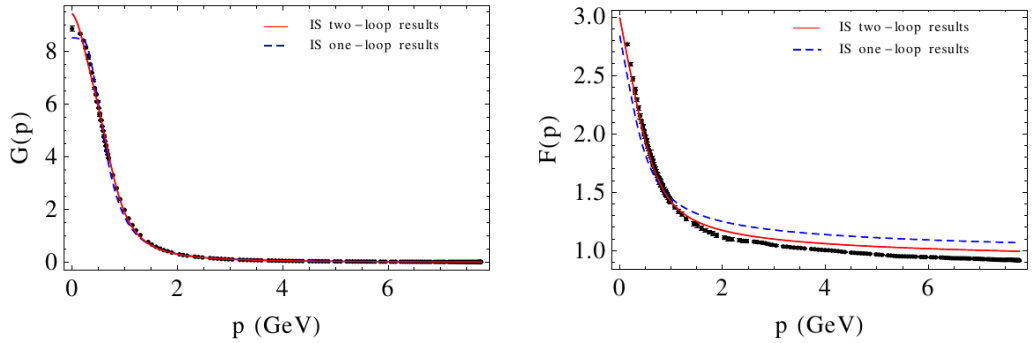

Figure 3.5: One- and two-loop gluon propagator (left) and ghost dressing function (right) from the CF model for the SU(3) gauge group as compared to lattice data from Refs. [203] and [204], respectively.

Group	$N=2$			$N=3$		
Params.	λ_0	m_0 (MeV)	χ	λ_0	m_0 (MeV)	χ
1-loop	0.34	450	10%	0.24	350	7%
2-loop	0.38	390	6%	0.27	330	4%

Table 3.1: Parameters in the IS scheme, as obtained from fitting the lattice results for the two-point functions, together with the corresponding error.

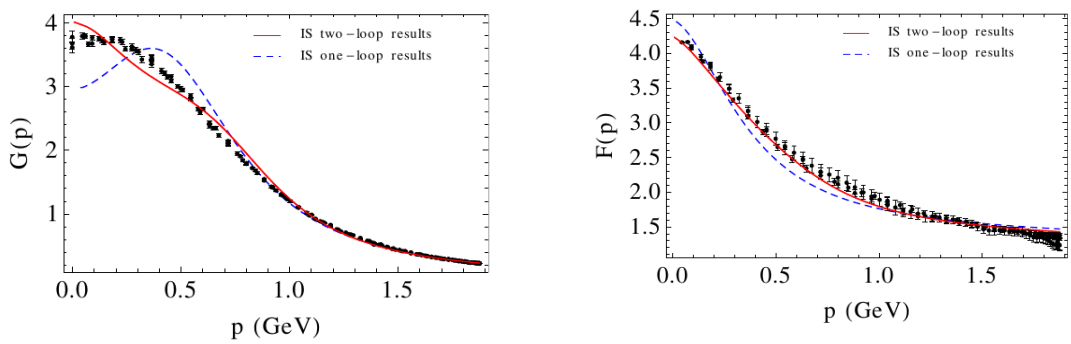

Figure 3.6: One- and two-loop gluon propagator (left) and ghost dressing function (right) from the CF model for the SU(2) gauge group as compared to lattice data from Ref. [29].

This is also confirmed by the corresponding error χ, displayed in Table 3.1. We note that the SU(3) case displays smaller errors than the SU(2) case. As we will see in subsequent chapters, such error difference is also verified by other Green's

functions in pure YM theory, and is always larger for the SU(2) gauge group. This phenomenon can be understood by looking at the expansion parameter of the perturbative series for each group. It turns out that this is larger for the SU(2) case, as can be seen in Fig. 3.7. As for SU(3), at two-loop order, λ is bounded by approximately 0.6 whereas for SU(2) that parameter overpasses 0.8 in some region of the flow, which makes questionable the use of a perturbative analysis there. Nonetheless, it is important to bear in mind the following parameter as well:

$$\tilde{\lambda} = \lambda \frac{\mu^2}{\mu^2 + m^2}, \tag{3.29}$$

which takes into account that most perturbative corrections including gluon lines are suppressed in the IR by at least one factor of order μ^2/m^2 (with $\mu^2 \ll m^2$). Which of the two expansion parameters λ or $\tilde{\lambda}$ governs the perturbative expansions is not fully clear and most likely depends on the renormalization scheme chosen.

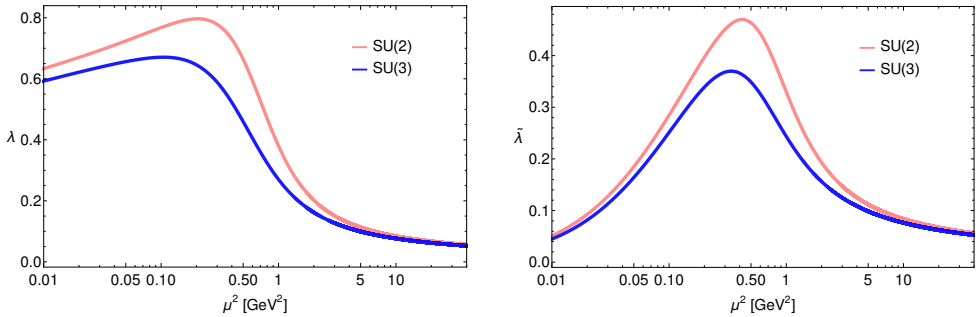

Figure 3.7: Two-loop running of the expansion parameters $\lambda(\mu^2)$ (left) and $\tilde{\lambda}(\mu^2)$ (right) in the IRS scheme for the gauge groups SU(2) and SU(3).

3.3.5 Scheme dependence

A complementary way of testing the perturbative CF approach in the evaluation of any quantity is to measure the scheme dependence of the result. At the exact level, the two-point functions are scheme independent, up to an overall normalization factor. However, as we are implementing a perturbative, and therefore an approximate, calculation, some scheme dependence is expected. Nonetheless, if the perturbative expansion is under control, the two-loop evaluation should be more accurate and, as such, should be less sensitive to variations in the renormalization scheme than the one-loop evaluation.

Vanishing momentum scheme

For the purpose of testing this dependence, in [54] the gluon and ghost two-point functions were computed by using the vanishing momentum scheme (VM) as well. Such scheme is characterized by the following renormalization conditions

$$G^{-1}(p=\mu) = m^2 + \mu^2, \;\; F(p=\mu) = 1, \;\; G^{-1}(p=0) = m^2 \text{ and } \sqrt{Z_\lambda Z_A} Z_c = 1. \tag{3.30}$$

This scheme features a Landau pole in the IR. A possible way of circumventing this problem is by choosing $\mu = \sqrt{p^2 + \alpha m_0^2}$ rather than $\mu = p$, with α a μ-independent

constant. Such election freezes the running at m_0, and avoids reaching the Landau pole. Similarly to the IRS scheme, in the VM scheme the β-functions can be expressed in terms of the anomalous dimensions of the fields. Since the condition $\sqrt{Z_\lambda Z_A} Z_c = 1$ is preserved the condition Eq. (3.15) also holds. Besides, as in the IRS scheme, from $\mu\partial_\mu m_B^2 = 0$ stems

$$\gamma_{m^2} = -\frac{\beta_{m^2}}{m^2}. \tag{3.31}$$

In addition, by assuming that the gluon propagator is analytic at low momentum and owing to both the pseudo-BRST symmetry of the CF model and the equation of motion of the antighost field, one can show that (see [43] for details)

$$G_B^{-1}(0) F_B^{-1}(0) = m_B^2, \tag{3.32}$$

which is equivalent to

$$Z_A^{-1} G^{-1}(0) F_B^{-1}(0) = Z_{m^2} m^2. \tag{3.33}$$

Then, by using that in VM $G^{-1}(0) = m^2$ and by taking logarithm at each side of the equation we get

$$\log Z_A^{-1} + \log F_B^{-1}(0) = \log Z_{m^2}. \tag{3.34}$$

As bare quantities do not depend on the renormalization scale μ, we have

$$\mu\partial_\mu(\log Z_A^{-1}) = -\gamma_A = \gamma_{m^2}. \tag{3.35}$$

By plugging this identity into Eq. (3.31) we obtain

$$\beta_{m^2} = m^2 \gamma_A. \tag{3.36}$$

Therefore, from this equation and from Eq. (3.15) we can express the γ-functions for the fields as

$$\gamma_A = \frac{\beta_{m^2}}{m^2}, \quad \gamma_c = \frac{1}{2}\left(\frac{\beta_\lambda}{\lambda} - \frac{\beta_{m^2}}{m^2}\right). \tag{3.37}$$

Consequently, by proceeding in the same manner as for the IRS scheme we get

$$z_A(\mu) = \frac{m^2(\mu)}{m^2(\mu_0)}, \quad z_c(\mu) = \sqrt{\frac{\lambda(\mu)}{\lambda(\mu_0)} \frac{m^2(\mu_0)}{m^2(\mu)}}. \tag{3.38}$$

Results

In order to estimate the scheme dependence, the authors of Ref. [54] introduce the quantity

$$\mathcal{H}(\alpha) = \sqrt{\frac{1}{N_{\text{latt.}}} \sum_{i=1}^{N_{\text{latt.}}} \frac{(X_{\text{VM}(\alpha)}(p_i) - X_{\text{IS}}(p_i))^2}{X_{\text{IS}}^2(p_i)}}, \tag{3.39}$$

with $X \in \{F, G\}$ and $N_{\text{latt.}}$ the number of lattice points. In Table 3.2 are presented the values of $\mathcal{H}$ for the gluon and ghost dressing functions using one- and two-loop results. The results are consistent with a valid perturbative expansion, since two-loop corrections are less sensitive to the renormalization scheme than one-loop calculations.

Quantity	Gluon dressing		Ghost dressing	
Order	One-loop	Two-loop	One-loop	Two-loop
VM $\alpha = 1$	0.03	0.02	0.06	0.05
VM $\alpha = 2$	0.06	0.03	0.08	0.03

Table 3.2: Estimate of the scheme dependence $\mathcal{H}$ between the IRS scheme and two VM schemes in SU(3) for the gluon and ghost dressing functions.

Chapter 4

Ghost-antighost-gluon vertex

In this chapter we present the two-loop evaluation of the ghost-antighost-gluon vertex from the Curci-Ferrari model in pure YM theory. We work in four dimensions and in Landau gauge for the gauge groups SU(3) and SU(2). The results presented in this chapter were published in [59]. As anticipated in the preceding chapter, the goal of this computation is to provide a further test on the perturbative CF model regarding its capability to describe the infrared of the pure gauge theory. Furthermore, this evaluation is a useful tool to test how controlled the perturbative series is.

The evaluation of the ghost-antighost-gluon vertex at two-loop order is as a *pure prediction* of the CF model. This is because the running functions of the only two parameters of the model, $m(\mu)$ and $\lambda(\mu)$, were determined in [54], when fitting the two-point functions to lattice data, see Section 3.3. In order to keep the calculation manageable, we perform the evaluation in the particular kinematical configuration where the momentum of the external gluon vanishes.

The ghost-antighost-gluon vertex has been studied by means of functional methods [18, 124, 205–210] and on the lattice [29, 55, 159, 211, 212]. As already stated before, the computation to be presented below is an extension of a previous calculation at one-loop order [57].

4.1 Generalities

To begin with, let us define the bare ghost-antighost-gluon vertex as

$$-V_\mu^{abc}(k,\ell) \equiv$$

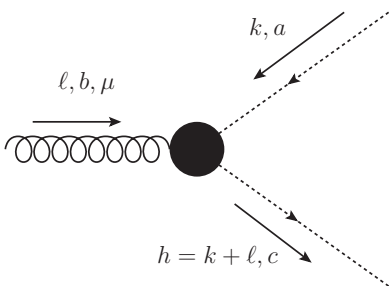

$$, \tag{4.1}$$

with k, ℓ and $h = k + \ell$, the (incoming) ghost, (incoming) gluon and (outgoing) antighost momenta, respectively. Because of Lorentz symmetry, the bare vertex

has in principle two tensor components,

$$V_\mu^{abc}(k,\ell) = k_\mu V^{abc}(k^2, k\cdot\ell, \ell^2) + \ell_\mu W^{abc}(k^2, k\cdot\ell, \ell^2). \tag{4.2}$$

However, since in Landau gauge, $\partial_\mu A_\mu = 0$, only transverse gluons are allowed, the only component of $V_\mu^{abc}(k,\ell)$ which contributes to connected correlation functions is

$$\begin{aligned} V_{\perp,\mu}^{abc}(k,\ell) &\equiv P_{\mu\nu}^{\perp}(\ell)\, V_\mu^{abc}(k,\ell) \\ &= P_{\mu\nu}^{\perp}(\ell)\, k_\nu V^{abc}(k^2, k\cdot\ell, \ell^2). \end{aligned} \tag{4.3}$$

Moreover, because the CF Lagrangian benefits from the symmetry

$$c^a \to \bar{c}^a, \quad \bar{c}^a \to -c^a, \quad ih^a \to ih^a - f^{abc}\bar{c}^b c^c, \tag{4.4}$$

in the absence of sources we have

$$\langle c^a(k) A_\mu^b(\ell) \bar{c}^c(-h)\rangle = -\langle \bar{c}^a(k) A_\mu^b(\ell') c^c(k)\rangle = \langle c^c(-h) A_\mu^b(\ell') \bar{c}^a(k)\rangle, \tag{4.5}$$

where in the last step we used that the ghost and antighost fields are Grassmannian. The argument of the fields refer to the incoming momenta in all cases. Therefore $\ell' = -h + k = -\ell$. This implies that $V_{\perp,\mu}^{abc}(k,\ell) = V_{\perp,\mu}^{cba}(-h,-\ell)$, which leads to

$$V^{abc}(k^2, k\cdot\ell, \ell^2) = -V^{cba}(h^2, h\cdot\ell, \ell^2)\,. \tag{4.6}$$

We are interested in the specific kinematical configuration where the momentum of the external gluon vanishes. Consequently, we define

$$V^{abc}(k^2) \equiv V^{abc}(k^2, 0, 0). \tag{4.7}$$

This quantity is antisymmetric in the indices a and c. Consequently, $V^{abc}(k^2)$ must be proportional to the completely antisymmetric tensor f^{abc}, since the other possible tensor in the color indices is symmetric under the transformation $a \leftrightarrow c$[1]. Then, we write

$$V^{abc}(k^2) \equiv i g_B \mu^\epsilon f^{abc} v_B(k^2). \tag{4.8}$$

We will refer to $v_B(k^2)$ as the bare vertex function. We are working in $d = 4 - 2\epsilon$ dimensions, with $\epsilon > 0$, and with the dimensionless bare gauge coupling g_B. The term μ^ϵ accounts for the dimensions we are missing because of working with the dimensionless coupling.

The scalar function $v_B(k^2)$ renormalizes as the vertex $V^{abc}(k^2)$. Therefore, according to Eq. (1.135), we have

$$v(k^2) = \sqrt{Z_A Z_\lambda}\, Z_c v_B(k^2). \tag{4.9}$$

We will compute this quantity in the IRS and VM schemes. In both schemes the relation $\sqrt{Z_A Z_\lambda} Z_c = 1$ holds. Accordingly,

$$v(k^2) = v_B(k^2). \tag{4.10}$$

As a consequence, the bare vertex is finite and it is already renormalized, as long as it is expressed in terms of the renormalized mass and coupling. Moreover, this implies that the ghost-antighost-gluon vertex is invariant under the renormalization group flow, i.e. it is invariant under changes in the renormalization scale μ.

[1] More generally, d^{abc} can be ruled out by invoking charge conjugation invariance [213].

4.2 Two-loop evaluation

4.2.1 Diagrams

It is convenient to express the two-loop bare vertex as

$$v(k^2) = 1 + \lambda_B\, v_1(k^2, m_B^2) + \lambda_B^2\, v_2(k^2, m_B^2)\,, \tag{4.11}$$

where $v_n(k^2, m_B^2)$ designates the sum of n-loop 1-PI Feynman diagrams. Since one- and two-loop diagrams are proportional to g_B^3 and g_B^5, respectively, and because we have factored out a g_B in the definition Eq. (4.8), by writing the vertex in the form (4.11), we have absorbed the remaining powers of the type g_B^{2n} in the coefficients λ_B^n. Likewise, the latter factor also absorbs the color factors, which are given by N^n. Furthermore, as it is customary, see for example Ref. [214] we have absorbed a factor $\mu^{2n\epsilon}(16\pi^2)^n$ in $v_n(k^2, m_B^2)$. As a consequence, to be coherent with this convention, whenever we compute a Feynman diagram, the d-dimensional momentum integrals associated with it are replaced by

$$\int \frac{d^d p}{(2\pi)^d} \to \int_p \equiv 16\pi^2 \mu^{2\epsilon} \int \frac{d^d p}{(2\pi)^d}\,. \tag{4.12}$$

We point out here that even tough this convention introduces factors of the type $\mu^{2\epsilon}$ in $v(k^2)$, at the end they all recombine to yield a μ-independent expression.

One-loop Feynman graphs, which make up $v_1(k^2, m_B^2)$ have already been computed in Ref. [57]. We can make use of such diagrams to organize two-loop diagrams by classifying them according to three categories: i) those corresponding to one-loop self-energy corrections to one-loop diagrams[2], ii) those corresponding to one loop vertex corrections to one-loop diagrams and iii) the rest. These diagrams are collected in Appendix A. This classification is also useful to write down sum of Feynman graphs in a simplified form. Let us see this idea at work with an example.

Let us consider the sum of the three diagrams displayed in Fig. 4.1, which can be viewed as a one-loop gluon self-energy inside a one-loop diagram.

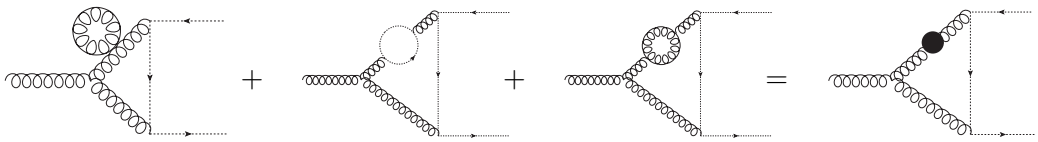

Figure 4.1: A sum of diagrams which can be interpreted as a one-loop gluon self-energy insertion in a one-loop diagram.

The sum from Fig. 4.1 can be written in terms of the one-loop correction to the gluon propagator, shown in the figure below. By applying the Feynman rules

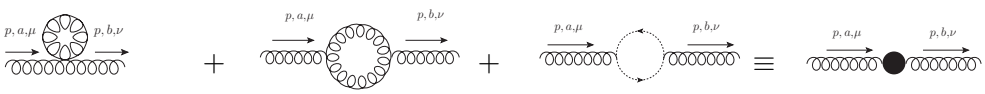

Figure 4.2: Feynman diagrams which contribute to the one-loop gluon self-energy.

[2]Self-energy refer to loop corrections to the a certain propagator.

and after simplification, the one-loop correction to the gluon propagator is

$$
\begin{aligned}
&= Ng^2\delta^{ab}\Bigg\{-\int_q \frac{q_\mu(q-p)_\nu}{(p-q)^2q^2} \\
&+\frac{1}{2}\int_q \left[(2q+p)_\mu\delta_{\rho\sigma}+2p_\sigma\delta_{\mu\rho}-2p_\rho\delta_{\mu\sigma}\right]\left[(2q+p)_\nu\delta_{\epsilon\eta}+2p_\epsilon\delta_{\nu\eta}-2p_\eta\delta_{\nu\epsilon}\right] \\
&\times\frac{P^\perp_{\sigma\epsilon}(p+q)P^\perp_{\eta\rho}(q)}{((p+q)^2+m^2)(q^2+m^2)}-\int_q\frac{q_\mu(q-p)_\nu}{(p-q)^2q^2}\Bigg\}\equiv Ng^2\delta^{ab}\,\Pi^{\mu\nu}(p)
\end{aligned}
\tag{4.13}
$$

This result can be exploited to compute the sum from Fig. 4.1 by means of the diagram from Fig. 4.3. Accordingly, by applying the Feynman rules to Fig. 4.1,

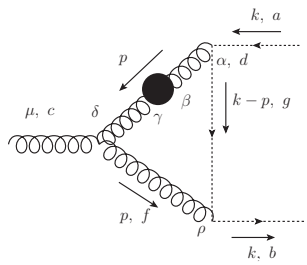

Figure 4.3: Feynman diagram corresponding to the sum from Fig. 4.1. The indices are the ones used for applying the Feynman rules.

we have

$$
2iNg^5 f^{efc}f^{gbf}f^{agd}\delta^{ed}\int_p \frac{p_\mu k_\rho(k-p)_\alpha P^\perp_{\rho\gamma}(p)P^\perp_{\alpha\beta}(p)\Pi_{\gamma\beta}(p)}{(k-p)^2(p^2+m^2)^3} \tag{4.14}
$$

The color factor is: $f^{efc}f^{gbf}f^{agd}\delta^{ed}=f^{dfc}f^{gbf}f^{agd}=f^{cdf}f^{bfg}f^{agd}$, and

$$
f^{cdf}f^{bfg}f^{agd}=i^3\mathrm{Tr}(T^cT^bT^a)=-\frac{N}{2}f^{abc}, \tag{4.15}
$$

where we used that the structure constants of the gauge group satisfy

$$
f^{abc}=i(T^a)^{bc}, \tag{4.16}
$$

where T^a are the generators of SU(N) in the adjoint representation.[3] Therefore, Eq. (4.14) transforms into

$$
-iN^2g^5f^{abc}\int_p \frac{p_\mu k_\rho k_\alpha P^\perp_{\rho\gamma}(p)P^\perp_{\alpha\beta}(p)\Pi_{\gamma\beta}(p)}{(k-p)^2(p^2+m^2)^3}, \tag{4.19}
$$

[3]The same calculation can be carried out graphically, as

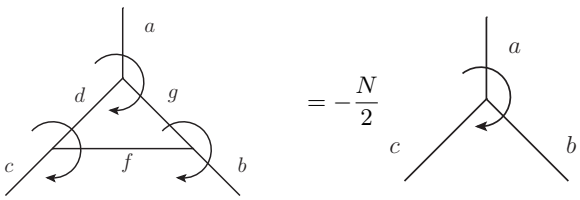

$$= -\frac{N}{2}f^{abc}, \tag{4.17}$$

where we have carried out some contractions. We can see that the one-loop gluon self energy is in between two transverse projectors. As a consequence, the only part of $\Pi_{\mu\nu}(p)$ which contributes to the diagram is $\Pi^{\perp}(p)P^{\perp}_{\mu\nu}(p)$. Finally, the diagram can be written as:

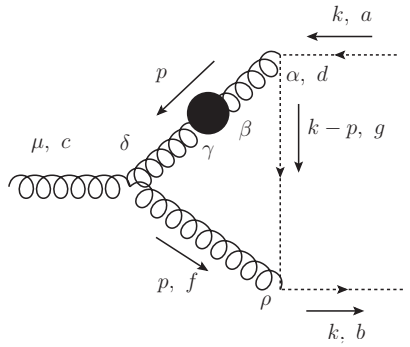

$$= -iN^2 g^5 f^{abc} \int_p \frac{p_\mu \; k \cdot P^{\perp}(p) \cdot k \; \Pi^{\perp}(p)}{(k-p)^2 (p^2+m^2)^3}. \tag{4.20}$$

Inside the category iii) we have four non-planar diagrams, all of them featuring the topology shown in Fig. 4.4. For a given diagram, solid lines must be appropriately replaced by gluon or ghost lines. Thanks to the color factor all of such diagrams vanish. According to the indices from Fig. 4.4 the color factor is proportional to

$$f^{ajd} f^{dhe} f^{egc} f^{jig} f^{ibh} = \mathrm{Tr}\Big(T^a T^h T^c T^i\Big) f^{ibh} = 0, \tag{4.21}$$

where in the last step we used that the contraction of a symmetric tensor in the indices i and h (because of the cyclic property of the trace) with the completely antisymmetric tensor f^{ibh} is zero.

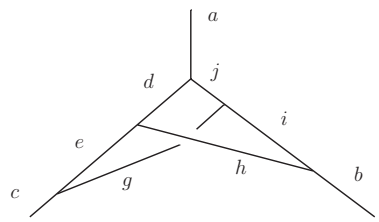

Figure 4.4: The only type of non-planar topology contributing to $v_2(k^2, m_B^2)$

4.2.2 Reduction to master integrals

Since we are interested in computing $v(k^2)$ in order to compare the result with lattice simulations, the first step to follow after we have written the mathematical

where we used that

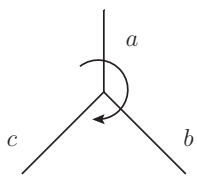

$$\equiv f^{abc}. \tag{4.18}$$

expressions associated to each diagram is to project them in the k_μ direction, see Eq. (4.3). Since we have only one external Lorentz index, μ, and only one external momentum, k, two loop Feynman integrals can be decomposed as sum of three different type of integrals:

$$I_{p,\mu} = \int_p \int_q A(m^2, k^2, p^2, q^2, k\cdot p, k\cdot q, p\cdot q) p_\mu, \tag{4.22}$$

$$I_{q,\mu} = \int_p \int_q A(m^2, k^2, p^2, q^2, k\cdot p, k\cdot q, p\cdot q) q_\mu, \tag{4.23}$$

$$I_{\mu} = \int_p \int_q A(m^2, k^2, p^2, q^2, k\cdot p, k\cdot q, p\cdot q) k_\mu. \tag{4.24}$$

The last type of integral is already projected. As for the first and second integral we can make use of

$$\int_q \int_p A(m^2, k^2, p^2, q^2, k\cdot p, k\cdot q, p\cdot q) q_\mu = I_1 k_\mu, \tag{4.25}$$

$$\int_q \int_p A(m^2, k^2, p^2, q^2, k\cdot p, k\cdot q, p\cdot q) p_\mu = I_2 k_\mu \tag{4.26}$$

where I_1 and I_2 are the projections we are looking for. They can be easily found by projecting along k_μ

$$I_1 = \frac{1}{k^2} \int_q \int_p A(m^2, k^2, p^2, q^2, k\cdot p, k\cdot q, p\cdot q)(k\cdot q), \tag{4.27}$$

$$I_2 = \frac{1}{k^2} \int_q \int_p A(m^2, k^2, p^2, q^2, k\cdot p, k\cdot q, p\cdot q)(k\cdot p). \tag{4.28}$$

As a second step we perform the following operations

$$\begin{aligned} G_m(q)G_0(q) &= \frac{1}{m^2}\left(G_0(q) - G_m(q)\right), \\ G_m(q)G_0(q)^{-1} &= 1 - m^2 G_m(q) \end{aligned} \tag{4.29}$$

where

$$G_m(p) \equiv \frac{1}{p^2 + m^2}, \tag{4.30}$$

since, as it will be clear later in this section, it is not convenient to have such products in $A(m^2, k^2, p^2, q^2, k\cdot p, k\cdot q, p\cdot q)$. Therefore, after these operations have been carried out on the projected Feynman integrals, each Feynman graph can be expressed as the sum of integrals of the form

$$\begin{aligned} &\tilde{I}_{m_1 m_2 m_3 m_4 m_5}(n_1, n_2, n_3, n_4, n_5, n_6, n_7, n_8) \equiv \int_p \int_q G^{n_1}_{m_1}(p) G^{n_2}_{m_2}(q) \\ &\times G^{n_3}_{m_3}(k-p) G^{n_4}_{m_4}(k-p) G^{n_5}_{m_5}(p-q)(k\cdot q)^{n_6}(k\cdot p)^{n_7}(p\cdot l)^{n_8}. \end{aligned} \tag{4.31}$$

The third step in the calculation consists in reducing these sort of terms to the so called self-energy *master integrals*.

One-loop master integrals are:

$$\begin{aligned} A_m &\equiv \int_p G_m(p) \\ B_{m_1 m_2}(k^2) &\equiv \int_p G_{m_1}(p) G_{m_2}(p+k), \end{aligned} \tag{4.32}$$

whereas two-loop master integrals are given by:

$$
\begin{aligned}
S_{m_1m_2m_3}(k^2) &\equiv \int_p\int_q G_{m_1}(p)G_{m_2}(p-q)G_{m_3}(k-q),\\
I_{m_1m_2m_3} &\equiv S_{m_1m_2m_3}(0),\\
U_{m_1m_2m_3m_4}(k^2) &\equiv \int_p\int_q G_{m_1}(p)G_{m_2}(p-k)G_{m_3}(k-q)G_{m_4}(p-q),\\
M_{m_1m_2m_3m_4m_5}(k^2) &\equiv \int_p\int_q G_{m_1}(p)G_{m_2}(q)G_{m_3}(p-k)G_{m_4}(k-q)G_{m_5}(p-q),
\end{aligned}
\tag{4.33}
$$

where we have kept a general notation in relation to the masses. In the calculation presented in this chapter the mass only admits two values, zero and the gluon mass, m.

The topology of the master integrals is displayed in Fig. 4.5. The advantage of

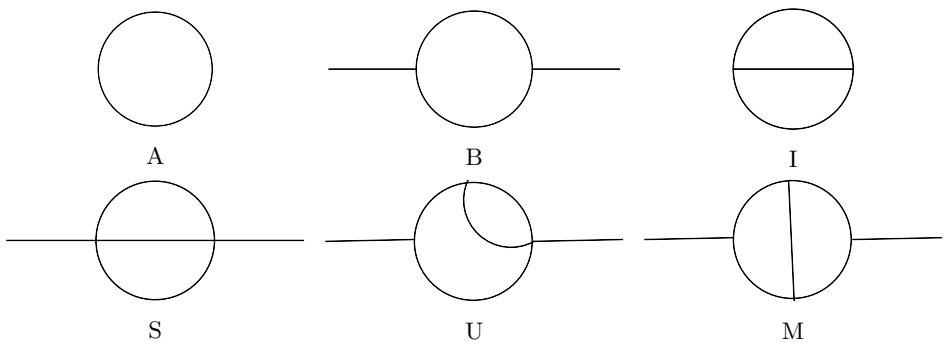

Figure 4.5: The topologies corresponding to one- and two-loop self-energy master integrals.

expressing the Feynman integrals entirely in terms of master integrals is that these have been widely studied, see e.g. [215–219]. Moreover, in $d = 4 - 2\epsilon$ dimensions, the poles in ϵ^{-2} and ϵ^{-1} have been determined analytically, see for example [215]. Analytical expressions for the finite parts have also been found in several cases. More importantly there is the possibility of determining all of them numerically. In this thesis we made this by means of the TSIL package [214].

In order to implement the reduction from integrals of the type (4.31) to master integrals we used the FIRE package [220, 221] in MATHEMATICA. For this package to work we need to make the transformations from Eq. (4.29) and to express the scalar products in terms of propagators. This can be carried out by making the replacement

$$
k \cdot q \to -\frac{1}{2}G_0(k-q) + G_0(k) + G_0(q), \tag{4.34}
$$

and similarly for $k \cdot p$ and $p \cdot q$. After this procedure has been performed for all

the scalar products, $v_2(k^2, m_B^2)$ is expressed as a sum of integrals of the form[4]

$$\begin{aligned} I_{m_1m_2m_3m_4m_5}(n_1,n_2,n_3,n_4,n_5) &\equiv \int_p\int_q G^{n_1}_{m_1}(p)G^{n_2}_{m_2}(q) \\ &\times G^{n_3}_{m_3}(k-p)G^{n_4}_{m_4}(k-q)G^{n_5}_{m_5}(p-q). \end{aligned} \tag{4.35}$$

The FIRE package makes an extensive use of the Laporta [222] and s-bases [223] algorithms, among other strategies, to carry out the reduction. Both of these algorithms use as starting point *integration by parts relations* (IBP)[224], which, in the case of two loop integrals with only one external momentum, k, acquire the form

$$\int_{q_1}\int_{q_2}\frac{\partial}{\partial(q_j)_\mu}\left(k_\mu G^{n_1}_{m_1}(q_1)G^{n_2}_{m_2}(q_2)G^{n_3}_{m_3}(k-q_1)G^{n_4}_{m_4}(k-q_2)G^{n_5}_{m_5}(q_1-q_2)\right)=0 \tag{4.36}$$

$$\int_{q_1}\int_{q_2}\frac{\partial}{\partial(q_j)_\mu}\left((q_l)_\mu G^{n_1}_{m_1}(q_1)G^{n_2}_{m_2}(q_2)G^{n_3}_{m_3}(k-q_1)G^{n_4}_{m_4}(k-q_2)G^{n_5}_{m_5}(q_1-q_2)\right)=0, \tag{4.37}$$

with $j,l=1,2$. These identities allow one to generate a system of equations relating the integral $I_{m_1m_2m_3m_4m_5}(n_1,n_2,n_3,n_4,n_5)$ with integrals of the same type but with lower values of the indices n_i. By successively applying these identities, one can find an expression for $I_{m_1m_2m_3m_4m_5}(n_1,n_2,n_3,n_4,n_5)$ in terms of master integrals, where the values each n_i takes are just zero or one.

After the reduction via FIRE, $v_1(k^2,m_B^2)$ and $v_2(k^2,m_B^2)$ are expressed in terms of master integrals with fractional coefficients which depend on the external momentum, k, the gluon mass, m and the space-time dimension d. For some diagrams, the FIRE output gave us non-master integrals with one of the propagators to the power -1, for instance, we found

$$I_{m00mm}(1,-1,0,1,1). \tag{4.38}$$

Fortunately, the integrals of this type can also be reduced to the master integrals listed above by proceeding as illustrated in Appendix D.

4.2.3 UV divergences

As already stated before, $v(k^2)$ is UV finite. In other words, it remains finite when we take the limit $\epsilon\to 0$. Of course, this becomes explicit only after this quantity is written in terms of the renormalized gauge coupling and gluon mass,

$$g_B = Z_g g, \quad m_B^2 = Z_{m^2}m^2, \tag{4.39}$$

and expanded to order g^4. Moreover, by defining the one-loop corrections to the Z-factors to be $\delta Z_\lambda \equiv Z_g^2-1$ and $\delta Z_{m^2}\equiv Z_{m^2}-1$ (by definition both of order $\lambda\propto g^2$), we have

$$v(k^2) = 1+\lambda\, v_1(k^2,m^2)+\lambda^2\, v_2(k^2,m^2)+\lambda\left(\delta Z_\lambda+\delta Z_{m^2}m^2\frac{\partial}{\partial m^2}\right)v_1(k^2,m^2)\,. \tag{4.40}$$

[4] Of course, as a result of this replacement we could have products of the type $G_m(q)G_0(q)^{-1}$ which should be removed again by using Eq. (4.29).

The derivative $\partial v_1/\partial m^2$ generates integrals of the type $\partial A_m/\partial m^2$ and $\partial B_{m0}(k^2)/\partial m^2$. The derivative of A_m can be easily obtained by means of dimensional analysis. The derivative of B_{m0} can be found via IBP relations, by writing the identities

$$0 = \int_p \frac{\partial}{\partial p_\mu} \frac{p_\mu}{(p^2+m^2)(p+k)^2}, \tag{4.41}$$

$$0 = \int_p \frac{\partial}{\partial p_\mu} \frac{k_\mu}{(p^2+m^2)(p+k)^2}, \tag{4.42}$$

as a linear system for $\partial B_{m0}(k^2)/\partial m^2$ and a second integral not needed for the calculation of $v(k^2)$. We find:

$$\frac{\partial A_m}{\partial m^2} = \left(\frac{d}{2}-1\right)\frac{A_m}{m^2}, \tag{4.43}$$

$$\frac{\partial B_{m0}(k^2)}{\partial m^2} = \frac{(d-3)B_{m0}(k^2) + \partial A_m/\partial m^2}{k^2+m^2}. \tag{4.44}$$

The first two terms in Eq. (4.40) correspond to the one-loop result. As can be seen, they do not involve any counterterm. This is because the quantity $v_1(k^2, m^2)$ is UV finite. Indeed, the two diagrams contributing to such quantity (see Appendix A) are finite. This is very clear if one looks at the vertex attached to the ghost leg in any of the one-loop diagrams. In both cases, the Feynman rules yield to a term $P^\perp_{\rho\sigma}(q+k)_\sigma = P^\perp_{\rho\sigma}(q)k_\sigma$, where q denotes the momentum of the gluon attached to the vertex. Then, due to the contraction with the transverse projector, one power of the internal momentum q is lost in the power counting, leading to a superficial degree of divergence of $D = -1$.

The same analysis can be extended to the two-loop diagrams. As a result, these diagrams have a superficial degree of divergence of $D = -1$ as well. Nonetheless, this does not imply that these diagrams are UV finite. They could also feature subdivergences, coming from UV divergent subdiagrams. These subdivergences are eliminated by the last term of Eq. (4.40). In fact, this is a non-trivial check on the reduction via Fire, since individual terms in the reduced expression of $v_2(k^2, m^2)$ show simple, double and even triple poles in $1/\epsilon$. Simple and double poles stem from two-loop master integrals or products of one-loop master integrals. The triple poles are a product of the reduction procedure, since it introduces an extra prefactor $(4-d)^{-1}$ over certain terms. These are:

$$\begin{aligned}\frac{(4-d)^{-1}}{96}\Bigg[&-\left(14+11\frac{k^2}{m^2}\right)\frac{A_m}{m^2}B_{00} - 3\left(2+\frac{k^2}{m^2}\right)B_{m0}B_{00}\\ &-\left(2-11\frac{k^2}{m^2}\right)\left(1+\frac{m^2}{k^2}\right)\frac{S_{m00}}{m^2} - \left(6+13\frac{k^2}{m^2}\right)\frac{S_{000}}{m^2}\\ &+\left(5+2\frac{m^2}{k^2}\right)\frac{I_{m00}}{m^2} - 8\left(1+\frac{k^2}{m^2}\right)U_{00m0} + 3\left(2+\frac{k^2}{m^2}\right)U_{0m00}\Bigg].\end{aligned} \tag{4.45}$$

We have checked that the triple poles cancel among the various terms in the above expression, as it should be, since there is no other source of triple poles. Double

poles in $v_2(k^2, m^2)$ are also canceled when considered altogether, in line with our expectations, since one-loop counterterms only provide simple poles. Finally, we have checked that the simple poles from the last term of Eq. (4.40) cancel the simple poles from $v_2(k^2, m^2)$.

We remind the reader that δZ_λ and δZ_{m^2} have already been determined, thanks to the renormalization of the gluon and ghost propagators and the two non-renormalization theorems, as we discussed in Section 3.3. At one-loop order, they read

$$\begin{aligned} \delta Z_\lambda &= \lambda \left(\frac{z_{\lambda 11}}{\epsilon} + z_{\lambda 10} \right) \\ \delta Z_{m^2} &= \lambda \left(\frac{z_{m^2 11}}{\epsilon} + z_{m^2 10}, \right) \end{aligned} \tag{4.46}$$

with $z_{\lambda 11} = -11/3$, $z_{m^2 11} = -35/12$ and where $z_{\lambda 10}$ and $z_{m^2 10}$ are more involved quantities, which depend on m and μ.

4.2.4 Finite parts

Leaving solved the matter of UV divergences, now we concentrate on the UV-finite contributions to $v(k^2)$. Due to the fact that the counterterms, the master integrals and even some prefactors multiplying such integrals contain poles in $1/\epsilon$, it is an issue of interest to which order in ϵ we must expand the various terms in Eq. (4.40) so as to not to miss any finite contribution. It is clear that, since $v_1(k^2, m^2)$ does not feature any pole in ϵ, the counterterms which multiply it in Eq. (4.40), δZ_λ and δZ_{m^2}, must be expanded only to order ϵ^0. On the contrary, since such counterterms are UV-divergent, see Eq. (4.46), $v_1(p^2, m^2)$ and the integrals in terms of which it is written, A and B, should be expanded to order ϵ^1. As for $v_2(p^2, m^2)$, the master integrals not involved in Eq. (4.45) must be considered to order ϵ^0, in the case of two-loop integrals, and to order ϵ^1 in what concerns the one-loop master integrals (since they come in products of two). One-loop master integrals that come with the prefactor $(4-d)^{-1}$, A_m, B_{m0} and B_{00} need to be expanded to order ϵ^2, whereas the two-loop master integrals which multiply it S_{000}, S_{m00}, I_{m00}, U_{0m00} and U_{00m0} must be expanded to order ϵ^1. To deal with these terms we used the expansions presented in Appendix E.

To end this section, we stress that the renormalized expression (4.40) is an expansion to order g^4 of the μ-independent quantity (4.11). As such, it should be μ-independent up to contributions of order g^6. The μ-independence here is crucial, since it allow us to choose a renormalization scale $\mu = k$ in order to avoid the appearance of potential large logarithms, see Section 1.5.2. We will implement this specific renormalization scale when presenting our results. Nevertheless, the crosschecks we introduce in what follows are valid for a fixed value of the renormalization scale.

4.3 Crosschecks

The reduction of $v(k^2)$ into master integrals generates a great amount of terms. So, we need to test such reduction in as many ways as possible. The tests we introduce here are all of them of the same nature. We know some specific behavior of $v(k^2)$

beforehand which is not necessarily described by the individual terms composing $v(k^2)$. Accordingly, different sorts of cancellations are needed in order for the vertex function behavior to be fulfilled. Actually, we have already introduced an example of this type of cancellation when discussing the elimination of the triple, double and simple poles in ϵ. The properties we will study in this section are: the UV and IR asymptotic behavior, the regularity for $k^2 = m^2$ and the limit when $m \to 0$ of $v(k^2)$.

4.3.1 UV behavior

To infer the large k^2 behavior of $v(k^2)$ we can use Weinberg's theorem [225]. For a given diagram, the theorem classifies the various contributions to the large momentum asymptotic expansion according to the possible ways that the large momentum k can flow inside the diagram. For each of such contributions it is possible to expand in powers of any scale (momentum or mass, except for k of course) that appear in a propagator whose total momentum is large. As a consequence, for a given diagram, the leading UV contribution can be evaluated by making the large momentum to flow through all of the internal lines. In other words, the behavior of the leading UV contribution is dictated by the superficial degree of divergence. As we have seen above, the superficial degree of divergence for each one of the diagrams contributing to $v(k^2)$ is $D = -1$. Based on this, we could naively expect that the UV leading behavior of $v(k^2)$ is $1/k$. However, as the reduction of the superficial degree of divergence, see discussion below Eq. (4.44), factors out a factor of k, $v(k^2)$ actually behaves logarithmically as $k^2 \to \infty$.

In contrast, the individual terms composing $v(k^2)$ can grow much faster. For the purpose of verifying that such contributions cancel when considered as a whole, we used UV expansions for the individual master integrals which make $v(k^2)$. So as to achieve this, we used our own implementation of the algorithm described in Ref. [226]. Such implementation was essentially developed for the investigation done in Ref. [54]. In that work the UV expansions were needed just to order ϵ^0 in the case of the two-loop master integrals. For $v(k^2)$, we had to extend that routine to include also the ϵ^1 order when necessary. More precisely, we needed to compute I_{m00} at order ϵ^1, which can be found by using Eq. (E.11). At leading order, we find

$$v(k^2 \to \infty) = \\ 1 + \frac{3\lambda}{4} + \lambda^2 \left(\frac{11 + 3z_{\lambda 11}}{4\epsilon} + \frac{317}{32} + z_{\lambda 11} + \frac{3z_{\lambda 10}}{4} + \frac{22 + 3z_{\lambda 11}}{4} \ln \frac{\bar{\mu}^2}{k^2} \right) + \mathcal{O}\left(\frac{m^2}{k^2}\right), \tag{4.47}$$

where $z_{\lambda 11}$ and $z_{\lambda 10}$ are given by Eq. (4.46) and $\bar{\mu}^2 \equiv 4\pi\mu^2 e^{-\gamma}$, with γ the Euler constant. By using that $z_{\lambda 11} = -11/3$, we get

$$v(k^2 \to \infty) = 1 + \frac{3\lambda}{4} + \lambda^2 \left(\frac{599}{96} + \frac{3z_{\lambda 0}}{4} - \frac{11}{4} \ln \frac{k^2}{\bar{\mu}^2} \right) + \mathcal{O}\left(\frac{m^2}{k^2}\right), \tag{4.48}$$

which verifies the expected behavior. The absence of logarithms at one-loop order stems from the fact that one-loop corrections are finite. Similarly, the simple

logarithm at two-loop order comes from the subdivergences and, moreover, signals the absence of global divergences.

Let us end this section by looking at the μ-dependence of $v(k^2 \to \infty)$:

$$\begin{aligned}\mu\partial_\mu v(k^2 \to \infty) = \frac{3}{4}\mu\partial_\mu\lambda + 2\mu\lambda\partial_\mu\lambda\left(\frac{599}{96} + \frac{3}{4}z_{\lambda 10} - \frac{11}{4}\ln\left(\frac{k^2}{\bar{\mu}^2}\right)\right) \\ + \frac{3}{4}\lambda^2\left(\mu\partial_\mu z_{\lambda 10} + \frac{11}{2}\right).\end{aligned} \tag{4.49}$$

This quantity can be calculated by taking into account that the running of λ satisfies

$$\begin{aligned}0 = \mu\partial_\mu \ln\left(\lambda_B \mu^{2\epsilon}\right) &= \mu(\partial_\mu Z_\lambda + \partial_\mu \ln\lambda) + 2\epsilon \\ &= \frac{\lambda}{Z_\lambda}\mu\partial_\mu z_{\lambda 10} + \left(1 + \frac{\delta Z_\lambda}{Z_\lambda}\right)\mu\partial_\mu\lambda + 2\epsilon,\end{aligned} \tag{4.50}$$

which is

$$\mu\partial_\mu\lambda = (2z_{\lambda 11} - \mu\partial_\mu z_{\lambda 10})\,\lambda^2 + \mathcal{O}(\lambda^3). \tag{4.51}$$

Plugging this identity into Eq. (4.49) and using that $z_{\lambda 11} = -11/3$ we can see that the μ-dependence in $v(k^2 \to \infty)$ appears formally only at order $\lambda^3 \propto g^6$, as expected. The corrections of order m^2/k^2 also contain logarithms and involve the finite part $z_{m^2 10}$ of δZ_{m^2}.

We note finally that the choice $\mu = k$ we will use in the context of the IRS scheme is perfectly consistent with the ordering in powers of m^2/k^2 in the UV-expansion, since $m(k) \to 0$ at large k. This is also the case for the running $\lambda(k)$, which implies that in the UV the term with less powers of λ dominates. As a result, once the running is taken into the calculation, $v(k^2)$ approaches one logarithmically in the UV.

4.3.2 IR behavior

The infrared behavior of the ghost-antighost-gluon vertex is limited by its diagramatic structure. Since the ghost legs can only be attached to a tree level ghost-antighost-gluon vertex, any loop correction presents the form shown in Fig. 4.6. Therefore, following the notation of the figure, the integrand of Feynman integrals are proportional to $k_\mu k_\sigma P^\perp_{\mu\nu}(q) P^\perp_{\rho\sigma}(\ell)$ for all loop corrections. Since the corrections enclosed in the black circle are not IR divergent in the CF model, see Appendix H, the loop contributions to $V^{abc}_\mu(k,0)$ tend to zero at least like k^2 as $k \to 0$. In other

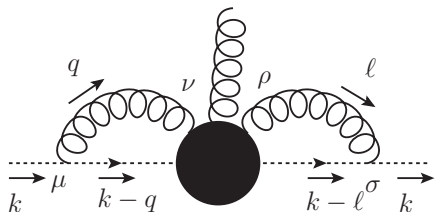

Figure 4.6: Any loop correction to the ghost-antighost-gluon vertex presents this form. The black circle refers to further loop corrections.

words $V_\mu^{abc}(k,0)$ approaches its tree level from as $k \to 0$, at least as k^2. Thus, the vertex function obeys $v(k^2 \to 0) \to 1$.

This property is not fulfilled by the individual terms contributing to $v(k^2)$. As occurred in the UV expansion, several cancellations must occur in order to yield the expected behavior. To test this, we used IR expansions for the various master integrals which intervene in the reduction of $v(k^2)$. Such expansions were obtained by implementing the algorithm described in Ref. [216]. In some instances this algorithm cannot be applied and a more sophisticated version is needed [227]. Concerning $v(k^2)$, luckily enough, the most problematic integrals are known analytically. For a few master integrals which do not have an analytic form to date, in particular for the order ϵ^1 of the masters U_{0m00} and U_{00m0} we used our own strategy, detailed in Appendix F.

At first non-trivial order, we find

$$\begin{aligned} v(k^2 \to 0) = 1 + \Bigg\{ \Bigg(\frac{17}{48} - \frac{1}{8} \ln \frac{k^2}{m^2} \Bigg) \lambda + \Bigg(\frac{2323}{1152} - \frac{29}{1152}\pi^2 - \frac{999}{128} S_2 + \frac{17}{48} z_{\lambda 10} \\ - \frac{11}{48} z_{m^2 10} + \frac{3}{32} \ln \frac{m^2}{\bar{\mu}^2} \ln \frac{k^2}{m^2} + \left[-\frac{5}{64} - \frac{z_{\lambda 10}}{8} + \frac{z_{m^2 10}}{8} \right] \ln \frac{k^2}{\bar{\mu}^2} \\ + \left[-\frac{53}{96} + \frac{z_{\lambda 10}}{8} - \frac{z_{m^2 10}}{8} \right] \ln \frac{m^2}{\bar{\mu}^2} \Bigg) \lambda^2 \Bigg\} \frac{k^2}{m^2} + \mathcal{O}\left(\frac{k^4}{m^4} \right), \end{aligned} \tag{4.52}$$

where

$$S_2 = \frac{4}{9\sqrt{3}} \operatorname{Im}(\operatorname{Li}_2(e^{i\pi/3})), \tag{4.53}$$

and $\operatorname{Li}_2(x)$ is the di-logarithm function. As expected $v(k^2 \to 0) \to 1$. The μ-independence of the expression (4.52) may be checked thanks to the running of the mass, which can be derived by writing

$$0 = \mu \partial_\mu \ln\Big(Z_{m^2} m^2 \Big), \tag{4.54}$$

then,

$$\begin{aligned} \mu \partial_\mu m^2 &= -m^2 \mu \partial_\mu \ln Z_{m^2} = -m^2 \mu \partial_\mu \left\{ \lambda \left(\frac{z_{m^2 11}}{\epsilon} + z_{m^2 10} \right) \right\} \\ &= -m^2 \mu \partial_\mu \left\{ \lambda_B \mu^{2\epsilon} \mu^{-2\epsilon} \left(\frac{z_{m^2 11}}{\epsilon} + z_{m^2 10} \right) \right\} = \lambda m^2 \left(2 z_{m^2 11} - \mu \partial_\mu z_{m^2 10} \right). \end{aligned} \tag{4.55}$$

Finally, this equation along with Eq. (4.51), allow to prove that $\mu \partial_\mu v(k^2 \to 0)$ is μ-independent up to contributions of order λ^3 or higher.

To end this section, we note that Eq. (4.52) shows that $v(k^2 \to 0) \to 1$ as long as $m \neq 0$, as anticipated. This property is not affected by the introduction of the running, since both $m(k)$ and $\lambda(k)$ approach zero logarithmically in the IR.

4.3.3 Regularity at $k^2 = m^2$

The function $v(k^2)$ is regular for any value of the momentum, including, as we just saw, $k^2 = 0$. Nevertheless, this is not the case for some of the terms entering in the reduced expression of the vertex function, which feature a singularity at

$k^2 = m^2$. However, if our result is correct, such contributions should be spurious and, similarly to the previous crosschecks, should cancel when considered as a whole. When adding all of these problematic contributions, the residue reads

$$\frac{\lambda^2}{64}\Big((d-2)(A_m B_{00}(m^2) + I_{m00}) + (d-3)m^2 B_{00}^2(m^2) + (8-3d)S_{m00}(m^2) + \frac{d-4}{2}m^4 M_{000m}(m^2)\Big). \tag{4.56}$$

All the integrals appearing in the above result are known analytically, see for instance [215, 217], which makes straightforward to verify that this residue vanishes. In this reasoning we are implicitly assuming that the gluon mass is nonzero. The case $m = 0$ leads to a genuine singularity, as we discuss in the following section.

4.3.4 Zero mass limit

A last check consists in taking the limit $m \to 0$ on $v(k^2)$. Such limit is regular for any $k^2 > 0$, and, moreover, the quantity $v_{m^2=0}(k^2)$ has already been computed in Ref. [228]. The non-regularity of this limit can be inferred from the fact that $v_{m^2\neq 0}(k^2 \to 0) \to 1$ whereas $v_{m^2=0}(k^2 \to 0) \to \infty$, as Eq. (4.52) shows, being the latter result in clear contradiction with lattice data, see Figs. 4.7 and 4.8.

The analysis of the zero mass limit is a double check on the reduction of $v(k^2)$ since, firstly, individual terms entering in the reduced expression of $v(k^2)$ are not necessarily regular when $m \to 0$ and, secondly, the limit should be equal to the result from Ref. [228].

In order to study this limit we used two different strategies. The first one exploits dimensional analysis so as to express any master integral $\mathcal{F}(p^2, m^2)$ as

$$(\mu^{2\epsilon})^L \mathcal{F}(p^2, m^2) = (\mu^{2\epsilon})^L (m^2)^{D_m/2} \mathcal{F}(p^2/m^2, 1), \tag{4.57}$$

where L is the number of loops and D_m the mass dimension of the integral (letting aside the powers of μ that multiply it). By writing the master integral in this way it is clear that the low mass and the UV expansions of $\mathcal{F}(p^2/m^2, 1)$ are equivalent. Consequently, the zero mass limit is simply the leading term in Eq. (4.47), which coincides with the result of [228] in Landau gauge (up to the fact that we considered general renormalization factors), as expected.

Another technique to calculate the limit $m \to 0$ consists in Taylor expanding the master integrals in powers of m^2. Simpler in principle, the actual reason why this procedure works has its subtleties as we explain later in this section and in more detail in Appendix G. Since we need to carry out an ϵ-expansion as well we have to decide which expansion we make first. Independently of this election, we will encounter singular terms in the $m \to 0$ limit which should cancel at the end of the calculation. We found the expansion much easier to deal with by first expanding in the mass for a generic dimension d.

We find potential singular terms proportional to m^{-4},

$$(8-3d)S_{000}(k^2) + (d-4)\left(k^2 U_{0000}(k^2) - I_{000}\right) \tag{4.58}$$

and proportional to m^{-2},

$$2(d-3)(d-4)k^2 B_{00}^2(k^2) + (d-4)^2 k^4 M_{00000}(k^2) - 2(3d-8)(3d-10)S_{000}(k^2). \tag{4.59}$$

Thankfully, both quantities vanish. The limit $m \to 0$ corresponds to the m^0 term in the mass expansion, which is proportional to

$$(d-4)(d-6)(d-8)\Big[(d-1)(d-4)k^4 M_{00000}(k^2) + 2(2d^4 - 28d^3 + 134d^2 \\ -252d + 147)k^2 B_{00}(k^2)\Big] + 2(88832 - 224384d + 223348d^2 - 113336d^3 \\ + 31705d^4 - 4895d^5 + 386d^6 - 12d^7)S_{000}(k^2). \tag{4.60}$$

By taking $d = 4 - 2\epsilon$ we can expand in ϵ, which, again, yields to the result of Ref. [228].

That a naive Taylor expansion in the mass leads to the correct result could, in principle, be in contradiction with the application of Weinberg's theorem to Eq. (4.57), since one should consider more terms. However, it turns out that these extra terms mutually cancel. This being the result of $v_{m^2}(k^2)$ being regular when $m \to 0$. We illustrate this in Appendix G.

4.4 Results

In this section we present our results for $v(k^2)$ in comparison to lattice simulations from Ref. [159] for the SU(2) gauge group and from Ref. [55, 212] in the SU(3) case. Unless otherwise stated, we work in the IRS scheme. We implement two strategies to obtain the results.

Firstly, we used the values $\lambda_0 = \lambda(\mu_0)$ and $m_0 = m(\mu_0)$ with $\mu_0 = 1$ GeV, determined in [54], by fitting the two-loop two-point functions to lattice data from [203, 204] for the SU(3) gauge group and to lattice data from [29] for the SU(2) gauge group, as explained in Section 3.3.3. Accordingly, with the aid of the β-functions we found the running functions $\lambda(k)$ and $m(k)$. As a result, there are no more free parameters to adjust and $v(k^2)$ arises as a pure prediction of the CF model.

Our results show an excellent agreement between the model and lattice simulations in SU(3) but much poorer results in SU(2). For this reason, in the latter case, we also opted for a less ambitious strategy, where we first carried out an independent fit of the vertex and the two-point functions so as to determine the optimal values of m_0 and λ_0 for which all of those functions can be reproduced to a reasonable accuracy.

4.4.1 Prediction

Our results are shown in Fig. 4.7 for the SU(3) case and in Fig. 4.8 for the SU(2) case. The colored bands display a simple estimate of our theoretical error, defined by the absolute difference between central values at a given order and the previous one. In the SU(3) case we note that two loop results are compatible with lattice simulations. Moreover, the estimated error diminishes from one- to two-loop corrections, except for a tiny region where the estimated error accidentally vanish (preventing us from estimating the error), which shows a good *apparent* convergence of the perturbative series[5].

[5] It is important to stress that the convergence can only be apparent. It is well known that the perturbative series is not convergent if one goes sufficiently high in the order of the expansion.

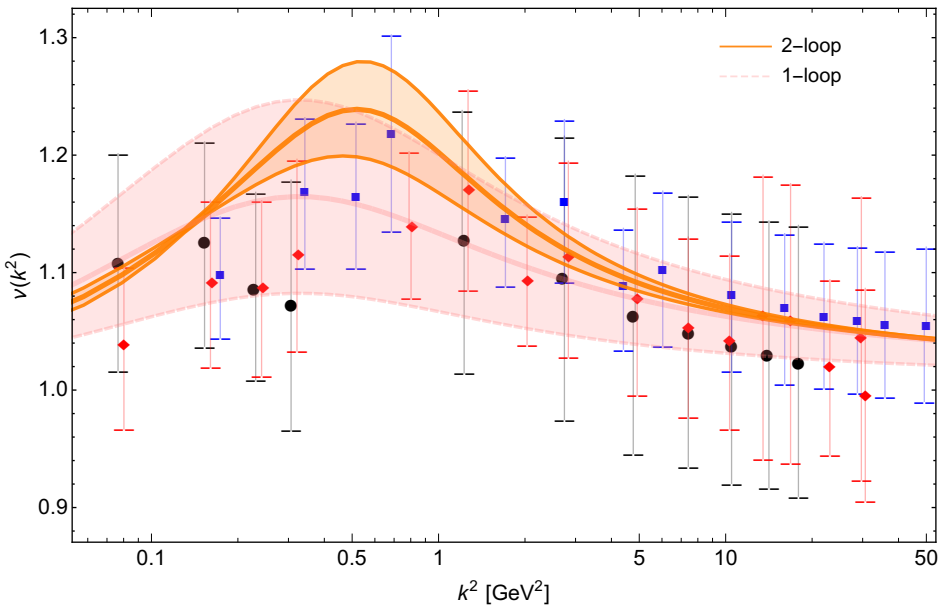

Figure 4.7: CF prediction for the function $v(k^2)$ in the SU(3) case in the IRS scheme, compared to lattice data in the Taylor scheme from [55, 212]. The lattice data were extracted manually from the plots of [55, 212] using WEBPLOTDIGITIZER [229]. We estimated the error related to the extraction procedure to be at most 0.8%.

In what concerns the SU(2) gauge group the situation is quite different. Even though the estimated error diminishes from one- to two-loop order, our results cannot describe accurately the lattice data. In particular, the scale at which $v(k^2)$ reaches a maximum is underestimated by a factor of two. The origin of such discrepancies is threefold. Firstly, given the large error bars and, more importantly, the dispersion of the lattice data depending on the various lattice parameters, one cannot exclude the possibility that the discrepancies stem from lattice artifacts, at least partially. Secondly, as we explained in Section 3.3.4, as the expansion parameter is larger in the SU(2) case, we expect that perturbation theory does not work as well as in the SU(3) case. Our calculations for $v(k^2)$ reveal that the theoretical error bars of the two-loop results are controlled by a parameter in between $\tilde{\lambda} = \lambda \frac{\mu^2}{\mu^2+m^2}$ and λ. This indicates that the situation is not as dramatic as if the parameter expansion were λ, in which case we would be reaching the limit of validity of the perturbative paradigm, but, anyway, caution is needed. Thirdly, the parameters have been adjusted to best reproduce the two-point functions. Therefore, any inaccuracy in the determination of such quantities (be it numerical or because perturbation theory features larger errors in SU(2)), necessarily impacts in the determination of the parameters and consequently in the prediction of $v(k^2)$.

For these reasons, it is interesting to adopt a less ambitious analysis in the SU(2) case, where the gluon and the ghost two-point functions as well as the vertex function are fitted independently. Being the goal of such fits to investigate if there exist a set of values, λ_0 and m_0, capable of reproducing to a reasonable accuracy the lattice data for the three functions at the same. Thankfully, such values exist. The analysis is presented in the following section.

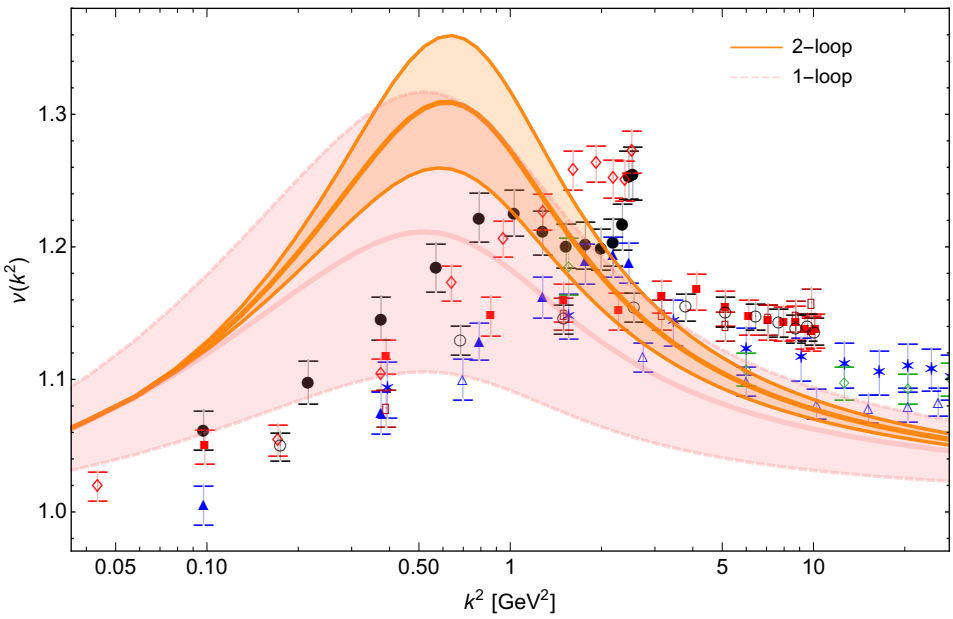

Figure 4.8: CF prediction for the function $v(k^2)$ in the SU(2) case in the IRS scheme, compared to lattice data in the Taylor scheme from [159].

4.4.2 Independent fit of the various vertex functions

In Fig. 4.9, the error regions associated to values (λ_0, m_0) are shown, both at one- and two-loop order. It is clear that the optimal parameters do not coincide. However, this tension is considerably reduced from one- to two-loop order, which shows consistency with the perturbative paradigm used for this calculation. If instead of fitting the two-point functions and the vertex altogether we fit $v(k^2)$ alone (as it has been done previously in other approaches), we can obtain an excellent agreement with lattice simulations, even for the SU(2) gauge group, as can be seen in Fig. 4.10. However, the information this fit provides regarding the quality of the model in describing the infrared of the vertex function is very limited, since it could lead to poor descriptions of the two-point functions. Moreover, the lattice data of these quantities is much more precise than the three-point functions and, thus, cannot be neglected.

To end this section, in Fig. 4.11 we show the plots for a set of parameters λ_0 and m_0 which reproduce the ghost dressing function, the gluon propagator and the vertex function $v(k^2)$ to a reasonable accuracy by minimizing a joint error.

4.4.3 Scheme dependence

Similarly to the analysis we presented in Section 3.3.5, in this section we investigate the scheme dependence of $v(k^2)$, by comparing the IRS scheme result with the the VM scheme, introduced in Section 3.3.5, for $\alpha = 1$ and $\alpha = 2$. The results are shown in Table 4.1. There we write our estimate for the relative error between the IRS and the VM scheme evaluations of $v(k^2)$. For calculating such error we used a definition slightly different to the one presented in Eq. (3.39). Rather than summing over the lattice points, here we carried out the sum over 1190 points $(k^2, v(k^2))$, equally spaced in the k^2 coordinate, keeping the rest of the definition

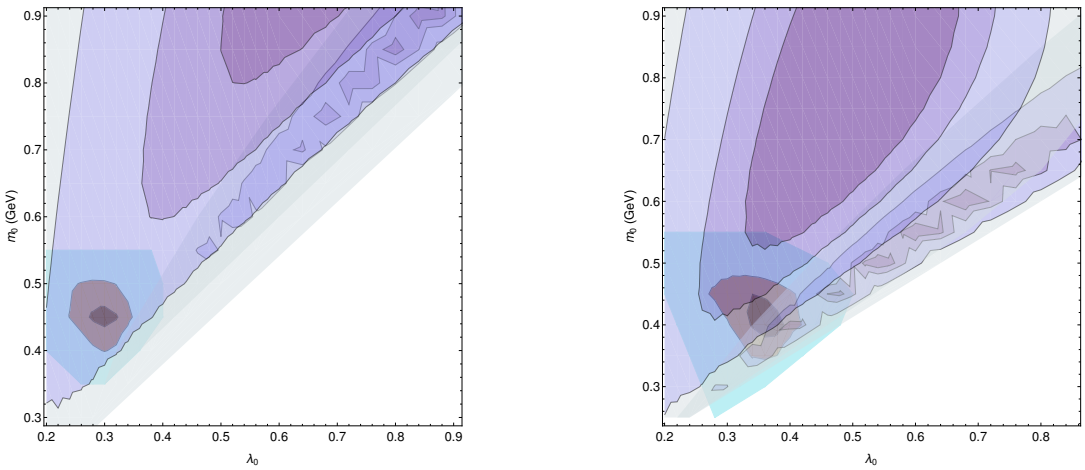

Figure 4.9: Error regions with 10%, 7%, 5% and 4% accuracy. Darker regions corresponding to lower errors. The errors were found by fitting the ghost dressing and the vertex function $v(k^2)$ in the SU(2) case in the IRS scheme to the lattice data in the Taylor scheme from Ref. [29, 159]. The wide region corresponds to the vertex function and the cigar-like region to the ghost dressing function. In the case of the gluon propagator, its error corresponds to the small region at the bottom left and it is subdivided in subregions corresponding to 20%, 10% and 7% accuracy. The parameters m and λ are fixed at the fixed scale μ_0. Left and right figures correspond to one- and two-loop evaluations, respectively.

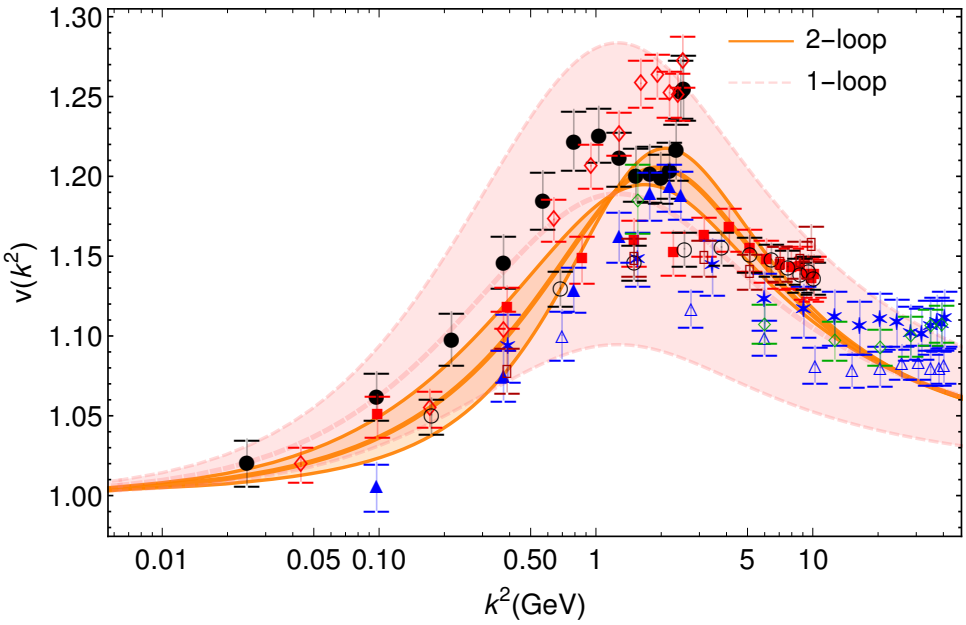

Figure 4.10: Best fit for $v(k^2)$ for the SU(2) gauge group in the IRS scheme, as compared to lattice data in the Taylor scheme from Ref. [159].

of $\mathcal{H}$ unchanged.

We note that the scheme dependence diminishes from one- to two-loop results in the SU(3) case, specially for $\alpha = 2$. Even though the effect is not as strong for $\alpha = 1$, it still remains compatible with a valid perturbative analysis. In contrast, in the SU(2) case the situation is exactly the opposite, in line with the

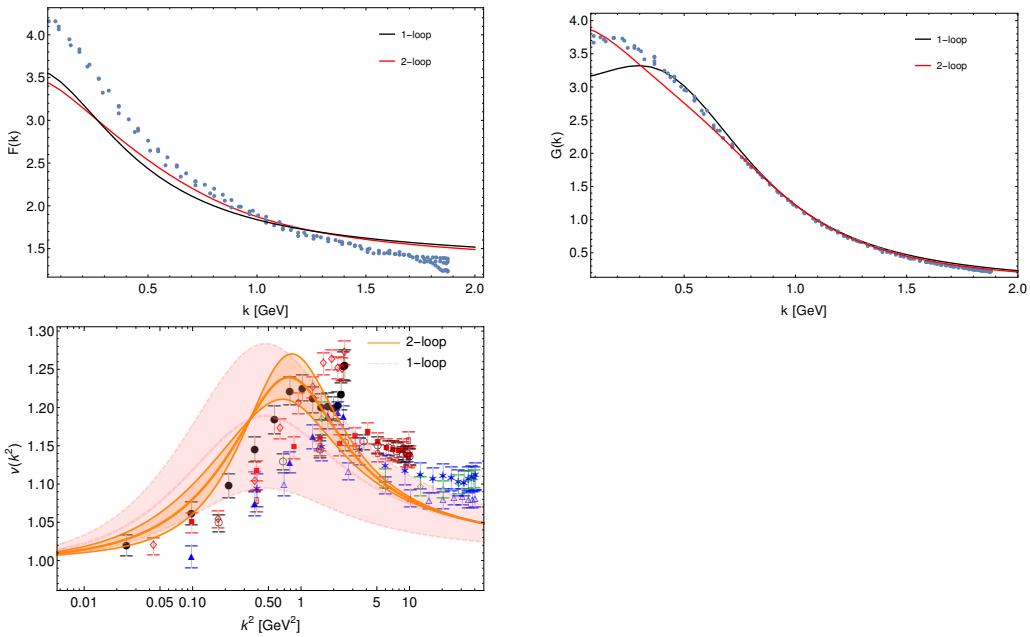

Figure 4.11: Plots of the ghost dressing function, $F(k)$, the gluon propagator, $G(k)$, and the vertex function, $v(k^2)$, for a choice of parameters, λ_0 and m_0, which reproduces to a reasonable accuracy the tree quantities. Lattice data from Refs. [29, 159].

Group	$N=2$		$N=3$	
VM	$\alpha=1$	$\alpha=2$	$\alpha=1$	$\alpha=2$
1-loop	0.9%	1.1%	0.9%	1.1%
2-loop	1.2%	2.0%	0.8%	0.7%

Table 4.1: Relative difference between the IS scheme and the VM schemes for $\alpha=1$ and $\alpha=2$.

previous observations that, in this case, we are close to the limit of validity of the perturbative paradigm within the CF model. For both references we note a decreasing in the estimated error when two-loop corrections are included.

Chapter 5

Three-gluon vertex

In this chapter we evaluate the three-gluon vertex at two-loop order from the CF model. The calculation is done for the pure gauge theory, in four dimensions and in the Landau gauge. Similarly to the ghost-antighost-gluon case, we computed this quantity in the asymmetric configuration. Since the parameters of the model λ_0 and m_0 are adjusted by fitting the two-point functions to lattice data, this calculation is a pure prediction of the model (up to a constant normalization factor).

The present computation is a continuation of the one we presented in the preceding chapter, in the sense that it is a way to test the quality of the perturbative CF model to reproduce the available lattice data. Moreover, the calculation will provide information on whether the perturbative expansion remains under control once two-loop corrections are included. On the whole, it will give us valuable information in order to determine if the model is suitable to describe the IR region of pure YM theory.

On the other hand, the evaluation of the three-gluon vertex is interesting in its own right, mainly in order to investigate the zero-crossing. Such phenomenon is characterized by the fact that the three-gluon dressing function (to be defined below) becomes negative in the deep IR. It is important to stress that current lattice data are not conclusive on this matter in four dimensions[1], see *e.g.* [19, 230]. As for the CF model, the one-loop evaluation of the three-gluon dressing function [57], showed that it does display a zero crossing. As we discuss in Section 5.1.1, this is actually an exact property of that quantity in the framework of the CF model and remains true at all orders of perturbation theory. The question of interest here is how the two-loop corrections modify the position of zero-crossing. As we will see, such modification is not negligible.

This work comes to complement several calculations that, in the last years, have permitted a better understanding of this fundamental quantity on the lattice [29, 158, 211, 231, 232] and within functional methods [19, 206, 207, 233–238].

The results presented in this chapter can also be found in [60].

[1] On the contrary, in three dimensions lattice simulations clearly indicate the existence of a zero crossing, see for instance [29, 211].

5.1 Generalities

As it is shown in Ref. [213], the color structure of the three-gluon vertex is simply the structure constant of the SU(N) gauge group, f^{abc}. Consequently, we can define the bare three-gluon vertex as

$$\Gamma^{(3)B}_{A^a_\mu A^b_\nu A^c_\rho}(p,k,r) \equiv -ig_B f^{abc}\Gamma^B_{\mu\nu\rho}(p,k,r), \tag{5.1}$$

where, as it is customary, we factorized out the bare gauge coupling. We will work in the asymmetric configuration, *i.e.* in the particular kinematical configuration where one of the external gluons has vanishing momentum. Therefore, it is convenient to define

$$\Gamma^B_{\mu\nu\rho}(p,-p,0) \equiv \Gamma^B_{\mu\nu\rho}(p). \tag{5.2}$$

Its corresponding renormalized expression, given by Eq. (1.135), reads

$$\Gamma_{\mu\nu\rho}(p,\mu) = Z_A^{3/2} Z_g \Gamma^B_{\mu\nu\rho}(p), \tag{5.3}$$

whose tensorial form can be written as

$$\Gamma_{\mu\nu\rho}(p,\mu) = 2\Gamma_a(p^2,\mu)\delta_{\mu\nu}p_\rho + \Gamma_b(p^2,\mu)(\delta_{\mu\rho}p_\nu + \delta_{\nu\rho}p_\mu) + \Gamma_c(p^2,\mu)p_\mu p_\nu p_\rho. \tag{5.4}$$

We are interested in comparing our results with lattice data from Refs. [19, 230] for the SU(3) gauge group and from Ref. [159] for the SU(2) gauge group. In all these studies the renormalized quantity the authors evaluate is, up to a constant factor,

$$\Gamma(p^2,\mu_0) = \frac{\Gamma^{\text{tree}}_{\mu'\nu'\rho}(p)P^\perp_{\mu'\mu}(p)P^\perp_{\nu'\nu}(p)\Gamma_{\mu\nu\rho}(p,\mu)}{\Gamma^{\text{tree}}_{\mu'\nu'\rho}(p)P^\perp_{\mu'\mu}(p)P^\perp_{\nu'\nu}(p)\Gamma^{\text{tree}}_{\mu\nu\rho}(p)}, \tag{5.5}$$

where $\Gamma^{\text{tree}}_{\mu\nu\rho}(p)$ is obtained from Eq. (5.2) at tree level order. By inserting Eq. (5.4) into Eq. (5.5) it is easy to deduce that

$$\Gamma(p^2,\mu) = \Gamma_a(p^2,\mu). \tag{5.6}$$

Hereafter, we will refer to this quantity as the *three-gluon dressing function*.

5.1.1 IR and zero-crossing

The infrared of the three gluon dressing function is particularly interesting because of the zero-crossing. The infrared structure of the CF model can be investigated by using the notion of asymptotically irreducible subgraphs [239, 240]. A short review on this subject is provided in Appendix H, for details see Apps. B and C from Ref. [60]. As a result of that analysis we find that the leading IR contribution to the bare three-gluon dressing function has the form of Fig. 5.1 at all orders of perturbation theory. The bare ghost propagators inside the boxes indicate we must retain uniquely the leading term in the low momentum Taylor expansion, which we denote as $\Sigma_B(k) \sim \sigma_B k^2$. In other words, the leading contribution to the IR expansion of the three-gluon dressing function is dictated by a one-loop ghost correction to the three-gluon vertex, where the Feynman rule for each tree level ghost propagator is replaced according to

$$\frac{1}{k^2} \to \frac{1}{k^2(1+\sigma_B)}, \tag{5.7}$$

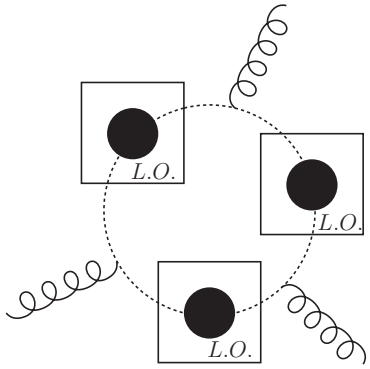

Figure 5.1: Leading IR contribution to the bare three-gluon dressing function.

where $1/(1+\sigma_B)$ corresponds to the bare ghost dressing function at zero-momentum, $F_B(0)$, see Eq. (3.8). Consequently, the leading term in the IR expansion of $\Gamma_B(p^2)$ is given a ghost loop multiplied by the cube of the exact ghost dressing function at vanishing momentum. In order to renormalize this expression we first note that the bare three-gluon dressing function renormalizes as $Z_A^{3/2} Z_g$, which can be conveniently written as

$$(Z_A^{1/2} Z_c Z_g)^3 Z_c^{-3} Z_g^{-2}. \tag{5.8}$$

The first factor is finite because of Taylor's non-renormalization theorem. Moreover, it equals one in both of the renormalization schemes to be used in this chapter, the IRS and the VM schemes. The third factor transforms the cube of the exact bare ghost dressing function at zero momentum into the cube of the exact renormalized ghost dressing function at zero momentum. Finally, the third factor transforms the λ_B that arises as a result of the one-loop ghost contribution into $\lambda(\mu)$. We end up with the following exact result

$$\Gamma(p^2,\mu) \sim \frac{\lambda(\mu)}{24} \ln \frac{p^2}{\mu^2} \times F(0)^3 \times (Z_A^{1/2} Z_c Z_g)^3, \tag{5.9}$$

where the last factor equals one in the IRS and VM schemes. The factor 1/24 arises from the strict one-loop computation [57]. In Section 5.3.2 we check that this identity holds at two-loop order.

The identity (5.9) confirms that the zero-crossing of the three-gluon dressing function is an exact property of the CF model in four dimensions, emerging as a result of an IR logarithmic divergence. Moreover, it shows that the power of such logarithm does not increment with the loop order, which indicates that it could be well described by perturbative means. In contrast, the powers of terms of the type $\ln m^2/\mu^2$, which come from $F(0)$, are not constrained and do increase with the loop order. Therefore, a running of the type $\mu = p$ invalidates the use of perturbation theory in the IR, since when $\ln m^2/\mu^2 \sim 1/\lambda(\mu)$ terms of the type $\lambda(\mu)^n (\ln m^2/\mu^2)^n$ are all of the same order. A way of curing this problem while keeping the large logarithms in the UV under control is to choose a renormalization scale such that $\mu = \sqrt{p^2 + m_0^2}$ with $m_0 = m(1\text{ GeV})$. As for the IRS scheme, this is the running we implement in the rest of this chapter.

5.2 Two-loop evaluation

In this section we address the two-loop evaluation of the three-gluon dressing function. We start by calculating its bare expression, $\Gamma_B(p^2)$. Afterwards we introduce its renormalization. We close this section by presenting the various crosschecks we implemented in order to reduce the chance of error.

5.2.1 Diagrams

At two-loop order, the bare expression of the three-gluon dressing function, $\Gamma_B(p^2)$, can be written as

$$\Gamma_B(p^2) = 1 + \lambda_B \Gamma_1(p^2, m_B^2) + \lambda_B^2 \Gamma_2(p^2, m_B^2), \tag{5.10}$$

where $\Gamma_n(p^2, m_B^2)$ represent the sum of n-loop diagrams, after projecting along $2\delta_{\mu\nu} p_\rho$. Similarly to the case of the ghost-antighost-gluon vertex we have factored out the term

$$\lambda_B \equiv \frac{g_B^2 N}{16\pi^2}, \tag{5.11}$$

which makes explicit the appropriate power of g_B^2 as well as the color factor of each loop contribution. As usual, we have absorbed the factors $(16\pi^2)^n$ and μ^ϵ in $\Gamma_n(p^2, m_B^2)$. This translates into making the following replacement on the Feynman integrals

$$\int \frac{d^d q}{(2\pi)^2} \to \int_q \equiv 16\pi^2 \mu^{2\epsilon} \int \frac{d^d q}{(2\pi)^d}, \tag{5.12}$$

and dividing the color factors by N^n.

The one-loop Feynman diagrams contributing to $\Gamma_1(p^2, m_B^2)$ can be treated essentially by hand from the writing of the Feynman integrals to their evaluation. As for the Feynman integrals deriving from two-loop diagrams, we wrote them down by hand and cross-checked them by means of an automatized routine in Mathematica together with qgraf [241].

For the purpose of organizing the diagrams, it is useful to take into account that in pure YM, the various elements of a Feynman graph satisfy the relations

$$L = I - (V_1 + V_3 + V_4 - 1) \tag{5.13}$$

$$2I_g + E_g = 3V_3 + 4V_4 + V_1 \tag{5.14}$$

$$2I_{gh} + E_{gh} = 2V_1, \tag{5.15}$$

where L is the total number of loops of the graph, and I and E denote the total amount of internal and external lines, respectively. The terms V_1, V_3 and V_4 refer to the number of ghost-gluon, three-gluon and four-gluon vertices, respectively. Finally, the quantities I_g and I_{gh} correspond to the gluon and ghost internal lines of a graph, respectively. From these equations it is easy to show that

$$2L + E = V_1 + V_3 + 2V_4 + 2. \tag{5.16}$$

As for the two-loop diagrams of the three-gluon vertex we have $E = 3$ and $L = 2$, which leads to

$$5 = V_1 + V_3 + 2V_4. \tag{5.17}$$

In order to determine which topologies are allowed in the computation it is enough to look only at the gluons, since the tree-level ghost-antighost-gluon vertex and the tree-level three-gluon vertex share the same topology. Thus, we can conclude that only three types of topologies are present in the calculation: $(V_3, V_4) = (3, 1) = (5, 0)$ and $(1, 2)$. A few examples are provided in Fig. 5.2.

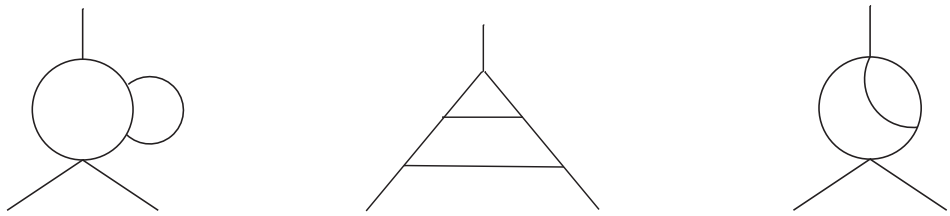

Figure 5.2: Examples of topologies of the type $V_3 = 3$, $V_4 = 1$ (left); $V_3 = 5$, $V_4 = 0$ (middle) and $V_3 = 1$, $V_4 = 2$ (right).

Non planar diagrams are only of the type $V_3 = 5$, $V_4 = 0$ and all of them vanish, owing to their color factor. The justification for this is exactly the same as the one we used for the non-planar diagrams of the ghost-antighost-gluon vertex, see end of Section 4.2.1.

In total, we evaluated 6 one-loop diagrams and 72 two-loop diagrams (excluding non-planar ones). Up to permutations, they are drawn in Appendix B.

5.2.2 Reduction to master integrals

In the same way we proceeded with the ghost-antighost-gluon vertex, see Section 4.2.2, after each two-loop diagram has been expressed in terms of Feynman integrals we reduced them to products of one-loop master integrals (4.32) and two-loop self energy master integrals (4.33). This reduction was implemented by means of a routine in Mathematica with the aid of the Fire6 package [242].

As a result of this reduction, each diagram is now expressed in terms of one- and two-loop master integrals with rational coefficients which depend on the gluon mass m, the external momentum p and the space-time dimension d. As occurred with the ghost-antighost-gluon vertex, the reduction routine we implemented produced, in addition to the master integrals, non-master integrals of the type (4.38), which, as we explain in Appendix D, can also be reduced to master integrals. Finally, we mention that at the end of the reduction we found integrals of the type

$$T_{m_1 m_2 m_3}(p^2) = -\frac{\partial S_{m_1 m_2 m_3}}{\partial m_1^2}(p^2), \tag{5.18}$$

whose poles in ϵ can be easily determined from the ones of the master integral S. Moreover, its finite part can be evaluated numerically with the aid of the Tsil package [214], which we also used to numerically evaluate all the master integrals appearing at the end of the reduction. Consequently, no further reduction is needed in this case.

5.2.3 Renormalization

The bare three-gluon dressing function is UV divergent both at one- and two-loop order. In order to make it finite we need to regularize the Feynman integrals and

renormalize the fields, the coupling and the gluon mass. Since we are working in $d = 4 - 2\epsilon$, with $\epsilon > 0$, the regularization is already in place. To renormalize $\Gamma_B(p^2)$ we use Eq. (1.135) in addition to $\lambda_B = Z_\lambda$ and $m_B^2 = Z_{m^2} m^2$, to get[2]

$$\Gamma(p^2) = \sqrt{Z_\lambda} Z_A^{3/2} (1 + \lambda Z_\lambda \Gamma_1(p^2, Z_{m^2} m^2) + \lambda^2 \Gamma_2(p^2, m^2)), \tag{5.19}$$

where $Z_\lambda = Z_g^2$. In the term $\lambda^2 \Gamma_2(p^2, m^2)$ bare quantities can be automatically replaced by dressed ones since corrections coming from the renormalization factors impact only on higher order corrections.

To get the final renormalized expression at two-loop order of $\Gamma(p^2)$ we need to expand Eq. (5.19) in λ up to order λ^2, neglecting terms of order λ^3 or higher. To this end, we consider the renormalization factors to two-loop order,

$$Z_X = 1 + \lambda Z_{X,1} + \lambda^2 Z_{X,2} + \mathcal{O}(\lambda^3), \tag{5.20}$$

where

$$Z_{X,1} = \frac{Z_{X,11}}{\epsilon} + Z_{X,10} + \epsilon Z_{X,1-1} + \mathcal{O}(\epsilon^2) \tag{5.21}$$

$$Z_{X,2} = \frac{Z_{X,22}}{\epsilon^2} + \frac{Z_{X,21}}{\epsilon} + Z_{X,20} + \mathcal{O}(\epsilon) \tag{5.22}$$

with $X \in \{A, \lambda, m^2\}$. Therefore, we have

$$\begin{aligned}\Gamma(p^2) = 1 + \lambda \left(\frac{3}{2} Z_{A,1} + \frac{1}{2} Z_{\lambda,1} + \Gamma_1(p^2, m^2) \right) + \lambda^2 \Big(\frac{3}{8} Z_{A,1}^2 + \frac{3}{2} Z_{A,2} \\ + \frac{3}{4} Z_{A,1} Z_{\lambda,1} - \frac{Z_{\lambda,1}^2}{8} + \frac{Z_{\lambda,2}}{2} + \frac{3}{2} Z_{A,1} \Gamma_1(p^2, m^2) + \frac{3}{2} Z_{\lambda,1} \Gamma_1(p^2, m^2) \\ + m^2 Z_{m^2,1} \frac{\partial \Gamma_1}{\partial m^2}(p^2, m^2) + \Gamma_2(p^2, m^2) \Big) + \mathcal{O}(\lambda^3).\end{aligned} \tag{5.23}$$

The derivative $\frac{\partial \Gamma_1}{\partial m^2}$ generates integrals of the type $\partial A_m / \partial m^2$, $\partial B_{m0}(p^2)/\partial m^2$ and $\partial B_{mm}(p^2)/\partial m^2$. All of them can be expressed in terms of one-loop master integrals by using integration by parts techniques. The expression for the first two were already presented in Eq. (4.44). The latter reads

$$\frac{\partial B_{mm}(p^2)}{\partial m^2} = \frac{d-2}{2m^2(p^2 + 4m^2)} A_m + \frac{d-3}{p^2 + 4m^2} B_{mm}(p^2). \tag{5.24}$$

The IRS Z-factors were already determined from the renormalization of the ghost and gluon two-point function along with the two non-renormalization theorems, see Section 3.3.1. As a result, a first test on our reduction of $\Gamma(p^2)$ comes from verifying that the various divergent terms appearing in Eq. (5.23) cancel when regarded altogether, rendering a finite expression. This is a non-trivial check since our result features poles in ϵ^{-1}, ϵ^{-2} and even ϵ^{-3}. Likewise the case of the ghost-antighost-gluon vertex, the pole in ϵ^{-3} is a consequence of the reduction

[2] Strictly speaking, we should write $\Gamma(p^2, \mu)$ rather than $\Gamma(p^2)$. However, we will use the latter notation unless we need to make μ explicit.

procedure, since it introduces some terms with an extra pre-factor $(4-d)^{-1}$. More precisely, these are

$$\frac{(4-d)^{-1}}{96}\left[\left(\frac{4}{m^2}-\frac{2}{3p^2}+\frac{7p^2}{3m^4}-\frac{p^4}{3m^6}\right)A_m B_{00}+\left(1-\frac{p^2}{m^2}\right)B_{00}B_{m0}\right.$$
$$+\left(-\frac{13}{3m^2}+\frac{2m^2}{3p^4}-\frac{2}{p^2}+\frac{p^2}{3m^4}\right)I_{m00}+\left(\frac{11}{3m^2}-\frac{2p^2}{3m^4}-\frac{p^4}{3m^6}\right)S_{000}$$
$$+\left(\frac{1}{3m^2}-\frac{2m^2}{3p^4}+\frac{8}{3p^2}-\frac{8p^2}{3m^4}+\frac{p^4}{3m^6}\right)S_{m00}$$
$$\left.+\left(3-\frac{2m^2}{3p^2}+\frac{10p^2}{3m^2}-\frac{p^4}{3m^4}\right)U_{00m0}+\left(\frac{p^2}{m^2}-1\right)U_{0m00}\right]. \tag{5.25}$$

All the terms appearing in this expression are known analytically to order ϵ^0 in the case of two-loop master integrals, and to order ϵ^1 in the case of one-loop master integrals see *e.g.* [214]. This allowed us to verify than no pole survives from this term. Additionally, we could check that all the remaining poles in $\Gamma(p^2, m^2)$ cancel.

5.2.4 Finite parts

Once we have checked that our expression of $\Gamma(p^2)$ is UV-finite, we must carefully analyze the ϵ-expansion of the various terms appearing in Eq. (5.23) in order to not to miss any finite contribution. Since in the products $Z_{A,1}^2$, $Z_{A,1}Z_{\lambda,1}$, $Z_{A,1}\Gamma_1$, $Z_{\lambda,1}\Gamma_1$ and $Z_{m^2,1}\frac{\partial\Gamma_1}{\partial m^2}$, all of them contributing to the order λ^2, both of the terms involved in each product feature poles in ϵ^{-1}, the ϵ^1 order of each factor yields a finite contribution. As a consequence, $\Gamma_1(p^2, m^2)$ and $Z_{X,1}$ must be expanded to order ϵ^1. In contrast, $\Gamma_2(p^2, m^2)$ as well as $Z_{X,2}$ must be retained just to order ϵ^0, since no product involving such quantities intervene at order λ^2.

In brief, one could argue that the one-loop master integrals A and B must be expanded to order ϵ^1 whereas two-loop master integrals I, S, U, M and also the non-master integral T must be expanded to order ϵ^0. However, since the term (5.25) introduces an extra pre-factor ϵ^{-1}, the integrals in there must be expanded to an order higher. More precisely, A_m, B_{00} and B_{m0} need to be expanded to order ϵ^2 whereas I_{m00}, S_{000}, S_{m00}, U_{00m0} and U_{0m00} need to be expanded to order ϵ^1. In the case of the two-loop master integrals, we found the coefficients associated to the ϵ^1 term by means of the procedure described in Appendix E.

5.3 Crosschecks

Since the reduction of $\Gamma_2(p^2, m_B^2)$ into master integrals employs a routine with several steps and generate a significant amount of terms, we need to test the reduced expression as much as possible. In what follows we briefly review the tests we implemented. All of them are of the same nature as those shown for the ghost-antighost-gluon vertex in Section 4.3: we know beforehand some specific behavior of $\Gamma(p^2)$ which is not necessarily described by the individual terms composing its

reduced expression. As a consequence, very precise cancellations among such term should occur in order to produce the appropriate behavior of $\Gamma(p^2)$.

Below we study the UV and IR behavior of $\Gamma(p^2)$ as well as the zero mass limit. In addition, the reduced expression of $\Gamma(p^2)$ displays an apparent divergence at $p^2 = m^2$. Since this Euclidean configuration is not special, it should be a spurious divergence, resulting from the particular procedure we implemented in order to carry out the reduction to master integrals. We verified that this is indeed the case.

5.3.1 UV asymptotic behavior

Due to the Weinberg's theorem [225], we know that the leading order of the UV expansion of the three-gluon dressing function is dictated by the superficial degree of divergence of the diagrams contributing to such quantity. This is $D = 1$. However, owing to the factorization of a factor p between this vertex and its corresponding dressing function, see Eq. (5.4), we infer that $\Gamma(p^2)$ features a logarithmic behavior at large p^2.

This behavior is not described by the individual terms contributing to $\Gamma(p^2)$, which can grow much faster. In order to test that the cancellations among these terms actually occur, we used UV expansions for all the master integrals involved in $\Gamma(p^2)$. Such expansions were found by using our own implementation of the algorithm described in Ref. [226].

At leading order of the $p \to \infty$ expansion, we find[3]

$$\begin{aligned}\Gamma(p \to \infty) = 1 + \lambda(\mu) &\left[\frac{37}{24} + \frac{17}{12}\ln\left(\frac{p^2}{\mu^2}\right)\right] \\ &+ \lambda^2(\mu)\left[\frac{153}{32} + \frac{143}{96}\ln\left(\frac{p^2}{\mu^2}\right) - \frac{51}{32}\ln\left(\frac{p^2}{\mu^2}\right)^2 + \frac{5}{16}\zeta(3)\right] + \mathcal{O}\left(\frac{m^2}{p^2}\right).\end{aligned} \tag{5.26}$$

As anticipated, the three-gluon dressing function grows logarithmically in the UV. In addition, we observe that the power of the logarithms increases with the loop order. This particular aspect of the expansion makes clear the need to choose a renormalization scale of the type $\mu(p) \sim p$ in the UV. Otherwise, when $\ln\left(\frac{p^2}{\mu^2}\right) \sim 1/\lambda$, we have one- and two-loop terms of the same order of magnitude which invalidates the use of perturbation theory.

5.3.2 IR asymptotic behavior

As we discussed in Section 5.1.1, the exact leading asymptotic behavior of the three gluon dressing function is given by a linear logarithm, which is in essence of one-loop origin, multiplied by the cube of the ghost dressing function at zero momentum. Expanding Eq. (5.9) to two-loop order and using the renormalization condition $Z_A^{1/2} Z_c Z_A = 1$, we find

$$\Gamma(p^2, \mu) \sim \frac{\lambda(\mu)}{24} \ln \frac{p^2}{\mu^2}(1 - 3\sigma_1), \tag{5.27}$$

[3] In the UV, since the perturbative expansions makes sense only with a running scale where $\mu \sim p$, we have also expanded with respect to μ.

where σ_1 is the k^2-coefficient of the one-loop ghost self-energy $\Sigma(k)$ in the $k \to 0$ limit.

Similarly to the UV case, this is not the behavior of the individual terms that make the reduced expression of $\Gamma(p^2)$. So, in order to find out if our expression of the three-gluon dressing function do behave according to Eq. (5.27), we determined the IR expansion for all the integrals involved in $\Gamma(p^2)$. We achieved this by implementing the algorithm described in Ref. [216]. In a few instances we also used the algorithm from [227].

At first non-trivial order of the $p \to 0$ expansion, we find

$$\begin{aligned}\Gamma(p^2,\mu) = 1 + \frac{\lambda(\mu)}{24}\left[\ln\left(\frac{p^2}{\mu^2}\right)(1-3\tau_1) + C_1(m^2/\mu^2)\right] \\ + \frac{\lambda^2(\mu)}{24}\left[C_2(m^2/\mu^2) + \mathcal{O}\left(\frac{p^2}{m^2}\right)\right],\end{aligned} \tag{5.28}$$

where

$$\tau_1 = \frac{\lambda(\mu)}{4}\frac{\mu^2}{m^2}\left(\frac{m^4}{\mu^4} + \frac{5}{2}\frac{m^2}{\mu^2} + \ln\frac{\mu^2}{m^2} - \left(1+\frac{m^2}{\mu^2}\right)^3 \ln\left[1+\frac{\mu^2}{m^2}\right]\right), \tag{5.29}$$

which we checked equals σ_1 in the IRS scheme. Thus, the IR expansion of the three-gluon dressing function is compatible with the exact relation (5.9).

5.3.3 Regularity at $p^2 = m^2$

As we just saw, our expression is not regular at $p = 0$. This is a genuine singularity, associated to the zero-crossing. However, other terms in the reduced expression of $\Gamma(p^2)$ are singular at $p^2 = m^2$. There is nothing special about this specific Euclidean configuration. Therefore, we expect this divergence to be spurious, *i.e.* an artifact coming from the particular reduction we implemented. The residue corresponding to the sum of all the singular contributions at $p^2 = m^2$ reads

$$\begin{aligned}\frac{\lambda^2}{64}\Bigg[\frac{2-d}{d-1}A_m B_{00}(m^2) - \frac{m^2(d-3)}{d-1}B_{00}(m^2) \\ + \frac{2-d}{d-1}I_{m00} - \frac{(4-d)m^4}{2(d-1)}M_{0000m}(m^2)\frac{3d-8}{d-1}S_{m00}(m^2)\Bigg].\end{aligned} \tag{5.30}$$

Since the one- and two-loop master integrals in the above equation are known analytically in $d = 4 - 2\epsilon$ dimensions to order ϵ^1 and ϵ^0, respectively, we could verified that Eq. (5.30) indeed vanishes, at least to order ϵ^0. Of course, higher orders in ϵ are irrelevant in our analysis.

5.3.4 Zero mass limit

As a final check on our calculation of the three-gluon dressing function, we can compute the zero mass limit $\Gamma_{m^2\to 0}(p^2)$. This is regular for any $p^2 > 0$ and has been computed in [228]. This check is double since individual terms in the expression of $\Gamma(p^2)$ are not necessarily regular in that limit and cancellations must occur in order to produce the correct result.

As explained in Section 4.3.4, by using dimensional analysis it is straightforward to see that the low mass expansion is equivalent to the large momentum expansion. As a consequence, $\Gamma_{m^2\to 0}(p^2)$ is simply the leading term in Eq. (5.26). Since the authors of [228] used a different renormalization than us, we compared the bare results, which do coincide in Landau gauge.

5.4 Renormalization group

As we mentioned in Section 5.3.1, in order to control the perturbative expansion in the UV we must work with a running scale such that $\mu(p) \sim p$ in the UV. In addition, there are potentially hazardous terms of the type $\ln(m^2/\mu^2)$ in the IR, as we discussed in Section 5.1.1. A way to elude both problem is to choose a variable renormalization scale of the form $\mu = \sqrt{p^2 + m_0^2}$, which ensures no large logarithms survive neither in the UV nor in the IR[4]. Nonetheless, for the purpose of comparing with the lattice simulations, we need to evaluate the dressing function at a fixed renormalization scale μ_0. In order to find such function we can exploit the Callan-Symanzik equation, see Section 1.5.3, whose solution is given by (1.142). As for a purely gluonic function it reads

$$\Gamma^{(n_A)}(p, \mu_0, \lambda_0, m_0^2) = z_A(\mu, \mu_0)^{-n_A/2}\Gamma^{(n_A)}(p, \mu, \lambda(\mu), m^2(\mu)), \tag{5.31}$$

where $z_A(\mu, \mu_0)$ is defined by Eq. (1.143). In our case, this equation is extremely useful, since it relates $\Gamma(p^2, \mu_0)$ with a quantity which can be safely computed within the perturbative approach, $\Gamma(p^2, \mu)$ with $\mu = \sqrt{p^2 + m_0^2}$:

$$\Gamma(p^2, \mu_0) = \frac{\lambda(\mu)}{\lambda(\mu_0)} \frac{\Gamma(p^2, \mu)}{z_A(\mu, \mu_0)^{3/2}}. \tag{5.32}$$

We have already computed the function $z_A(\mu, \mu_0)$ in the IRS scheme, see Eq. (3.23). By plugging that result into Eq. (5.32), we finally arrive at

$$\Gamma(p^2, \mu_0) = \frac{\lambda^{5/2}(\mu)}{\lambda^{5/2}(\mu_0)} \frac{m^6(\mu_0)}{m^6(\mu)} \Gamma(p^2, \mu). \tag{5.33}$$

5.5 Results

In this section we present the results of the two-loop evaluation of the three-gluon dressing function in the CF model and their comparison to lattice data for the SU(3) and SU(2) gauge groups. We remark that these results are, up to a normalization constant, a pure prediction of the model because the parameters λ_0 and m_0 are determined by fitting the ghost and gluon two-point functions to lattice data. Since the lattice data of the three-gluon dressing function, to which we compare our results with, were not generated in the same renormalization scheme as the one we used, we must allow an overall normalization constant $\mathcal{N}$[5]. This quantity is adjusted so as to minimize the absolute error, χ, between the

[4] It is important to note that the genuine logarithm in the IR, associated with the zero-crossing, does survive when using this prescription.

[5] At an exact level, the normalization factors associated to the gluon and ghost two-point functions are related to the three-gluon dressing function normalization factor provided that one

predicted three-gluon dressing function, $\Gamma(p^2, \mu_0)$ (from now on denoted as $\Gamma(p^2)$), and the lattice data:

$$\chi^2_\Gamma = \frac{1}{N}\sum_{i=1}^{N}\left(\frac{\Gamma_{\text{latt.}}(p_i^2) - \mathcal{N}\,\Gamma(p_i^2)}{\Gamma_{\text{latt.}}(p_N^2)}\right)^2, \tag{5.34}$$

where the sum runs over the lattice points. Consequently,

$$\mathcal{N} = \frac{\sum_{i=1}^{N}\Gamma_{\text{latt.}}(p_i^2)\Gamma(p_i^2)}{\sum_{i=1}^{N}\Gamma(p_i^2)^2}. \tag{5.35}$$

Even though at first sight one might think that the relative or averaged error, such as the one from Eq. (3.27), is better for estimating the error, actually this is not the case. In any of those definitions, the relative error overweights the deep IR region, since the lattice values are very close to zero. Moreover, such error definitions do not lead to reasonable values of the normalization constant $\mathcal{N}$.

5.5.1 SU(3)

In the case of the SU(3) group we compared our results with two sets of lattice data [19, 230], while the fits of the ghost and gluon two point functions were done using lattice data from Ref. [203, 204][6]. The comparison between the CF prediction of the three-gluon dressing function and the lattice data is displayed in Fig. 5.3. In that plot, as any other plot we show in the rest of this chapter, the vertical axis refers to the dressing function, $\Gamma(p)$, whereas the horizontal axis refers to the momentum in GeV.

Concerning the zero-crossing, two-loop corrections move its position deep in the IR, where no lattice data are available[7]. More precisely, whereas the location of the zero-crossing is around $p = 313$ MeV at one-loop order, it is pushed down to $p = 1.96$ MeV approximately at two-loop order. Of particular interest is the comparison of the model outcome with the lattice results from Ref. [230] in Fig. 5.3, in which the zero-crossing is absent, thus contradicting the one-loop result. Quite impressively, this discrepancy is fixed once two-loop corrections are included in the calculation.

Moreover, as can be observed in Fig. 5.3, the two-loop evaluation yields qualitative differences in the IR in relation to the one-loop evaluation. More precisely, at a scale of around 0.5 GeV the two-loop result of $\Gamma(p^2)$ features an upbending behavior not observed at one-loop order.

is working with a scheme where the identity $Z_A^{1/2} Z_c Z_g = 1$ holds. As a consequence, we should be able of determining $\mathcal{N}$ entirely in terms of the normalization constants used when fitting the two-point functions if we had exactly the same numerical setup for the lattice data of the three quantities involved. Unfortunately, this is not the case.

[6] Although the CF ghost and gluon two-point functions in the IRS scheme were already fitted to lattice data in Ref. [54], for this work we had to redo the fits since instead of $\mu(p) = p$ we used $\mu(p) = \sqrt{p^2 + m_0^2}$. The differences between the fits of the two-point functions, deriving from using either $\mu(p) = p$ or $\mu(p) = \sqrt{p^2 + m_0^2}$, are about 0.4%. The latter tends to improve the one-loop fits, while it worsens the two-loop fits by the same amount. For completeness, we also used the (invalid) prescription $\mu = p$ to predict the three-gluon dressing function obtaining much poorer results than for $\mu(p) = \sqrt{p^2 + m_0^2}$, as expected. The same applies for the SU(2) case.

[7] As we discussed in Section 5.1.1, the three-gluon dressing function from the CF model features a zero-crossing at all orders of perturbation theory, due to the presence of an exact IR logarithmic divergence.

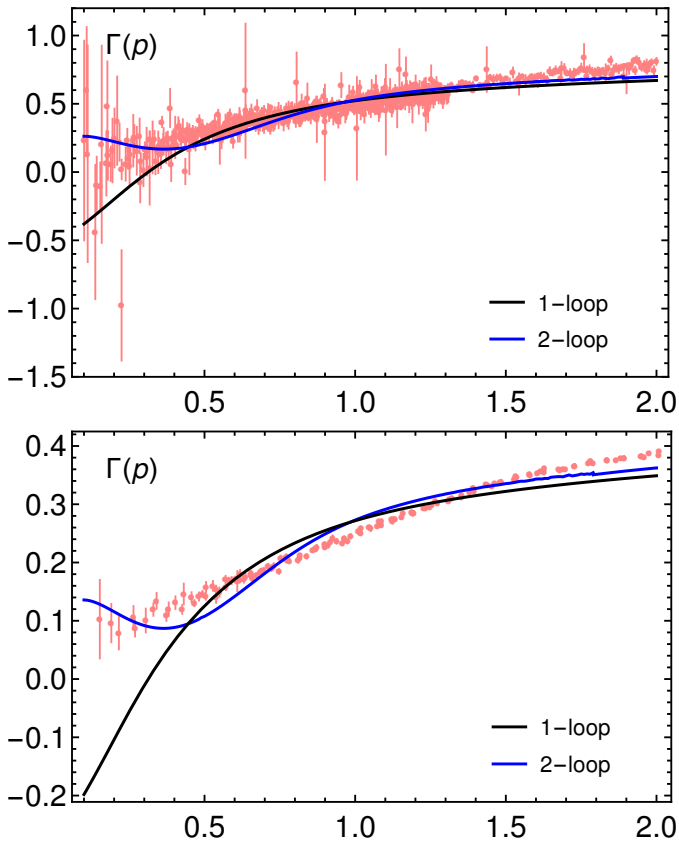

Figure 5.3: Predicted one- and two-loop three-gluon dressing function from the CF model compared with the SU(3) lattice results from Ref. [19] (top) and Ref. [230] (bottom).

In Table 5.1 we show the absolute error between the CF prediction of $\Gamma(p^2)$ and lattice simulations. For completeness we also show the joint error associated to the ghost and gluon dressing functions, F and D, defined as

$$\chi^2_{FD} = \frac{1}{2}(\chi^2_F + \chi^2_D), \tag{5.36}$$

with χ_F and χ_D defined according to Eq. (3.26).

Concerning the three-gluon dressing function, as for Ref. [230] we find a much lower error at one- and two-loop order. This could be attributed to a smaller incertitude of the data in comparison to lattice results from [19], particularly in the deep IR, where the data displays larger error bars and a much larger number of points. In any case, both the one- and two-loop calculation of $\Gamma(p^2)$ is totally compatible with lattice data from [19]. We emphasize, again, that these results are a pure prediction of CF.

We can conclude that, for the SU(3) gauge group, in line with the two-loop evaluation of the two-point functions as well as the ghost-antighost-gluon vertex, the perturbative CF model is able to describe both at a qualitative and at a quantitative level the available lattice data. More importantly, successive perturbative orders tend to improve the agreement with the lattice simulations, which is consistent with a controlled perturbative expansion.

order	λ_0	m_0 (MeV)	$\chi_{FD}(\%)$	$\chi_{\Gamma,A}(\%)$	$\chi_{\Gamma,C}(\%)$
1-loop	0.30	350	4.6	13.0	11.6
2-loop	0.27	320	3.2	10.6	5.5

Table 5.1: This table shows, depending on the loop order, the values of the parameters which best fit the lattice data from Ref. [203, 204] for the ghost and gluon two-point functions; the joint error, see, of the gluon and ghost dressing functions for such fits and the individual errors of the predicted three-gluon dressing function with respect to lattice simulations from Ref. [19], denoted as $\chi_{\Gamma,A}$ and from Ref. [230], denoted as $\chi_{\Gamma,C}$.

5.5.2 SU(2)

For the SU(2) gauge group we compared the CF prediction of $\Gamma(p^2)$ with the lattice data from Ref. [159], while the ghost and gluon two-point functions were fitted to lattice data from [50]. The plot comparing the lattice data with the two-loop CF evaluation of $\Gamma(p)$ is displayed in Fig. 5.4.

Two-loop corrections present a qualitative behavior similar than the one of the SU(3) case. Also in this case, two-loop corrections move the position of the zero-crossing deeper in the IR. Both calculations, at one- and two-loop order reproduce very well the lattice data.

The absolute error between the predicted CF three-gluon dressing function and the lattice data is provided in Table 5.2. We also include the joint error of the ghost and gluon dressing functions. In line with results from Chapters 3 and 4, the errors are larger than for the SU(3) case. In any case, at a much modest scale than for the SU(3) gauge group, we also observe that the two-loop evaluation features a smaller error in comparison with the one-loop calculation, which is consistent with the perturbative approach we used. Finally, we could also argue that, given the incertitude of the lattice data, a much smaller error would not have much sense.

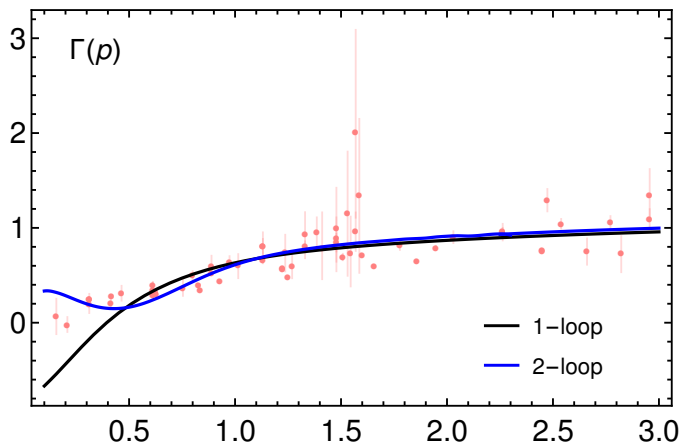

Figure 5.4: Predicted one- and two-loop three-gluon dressing function from the CF model compared with the SU(2) lattice data from Ref. [159].

order	λ_0	m_0 (MeV)	$\chi_{FD}(\%)$	$\chi_\Gamma(\%)$
1-loop	0.42	400	7.5	15.5
2-loop	0.38	400	4.9	12.2

Table 5.2: This table shows, depending on the loop order, the values of the parameters which best the lattice data from Ref. [50] for the ghost and gluon two point functions; the joint error of the gluon and ghost dressing functions for such fits and the individual error of the predicted three-gluon dressing function in comparison to lattice data from Ref. [159].

5.5.3 Scheme dependence

A complementary way of testing the perturbative approach within the CF model is given by estimating the scheme dependence of the three-gluon dressing function, as we explained in Section 3.3.5. If our perturbative expansion becomes more precise as we include higher orders of the perturbative expansion, two-loop corrections should be less sensitive to a change in the renormalization scheme. To test this, we also computed the three-gluon different by using the VM scheme, see Section 3.3.5. Since this renormalization scheme features a Landau pole in the IR we need to stop the flow before reaching that scale. This can be accomplished by using a renormalization scale such that $\mu = \sqrt{p^2 + \alpha m_0^2}$. We carried out the evaluation of $\Gamma(p^2)$ in the VM scheme with $\alpha = 1$ and $\alpha = 2$.

In order to estimate the difference between the IRS and the VM scheme we used the quantity $\mathcal{H}$, defined by Eq. (3.39). The results are shown in Tables 5.3 and 5.4 for the SU(3) and SU(2) gauge groups, respectively. We note that the scheme dependence systematically improves once two-loop corrections are included. Moreover, we observe a stronger dependence in the the case of SU(2), in line with the previous observations.

order	$\mathcal{H}_{\alpha=1,\mathrm{A}}(\%)$	$\mathcal{H}_{\alpha=2,\mathrm{A}}(\%)$	$\mathcal{H}_{\alpha=1,\mathrm{C}}(\%)$	$\mathcal{H}_{\alpha=2,\mathrm{C}}(\%)$
1-loop	5.1	5.3	2.4	2.5
2-loop	3.1	2.9	1.6	1.5

Table 5.3: Scheme dependence for the SU(3) gauge group. The normalization of the three-gluon dressing function was chosen so as to minimize the disagreement with lattice simulations from Ref. [19], in the case of $\mathcal{H}_{\alpha,\mathrm{A}}$, and with lattice data from Ref. [230], in the case of $\mathcal{H}_{\alpha,\mathrm{C}}$.

order	$\mathcal{H}_{\alpha=1,\mathrm{A}}(\%)$	$\mathcal{H}_{\alpha=2,\mathrm{A}}(\%)$
1-loop	11.6	11.3
2-loop	5.1	5.7

Table 5.4: Scheme dependence for the SU(2) gauge group. The normalization of the three-gluon dressing function was chosen so as to minimize the disagreement with lattice simulations from Ref. [159].

For completeness we present the values of the parameters which best fit the gluon and ghost dressing functions in VM for SU(3), Table 5.5 and SU(2) Table 5.6.

	$\lambda_{0,2\text{ loop}}$	$m_{0,2\text{ loop}}$ (MeV)	$\lambda_{0,1\text{ loop}}$	$m_{0,1\text{ loop}}$ (MeV)
VM $\alpha = 1$	0.39	500	0.36	500
VM $\alpha = 2$	0.36	500	0.42	600

Table 5.5: Values which best fit the CF gluon and ghost dressing functions to lattice data from Refs. [203] (gluon) and [204] (ghost), corresponding to the SU(3) gauge group in the VM scheme.

	$\lambda_{0,2\text{ loop}}$	$m_{0,2\text{ loop}}$ (MeV)	$\lambda_{0,1\text{ loop}}$	$m_{0,1\text{ loop}}$ (MeV)
VM $\alpha = 1$	0.46	600	0.20	600
VM $\alpha = 2$	0.36	600	0.22	600

Table 5.6: Values which best fit the CF gluon and ghost dressing functions to lattice data from Ref. [50], corresponding to the SU(2) gauge group in the VM scheme.

Chapter 6

QCD two-point functions

In the previous chapters we investigated the two-loop corrections to correlation functions in the pure gauge sector from the CF model. In this chapter we extend that analysis to all two-point functions in the presence of two mass-degenerate quark flavors. We compare our evaluations to lattice data from [11, 163]. These results were published in [61].

Within the functional method approaches to QCD, the quark propagator is of central importance and as such it has been widely investigated, see e.g. [22, 126, 243–247]. Lattice studies have also provided valuable information regarding this matter [11, 160, 161, 163, 248, 249]. Recently, the quark propagator has also been addressed in the context of the screened perturbation theory approach [187].

Before proceeding with the calculation, in the next section we make some preliminary remarks about what changes are introduced in the CF model once we abandon the quenched approximation. More precisely, we clearly state what outcomes do we expect from the model and what limitations naturally arise as a result of maintaining a purely perturbative approach.

6.1 Some preliminary remarks

The comparisons between the two-loop evaluations and lattice data, presented in the previous chapters, are compatible with a perturbative analysis in the pure gauge sector within the CF model. This is reinforced by lattice simulations which show a coupling compatible with a perturbative analysis both in the IR and in the UV *in the absence of quarks*. As we discussed in Section 3.2, in the unquenched theory the situation is less auspicious, since the perturbative expansion on the lattice could, in principle, take values beyond the range of validity of any perturbative approach. As it is not fully clear which parameter governs the perturbative expansion in the CF model, the perturbative evaluation of the two-point functions is of great importance in order to test the validity of the model in the presence of quarks.

This work is a continuation of a one-loop investigation of the two-point functions from the CF model in Landau gauge, in the presence of quarks [58]. The functions were evaluated in the IRS scheme for an arbitrary number of colors (N), degenerate flavors (N_f) and dimensions d, and compared with lattice data for $d = 4$, $N = 3$ and $N_f = 2$, $2 + 1$ or $2 + 1 + 1$ flavors [160, 161, 163, 249]. The results described very well the gluon and ghost two-point functions. In con-

trast, the quark dressing function was wrongly described by the model even at a qualitative level.

In principle, such disappointing result could be attributed to a limitation of the perturbative CF model. However, as the authors of [58] pointed out, the two-loop evaluation of the quark dressing function is completely necessary in order to discard the following alternative explanation. In the massless gluon case, the one-loop correction to the quark dressing function identically vanishes, which makes of the two-loop correction the actual leading term in the perturbative expansion. To some extent, the CF model could feature a similar behavior. Despite being non-zero, the one-loop contribution could be abnormally tiny and, as a result, two-loop corrections would be fundamental to consistently include the leading term of the perturbative series. Moreover, the authors of [58] estimated the potential two-loop contribution and they concluded that it could greatly diminish the tension between the model and the lattice data. This is one of the central motivations to extend the computation of [58] to two-loop order.

Another quantity derived from the quark propagator is the quark mass function, which is directly related to the chiral symmetry breaking (χSB). Being a key aspect of infrared QCD, since it is responsible for the overwhelming majority of the mass of the hadrons, χSB cannot be grasped by using purely perturbative approaches, see for instance [62][1]. Nonetheless, the perturbative CF model still could be useful for studies where the quark masses are artificially large. As a consequence, it is a matter of interest of the present work to investigate to which extent the accuracy of the perturbative CF model varies as we approach the chiral limit. To that end, we compared our results with two sets of lattice data, one close to the chiral limit ($M_\pi = 150$ MeV) and other far from it ($M_\pi = 422$ MeV).

It is important to bear in mind that the fact that the perturbative CF model is unable to reproduce χSB, reveals a deficiency of the pertubrative framework rather than the CF model itself. In fact, the CF model has been used beyond perturbation theory by using the so called Rainbow Improved (RI) expansion scheme [192, 250]. This approximation consists in preserving the standard perturbative expansion in the pure gauge sector whereas in the quark sector the expansion is performed in the inverse of the number of colors $1/N_C$, retaining all the orders in the quark coupling. Despite $N_c = 3$ in QCD, it is well-known that a $1/N_c$ expansion captures essential aspects of the dynamics, see [251–253]. Proceeding in this way the CF is able to reproduce the χSB, even close to the chiral limit.

Finally, we mention that, regardless of whether the perturbative model is capable of describing the quark mass function, it is interesting in its own right to test whether the gluon, ghost and quark dressing functions admit a perturbative description within the CF approach. Of course, we cannot completely separate that investigation from the quark mass function. So, we also implement a couple of strategies to analyze the impact of the χSB on the two-loop dressing functions.

6.2 Generalities

We begin by fixing the notation and by defining the quark dressing function and the quark mass function. We continue by reintroducing the IRS scheme, now in

[1] This is because the loop corrections are proportional to the tree-level mass. Consequently, if we set $M = 0$ at tree-level, all the loop corrections will vanish.

the presence of quarks.

6.2.1 Notation

The ghost and gluon dressing functions, F and D, have already been defined in Eqs. (1.102) and (1.116), respectively. Since, for a two-point function, Feynman diagrams, see Eq. (3.8), are associated with the inverse of the propagator, it is convenient to work with

$$\Gamma(k) \equiv \frac{k^2}{F(k)}, \quad \text{and} \quad \Gamma^{\perp} = \frac{k^2}{D(k)}, \tag{6.1}$$

which are nothing but the inverse of the ghost and gluon propagator, respectively. As for the quark propagator, it is convenient to begin by taking into account that the derivative of the effective action, $\Gamma^{(2)}_{\psi\bar{\psi}}(k)$, can be written as

$$\Gamma^{(2)}_{\psi\bar{\psi}}(k) \equiv -i\not{k}\Gamma^{\gamma}(k) + \mathbb{1}\Gamma^{\mathbb{1}}(k). \tag{6.2}$$

The quark propagator is obtained by inverting this quantity. Its final expression can be easily found by multiplying and dividing by $i\not{k}\Gamma^{\gamma}(k)+\mathbb{1}$ and by taking into account that $\not{k}^2 = k^2$, which yields

$$S(k) = \frac{i\not{k}\Gamma^{\gamma}(k) + \mathbb{1}\,\Gamma^{\mathbb{1}}(k)}{k^2(\Gamma^{\gamma}(k))^2 + (\Gamma^{\mathbb{1}}(k))^2}. \tag{6.3}$$

It is customary to rewrite it as

$$S(k) = Z(k)\frac{i\not{k} + \mathbb{1}M(k)}{k^2 + M^2(k)}, \tag{6.4}$$

with

$$Z(k) \equiv 1/\Gamma^{\gamma}(k) \quad \text{and} \quad M(k) \equiv \Gamma^{\mathbb{1}}(k)/\Gamma^{\gamma}(k)\,. \tag{6.5}$$

By defining the *quark mass function*, $M(k)$, in this way, it becomes clear that it is a finite and renormalization group invariant quantity, since it is expressed as the quotient of two tensor components of the same two-point function.

6.2.2 Infrared safe scheme

As we did in Chapters 4 and 5 we will carry out the calculation in the IRS scheme. To completely characterize this scheme we must add to the renormalization conditions of the gauge sector, see Eqs. (3.10) and (3.11), the conditions

$$\Gamma^{\gamma}(k=\mu;\mu) = 1, \quad \Gamma^{\mathbb{1}}(k=\mu;\mu) = M(\mu). \tag{6.6}$$

The quantity $M(\mu)$ referrers to the *renormalized mass*. In the IRS scheme this mass coincide with the quark mass function defined above[2]. This derives from the fact that the bare components $\Gamma^{\gamma}(k)$ and $\Gamma^{\mathbb{1}}(k)$ renormalize identically, this is:

$$\frac{\Gamma^{\mathbb{1}}(k)}{\Gamma^{\gamma}(k)} = \frac{\Gamma^{\mathbb{1}}(k;\mu)}{\Gamma^{\gamma}(k;\mu)} = \frac{\Gamma^{\mathbb{1}}(k;k)}{\Gamma^{\gamma}(k;k)}, \tag{6.7}$$

where the left and right hand side of the equation correspond to the quark mass function and the renormalized mass in the IRS scheme at the scale $\mu = k$, respectively.

[2]For a generic renormalization scheme the renormalized mass and the quark mass function differ.

6.3 Two-loop evaluation

We begin this section by presenting the various elements we needed in order to carry out the calculation. Afterwards, we give a short review on the crosschecks we made to detect any possible error.

6.3.1 Diagrams

Since we will often refer to the various two-point functions simultaneously, it is convenient to denote them generically as Γ^C with $C \in \{\emptyset, \perp, \|, \gamma, \mathbb{1}\}$, where the symbol $\emptyset$ refers to the ghost component $\Gamma(k)$. By using this notation, we can write the bare two-loop expansion of any Γ^C as

$$\Gamma^C_B(k) = \Gamma^C_0(k^2, m_B^2, M_B) + \lambda_B \Gamma^C_1(k^2, m_B^2, M_B) + \lambda_B^2 \Gamma^C_2(k^2, m_B^2, M_B), \tag{6.8}$$

where $\Gamma^C_n(k^2, m_B^2, M_B)$ is the sum of n-loop diagrams contributing to $\Gamma^C(k)$. In the same way as we did for the ghost-antighost-gluon and the three-gluon vertex, we have factored out a term $\lambda_B \equiv \frac{g_B^2 N}{16\pi^2}$, where g_B is the dimensionless coupling. As usual, this translates into making the following replacement on the Feynman integrals

$$\int \frac{d^d p}{(2\pi)^2} \to \int_p \equiv 16\pi^2 \Lambda^{2\epsilon} \int \frac{d^d p}{(2\pi)^d}, \tag{6.9}$$

and dividing the color factors by N^n. The quantity Λ has mass dimensions and we introduced it to absorb the actual dimensions of the coupling.

The tree-level contributions $\Gamma^C_0(k^2, m_B^2, M_B)$ are given by

$$\Gamma_0 = k^2 \,,\, \Gamma_0^{\perp} = k^2 + m_B^2 \,,\, \Gamma_0^{\|} = m_B^2 \,,\, \Gamma_0^{\gamma} = 1 \,,\, \Gamma_0^{\mathbb{1}} = M_B \,. \tag{6.10}$$

There are 4, 1 and 1 Feynman diagrams for the gluon, ghost and quark two-point functions at one-loop order, respectively. These graphs were already computed in [58], the results being expressed in terms of the one-loop master integrals A and B, defined in Eq. (4.32).

At two-loop order there are a total of 23, 7 and 7 diagrams for the gluon, ghost and quark two-point functions, respectively. The diagrams were generated using the Fortran based Qgraf package [241]. One- and two-loop diagrams for all the two-point functions are displayed in Appendix C.

The two loop contributions to $\Gamma^C_2(k^2, m_B^2, M_B)$ can systematically be reduced to the evaluation of two-loop master integrals (4.33), as explained in Section 4.2.2. In this calculation we carried out such reduction by means of the Reduze implementation [254, 255] written in C++ with GiNaC [256]. We also used the symbolic manipulation language Form [257, 258] to deal with the algebra.

After this reduction, each function $\Gamma^C_2(k^2, m_B^2, M_B)$ is entirely expressed as a sum of two-loop master integrals and products of one-loop master integrals with rational coefficients that depend on the masses m and M, the momentum k, and the space-time dimension d. In addition, in the reduced expression we also found the non-master integrals

$$T_{m_1 m_2 m_3} = -\frac{\partial S_{m_1 m_2 m_3}}{\partial m_1^2} \quad \text{and} \quad V_{m_1 m_2 m_3 m_4} = -\frac{\partial U_{m_1 m_2 m_3 m_4}}{\partial m_1^2}. \tag{6.11}$$

There is no need to further reduce the integrals T and V since in $d = 4 - 2\epsilon$, the coefficients of the poles in ϵ can be easily extracted from the master integrals S and U. Moreover, the TSIL package we employed to numerically evaluate the finite parts of the two-loop master integrals can also be used to find the finite parts of T and V.

6.3.2 Renormalization

Once $\Gamma_1^C(k^2, m_B^2, M_B)$ and $\Gamma_2^C(k^2, m_B^2, M_B)$ have been reduced to master integrals, we proceed with the regularization of the integrals and the renormalization of the two-point functions. The former step is automatically satisfied because we are working in $d = 4 - 2\epsilon$ dimensions. The renormalization of the fields yields the identity Eq. (1.135), which in the context of this chapter is useful to write in the following way

$$\Gamma^C(k) = Z_C \Gamma_B^C(k), \tag{6.12}$$

with $Z_C \in \{Z_c, Z_A, Z_\psi\}$. In addition, we need to rewrite the bare masses and couplings in terms of the renormalized ones,

$$\lambda_B = Z_\lambda \lambda, \;\; m_B^2 = Z_{m^2} m^2, \;\; M_B = Z_M M. \tag{6.13}$$

Consequently, the renormalized counterpart of $\Gamma_B^C(k)$ is

$$\begin{aligned}\Gamma^C(k) = Z_C \Big(&\Gamma_0(k^2, Z_{m^2} m^2, Z_M M) + Z_\lambda \lambda \, \Gamma_1(k^2, Z_{m^2} m^2, Z_M M) \\ &+ (Z_\lambda \lambda)^2 \Gamma_2(k^2, Z_{m^2} m^2, Z_M M)\Big).\end{aligned} \tag{6.14}$$

Of course, since we are performing a two-loop calculation, we need to expand to the order λ^2. To do so, it is convenient to write the Z-factors as

$$Z_X = 1 + \delta Z_X, \tag{6.15}$$

where δZ_X is a shorthand notation for the loop contributions, i.e.

$$\delta Z_X = \lambda Z_{X,1} + \lambda^2 Z_{X,2} + \mathcal{O}(\lambda^3), \tag{6.16}$$

with $X \in \{c, A, \psi, \lambda, m^2, M\}$. Due to the fact that the term $\Gamma_2(k^2, Z_{m^2} m^2, Z_M M)$ in Eq. (6.14) is proportional to λ^2, we can safely make the replacement

$$Z_C (Z_\lambda \lambda)^2 \Gamma_2(k^2, Z_{m^2} m^2, Z_M M) \to \lambda^2 \Gamma_2(k^2, m^2, M). \tag{6.17}$$

For the other terms in Eq. (6.14) we certainly do have to consider the loop corrections. To that end, it is useful to introduce the operator

$$\mathcal{R} \equiv \delta Z_C + \delta Z_{m^2} m^2 \partial_{m^2} + \delta Z_M M \partial_M, \tag{6.18}$$

whose truncation to the n-order in λ will be written as $\mathcal{R}^n$. Thanks to this operator we can easily write the expansion to order λ^2 of Eq. (6.14) as

$$\begin{aligned}\Gamma^C(k) =& \Gamma_0^C(k^2, m^2, M) + \lambda \Gamma_1^C(k^2, m^2, M) + \lambda^2 \Gamma_2^C(k^2, m^2, M) \\ &+ \lambda(\lambda Z_{\lambda,1} + \mathcal{R}^1) \Gamma_1^C(k^2, m^2, M) + \mathcal{R}^2 \Gamma_0^C(k^2, m^2, M).\end{aligned} \tag{6.19}$$

6.3.3 Finite parts

Since Eq. (6.19) refers to a renormalized quantity, it must be UV finite, i.e. the various poles in ϵ, coming from the Z-factors and also from the one- and two-loop diagrams must cancel when considered as a whole. Thus, by imposing this condition we can determine part of the divergences of the Z-factors.

To go a little further with the analysis, let us make explicit the UV-divergences of the loop contributions to the Z-factors by writing them as

$$\begin{aligned} Z_{X,1} &= \frac{z_{x,11}}{\epsilon} + z_{x,10} + z_{x,1(-1)}\epsilon, \\ Z_{X,2} &= \frac{z_{x,22}}{\epsilon^2} + \frac{z_{x,21}}{\epsilon} + z_{x,20}. \end{aligned} \tag{6.20}$$

The divergences of the type ϵ^{-1} to order λ in Eq. (6.19) have only two possible sources, either $\Gamma_1^C(k^2, m^2, M)$ or $\mathcal{R}^1\Gamma_0^C(k^2, m^2, M)$. At the end, the coefficient corresponding to the term $\lambda\epsilon^{-1}$ must vanish, which allows us to determine the coefficients $z_{x,11}$. These terms are scheme-independent constants. We checked that the values we obtained coincide with the well- known results for them, see for example [259, 260]. The order λ^2 in Eq. (6.19) has potential poles in ϵ^{-2} and ϵ^{-1}. The former leads to the values of $z_{x,22}$ which, again, are scheme independent. We checked our values with the ones obtained by the authors of Refs. [259, 260] and they coincide. The pole ϵ^{-1} is related to the values of $z_{x,21}$, which do depend on the scheme. This can be seen by taking into account that, for instance, the term $\lambda^2 Z_{\lambda,1}\Gamma_1^C(k^2, m^2, M)$ contributes with a UV-term of the type $\lambda^2 1/\epsilon$, which is the sum of the two terms of the type $\epsilon^0 \times 1/\epsilon$. This implies that the scheme dependent, finite, part of $Z_{\lambda,1}$ intervenes in the final result of $z_{x,21}$.

To end this section, we mention that the term $z_{x,1(-1)}$ in $Z_{X,1}$ is absolutely necessary in our two-loop evaluation since it yields finite contributions. By looking, for instance, at the term $\mathcal{R}^1\Gamma_1^C(k^2, m^2, M)$ in Eq. (6.19), it is clear that the part proportional to ϵ in $\mathcal{R}^1$ leads to a finite contribution when multiplied with the term proportional to $1/\epsilon$ in $\Gamma_1^C(k^2, m^2, M)$.

6.4 Crosschecks

In this section we present the various crosschecks we performed on our expression for $\Gamma^C(k)$. Similarly to the cases of the ghost-antighost-gluon vertex and the three-gluon vertex, the resulting expression of $\Gamma^C(k)$ in terms of master integrals is made of a great amount of terms, which need to be tested in order to diminish the chance of error. We finally mention that all the crosschecks presented below can be performed prior to renormalization.

6.4.1 MS scheme and quenched limit

As a first crosscheck we verified that with our expressions we can retrieve the well-known values of the Z-factors in the minimal substraction (MS) scheme [259, 260].

Another initial test in the same direction consisted in taking the quenched limit on the reduced expressions for ghost and gluon two-point functions, which simply translates into taking the limit $N_f \to 0$. As we presented in detail in

Section 3.3, these two-point functions have already been evaluated in the quenched approximation in Ref. [54]. We verified the latter results coincide with the $N_f \to 0$ limit.

6.4.2 Ultraviolet behavior

From Weinberg's theorem, see Section 4.3.1, we know that the leading UV contribution of a certain Feynman graph is typically dictated by its superficial degree of divergence. As a consequence, we have

$$\lim_{k\to\infty} \frac{\Gamma(k)}{|k|^3} = 0, \quad \lim_{k\to\infty} \frac{\Gamma^{\perp}(k)}{|k|^3} = 0, \quad \lim_{k\to\infty} \frac{\Gamma^{\gamma}(k)}{|k|} = 0, \quad \text{and} \quad \lim_{k\to\infty} \frac{\Gamma^{\mathbb{1}}(k)}{|k|} = 0. \tag{6.21}$$

Typically, such behaviors are not those described by the individual terms that make up the expression of each $\Gamma^C(k)$ and very precise cancellations need to occur so as to produce the expected UV-behavior of $\Gamma^C(k)$. To check this, we UV-expanded each of the master integrals composing $\Gamma^C(k)$, by following essentially the same procedure as described in Section 4.3.1.

At leading order in $k \to \infty$ we find

$$\begin{aligned}\frac{\Gamma(k)}{k^2} = 1 - \lambda \left[1 + \frac{3}{4}\ln\left(\frac{\mu^2}{k^2}\right)\right] - \lambda^2 \left[\frac{1751}{192} - \frac{15}{16}\zeta(3) - \frac{95}{48}\frac{N_f}{N}\right.\\ \left. + \left(\frac{235}{48} - \frac{13}{12}\frac{N_f}{N}\right)\ln\left(\frac{\mu^2}{k^2}\right) + \left(\frac{35}{32} - \frac{1}{4}\frac{N_f}{N}\right)\ln^2\left(\frac{\mu^2}{k^2}\right)\right] + \mathcal{O}\left(\frac{m^2}{k^2}, \frac{M^2}{k^2}\right),\end{aligned} \tag{6.22}$$

$$\begin{aligned}\frac{\Gamma^{\perp}(k)}{k^2} &= 1 - \lambda \left[\frac{97}{36} - \frac{10}{6}\frac{N_f}{N} + \left(\frac{13}{6} - \frac{2}{3}\frac{N_f}{N}\right)\ln\left(\frac{\mu^2}{k^2}\right)\right]\\ &- \lambda^2 \left[\frac{2381}{96} - \frac{59}{8}\frac{N_f}{N} - \frac{55}{6}\frac{C_F}{N}\frac{N_f}{N} - \zeta(3)\left(3 + 4\frac{N_f}{N} - 8\frac{C_F}{N}\frac{N_f}{N}\right)\right.\\ &\left. + \left(\frac{137}{12} - \frac{25}{6}\frac{N_f}{N} - 2\frac{C_F}{N}\frac{N_f}{N}\right)\ln\left(\frac{\mu^2}{k^2}\right) + \left(\frac{13}{8} - \frac{1}{2}\frac{N_f}{N}\right)\ln^2\left(\frac{\mu^2}{k^2}\right)\right]\\ &+ \mathcal{O}\left(\frac{m^2}{k^2}, \frac{M^2}{k^2}\right),\end{aligned} \tag{6.23}$$

$$\begin{aligned}\Gamma^{\gamma}(k) =& 1 + \lambda^2 \frac{C_F}{N}\left[\frac{41}{4} - 3\zeta(3) - \frac{5}{8}\frac{C_F}{N} - \frac{7}{4}\frac{N_f}{N} + \left(\frac{25}{4} - \frac{3}{2}\frac{C_F}{N} - \frac{N_f}{N}\right)\ln\left(\frac{\mu^2}{k^2}\right)\right]\\ &+ \mathcal{O}\left(\frac{m^2}{k^2}, \frac{M^2}{k^2}\right),\end{aligned} \tag{6.24}$$

and

$$\frac{\Gamma^{\mathbb{1}}(k)}{M} = 1 + \lambda\frac{C_F}{N}\left[4 + 3\ln\left(\frac{\mu^2}{k^2}\right)\right] + \lambda^2\frac{C_F}{N}\left[\frac{1531}{24} + 13\frac{C_F}{N} - \frac{26}{3}\frac{N_f}{N}\right.$$
$$-\zeta(3)\left(21 - 12\frac{C_F}{N}\right) + \left(\frac{445}{12} + 12\frac{C_F}{N} - \frac{16}{3}\frac{N_f}{N}\right)\ln\left(\frac{\mu^2}{k^2}\right)$$
$$\left. + \left(\frac{11}{2} + \frac{9}{2}\frac{C_F}{N} - \frac{N_f}{N}\right)\ln^2\left(\frac{\mu^2}{k^2}\right)\right] + \mathcal{O}\left(\frac{m^2}{k^2}, \frac{M^2}{k^2}\right), \tag{6.25}$$

where $C_F = (N^2-1)/(2N)$. We note that, as expected, all the expansions satisfy Eq. (6.21).

To conclude the analysis in relation to the UV behavior, we mention that the following Slavnov-Taylor identity holds in the CF model [43]

$$\Gamma^{\parallel}_B(k)F_B^{-1}(k) = m_B^2, \tag{6.26}$$

where $\Gamma^{\parallel}$ is defined as

$$\Gamma^{(2)}_{A^a_\mu A^b_\nu}(k) \equiv \delta^{ab}\left(P^{\perp}_{\mu\nu}(k)\Gamma^{\perp}(k) + P^{\parallel}_{\mu\nu}(k)\Gamma^{\parallel}(k)\right). \tag{6.27}$$

By making a double expansion on (6.26), to the order λ^2 followed by a UV expansion, we have verified that this relation holds for large $|k|$.

6.4.3 Infrared behavior

In the limit $|k| \to 0$ we expect the functions $\Gamma^C(k)$ to be regular, since there are always enough massive propagators as to avoid any potential IR divergence. As for the ghost propagator, its IR behavior is even more limited because of its diagramatic structure. Since the external ghost and antighost legs can only be attached to a tree level ghost-gluon vertex, any loop correction has the form shown in Fig. 6.1. Then, following the notation of that figure, we can infer that any loop contribution will be proportional to a term of the type $k_\mu k_\sigma$. Consequently, since the loop diagram corresponding to the black circle is IR-finite, see end of Appendix H, we can affirm that the this correction tends to zero at leas as k^2 as $|k| \to 0$. In order to verify that our results for the various $\Gamma^C(k^2)$ do behave as we

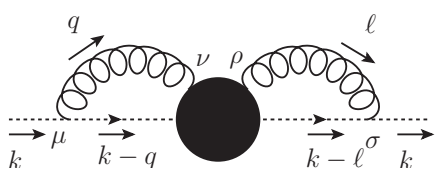

Figure 6.1: Diagramatic structure of any loop correction to the ghost propagator. The black circle represents further loop corrections.

expect, we IR-expanded each of the master integrals involved in such quantities. Luckily enough, all the master integrals had enough massive propagators to route the small momentum k to a massive propagator. By doing so, we can safely use the algorithm from Ref. [216], which ends up writing the expansion in powers

of k^2 with coefficients given by the k-independent masters A and I and their derivatives. The latter can always be computed by using iteratively the following relations

$$\partial_m A_m = \left(\frac{d}{2} - 1\right) \frac{A_m}{m^2}, \tag{6.28}$$

$$\begin{aligned}\Delta_{m_1 m_2 m_3} \partial_{m_3^2} I_{m_1 m_2 m_3} &= (d-3)(m_1^2 + m_2^2 - m_3^2) I_{m_1 m_2 m_3} \\ &+ (d-2)\left[A_{m_1} A_{m_2} + \frac{m_1^2 - m_2^2 - m_3^2}{2m_3^2} A_{m_1} A_{m_3} + \frac{m_2^2 - m_1^2 - m_3^2}{2m_3^2} A_{m_2} A_{m_3}\right],\end{aligned} \tag{6.29}$$

where the first derivative can be easily deduced by dimensional analysis and the second one by means of integration by parts techniques, see [216, 261]. By proceeding in this way we could, indeed, check that our reduced expressions for the two-point functions have the correct IR behavior.

6.4.4 Spurious singularities

The reduction from Feynman integrals to master integrals introduces some terms which are singular in some specific configurations. Nothing physically relevant occurs for such (Euclidean) configurations, so we expect the corresponding singularities to be spurious. More precisely, in the case of the ghost and gluon two-point functions we found potential singularities at $k^2 = 2m^2$ and $k^2 = 2M^2$. The residue corresponding to the pole $1/(k^2 - 2x^2)$ with $x = m$ and $x = M$ indeed vanishes, because of the following identity

$$\begin{aligned}&2(d-3)x^2 \left[6(d-4)x^4 M_{xxxx0}(2x^2) - (3d-8) S_{xx0}(2x^2)\right] \\ &= \left[(d-2)A_x - 2(d-3)x^2 B_{xx}(2x^2)\right]^2 - 8(d-3)^2 x^4 B_{xx}^2(2x^2),\end{aligned} \tag{6.30}$$

which can be derived by means of the Laporta algorithm.

In addition, all the two-point functions featured potential singular terms at $m = 2M$. For instance, as for $\Gamma^{\mathbb{1}}(k)$ the residue of $1/(m - 2M)$ is proportional to

$$\begin{aligned}&(d-2)(2A_M - A_{2M}) B_{M(2M)}(k) \\ &+ 4M^2 (T_{M(2M)(2M)}(k) - 2T_{(2M)(2M)M}(k) - (d-3) U_{(2M)M(2M)M}(k)),\end{aligned} \tag{6.31}$$

which, again, thanks to Laporta algorithm we could verify is zero. In the case of the gluon we had to check several cancellations in order to make sure that the residue of $1/(m - 2M)$ vanishes. These are:

$$\begin{aligned}&(d-2)(2A_M - A_{2M}) B_{MM}(k) \\ &- 4M^2 (T_{M(2M)M}(k) - 2T_{(2M)MM}(k) - (d-3) U_{MM(2M)M}(k)) = 0,\end{aligned} \tag{6.32}$$

$$(d-2) A_M B_{(2M)(2M)} + 2M^2 (T_{M(2M)M}(k) + (d-3) U_{(2M)(2M)MM}) = 0, \tag{6.33}$$

and

$$
\begin{aligned}
&(d-3)\left[(d-4)k^2M^2(k^2+4M^2)^2M_{MMMM0}(k)-2(3d-8)(k^2+4M^2)S_{MM0}\right]\\
&=\left[(d-2)^2A_M^2-2(d-2)(d-3)k^2A_MB_{MM}-2(d-3)^2k^2M^2B_{MM}^2\right](k^2+4M^2)\\
&-4(d-3)\left[3k^2T_{MM0}+4(d-3)(k^2+M^2)U_{0(2M)MM}\right.\\
&\left.-2(d-2)(k^2+M^2)A_MB_{(2M)M}\right](k^2-2M^2),
\end{aligned}
\tag{6.34}
$$

which we also checked.

6.4.5 Zero mass limit

The last check we implemented consisted in taking the limits $m \to 0$ and $M \to 0$ of the two-point functions at the same time, and comparing the results with an independent calculation for the same two-point functions but where m and M are set to zero from the beginning. Thus, this check works as a self-consistency test.

To calculate the limit we note that any master integral depending on the external momentum and the masses can be written as

$$
(\mu^{2\epsilon})^L\mathcal{F}(k^2,m^2,M^2)=(\mu^{2\epsilon})^L(k^2)^D\mathcal{F}(1,m^2/k^2,M^2/k^2),
\tag{6.35}
$$

where L is the number of loops and D is the mass dimension of the the integral. From this relation it is clear that, as we also discussed in Sections 4.3.4 and 5.3.4, the zero mass limit is equivalent to the leading term of the large $|k|$ expansion. As a result, the zero mass limit of the various $\Gamma^C(k^2)$ are nothing but the leading contributions in Eqs. (6.22) to (6.25). We have verified that these terms coincide with the independent calculation with $m = M = 0$ in the MS scheme.

6.5 Renormalization group

To compare our results with the lattice simulations it is enough to evaluate the two-point functions at a fixed renormalization scale μ_0. However, as we discussed in previous chapters, this introduces large logarithms in the UV, which invalidate the use of perturbation theory. To avoid them, one must choose a variable renormalization scale such that $\mu(p) \sim p$. Therefore, we will evaluate the two-point functions by using the renormalization scale $\mu = p$ and via the Callan-Symanzik equation Eq. (1.139) we will be able to determine the two-point functions at the fixed renormalization scale μ_0. For any of the two-point functions $\Gamma^C(k)$, the solution to the Callan-Symanizik equation is given by

$$
\Gamma^C(k;m_0^2,M_0,\lambda_0,\mu_0)=z_C^{-1}(\mu,\mu_0)\Gamma^C(k;m^2(\mu),M(\mu),\lambda(\mu),\mu),
\tag{6.36}
$$

where z_C is related to the anomalous dimension of the respective field, γ_C via Eq. (1.143). The latter, we recall, is defined as

$$
\gamma_C \equiv \frac{d\ln Z_C}{d\ln\mu}.
\tag{6.37}
$$

We have also used the definitions $m_0 \equiv m(\mu_0)$, $\lambda_0 \equiv \lambda(\mu_0)$ and $M_0 = M(\mu_0)$. In what follows we will write $\Gamma^C(k;m^2(\mu),M(\mu),\lambda(\mu),\mu)$ simply as $\Gamma^C(k,\mu)$.

After we have derived $\Gamma^C(k)$, we determine the Z-factors, evaluated at the scale μ, by means of the IRS scheme renormalization conditions. Next, the anomalous dimensions can be found by using Eq. (6.37)[3]. In the case of the ghost and gluon two-point functions, the relations from Section 3.3.1, derived for the pure YM theory in the IRS scheme, remain valid. Consequently, with the γ-functions we can determine the β-functions thanks to the identities

$$\beta_\lambda = \lambda(2\gamma_c + \gamma_A), \quad \text{and} \quad \beta_{m^2} = m^2(\gamma_A + \gamma_c). \tag{6.40}$$

From these functions, and using $\mu = k$, it is possible to determine the gluon and ghost dressing functions, see Section 3.3.2, as

$$F(k,\mu_0) = \frac{\lambda(k)}{\lambda_0}\frac{m_0^2}{m^2(k)}, \tag{6.41}$$

$$D(k,\mu_0) = \frac{\lambda_0}{\lambda(k)}\frac{m^4(k)}{m_0^4}\frac{k^2}{k^2+m^2(k)}, \tag{6.42}$$

respectively.

As for the quark mass function, since it coincides with the renormalized quark function in the IRS scheme, it can be derived from

$$\frac{\beta_M}{M} = -\frac{d\ln Z_M}{d\ln\mu}, \tag{6.43}$$

which stems from the fact that the bare quark mass is renormalization scale independent, i.e. $\frac{dM_B}{d\ln\mu} = 0$. In the case of the quark dressing function, by taking into account that $Z(k,\mu_0) = 1/\Gamma^\gamma(k,\mu_0)$ and $\Gamma^\gamma(k,\mu_0) = z_\psi^{-1}(k,\mu_0)\Gamma^\gamma(k,k)$, and by using the IRS renormalization condition $\Gamma^\gamma(k,k) = 1$, we get

$$Z(k,\mu_0) = z_\psi(k,\mu_0). \tag{6.44}$$

6.5.1 Asymptotic behaviors

We have computed the UV- and IR-asymptotic expansions of the various two-loop γ-functions at next-to-leading order. There are rather lengthy, so we collect them in Appendix I.

[3]The anomalous dimension can be expressed in terms of the factors introduced in Eq. (6.20) as, see App. B of Ref. [61] for details,

$$\gamma_X = g^2\frac{\partial z_{X,10}}{\partial\ln\mu} + g^4\left(\frac{\partial z_{X,20}}{\partial\ln\mu} - \left(\frac{\partial z_{X,10}}{\partial\ln\mu} + \frac{\partial z_{g^2,10}}{\partial\ln\mu}\right)z_{X,10} - \left(\frac{\partial z_{X,1(-1)}}{\partial\ln\mu} + \frac{\partial z_{g^2,1(-1)}}{\partial\ln\mu}\right)z_{X,11} - \sum_i \frac{\partial z_{m_i^2,10}}{\partial\ln\mu}\frac{\partial z_{X,10}}{\partial\ln m_i^2}\right), \tag{6.38}$$

where the sum is taken over the possible mass values of the theory in question. In our case this is $m_i = m$ and $m_i = M$. Furthermore, this derivation, imposes, in order to obtain a finite expression for γ_X the constraints

$$0 = \frac{\partial z_{X,11}}{\partial\ln\mu} = \frac{\partial z_{X,22}}{\partial\ln\mu} = \frac{\partial}{\partial\ln\mu}(z_{X,21} - (z_{X,10} + z_{g^2,10})z_{X,11}). \tag{6.39}$$

The first two conditions hold automatically, as we have already seen in Section 6.3.3. We checked that the Z-factors we obtained in this calculation also verify the last condition.

6.6 Results

As already stated above, a fully perturbative investigation only makes sense for those quantities which are in principle less sensitive to the χSB. Thus, in a first stage we concentrate our analysis on the ghost, gluon and quark dressing functions. To carry out such analysis we adopt two different strategies. The first one consists simply in determining the parameters λ_0, m_0 and M_0 which best fit the dressing functions to the lattice data. The second one studies the prediction of one of the dressing functions by fitting to lattice data the other two. All the fits are performed for two sets of lattice data, one close to the chiral limit and another far from it. This would allow us to detect any significant modification of the CF dressing functions in relation to lattice data when approaching the chiral limit. Both strategies leave aside any information directly related to the lattice quark mass function.

In a second stage we investigate the quark mass function. At first, we test to which extent the CF model is able to predict the lattice quark mass. Of course, in this analysis we expect different outcomes depending on how close to the chiral limit the quark mass is, so we perform the analysis for the two sets of lattice data mentioned in the preceding paragraph. In a second analysis we perform a global fit to lattice data for the three dressing functions and the quark mass. We know beforehand that we are taking the perturbative model beyond its limits when trying to include the quark mass in the fit. However, such analysis is still useful to make explicit the limitations within the perturbative approach.

We close this chapter by investigating the impact of the non-perturbative mass on the perturbative description of the dressing functions from the CF model. This analysis comes to complement the first investigation, in which we fit the dressing functions without taking into account the lattice quark mass.

6.6.1 Dressing functions

As we explained in the previous section, a set of values λ_0, m_0 and M_0 determines, up to a normalization factor, the gluon, ghost and quark dressing functions. Thus, the fits to lattice data were preformed by using the values λ_0, m_0 and M_0 which minimized the error between the CF model outcome and the lattice data. In this section we choose $\mu_0 = 1$ GeV.

Global fit

In this section we fit simultaneously the gluon, ghost and quark dressing functions to lattice data from Refs. [11, 163]. To achieve this, we minimized the joint error χ_{DFZ}, defined as

$$\chi^2_{DFZ} \equiv \frac{1}{3}\left[\chi^2_D + \chi^2_F + \chi^2_Z\right], \tag{6.45}$$

where

$$\chi^2_X = \frac{1}{N}\sum_i \left(\mathcal{N}_X \frac{X_{\mathrm{CF}}(k_i)}{X_{\mathrm{latt.}}(k_i)} - 1\right)^2, \tag{6.46}$$

with $X \in \{D, F, Z\}$. For the individual errors, χ_X, we have used the relative error definition. In addition, we have introduced a normalization constant between our calculation, X_{CF}, and the lattice simulations results, $X_{\mathrm{latt.}}$, which we denoted $\mathcal{N}_X$.

This normalization constant must be introduced since the renormalization scheme from the lattice studies do not coincide with one implemented in the present calculation. We determined the value of $\mathcal{N}_X$ by imposing that it minimizes the error χ_X. Therefore,

$$\mathcal{N}_X = \frac{\sum_i X_{\rm CF}(k_i)/X_{\rm latt.}(k_i)}{\sum_i X^2_{\rm CF}(k_i)/X^2_{\rm latt.}(k_i)}. \tag{6.47}$$

In the case far from the chiral limit, the one- and two-loop fits to lattice data are shown in Fig. 6.2. In the rest of this chapter, the horizontal axis of all the plots refers to momenta in GeV, whereas the unit used on each vertical axis is in GeV elevated to the mass dimension of the plotted quantity.

We can see that both, one- and two-loop corrections agree with the lattice data in the case of the gluon and ghost dressing functions. In both cases, two-loop corrections clearly represent an improvement with respect to the one-loop evaluation. As for the quark dressing function we confirm that two-loop corrections are essential (and sufficient) in order to accurately describe the lattice data. The corresponding errors are displayed in Table 6.1.

order	$\chi_{DFZ}(\%)$	$\chi_D(\%)$	$\chi_F(\%)$	$\chi_Z(\%)$
1-loop	7.3	4.6	4.8	10.8
2-loop	2.7	3.2	3.1	1.2

Table 6.1: Global and individual errors as obtained from the global fit of D, F and Z in the case $M_\pi = 422$ MeV.

As for the case $M_\pi = 150$ MeV, the plots are shown in Fig. 6.3 and the corresponding errors with respect to the lattice data are gathered in Table 6.2. We do not observe any impact from the fact that we are closer to the physical case when compared to the case $M_\pi = 422$ MeV. Moreover, the error table indicates that errors are smaller in this case.

order	$\chi_{DFZ}(\%)$	$\chi_D(\%)$	$\chi_F(\%)$	$\chi_Z(\%)$
1-loop	9.2	3.6	4.4	14.9
2-loop	1.8	2.6	1.5	1.1

Table 6.2: Global and individual errors as obtained from the global fit of D, F, Z in the case $M_\pi = 150$ MeV.

Partial fits

Another way of testing the validity of the perturbative CF model to describe the gluon, ghost and quark dressing functions consists in predicting one of these quantities by fitting the remaining two to lattice data. To do this, we minimized the joint error, χ_{XY} associated to two dressing functions only, X and Y,

$$\chi^2_{XY} = \frac{1}{2}(\chi^2_X + \chi^2_Y), \tag{6.48}$$

with $X, Y \in \{F, D, Z\}$.

The resulting plots for $M_\pi = 422$ MeV and $M_\pi = 150$ MeV are displayed in Figs. 6.4 and 6.5, respectively. The corresponding error values are collected in

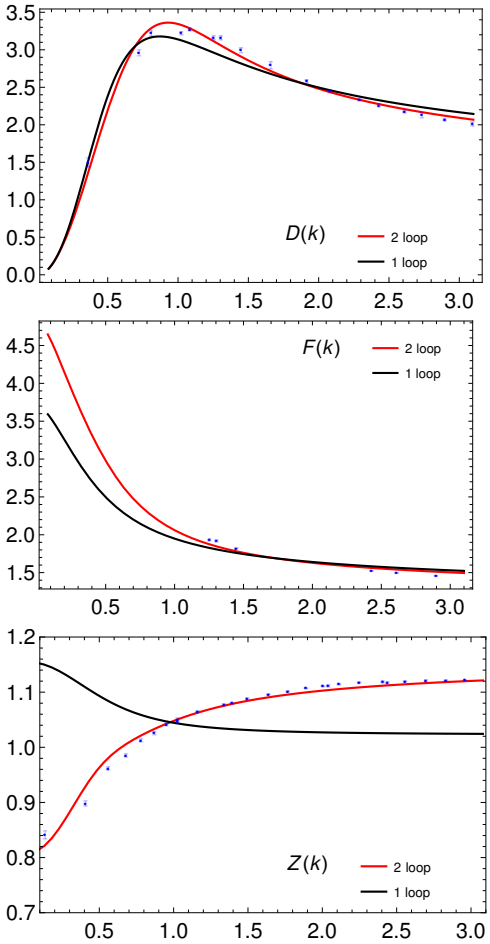

Figure 6.2: One- and two-loop fit of the gluon (top left), ghost (top right) and quark (bottom) dressing functions. The values λ_0, m_0 and M_0 were chosen so as to minimize the joint error χ_{FDZ}. Blue points correspond to lattice data from [11, 163] with $M_\pi = 422$ MeV. At one-loop we found $\lambda_0 = 0.28$, $m_0 = 390$ MeV and $M_0 = 300$ MeV. At two-loop, $\lambda_0 = 0.32$, $m_0 = 350$ MeV and $M_0 = 100$ MeV.

Table 6.3. As expected, the error of the predicted quantity is larger than the one corresponding to the triple fit. Anyway, it remains small and compatible with the CF model. For both sets of lattice data, $M_\pi = 422$ MeV and $M_\pi = 150$ MeV, the error associated to the predicted gluon dressing function is the largest. This is reasonable, since we are fixing the value of the gluon mass, the key parameter of the CF model, without any input about the lattice gluon propagator. The case $M_\pi = 422$ MeV is quite striking since the error acquires a value above 12%. In addition to the previous argument, this atypical number can also be explained because of the small number of lattice points for the ghost dressing function in this case, which turns out in a much less precise prediction. Indeed, in the case $M_\pi = 150$ MeV, the predicted gluon dressing function displays an error of 4.2%, which coincides with more lattice points for the ghost dressing function.

As a conclusion, in both scenarios, close and far from the chiral limit, the perturbative CF model seems to be able to describe the gluon, ghost and dressing functions. Moreover, the precision of the model improves when we include higher

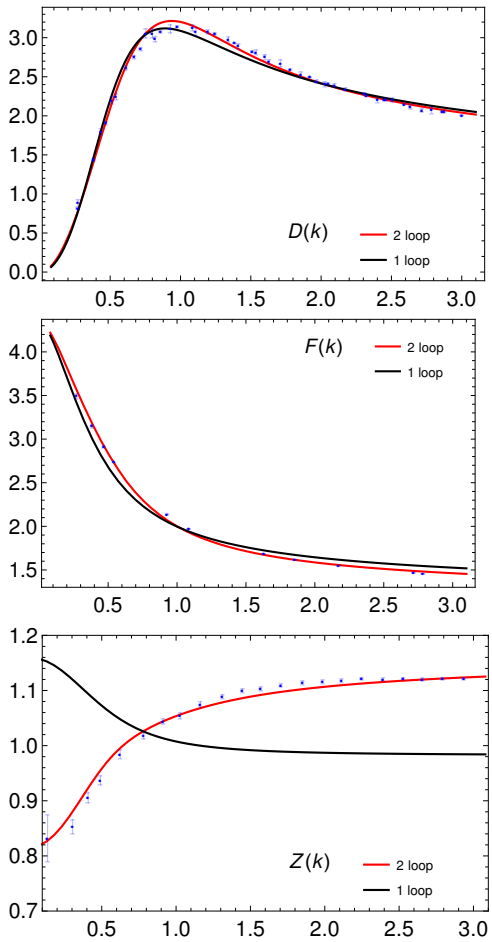

Figure 6.3: One- and two-loop fit of the gluon (top left), ghost (top right) and quark (bottom) dressing functions. The values λ_0, m_0 and M_0 were chosen so as to minimize the joint error χ_{FDZ}. Blue points correspond to lattice data from [11, 163] with $M_\pi = 150$ MeV. At one-loop we found $\lambda_0 = 0.33$, $m_0 = 410$ MeV and $M_0 = 250$ MeV. At two-loop, $\lambda_0 = 0.32$, $m_0 = 370$ MeV and $M_0 = 160$ MeV.

orders of the perturbative series, which is in line with the use of the perturbative paradigm.

6.6.2 The quark mass function

In this section we carry out an analysis on the quark mass function. Of course, we do expect to detect significant differences between the case close to the chiral limit and the case far from it. More precisely, we expect that the non-perturbative effects of the χSB will lead to a failure of the perturbative CF model when describing the running of the quark mass close to the physical case. However, these effects could be attenuated in the case of artificially large masses in the UV. With the analysis we present below, we aim, in part, at elucidating this question.

In all the cases, the error definition for the quark mass is given by

$$\chi^2_M = \frac{1}{2N}\sum_i \left(\frac{1}{\bar{M}^2_{\text{latt.}}} + \frac{1}{M^2_{\text{latt.}}(k_i)}\right)(M_{\text{latt.}}(k_i) - M_{\text{CF}}(k_i))^2, \tag{6.49}$$

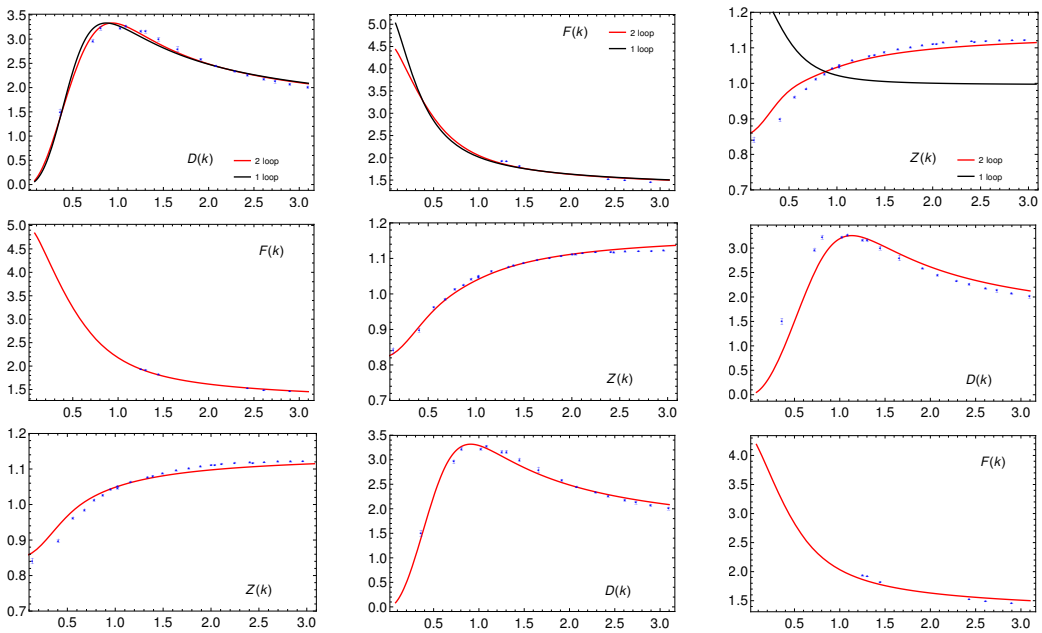

Figure 6.4: Fits of the two-loop CF results for the dressing functions X (left) and Y (middle) to the lattice data from [11, 163] using $M_\pi = 422$ MeV and the corresponding prediction of the third dressing function compared to data from the same references. The parameters are found to be $\lambda_0 = 0.31$, $m_0 = 350$ MeV, $M_0 = 90$ MeV in the case $XY = DF$, $\lambda_0 = 0.43$, $m_0 = 490$ MeV, $M_0 = 200$ MeV in the case $XY = FZ$, and $\lambda_0 = 0.31$, $m_0 = 350$ MeV, $M_0 = 120$ MeV in the case $XY = ZD$.

which corresponds to an average between the relative and absolute error (the latter is normalized by the largest value of the lattice quark mass, $\bar{M}_{\text{latt.}}$). We use this definition because it puts the UV and IR tails on an equal footing. In contrast, the absolute error overweights the IR region whereas the relative error overweights the UV region.

Prediction

We first study, assuming the perturbative nature of the gluon, ghost and quark dressing functions, how well the perturbative CF is able to predict the quark mass function. In principle, we could do this by evaluating the quark mass function using the values of λ_0, m_0 and M_0 determined in Section 6.6.1. However, this is note the best way of making the prediction, since M_0 is fixed without providing information about the lattice quark mass. The difficulty is similar to the one described in the partial fits section, where we intended to predict the gluon dressing function from the ghost and quark dressing functions. A more reliable prediction, which we present below, can be done by choosing the values of λ_0 and m_0 so as to fit the gluon and ghost dressing functions to lattice data, whereas we impose the CF quark mass to be equal to a value of the lattice data in the UV.

The plots for the predicted quark mass are displayed in Fig. 6.6. As anticipated, we observe two contrasting outcomes. In Table 6.4 we show the corresponding errors. As for $M_\pi = 422$ MeV, two-loop corrections greatly improve the one-loop evaluation. Moreover, in the plot we clearly see that the perturbative CF model can generate a significant amount of mass in the IR. Even though the quark

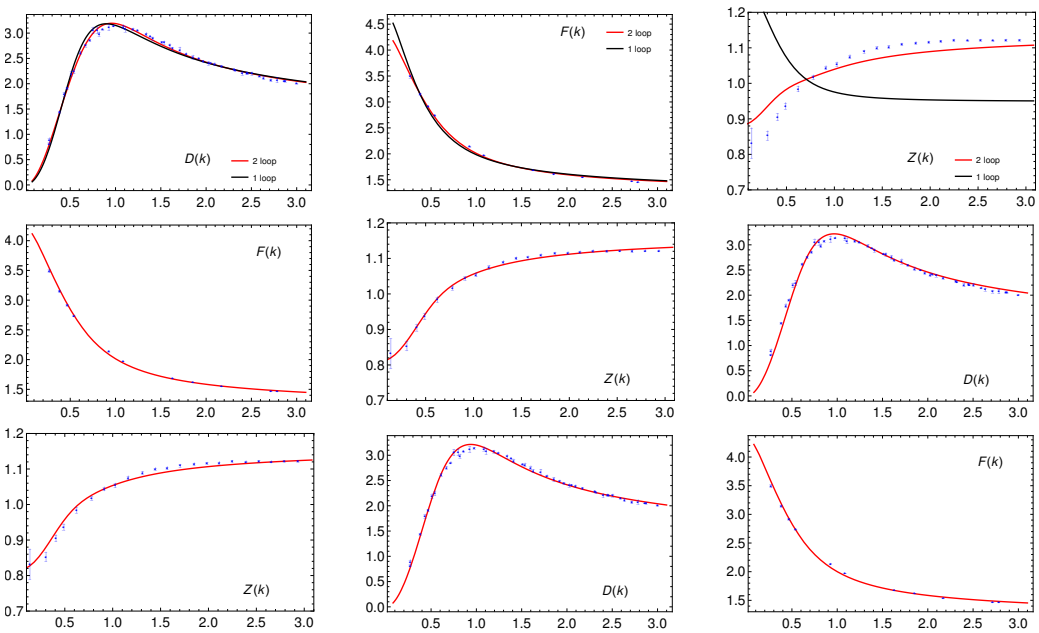

Figure 6.5: Two-loop fits of the dressing functions X (left) and Y (middle) from the CF model to the lattice data from [11, 163] using $M_\pi = 150$ MeV and the corresponding prediction of the third dressing function compared to data from the same references. The parameters are found to be $\lambda_0 = 0.31$, $m_0 = 360$ MeV, $M_0 = 90$ MeV in the case $XY = DF$, $\lambda_0 = 0.38$, $m_0 = 400$ MeV, $M_0 = 250$ MeV in the case $XY = FZ$, and $\lambda_0 = 0.32$, $m_0 = 370$ MeV, $M_0 = 160$ MeV in the case $XY = ZD$.

mass error is large in comparison with the functions D, F and Z, it remains acceptable and consistent with the perturbative framework. As for $M_\pi = 150$ MeV, the plot clearly indicate that we are unable reproduce the lattice data in the IR. Despite the fact that the two-loop evaluation represents a tiny improvement with respect to the one-loop calculation, this result is pointing out a limitation of the perturbative CF model.

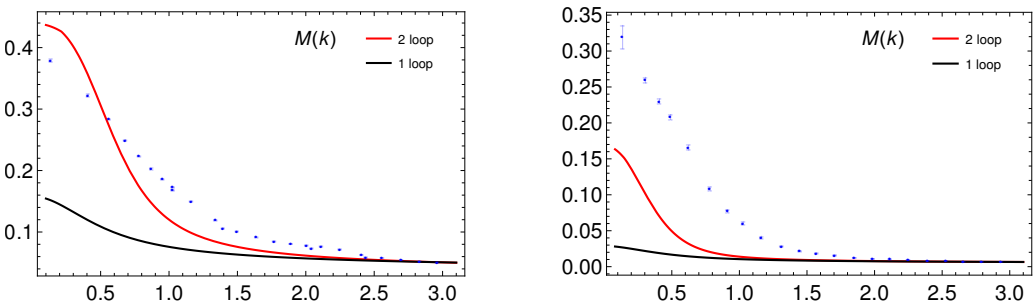

Figure 6.6: One- and two-loop predicted quark mass from the CF model. Lattice data from Refs. [11, 163] for $M_\pi = 422$ MeV (left) and $M_\pi = 150$ MeV (right). The parameters are determined from a global fit using the three functions D, F, Z and imposing to the quark mass equal to a lattice value in the UV. The parameters are found to be $\lambda_0 = 0.24$, $m_0 = 364$ MeV and $\lambda_0 = 0.28$ and $m_0 = 392$ MeV at one-loop and $\lambda_0 = 0.34$ and $m_0 = 377$ MeV $\lambda_0 = 0.30$ and $m_0 = 291$ MeV at two-loop order for $M_\pi = 422$ MeV and $M_\pi = 150$ MeV respectively.

XY	$\chi_{XY}(\%)$	$\chi_X(\%)$	$\chi_Y(\%)$	$\chi_{\text{pred.}}(\%)$
DF	3.1	3.0	3.2	1.9
FZ	0.7	1.0	0.4	12.3
ZD	2.3	1.2	3.1	3.3

XY	$\chi_{XY}(\%)$	$\chi_X(\%)$	$\chi_Y(\%)$	$\chi_{\text{pred.}}(\%)$
DF	1.8	2.0	1.5	3.6
FZ	0.9	1.1	0.9	4.2
ZD	2.0	1.1	2.6	1.5

Table 6.3: Global and individual errors obtained from the partial fit of X and Y using the two-loop expressions and the corresponding error on the predicted dressing function in the case $M_\pi = 422$ MeV (top) and in the case $M_\pi = 150$ MeV (bottom).

order	$\chi_{DFZ}(\%)$	$\chi_D(\%)$	$\chi_F(\%)$	$\chi_Z(\%)$	$\chi_M(\%)$
1-loop	8.9	5.6	5.3	12.1	34.6
2-loop	3.0	4.5	2.7	0.9	16.0

order	$\chi_{DFZ}(\%)$	$\chi_D(\%)$	$\chi_F(\%)$	$\chi_Z(\%)$	$\chi_M(\%)$
1-loop	11.0	3.2	7.0	16.9	50.9
2-loop	5.5	6.6	3.0	6.1	41.8

Table 6.4: Global and individual errors, obtained from the global fit of D, F, Z imposing to the quark mass equal to a lattice value in the UV. In the case of $M_\pi = 422$ MeV (top) this is $M(3.0\text{ GeV}) = 5.1$ MeV, whereas in the case where $M_\pi = 150$ MeV (bottom) this corresponds to impose $M(2.9\text{ GeV}) = 6.6$.

Global fit

Another direction we can point to in order to analyze to which extent the quark mass function admits a perturbative description within the CF approach is based on performing a simultaneous fit of the three dressing functions and the quark mass. It is clear that in the case close to the physical case we are artificially trying to fit a quantity we know, beforehand, we cannot describe. Nonetheless, it is interesting to test how this added tension modifies the dressing functions behavior. To carry out this study we use the joint error χ_{DFZM}, defined as

$$\chi^2_{DFZM} = \frac{1}{4}\left(\chi^2_D + \chi^2_F + \chi^2_M + \chi^2_Z\right). \tag{6.50}$$

The plots corresponding to the quark mass are displayed in Fig. 6.7. The errors associated to the dressing functions and the quark mass are gathered in Table 6.5. We note no significant changes in relation to the quark mass prediction, see Table 6.4, except that in this case, the errors come essentially from the UV tails.

In line with the previous observations, the case $M_\pi = 422$ MeV is consistent with a perturbative description within the CF framework, whereas the case $M_\pi = 150$ MeV shows that we have pushed the perturbative model too far. This becomes even more evident when looking at the errors of the latter case: two-loop corrections for the quark mass and the gluon dressing function display larger er-

rors than one-loop corrections. It is worth emphasizing, again, that this limitation derives from the use of perturbation theory rather than the CF model itself.

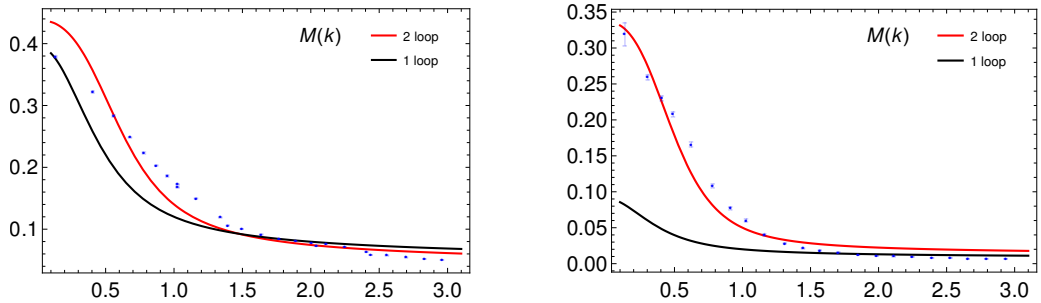

Figure 6.7: One- and two-loop fit for quark mass from the CF model. Lattice data from Ref. [11, 163], for $M_\pi = 422$ MeV (left) and $M_\pi = 150$ MeV (right). The parameters were obtained by minimizing the joint error χ_{DFZM}. As for $M_\pi = 422$ MeV these are $\lambda_0 = 0.43$, $m_0 = 430$ MeV, $M_0 = 130$ MeV at one-loop order and $\lambda_0 = 0.33$, $m_0 = 390$ MeV, $M_0 = 150$ MeV at two-loop order. As for $M_\pi = 150$ MeV the parameters are $\lambda_0 = 0.43$, $m_0 = 430$ MeV, $M_0 = 20$ MeV at one-loop order and $\lambda_0 = 0.39$, $m_0 = 400$ MeV , $M_0 = 50$ MeV at two-loop order.

order	$\chi_{DFMZ}(\%)$	$\chi_D(\%)$	$\chi_F(\%)$	$\chi_Z(\%)$	$\chi_M(\%)$
1-loop	13.2	5.6	3.1	15.9	18.1
2-loop	5.9	4.7	2.8	1.6	10.3

order	$\chi_{DFMZ}(\%)$	$\chi_D(\%)$	$\chi_F(\%)$	$\chi_Z(\%)$	$\chi_M(\%)$
1-loop	25.3	7.2	4.9	21.5	45.0
2-loop	31.9	9.1	4.7	3.4	62.8

Table 6.5: Global and individual errors as obtained from the global fit of D, F, M and Z in the case $M_\pi = 422$ MeV (top) and in the case $M_\pi = 150$ MeV (bottom).

We end this section by mentioning that, in the case close to the chiral limit, the perturbative CF model still could be helpful in the investigation of observables which are mostly sensitive to the IR scale. For instance, by using the CF quark mass resulting from the minimization of the joint error χ_{DFZM}. In fact, we have checked that error definitions which put more weight on the IR region typically give errors of the order of 15% at two-loop order for both $M_\pi = 422$ MeV and $M_\pi = 150$ MeV.

6.6.3 Impact of the non-perturbative quark mass on the dressing functions

We have seen previously that the gluon, ghost and quark dressing functions admit a perturbative description within the CF model, even in the case close to the chiral limit. However, one could argue that such analysis is not fully convincing since it neglects the impact of the χSB on such functions. In other words, the quark mass function from lattice simulations was not properly described in the various fits we presented, at least in the case $M_\pi = 150$ MeV. As a result, we might be

getting artificially good fits at the expense of not accurately describing the quark mass function.

Therefore, in order to estimate the impact of the non-perturbative mass on the fits for the three dressing functions, we remove the perturbative quark mass function from the analysis. Rather, we extract the running of the quark mass, $M(k)$, directly from the lattice data, by realizing a simple interpolation of the lattice points. The remaining parameters of the model, λ_0 and m_0, are found by minimizing the joint error of the three dressing functions χ_{DFZ}, defined in Eq. (6.45). As we already discussed, with the aid of the $\beta-$functions one can easily determine the running functions $\lambda(\mu)$ and $m(\mu)$ afterwards. Proceeding in this way, we fit the three dressing functions whereas χSB automatically holds since it is taken as an input from lattice simulations. Of course, by doing this we are propagating the systematic errors from lattice data to the fits of the dressing functions. Anyway, the analysis is still useful so as to give an estimate of the impact of the non-perturbative quark mass on our results for the three dressing functions.

The resulting plots are shown in Fig. 6.8 and the errors are listed in Table 6.6. We do not observe significant differences with the fits provided in Section 6.6.1. In all cases, two-loop evaluations reproduce with very good accuracy the lattice data and represent an improvement with respect to one-loop results. As it occurred with previous fits, the case of the quark dressing function is quite remarkable, since the one-loop evaluation is unable to reproduce the lattice simulations even at a qualitative level. As expected, these results show a marginal impact of the χSB on the perturbative description of the gluon, ghost and quark dressing functions even close to the chiral limit. We can conclude now that our investigation strongly suggests that such dressing functions admit a perturbative treatment within the CF approach.

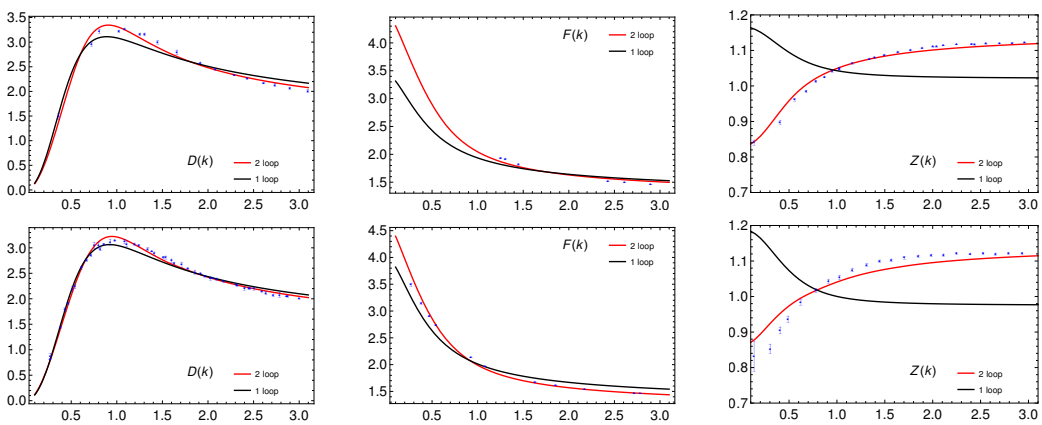

Figure 6.8: One- and two-loop CF fits of the gluon (left), ghost (middle) and quark dressing function (right) to lattice data from [11, 163], using $M_\pi = 422$ MeV (top) and $M_\pi = 150$ MeV (bottom). The parameters are determined from an interpolation of the lattice quark mass and the minimization of the joint error of D, F and Z. These are $\lambda_0 = 0.31$, $m_0 = 360$ MeV; $\lambda_0 = 0.32$, $m_0 = 350$ MeV at two-loop order and $\lambda_0 = 0.31$, $m_0 = 400$ MeV; $\lambda_0 = 0.26$, $m_0 = 380$ MeV at one-loop order for $M_\pi = 422$ MeV and $M_\pi = 150$ MeV, respectively.

order	$\chi_{DFZ}(\%)$	$\chi_D(\%)$	$\chi_F(\%)$	$\chi_Z(\%)$
1-loop	7.7	5.3	5.1	11.1
2-loop	2.8	3.4	3.3	1.0

order	$\chi_{DFZ}(\%)$	$\chi_D(\%)$	$\chi_F(\%)$	$\chi_Z(\%)$
1-loop	9.9	3.1	6.1	15.4
2-loop	2.6	2.4	2.3	3.2

Table 6.6: Global and individual errors obtained from the global fit of D, F, Z and the interpolation of the quark mass lattice data in the case $M_\pi = 422$ MeV (top) and $M_\pi = 150$ MeV (bottom).

Chapter 7

Conclusions and outlook

In this thesis we investigate to which extent various two- and three-point functions from Yang-Mills (YM) theory (pure gauge) and Quantum Chormodynamics (QCD) admit a perturbative description within the Curci-Ferrari model in Landau gauge [41], by comparing several two-loop evaluations with available lattice data.

The model is a gluon massive extension of the textbook Faddeev-Popov gauge fixed action, which is retrieved at very high momenta [42]. This ensures that all the good properties featured by the latter in the deep ultraviolet are retained by the CF model. It is motivated by the decoupling solution of the gluon propagator, observed in lattice simulations[28–37]. The model has been proven to be renormalizable [41, 44, 46] and benefits from certain renormalization group trajectories, corresponding to the so called infrared safe renormalization scheme, in which the coupling remains small for the whole range of momenta, being compatible with a perturbative treatment [43, 53, 54]. More importantly, this analysis seems to be consistent with the lattice simulations for that quantity in the pure gauge case [29, 32, 55, 56].

Based on this behavior, over the last decade various two- and three-point correlation functions from the CF model have been evaluated at one-loop order of perturbation theory and compared to available lattice data [42, 43, 57, 58, 85]. In general terms, the error between the lattice and the model outcome was in between 10% and 20% as for pure YM theory. In the presence of quarks, some quantities seem to admit a perturbative description, such as the gluon and ghost two-point functions while others not, such as the quark mass function close to the quiral limit. Recently, a two-loop evaluation of the two-point functions in the pure gauge case was performed [54]. The comparison with lattice data showed that the two-loop corrections allow to describe more accurately the lattice simulations, which strongly suggests that the perturbative expansion is under control.

In this thesis we have continued that work and investigated several correlation functions to two-loop order from the CF model in Landau gauge, with the purpose of testing to which extent the perturbative version of this model is capable of describing the infrared of pure YM theory and QCD.

In Chapter 4 we presented the two-loop evaluation of the ghost-antighost-gluon vertex in pure YM theory, based on the groups SU(3) and SU(2), and compared those results with available lattice data. This calculation is an extension of the one-loop evaluation from [57]. With the purpose of keeping the calculation manageable we used a particular kinematical configuration where the momentum of the gluon

vanishes. This evaluation was a pure prediction of the CF model since the running functions of the gauge coupling and the gluon mass were completely determined in [54], by fitting the two-point functions to lattice data. In the case of the SU(3) gauge group, the plots show that both one- and two-loop corrections have a very good agreement with the lattice data. As for SU(2), the prediction quality clearly deteriorates as compared to SU(3). A complementary way of testing the control of the perturbative expansion is by measuring the scheme dependence of the result. In line with the plots, whereas for the SU(3) gauge group the scheme dependence diminishes from one- to two-loop order, this is not the case for SU(2). We believe that the differences between groups is directly related to the gauge coupling, which is larger for the SU(2) group. Indeed, the fits of the two-point functions already feature larger errors for the SU(2) group. Then, in order to avoid the potential error propagation from the fits of the two-point functions to the ghost-antighost-gluon vertex prediction in the SU(2) case, we opted for fitting the two-point functions *and* the vertex simultaneously, obtaining reasonable results. Moreover, two-loop corrections show a better agreement with lattice simulations than one-loop corrections. In brief, our results indicate that the perturbative CF model is able to reproduce to a very good extent the lattice data of the ghost-antighost-gluon vertex in pure YM theory, based on the SU(3) gauge group. As for SU(2), the perturbative CF model gives reasonable results. However caution is needed in this case, since the errors are expected to be larger. As a final remark, we mention that the error bars from lattice simulations are quite large in the particular kinematical configuration we are looking at. As a result, it could be the case that part of the discrepancies we note in the SU(2) case have their origin in the simulations rather than the model. These results were published in [59].

In Chapter 5 we presented the two-loop evaluation of the three-gluon vertex in pure YM theory, based on the groups SU(3) and SU(2), in the particular kinematical configuration where the momentum of one of the gluons vanishes. This calculation is an extension of the one-loop evaluation from [57]. Similarly to the ghost-antighost-gluon vertex, this calculation is a pure prediction of the model, up to an overall normalization factor. For both gauge groups we observe a very good agreement with lattice data. Moreover, the two-loop evaluation describes more accurately the lattice simulations than the one-loop evaluation, which reinforces the idea that the CF model is able to perturbatively describe the infrared of YM theory. This is confirmed by the analysis of the renormalization scheme dependence, which diminishes from one- to two-loop order in both SU(3) and SU(2). In line with the previous perturbative calculations in the framework of the CF model, we observe that the SU(3) case leads to smaller errors and is less scheme dependent than the SU(2) case. Finally, we studied the zero-crossing of the three-gluon vertex dressing function. We proved that it occurs at all order of perturbation theory. Moreover, we found an expression for the leading contribution in the infrared at each loop order. We checked that it coincides with the leading term in the infrared expansion at two-loop order. We note, however, that the scale at which the zero-crossing occurs is significantly reduced from one- to two-loop order, which seems to be consistent with the lattice data from [230]. An article on this work will soon be submitted to a journal. Its preprint can be found in [60].

In Chapter 6 we presented the two-loop evaluation of all the two-point func-

tions in the presence of two mass-degenerate quark flavors and the corresponding fits to lattice data from [11, 163]. In the presence of quarks the coupling governing the perturbative expansion is larger than in pure YM theory, so the information provided by this calculation is crucial in order to test the validity of the perturbative CF model. In addition, we have the fact that, as it is well-known, the spontaneous breaking of chiral symmetry (χSB) does not admit any sort of perturbative description. Thus, in order to study the impact of χSB, we compared our results with two sets of lattice data, one close to the quiral limit and another far from it. We computed the gluon and ghost dressing functions, related to their respective propagators, and the quark dressing and quark mass functions, both related to the quark propagator. Our results show that the quantities not directly impacted by χSB, *i.e.* the gluon, ghost and quark dressing functions, admit a perturbative description within the CF model. This is supported by the fact that two-loop results systematically improve the agreement with lattice data when compared to one-loop results. In the case of the ghost and gluon dressing functions this was already confirmed in Ref. [58], at one-loop order. As for the quark dressing function, the one-loop result is unable of reproducing the lattice data even at a qualitative level, where it features the wrong monotonicity. However, this is corrected at two-loop order, and the lattice data is reproduced with high accuracy, as anticipated in Ref. [58]. In the case of the quark mass function, our results confirm that the perturbative approach is unable of describing the lattice data close to the chiral limit. Nonetheless, in the case far from that limit the model becomes useful again, giving reasonable results even in the case of the quark mass function. We also studied the impact of the non-perturbative mass, provided by lattice simulations, on the fits of the dressing functions and found it minimal. This is another confirmation of the perturbative nature of the ghost, gluon and quark dressing functions within the CF model. These results were published in [61].

All the results mentioned above, in addition to other works for finite temperature and density [193–199] as well as chemical potential [200], support the idea that pure YM theory can be well described by the perturbative CF model. This extends to QCD as far as we are referring to quantities not directly affected by the χSB. But even in the case of the quark mass function this remains true as long as we stay far from the chiral limit. To further check this claim we plan to evaluate the quark-gluon vertex at two-loop order in the near future. This quantity arises as a pure prediction of the model once the running functions have been determined by the fits provided in Chapter 6. After this calculation, a final interesting test on the model we are planning to carry out is the two-loop evaluation of all the two- and three-point functions of pure YM theory in three dimensions.

For physical situation close to the chiral limit, one can still make use of the CF model but using some approach which goes beyond perturbation theory, such as the one described in [192, 250]. In those works, the pure gauge sector is treated in a purely perturbative approach whereas in the quark sector all the orders in the quark coupling are retained, at the expense of performing another expansion in the inverse of the number of colors. This opens the door to extend the use of CF model to compute physical observables, such as the hadron mass spectrum.

A great task to achieve in the long term is to make progress in the questions concerning the origin of the gluon mass term and the construction of the physical

space of the CF model.

Appendix A

Ghost-antighost-gluon vertex Feynman diagrams

Firstly, we have one-loop diagrams which are drawn in Fig. A.1.

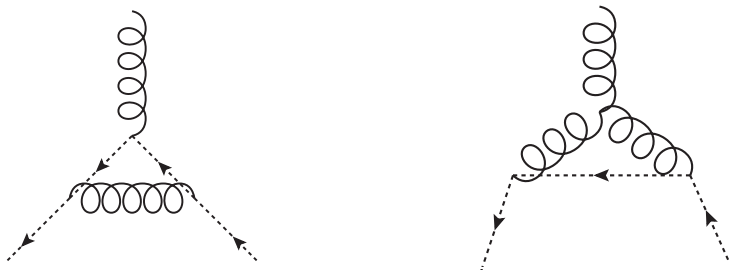

Figure A.1: One-loop contributions to the ghost-gluon vertex.

Secondly, we have two-loop corrections. In order to organize the corresponding diagrams it is useful to classify them according to the following criteria: i) those corresponding to one-loop self-energy insertions in one-loop diagrams, ii) those corresponding to one-loop vertex insertions in one-loop diagrams and iii) the rest. In the case of i) we can distinguish between ghost and gluon self-energy corrections, shown in Fig. A.2 and Fig. A.3, respectively. In the case of ii) we have ghost-gluon, see Fig. A.4, and three-gluon one-loop insertions, see Fig. A.5. Inside the category iii) we have the non-planar diagrams, which vanish due to the color factor and the diagram showed in Fig. A.6.

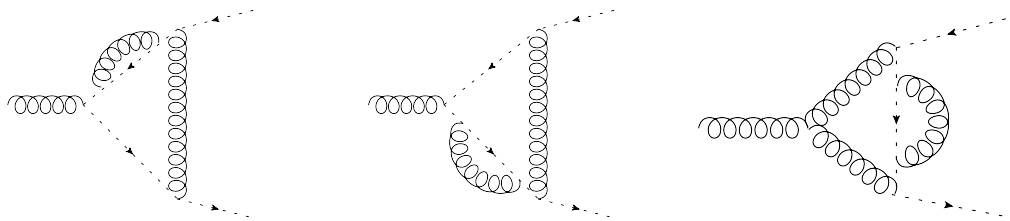

Figure A.2: Two-loop diagrams corresponding to ghost self-energy corrections inserted in one-loop diagrams.

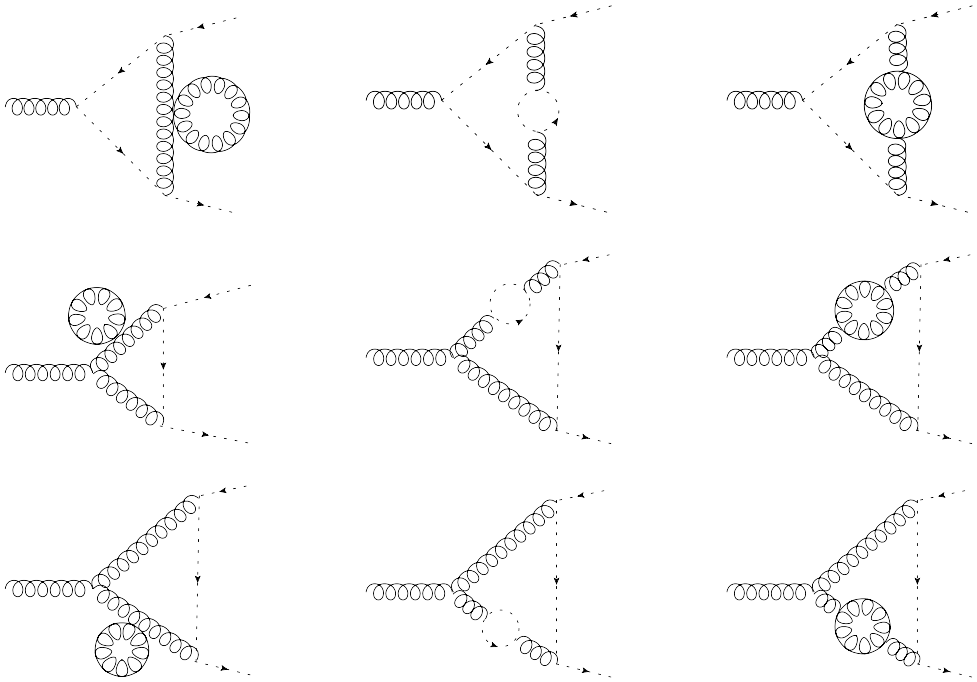

Figure A.3: Two-loop diagrams corresponding to gluon self-energy corrections inserted in one-loop diagrams.

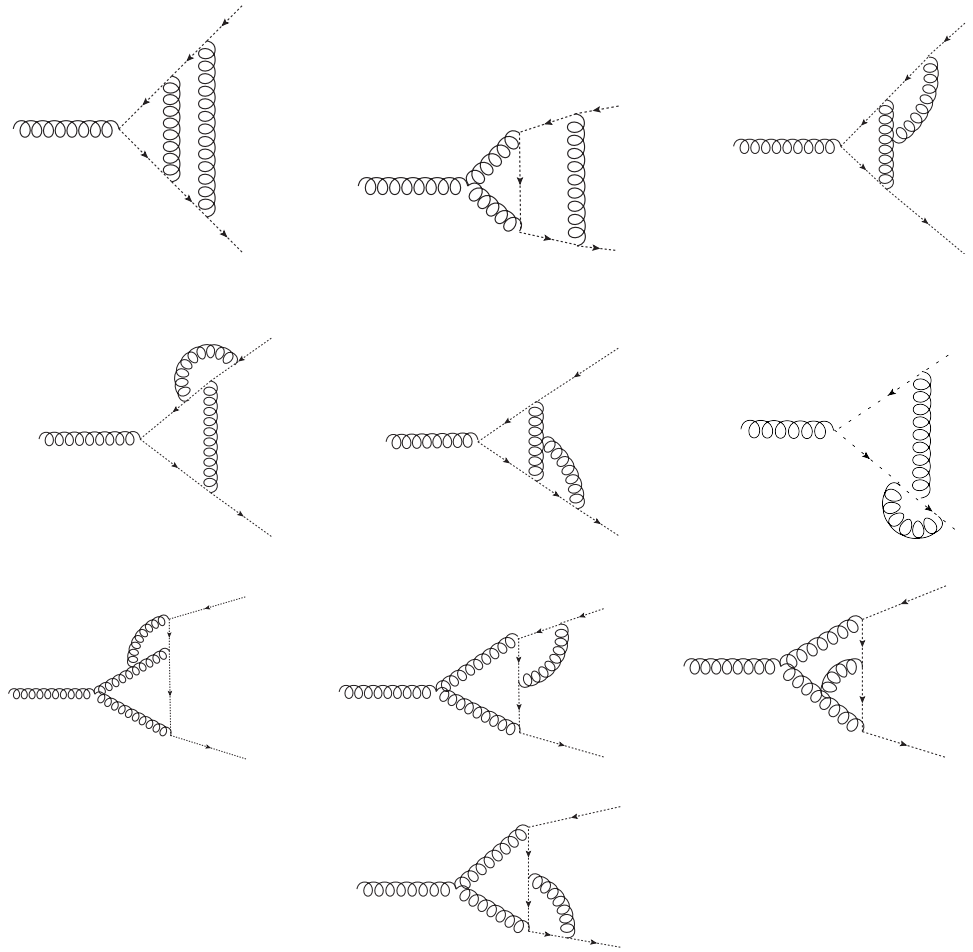

Figure A.4: Two-loop diagrams corresponding to one-loop ghost-gluon vertex insertions in one-loop diagrams.

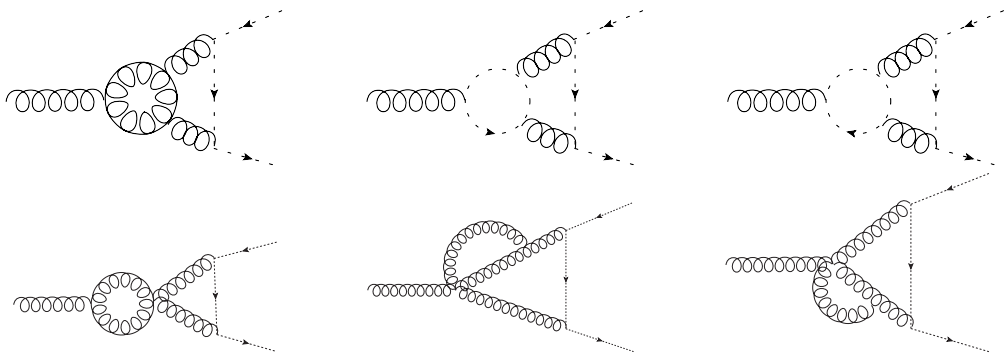

Figure A.5: Two-loop diagrams corresponding to one-loop three gluon vertex insertions in one-loop diagrams.

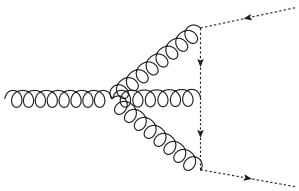

Figure A.6: The only nonvanishing diagram that cannot be described in terms of a one-loop correction to a one-loop ghost-gluon diagram.

Appendix B

Three-gluon vertex Feynman diagrams

B.1 One-loop diagrams

In this section we show the one-loop diagrams contributing to $\Gamma(p^2)$. We do not draw diagrams which are permutations of the ones below.

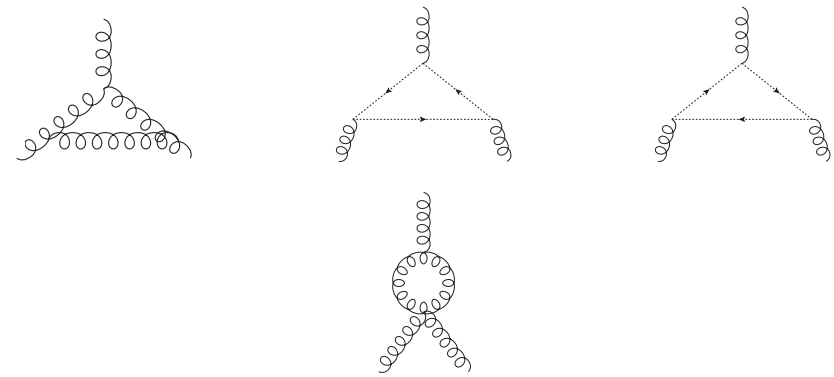

B.2 Two-loop diagrams

In this section we show the two-loop diagrams contributing to $\Gamma(p^2)$. We do not draw diagrams which are permutations of the ones below.

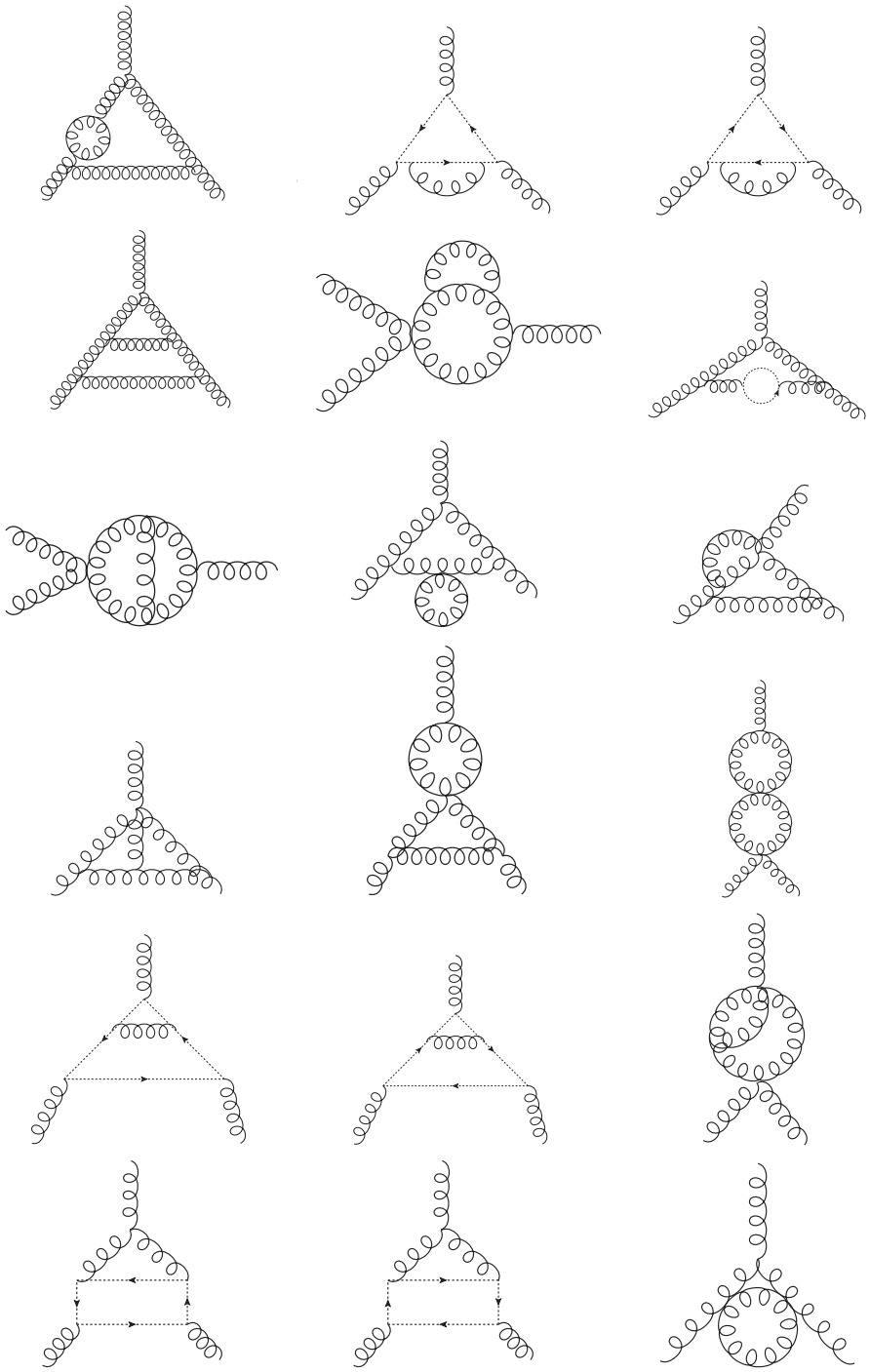

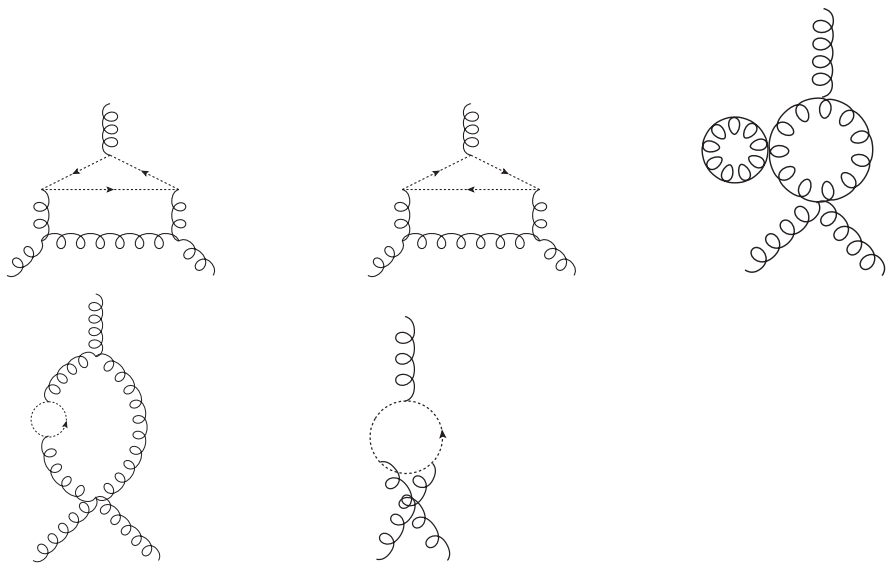

Appendix C

QCD two-point functions Feynman diagrams

C.1 Gluon two-point function

In this section we show the Feynman diagrams contributing to the gluon two-point function.

C.1.1 One-loop diagrams

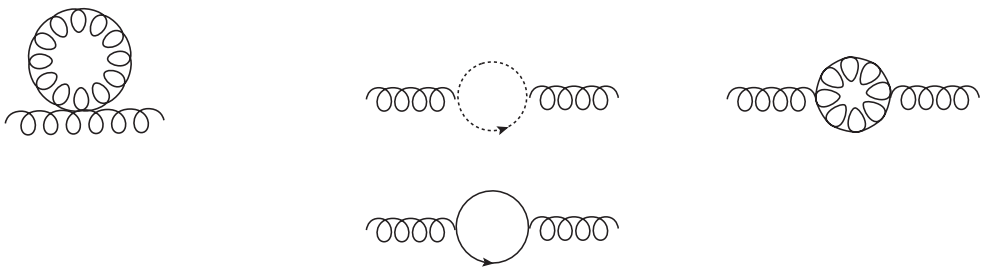

C.1.2 Two-loop diagrams

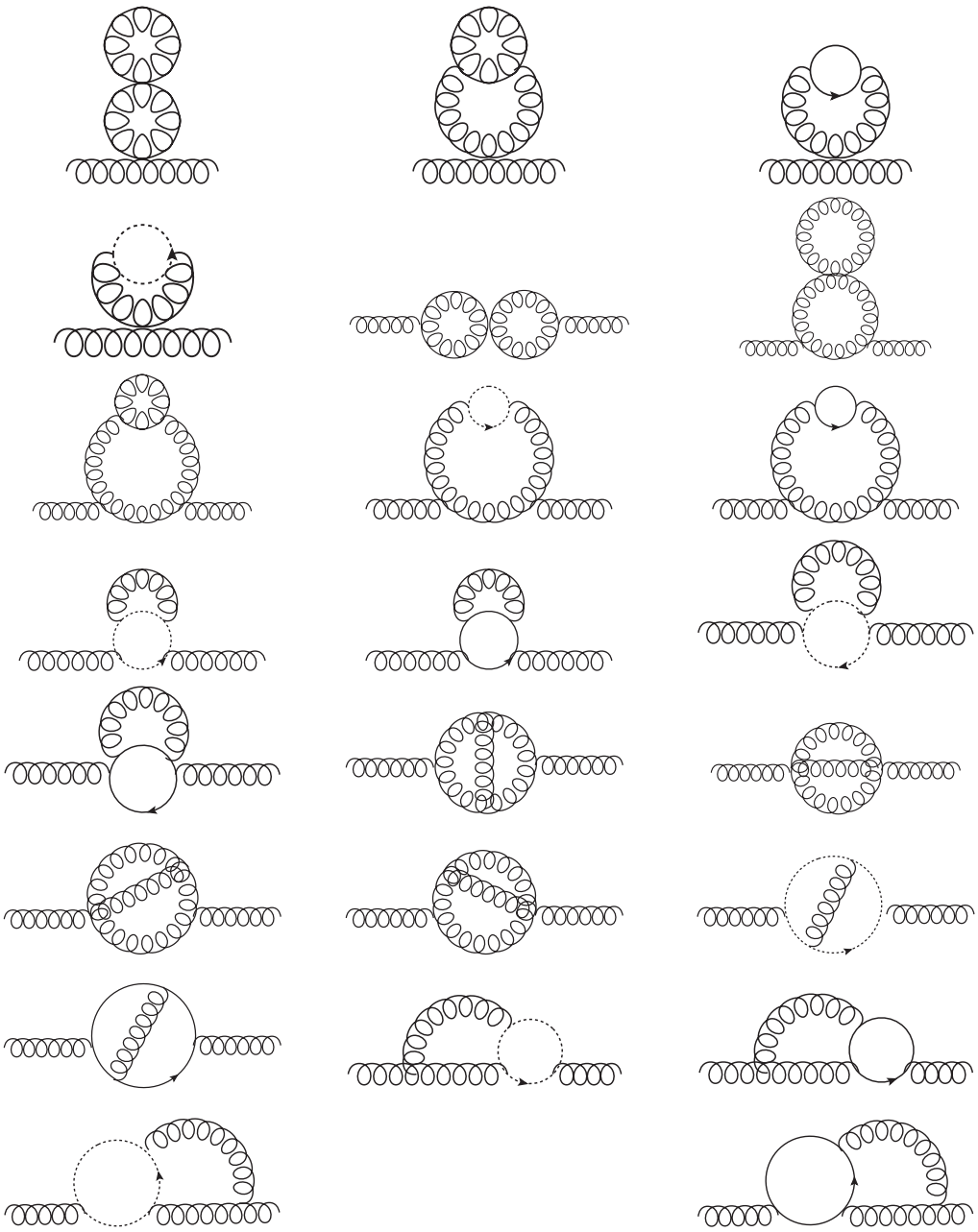

C.2 Ghost two-point function

In this section we show the Feynman diagrams contributing to the ghost two-point function.

C.2.1 One-loop diagram

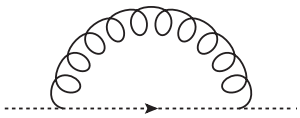

C.2.2 Two-loop diagrams

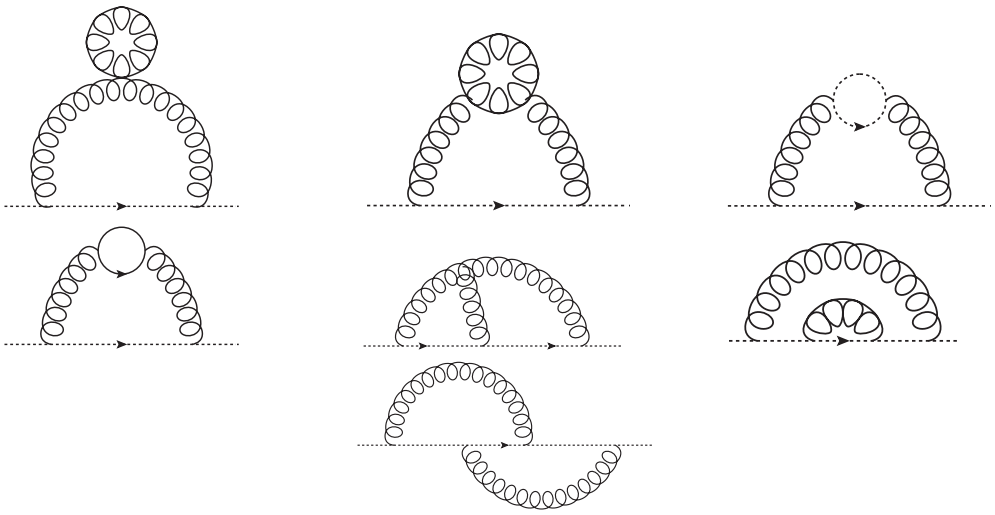

C.3 Quark two-point function

In this section we show the Feynman diagrams contributing to the quark two-point function.

C.3.1 One-loop diagram

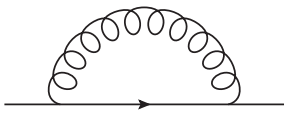

C.3.2 Two-loop diagrams

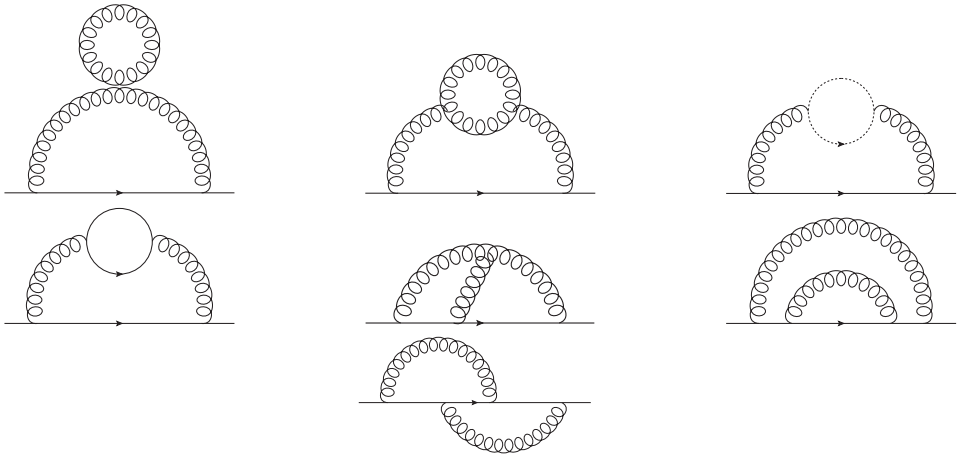

Appendix D

Reduction of integrals with one inverted propagator

When implementing the FIRE reduction package, it may happen that not all the resulting integrals are master ones. In some instances one of the propagators could be elevated to the power -1. In this appendix we show a generic example in order to illustrate how to operate on this type of integrals so as to expressed them entirely in terms of master ones. Let us begin by introducing the following notation:

$$\begin{aligned} I_{m_1 m_2 m_3 m_4 m_5}(n_1, n_2, n_3, n_4, n_5) &\equiv \int_p \int_q G_{m_1}^{n_1}(p) G_{m_2}^{n_2}(q) \\ &\times G_{m_3}^{n_3}(k-p) G_{m_4}^{n_4}(k-q) G_{m_5}^{n_5}(p-q)\,, \end{aligned} \tag{D.1}$$

with $G_{m_i}(\ell) \equiv 1/(\ell^2 + m_i^2)$.

Let us consider the integral $I_{m_1 00 m_4 m_5}(1, -1, 0, 1, 1)$ which has one propagator elevated to the power -1. By using

$$q^2 = (k-q)^2 + m_4^2 - k^2 - m_4^2 + 2(k \cdot q)\,, \tag{D.2}$$

the integral can be written as

$$\begin{aligned} I_{m_1 00 m_4 m_5}(1, -1, 0, 1, 1) =& I_{m_1 m_5 000}(1, 1, 0, 0, 0) \\ &- (k^2 + m_4^2) I_{m_1 00 m_4 m_5}(1, 0, 0, 1, 1) \\ &+ \int_p \int_q 2(k \cdot q) G_{m_1}(p) G_{m_4}(k-q) G_{m_5}(p-q)\,. \end{aligned} \tag{D.3}$$

By performing the change of variables $p \to k-p$ and $q \to k-q$, followed by $p \leftrightarrow q$, we arrive at

$$\begin{aligned} I_{m_1 00 m_4 m_5}(1, -1, 0, 1, 1) =& \; I_{m_1 m_5 000}(1, 1, 0, 0, 0) + 2k^2 I_{m_4 00 m_1 m_5}(1, 0, 0, 1, 1) \\ &- (k^2 + m_4^2) I_{m_1 00 m_4 m_5}(1, 0, 0, 1, 1) \\ &- \frac{1}{2} \int_q 2k\, G_{m_1}(k-q) \cdot \int_p 2p\, G_{m_4}(p) G_{m_5}(p-q). \end{aligned} \tag{D.4}$$

It follows that

$$\begin{aligned}
&I_{m_1 00 m_4 m_5}(1,-1,0,1,1) = I_{m_1 m_5 000}(1,1,0,0,0) + 2k^2 I_{m_4 00 m_1 m_5}(1,0,0,1,1) \\
&- (k^2+m_4^2) I_{m_1 00 m_4 m_5}(1,0,0,1,1) \\
&- \frac{1}{2}\int_q 2(k\cdot q) G_0(q) G_1(k-q) \int_p 2(p\cdot q) G_{m_4}(p) G_{m_5}(p-q)
\end{aligned} \tag{D.5}$$

Then, inserting the identities

$$2(k\cdot q) = k^2 + m_1^2 + q^2 - (k-q)^2 - m_1^2\,, \tag{D.6}$$

$$2(p\cdot q) = q^2 + m_5^2 - m_4^2 + p^2 + m_4^2 - (p-q)^2 - m_5^2\,, \tag{D.7}$$

and identifying the corresponding master integrals, we have

$$\begin{aligned}
&2I_{m_1 00 m_4 m_5}(1,-1,0,1,1) + I_{m_4 00 m_1 m_5}(1,-1,0,1,1) \\
&= A_{m_1}A_{m_4} + A_{m_4}A_{m_5} + A_{m_5}A_{m_1} - (k^2+m_1^2)(A_{m_5}-A_{m_4})B_{m_1 0} \\
&+ (m_5^2-m_4^2) I_{m_4 m_5 0} + (k^2-m_1^2-m_4^2-m_5^2) S_{m_1 m_4 m_5} \\
&- (k^2+m_1^2)(m_5^2-m_4^2) U_{m_1 0 m_4 m_5}\,.
\end{aligned} \tag{D.8}$$

In the case where $m_1 = m_4$, we obtained an explicit expression of $I_{m_1 00 m_4 m_5}(1,-1,0,1,1)$ in terms of the master integrals. In the case where $m_1 \neq m_4$ we can simply consider the same equation with $m_1 \leftrightarrow m_4$:

$$\begin{aligned}
&I_{m_1 00 m_4 m_5}(1,-1,0,1,1) + 2I_{m_4 00 m_1 m_5}(1,-1,0,1,1) \\
&= A_{m_1}A_{m_4} + A_{m_4}A_{m_5} + A_{m_5}A_{m_1} - (k^2+m_4^2)(A_{m_5}-A_{m_1})B_{m_4 0} \\
&+ (m_5^2-m_1^2) I_{m_1 m_5 0} + (k^2-m_1^2-m_4^2-m_5^2) S_{m_1 m_4 m_5} \\
&- (k^2+m_4^2)(m_5^2-m_1^2) U_{m_4 0 m_1 m_5}\,.
\end{aligned} \tag{D.9}$$

Together with Eq. (D.8), this provides an invertible linear system whose solution allows us to write $I_{m_1 00 m_4 m_5}(1,-1,0,1,1)$ in terms of the master integrals only.

Appendix E

Master integrals to order ϵ

Let us start this appendix by introducing some useful identities. In all the cases we work with dimensional regularization in $d = 4 - 2\epsilon$ dimensions. Firstly, we introduce the well known integral

$$J_\alpha(m^2) \equiv \int_q \frac{1}{(q^2+m^2)^\alpha} = \frac{(m^2)^{2-\alpha-\epsilon}}{(4\pi\mu^2)^{-\epsilon}} \frac{\Gamma(\alpha-2+\epsilon)}{\Gamma(\alpha)} \tag{E.1}$$

which can be found, for instance, in [262]. A widely used technique to deal with Feynman integrals is the famous Feynman trick. It consists in introducing the parameters $x_1 \dots x_n$ such that

$$\begin{aligned} &\frac{1}{D_1^{\nu_1} \dots D_n^{\nu_n}} \\ &\quad = \int_0^1 dx_1 \dots dx_n \delta(\sum x_i - 1) \frac{\prod x_i^{\nu_i - 1}}{(x_1 D_1 + \dots + x_n D_n)^{\sum \nu_i}} \frac{\Gamma(\nu_1 + \dots + \nu_n)}{\Gamma(\nu_1) \dots \Gamma(\nu_n)}, \end{aligned} \tag{E.2}$$

where D_i denotes a particular propagator and $\Gamma(x)$ is the Euler Gamma function. Note that the number of Feynman parameters, x_i, coincides with the number of propagators. Let us apply it to the integral

$$I_{\alpha,\beta}(p^2) \equiv \int_q \frac{1}{(q^2)^\alpha ((q+p)^2)^\beta} = I_{\beta,\alpha}(p^2), \tag{E.3}$$

which will be of use further in this appendix,

$$\int_q \frac{1}{(q^2)^\alpha ((q+p)^2)^\beta} = \int_0^1 dx_1 dx_2 \int_q \frac{\delta(x_1+x_2-1) x_1^{\alpha-1} x_2^{\beta-1}}{(x_1 q^2 + x_2 (p+q)^2)^{\alpha+\beta}} \frac{\Gamma(\alpha+\beta)}{\Gamma(\alpha)\Gamma(\beta)}. \tag{E.4}$$

By using the change of variables $\ell = q + xp$ we can write

$$I_{\alpha,\beta}(p^2) = \frac{\Gamma(\alpha+\beta)}{\Gamma(\alpha)\Gamma(\beta)} \int_\ell \int_0^1 dx \frac{(1-x)^{\alpha-1} x^{\beta-1}}{(\ell^2 + p^2 x(1-x))^{\alpha+\beta}}. \tag{E.5}$$

Now, it is possible to compute the integral in ℓ thanks to Eq. (E.1), obtaining

$$I_{\alpha,\beta}(p^2) = \frac{(p^2)^{2-\alpha-\beta-\epsilon}}{(4\pi\mu^2)^{-\epsilon}} \frac{\Gamma(\alpha+\beta-2+\epsilon)}{\Gamma(\alpha)\Gamma(\beta)} \int_0^1 dx (1-x)^{1-\beta-\epsilon} x^{1-\alpha-\epsilon}. \tag{E.6}$$

Finally, we get

$$\begin{aligned} I_{\alpha,\beta}(p^2) &\equiv \int_q \frac{1}{(q^2)^\alpha((q+p)^2)^\beta} = I_{\beta,\alpha}(p^2) \\ &= \frac{(p^2)^{2-\alpha-\beta-\epsilon}}{(4\pi\mu^2)^{-\epsilon}} \frac{\Gamma(2-\alpha-\epsilon)\Gamma(2-\beta-\epsilon)\Gamma(\alpha+\beta-2+\epsilon)}{\Gamma(\alpha)\Gamma(\beta)\Gamma(4-\alpha-\beta-2\epsilon)}, \end{aligned} \tag{E.7}$$

where we used the identity

$$\int_0^1 dx x^{\alpha-1}(1-x)^{\beta-1} = \frac{\Gamma(\alpha)\Gamma(\beta)}{\Gamma(\alpha+\beta)}. \tag{E.8}$$

Additionally, we will also need the relation

$$\begin{aligned} J_{\alpha,\beta}(m^2) &\equiv \int_q \frac{1}{(q^2+m^2)^\alpha (q^2)^\beta} \\ &= \frac{(m^2)^{2-\alpha-\beta-\epsilon}}{(4\pi\mu^2)^{-\epsilon}} \frac{\Gamma(2-\beta-\epsilon)\Gamma(\alpha+\beta-2+\epsilon))}{\Gamma(2-\epsilon)\Gamma(\alpha)} \end{aligned} \tag{E.9}$$

which can be obtained by interpreting $J_{\alpha,\beta}(m^2)$ as the integral $J_\alpha(m^2)$ in $d-2\beta$ dimensions, this is:

$$\int_q \frac{1}{(q^2+m^2)^\alpha (q^2)^\beta} = \frac{\Omega_d}{(2\pi)^d} \int_0^\infty dq \frac{q^{d-1} q^{-2\beta}}{(q^2+m^2)^\alpha}, \tag{E.10}$$

where $\Omega_d = 2\pi^{d/2}/\Gamma(d/2)$ is the d-dimensional solid angle and the integral in q can be easily solved by performing the change of variables $q^2 \to u$, $u \to m^2 y$ and $y \to 1/x - 1$. Combining Eq. (E.9) with Eq. (E.7), one also finds

$$\begin{aligned} I_{\alpha,\beta,\gamma}(m^2) &\equiv \int_p \int_q \frac{1}{(p^2+m^2)^\alpha (q^2)^\beta ((q+p)^2)^\gamma} = I_{\alpha,\gamma,\beta}(m^2) \\ &= \frac{(m^2)^{4-\alpha-\beta-\gamma-2\epsilon}}{(4\pi\mu^2)^{-2\epsilon}} \frac{\Gamma(2-\beta-\epsilon)\Gamma(2-\gamma-\epsilon)}{\Gamma(\alpha)\Gamma(\beta)\Gamma(\gamma)} \\ &\quad \times \frac{\Gamma(\beta+\gamma-2+\epsilon)\Gamma(\alpha+\beta+\gamma-4+2\epsilon)}{\Gamma(2-\epsilon)}. \end{aligned} \tag{E.11}$$

Finally, we will use the following result by Berends et al. [227]:

$$\begin{aligned} I_{\alpha,\beta,\gamma}(m^2,m^2) &\equiv \int_p \int_q \frac{1}{(p^2+m^2)^\alpha (q^2+m^2)^\beta ((q+p)^2)^\gamma} = I_{\beta,\alpha,\gamma}(m^2,m^2) \\ &= \frac{(m^2)^{4-\alpha-\beta-\gamma-2\epsilon}}{(4\pi\mu^2)^{-2\epsilon}} \frac{\Gamma(2-\gamma-\epsilon)\Gamma(\alpha+\gamma-2+\epsilon)\Gamma(\beta+\gamma-2+\epsilon)}{\Gamma(\alpha)\Gamma(\beta)\Gamma(2-\epsilon)} \\ &\quad \times \frac{\Gamma(\alpha+\beta+\gamma-4+2\epsilon)}{\Gamma(\alpha+\beta+2\gamma-4+2\epsilon)}. \end{aligned} \tag{E.12}$$

As described in Chapters 4 and 5, we need to expand the master integrals A_m, B_{m0} and B_{00} to order ϵ^2, as well as S_{000}, S_{m00}, I_{m00}, U_{0m00} and U_{00m0} to order ϵ^1. The ϵ^2 order of the integrals A_m and B_{00} can be easily deduced from (E.1)

and (E.7). Likewise, the ϵ^1 term for S_{000} can be obtained by using (E.7) twice. The corresponding term for I_{m00} can be obtained by means of Eq. (E.11).

To treat the integral $B_{m0}(k^2)$, we use the Feynman trick in the following way

$$B_{m0}(k^2) = \frac{\Gamma(\epsilon)}{(4\pi\mu^2)^{-\epsilon}} \int_0^1 dx (xm^2 + x(1-x)k^2)^{-\epsilon} \,. \tag{E.13}$$

Since the prefactor of the integral diverges as $1/\epsilon$[1], we need to expand the integral in the Feynman parameter to order ϵ^3, where each of the coefficients of ϵ^0, ϵ^1 and ϵ^2 is nothing but an integral which can be computed analytically in terms of logarithms and di-logarithms.

Concerning the integral $S_{m00}(k^2)$, its expansion can be found by writing

$$\begin{aligned} S_{m00}(k^2) &= \int_p \frac{I_{1,1}((p+k)^2)}{p^2+m^2} \\ &= \frac{\Gamma(1-\epsilon)^2\Gamma(\epsilon)}{(4\pi\mu^2)^{-\epsilon}\Gamma(2-2\epsilon)} \int \frac{d^dp}{(2\pi)^d} \frac{((p+k)^2)^{-\epsilon}}{p^2+m^2} \\ &= \frac{\Gamma(1-\epsilon)^2\Gamma(-1+2\epsilon)}{(4\pi\mu^2)^{-2\epsilon}\Gamma(2-2\epsilon)} \int_0^1 dx\,(1-x)^{-1+\epsilon}(xm^2)^{1-2\epsilon} \left(1+(1-x)\frac{k^2}{m^2}\right)^{1-2\epsilon} , \end{aligned} \tag{E.14}$$

where, again, we used the Feynman trick in the last step. An ϵ-expansion at this point would generate a singularity stemming from the term $\int^1 dx\,(1-x)^{-1}$. To avoid it we can work with the identity

$$\left(1+(1-x)\frac{k^2}{m^2}\right)^{1-2\epsilon} = 1 + \left[\left(1+(1-x)\frac{k^2}{m^2}\right)^{1-2\epsilon} - 1\right] \tag{E.15}$$

When we insert back this term in Eq. (E.14), the first term leads to an analytically computable integral which contains the divergence of the integral as $\epsilon \to 0$. In contrast, the second term leads to an integral regular in the limit $\epsilon \to 0$, thus allowing a safe ϵ-expansion. As a result, we obtain

$$\begin{aligned} S_{m00}(k^2) &= \frac{(m^2)^{1-2\epsilon}}{(4\pi\mu^2)^{-2\epsilon}} \frac{\Gamma(1-\epsilon)^2\Gamma(-1+2\epsilon)\Gamma(\epsilon)}{\Gamma(2-\epsilon)} \\ &+ \frac{(m^2)^{1-2\epsilon}}{(4\pi\mu^2)^{-2\epsilon}} \frac{\Gamma(1-\epsilon)^2\Gamma(-1+2\epsilon)}{\Gamma(2-2\epsilon)} \int_0^1 dx\, x^{1-2\epsilon}(1-x)^{-1+\epsilon} \\ &\quad \times \left[\left(1+(1-x)\frac{k^2}{m^2}\right)^{1-2\epsilon} - 1\right] . \end{aligned} \tag{E.16}$$

Since the prefactor of the integral diverges as $1/\epsilon$ as $\epsilon \to 0$, we need to expand the integrand to order ϵ^2. Again, all the integrals coming as coefficients of ϵ^0, ϵ^1 and ϵ^2 admit an analytic expression in terms of logarithms and di-logarithms.

[1] This is due to the property $\Gamma(\epsilon) = \frac{1}{\epsilon}\Gamma(1+\epsilon)$, where $\Gamma(1+\epsilon)$ is regular when $\epsilon \to 0$.

Next, we consider the integral $U_{0m00}(k^2)$. To begin with, we conveniently write it as

$$\begin{aligned}
U_{0m00}(k^2) &= \int_p \frac{I_{1,1}(p^2)}{p^2+m^2}\frac{1}{(p-k)^2} \\
&= \frac{\Gamma(1-\epsilon)^2\Gamma(\epsilon)}{(4\pi\mu^2)^{-\epsilon}\Gamma(2-2\epsilon)}\int_p \frac{(p^2)^{-\epsilon}}{p^2+m^2}\frac{1}{(p-k)^2} \\
&= \frac{\Gamma(1-\epsilon)^2\Gamma(2\epsilon)}{(4\pi\mu^2)^{-2\epsilon}\Gamma(2-2\epsilon)}(m^2)^{-2\epsilon} \\
&\quad \times \int_0^1 dx\, x^{-1+\epsilon}\int_0^{1-x} dy\left(1-x-y+y(1-y)\frac{k^2}{m^2}\right)^{-2\epsilon}. \qquad \text{(E.17)}
\end{aligned}$$

As occurred with $S_{m00}(k^2)$, a naive $\epsilon-$expansion is not valid since it leads to an artificial singularity at $x=0$. Rather, we can add and subtract to the integral over y its value at $x=0$. The advantage of doing this is that the added term can be calculated analytically whereas the subtracted term is regular in the $\epsilon\to 0$ limit, thus admitting an $\epsilon-$expansion. Provided that $\epsilon>0$ the result is

$$\begin{aligned}
U_{0m00}(k^2) &= \frac{\Gamma(1-\epsilon)^2\Gamma(2\epsilon)}{(4\pi\mu^2)^{-2\epsilon}\Gamma(2-2\epsilon)}\frac{(m^2)^{-2\epsilon}}{\epsilon}\int_0^1 dy\left(1-y+y(1-y)\frac{k^2}{m^2}\right)^{-2\epsilon} \\
&+ \frac{\Gamma(1-\epsilon)^2\Gamma(2\epsilon)}{(4\pi\mu^2)^{-2\epsilon}\Gamma(2-2\epsilon)}(m^2)^{-2\epsilon}\int_0^1 dx\, x^{-1+\epsilon} \\
&\left[\int_0^{1-x} dy\left(1-x-y+y(1-y)\frac{k^2}{m^2}\right)^{-2\epsilon}\right. \\
&\left. \qquad -\int_0^1 dy\left(1-y+y(1-y)\frac{k^2}{m^2}\right)^{-2\epsilon}\right]. \qquad \text{(E.18)}
\end{aligned}$$

Since the first integral is multiplied by a double pole in ϵ, it must be expanded to order ϵ^3 in order to calculate the term of order ϵ^1 in U_{0m00}. Since the integral multiplying the ϵ^3 term cannot be computed analytically, we implemented a numerical evaluation for it. As for the subtracted integral, since it is multiplied by a simple pole in ϵ, we need to expand it to order ϵ^2. Also for this term the corresponding coefficient was evaluated numerically.

To end with this appendix, let us analyze the case of the integral $U_{00m0}(k^2)$, which we write as

$$\begin{aligned}
U_{00m0}(k^2) &= \int_q \frac{1}{q^2+m^2}\int_p \frac{1}{p^2(p-q)^2(p-k)^2} \\
&= \frac{\Gamma(1+\epsilon)}{(4\pi\mu^2)^{-\epsilon}}\int_0^1 dx\int_0^{1-x} dy\int_q \frac{(x(1-x)q^2+y(1-y)k^2-2xyq\cdot k)^{-1-\epsilon}}{q^2+m^2}.
\end{aligned} \qquad \text{(E.19)}$$

By factoring out a term $(x(1-x))^{-1-\epsilon}$ in the numerator of the second integral, we can interpret the latter as a propagator to the power $1+\epsilon$. By applying once more the Feynman trick we get

$$
\begin{aligned}
U_{00m0}(k^2) &= \frac{\Gamma(2+\epsilon)}{(4\pi\mu^2)^{-\epsilon}} \int_0^1 dx\, x^{-1-\epsilon}(1-x)^{-1-\epsilon} \int_0^{1-x} dy \int_0^1 dz\, z^\epsilon \\
&\times \int_q \frac{1}{\left(q^2 + (1-z)m^2 + \frac{yz(1-x-y+xy(1-z))}{x(1-x)^2}k^2\right)^{2+\epsilon}} \\
&= \frac{\Gamma(2\epsilon)}{(4\pi\mu^2)^{-2\epsilon}} \int_0^1 dx\, x^{-1+\epsilon}(1-x)^{-1+3\epsilon} \\
&\times \int_0^{1-x} dy \int_0^1 dz\, z^\epsilon \left(x(1-x)^2(1-z)m^2 + yz(1-x-y+xy(1-z))k^2\right)^{-2\epsilon} .
\end{aligned}
\tag{E.20}
$$

In the limit $\epsilon \to 0$ the integrand features a divergence at $x = 0$. As before, a possible way to overcome this difficulty is by adding and subtracting from the yz-integral its value at $x = 0$. The added integral can be computed analytically, whereas the subtracted integral, being regular in the limit $\epsilon \to 0$, can safely be ϵ-expanded. We finally arrive at

$$
\begin{aligned}
U_{00m0}(k^2) &= \frac{(k^2)^{-2\epsilon}}{(4\pi\mu^2)^{-2\epsilon}} \frac{\Gamma(2\epsilon)\Gamma(\epsilon)\Gamma(3\epsilon)\Gamma(1-2\epsilon)^2}{\Gamma(4\epsilon)\Gamma(2-4\epsilon)(1+\epsilon)} \\
&+ \frac{\Gamma(2\epsilon)}{(4\pi\mu^2)^{-2\epsilon}} \int_0^1 dx\, x^{-1+\epsilon}(1-x)^{-1+3\epsilon} \\
&\times \left[\int_0^{1-x} dy \int_0^1 dz\, z^\epsilon \left(x(1-x)^2(1-z)m^2 + yz(1-x-y+xy(1-z))k^2\right)^{-2\epsilon}\right. \\
&\qquad \left. - \int_0^1 dy \int_0^1 dz\, z^\epsilon \left(yz(1-y)k^2\right)^{-2\epsilon}\right] .
\end{aligned}
\tag{E.21}
$$

Due to the presence of a simple pole in the last term, we need to expand the corresponding triple integral to order ϵ^2. The corresponding integral was evaluated numerically.

Appendix F

Small momentum expansion

In this appendix we derive IR expansions for the master integrals U_{0m00}, U_{00m0}, U_{0mm0}, S_{m00} and S_{mm0} for which, up to our knowledge, there are not analytic expressions in the literature. These expressions can be safely ϵ-expanded, thus allowing us to determine the low momentum expansion for the order ϵ^1 coefficient of the masters U_{0m00}, U_{00m0} and S_{m00}. These specific expansions are needed for the low momentum evaluation of the ghost-antighost-gluon and the three-gluon vertex.

In this appendix, we will use the integrals introduced in Appendix E. For convenience, we write them as $J_\alpha(m^2) = (m^2)^{2-\alpha-\epsilon} J_\alpha(1)$, $J_{\alpha,\beta}(m^2) = (m^2)^{2-\alpha-\beta-\epsilon} J_{\alpha,\beta}(1)$ and $I_{\alpha,\beta}(p^2) = (p^2)^{2-\alpha-\beta-\epsilon} I_{\alpha,\beta}(1)$, where the '1' in the argument of each function means that we replace m^2 and p^2 formally by 1 in the corresponding analytical expression. Similarly, $I_{\alpha,\beta,\gamma}(m^2) = (m^2)^{4-\alpha-\beta-\gamma-2\epsilon} I_{\alpha,\beta,\gamma}(1)$, $I_{\alpha,\beta,\gamma}(m^2, m^2) = (m^2)^{4-\alpha-\beta-\gamma-2\epsilon} I_{\alpha,\beta,\gamma}(1,1)$, and we note that $I_{\alpha,\beta,\gamma}(1) = B_{\beta,\gamma}(1) J_{\alpha,\beta+\gamma-2+\epsilon}(1)$.

Before starting, we note that the integrals $J_{\alpha,\beta}(m^2)$, $I_{\alpha,\beta}(p^2)$, $I_{\alpha,\beta,\gamma}(m^2)$ and $I_{\alpha,\beta,\gamma}(m^2, m^2)$ are IR divergent when some of their indices are large enough. Although these divergences are regularized in dimensional regularization (this is, the integrals do have a well defined expression as long as $\epsilon \neq 0$),[1] they mix with the UV divergences, so the integrals must be manipulated with care.

F.0.1 Small k^2 expansion of $U_{0m00}(k^2)$

Let us start by studying the integral

$$U_{0m00}(k^2) = I_{1,1}(1) \int_p \frac{(p^2)^{-\epsilon}}{p^2 + m^2} \frac{1}{(p+k)^2} \tag{F.1}$$

We aim at expanding $U_{0m00}(k^2)/I_{1,1}(1)$ for small k^2. The first term in the expansion is simply the limit $k^2 \to 0$ whose result is

$$\frac{U_{0m00}(0)}{I_{1,1}(1)} = J_{1,1+\epsilon}(m^2) = (m^2)^{-2\epsilon} J_{1,1+\epsilon}(1)\,, \tag{F.2}$$

[1] There are two exceptions to this: 1) when one of those indices equals exactly $d/2$, and dimensional regularization does not regularize IR divergences and 2) when the sum of all indices is equal to $d/2$, in which case dimensional regularization does not regularize the UV divergences. Luckily enough, we did not find such undefined integrals in our calculations.

and so

$$\frac{U_{0m00}(k^2)}{I_{1,1}(1)} = (m^2)^{-2\epsilon} J_{1,1+\epsilon}(1) + \mathcal{O}(k^2)\,, \tag{F.3}$$

In principle, so as to get the next term in the expansion we could write

$$\begin{aligned}\frac{1}{(p+k)^2} &= \frac{1}{p^2}\frac{1}{1+\frac{2(p\cdot k)+k^2}{p^2}} \\ &= \frac{1}{p^2}\left[1 - \frac{2(p\cdot k)}{p^2} - \frac{k^2}{p^2} + \frac{4(p\cdot k)^2}{p^4} + \dots\right],\end{aligned} \tag{F.4}$$

where the first term in the bracket would correspond the leading order contribution, the second term vanishes (because it is an odd function of the internal momentum p), the third and the fourth terms may be written in terms of $J_{1,2+\epsilon}$, leading to

$$\frac{U_{0m00}(k^2)}{I_{1,1}(1)} = (m^2)^{-2\epsilon}\left[J_{1,1+\epsilon}(1) + \frac{2\epsilon}{d}\frac{k^2}{m^2}J_{1,2+\epsilon}(1)\right] + \mathcal{O}(k^4) \tag{F.5}$$

However, it is easy to infer that Eq. (F.5) is not right. By simple power counting we know that $dU_{0m00}(k^2)/dk^2$ has a logarithmic divergence as $k \to 0$. This feature is not reflected by the right hand side of Eq. (F.5). Indeed, because of power counting, we can see that $J_{1,2+\epsilon}(1)$ is one of the IR divergent integrals discussed above and as such we can safely work with it only when it arises from the expansion of an IR-safe quantity. The quantity $U_{0m00}(k^2)/I_{1,1}(1)$ certainly is IR-safe, but $U_{0m00}(k^2)/I_{1,1}(1) - (m^2)^{-2\epsilon}J_{1,1+\epsilon}(1)$ (which we need to obtain the next term in the expansion) is not.

In order to circumvent this problem we can split the integrand in (F.1) into two pieces. A first piece which we can treat analytically and a second one, where the IR singularity can be removed by taking the k-expansion one order higher. To this end it is useful to write

$$\frac{1}{p^2+m^2} = \frac{1}{m^2} + \left[\frac{1}{p^2+m^2} - \frac{1}{m^2}\right] = \frac{1}{m^2}\left[1 - \frac{p^2}{p^2+m^2}\right]. \tag{F.6}$$

By inserting this identity into Eq. (F.1), we get

$$\frac{U_{0m00}(k^2)}{I_{1,1}(1)} = \frac{1}{m^2}\left[(k^2)^{1-2\epsilon}I_{1,\epsilon}(1) - \int_p \frac{(p^2)^{1-\epsilon}}{p^2+m^2}\frac{1}{(p+k)^2}\right]. \tag{F.7}$$

In the above equation, the first term in right hand side is known exactly, see Eq. (E.7). In the second term, the small k^2 expansion can be pushed to one order higher. In this case, we have an extra power of p^2 in the numerator of the integrand, thus avoiding the potential IR divergence. Inserting (F.4) into (F.7) leads to

$$\frac{U_{0m00}(k^2)}{I_{1,1}(1)} = \frac{k^2}{m^2}(k^2)^{-2\epsilon}B_{1,\epsilon}(1) - (m^2)^{-2\epsilon}\left[J_{1,\epsilon}(1) + \frac{2\epsilon}{d}\frac{k^2}{m^2}J_{1,1+\epsilon}(1)\right] + \mathcal{O}(k^4)\,. \tag{F.8}$$

The first term is of dimension $2-4\epsilon$. It contains poles in $1/\epsilon$ due to the UV divergences. This yields terms of the form $k^2 \ln k^2/\mu^2$, in consistency with the $k \to 0$ limit of $dU_{0m00}(k^2)/dk^2$. The remaining terms are regular in k^2. The leading term now appears as $-(m^2)^{-2\epsilon} J_{1,\epsilon}(1)$ instead of $(m^2)^{-2\epsilon} J_{1,1+\epsilon}(1)$. This makes perfect sense since $J_{1,\beta}(1) = -J_{1,\beta-1}(1)$[2]. Finally, we mention that (F.8) can be expanded to any order in ϵ.

The same strategy can be applied at any order in k^2. To do so, we iterate Eq. (F.6)

$$\begin{aligned}\frac{1}{p^2+m^2} &= \frac{1}{m^2}\left[1-\frac{p^2}{p^2+m^2}\right] \\ &= \frac{1}{m^2}\left[1-\frac{p^2}{m^2}+\frac{p^2}{m^2}\frac{p^2}{p^2+m^2}\right] \\ &= \frac{1}{m^2}\left[\sum_{j=0}^{n}\left(-\frac{p^2}{m^2}\right)^j-\left(-\frac{p^2}{m^2}\right)^n\frac{p^2}{p^2+m^2}\right],\end{aligned} \tag{F.9}$$

then,

$$\frac{U_{0m00}(k^2)}{I_{1,1}(1)} = \frac{1}{m^2}\left[\sum_{j=0}^{n}(-1)^j\frac{(k^2)^{1+j-2\epsilon}}{(m^2)^j}I_{1,\epsilon-j}(1)-\frac{(-1)^n}{(m^2)^n}\int_p\frac{(p^2)^{1+n-2\epsilon}}{p^2+m^2}\frac{1}{(p+k)^2}\right]. \tag{F.10}$$

The terms in the sum are known exactly and generate terms of the form $\ln k^2/\mu^2$, since all the functions $I_{1,\epsilon-j}(1)$ are UV divergent (thus featuring poles in $1/\epsilon$). The integral in (F.10) can be expanded to order $(k^2)^{n+1}$ without finding any IR divergence, thanks to the term $(p^2)^{1+n-2\epsilon}$ in the numerator. The corresponding regular expansion can be written in terms of integrals of the type $J_{\alpha,\beta}(1)$. To see this, we generalize (F.4) as

$$\begin{aligned}\frac{1}{(p+k)^2} &= \frac{1}{p^2}\sum_{j=0}^{2(n+1)}(-1)^j\left(\frac{2(p\cdot k)+k^2}{p^2}\right)^j+\dots \\ &= \sum_{j=0}^{2(n+1)}\frac{(-1)^j}{(p^2)^{j+1}}\sum_{\ell=0}^{j}\frac{j!}{\ell!(j-\ell)!}(2\,p\cdot k)^\ell(k^2)^{j-\ell}+\dots\end{aligned} \tag{F.11}$$

We consider the sum up to $2(n+1)$ to be sure that we generate all powers of k^2 up to $(k^2)^{n+1}$. However, it is understood that we must truncate any term beyond that order.

At this point it is convenient to introduce the following formula (for ℓ even, otherwise the integral vanishes) [216]:

$$\int_p f(p^2)\,(2\,p\cdot k)^\ell = \frac{\ell!}{(\ell/2)!}\frac{(k^2)^{\ell/2}}{(2-\epsilon)_{\ell/2}}\int_p f(p^2)\,(p^2)^{\ell/2}\,, \tag{F.12}$$

[2]This follows from Eq. (E.9) provided that $J_{1,\beta}(1)$ and $J_{1,\beta-1}(1)$ are well defined.

where we used the standard notation for the Pochhammer symbol in $(2-\epsilon)_{\ell/2}$.

Then, by plugging (F.11) into the last term of (F.10) and by using the above formula we arrive at

$$\int_p \frac{(p^2)^{1+n-\epsilon}}{p^2+m^2}\frac{1}{(p+k)^2} = (m^2)^{1+n-2\epsilon}\sum_{j=0}^{2(n+1)}\sum_{\ell(even)=0}^{j}(-1)^j\frac{j!}{(\ell/2)!(j-\ell)!}\left(\frac{k^2}{m^2}\right)^{j-\ell/2}\frac{J_{1,\epsilon-n+j-\ell/2}(1)}{(2-\epsilon)_{\ell/2}}\Bigg|_{(k^2)^{n+1}} + \cdots \tag{F.13}$$

So, we get

$$\frac{U_{0m00}(k^2)}{I_{1,1}(1)} = (k^2)^{-2\epsilon}\sum_{j=0}^{n}(-1)^j\left(\frac{k^2}{m^2}\right)^{j+1} I_{1,\epsilon-j}(1) - (m^2)^{-2\epsilon}\sum_{j=0}^{2(n+1)}\sum_{\ell=0}^{[j/2]}(-1)^{n+j}\frac{j!}{\ell!(j-2\ell)!}\left(\frac{k^2}{m^2}\right)^{j-\ell}\frac{J_{1,\epsilon-n+j-\ell}(1)}{(2-\epsilon)_\ell}\Bigg|_{(k^2)^{n+1}} + \mathcal{O}((k^2)^{n+2})\,. \tag{F.14}$$

We checked that this formula leads to the known low-k^2 expansion for the ϵ^0 contributions, see *e.g.* [215]. Afterwards, we used it to evaluate the corresponding expansion for the contributions of order ϵ^1. We checked that the latter matches with a numerical evaluation of the corresponding ϵ^1 contributions to $U_{0m00}(k^2)$ at small k^2.

F.0.2 Small k^2 expansion of $U_{00m0}(k^2)$

Now we consider the integral

$$U_{00m0}(k^2) = \int_p \frac{1}{p^2}\frac{1}{(p+k)^2}\int_q \frac{1}{q^2+m^2}\frac{1}{(q+p)^2}\,. \tag{F.15}$$

In this case the leading term of the low-k^2 expansion is already delicate, so it is convenient to work with the identity

$$\frac{1}{(q+p)^2} = \frac{1}{q^2} + \left[\frac{1}{(q+p)^2} - \frac{1}{q^2}\right] = \frac{1}{q^2}\left[1 - \frac{2(p\cdot q)+p^2}{(q+p)^2}\right] \tag{F.16}$$

to arrive at

$$U_{00m0}(k^2) = -\frac{1}{m^2}J_1(m^2)\,I_{1,1}(k^2) - \int_q \frac{1}{q^2(q^2+m^2)}\int_p \frac{2(q\cdot p)+p^2}{p^2(p+k)^2(q+p)^2}\,. \tag{F.17}$$

The first term is known exactly while the second one is regular in the $k^2 \to 0$ limit. We can evaluate it by writing

$$\begin{aligned}\int_p \frac{2(q\cdot p)+p^2}{p^4(q+p)^2} &= \int_p \frac{(q+p)^2-q^2}{p^4(q+p)^2} \\ &= \int_p \frac{1}{p^4} - q^2\int_p \frac{1}{p^4(q+p)^2}\,.\end{aligned} \tag{F.18}$$

We note here that Eq. (F.18) is by itself another example of the use of dimensionally regularized IR divergent integrals. As the left hand side of Eq. (F.18) is IR safe, its decomposition in terms of IR divergent integrals can be carried out safely. In order to evaluate the second line one can add a mass regulator to both quartic propagators (because the left hand is infrared safe) as $1/p^4 \to 1/(p^2+m^2)^2$ or even $1/p^2 \to 1/(p^2(p^2+m^2))$ and end the calculation. We checked that the same result is obtained by applying the Feynman trick directly to the left hand side of Eq. (F.18). Moreover, we verified that this result is also retrieved by using the well known result $\int d^dp/p^4 = 0$ [64], therefore, we are allowed to write

$$\begin{aligned}\int_p \frac{2(q\cdot p)+p^2}{p^4(q+p)^2} &= -q^2\int_p \frac{1}{p^4(q+p)^2} \\ &= -\frac{(q^2)^{-\epsilon}}{(4\pi\mu^2)^{-\epsilon}}\Gamma(1+\epsilon)\frac{\Gamma(1-\epsilon)\Gamma(-\epsilon)}{\Gamma(1-2\epsilon)}\,.\end{aligned} \tag{F.19}$$

We can insert back this result into (F.17), obtaining the known integral $J_{1,1+\epsilon}$.

Similarly to the U_{0m00} case, we can compute higher orders by iterating (F.16)

$$\begin{aligned}\frac{1}{(q+p)^2} &= \frac{1}{q^2}\left[1-\frac{2(p\cdot q)+p^2}{(q+p)^2}\right] \\ &= \frac{1}{q^2}\left[1-\frac{2(p\cdot q)+p^2}{q^2}+\frac{2(p\cdot q)+p^2}{q^2}\frac{2(p\cdot q)+p^2}{(q+p)^2}\right] \\ &= \frac{1}{q^2}\left[\sum_{j=0}^{n}\left(-\frac{2(p\cdot q)+p^2}{q^2}\right)^j-\left(-\frac{2(p\cdot q)+p^2}{q^2}\right)^n\frac{2(p\cdot q)+p^2}{(q+p)^2}\right].\end{aligned} \tag{F.20}$$

Then

$$\begin{aligned}U_{00m0}(k^2) &= \sum_{j=0}^{n}(-1)^j\int_q\frac{(q^2)^{-j-1}}{(q^2+m^2)}\int_p\frac{(2(p\cdot q)+p^2)^j}{p^2(p+k)^2} \\ &- (-1)^n\int_q\frac{(q^2)^{-n-1}}{(q^2+m^2)}\int_p\frac{(2(p\cdot q)+p^2)^{n+1}}{p^2(p+k)^2(q+p)^2}\,.\end{aligned} \tag{F.21}$$

The first line can be computed analytically while in the second line we can safely expand to the relevant order in k^2 without generating any IR divergence. In addition, the corresponding coefficients can be computed analytically. In order to solve the first line, it is useful to begin by performing the integral over q,

$$\begin{aligned}\int_q\frac{(2(p\cdot q)+p^2)^j}{(q^2)^{j+1}(q^2+m^2)} &= \sum_{\ell=0}^{j}\frac{j!}{\ell!(j-\ell)!}(p^2)^{j-\ell}\int_q\frac{(2(p\cdot q))^\ell}{(q^2)^{j+1}(q^2+m^2)} \\ &= (m^2)^{d/2-2}\sum_{\ell(even)=0}^{j}\frac{j!}{(\ell/2)!(j-\ell)!}\left(\frac{p^2}{m^2}\right)^{j-\ell/2}\frac{J_{1,1+j-\ell/2}(1)}{(2-\epsilon)_{\ell/2}}\,,\end{aligned} \tag{F.22}$$

where in the last line we used the formula (F.12). So as to carry out the expansion in the last line of Eq. (F.21) we can make use of the identity

$$\frac{(2(p\cdot q)+p^2)^{n+1}}{p^2(p+k)^2} = \sum_{j=0}^{2n}\frac{(-1)^j}{(p^2)^{j+2}}(2(p\cdot q)+p^2)^{n+1}(2(p\cdot k)+k^2)^j\Big|_{(k^2)^n} + \dots \tag{F.23}$$

Therefore, we must evaluate

$$\begin{aligned}
&\int\frac{d^dp}{(2\pi)^d}\frac{(2(p\cdot q)+p^2)^{n+1}(2(p\cdot k)+k^2)^j}{(p^2)^{j+2}(q+p)^2}\\
&= -q^2\int\frac{d^dp}{(2\pi)^d}\frac{(2(p\cdot q)+p^2)^{n}(2(p\cdot k)+k^2)^j}{(p^2)^{j+2}(q+p)^2}\\
&= (-q^2)^k\int\frac{d^dp}{(2\pi)^d}\frac{(2(p\cdot q)+p^2)^{n+1-k}(2(p\cdot k)+k^2)^j}{(p^2)^{j+2}(q+p)^2}\\
&= (-q^2)^{n+1}\int\frac{d^dp}{(2\pi)^d}\frac{(2(p\cdot k)+k^2)^j}{(p^2)^{j+2}(q+p)^2}\,,
\end{aligned} \tag{F.24}$$

where we used similar tricks as in (F.18). By plugging these formulas into (F.21) and by invert the order of the integrals, we get

$$\begin{aligned}
U_{00m0}(k^2) &= (k^2m^2)^{-\epsilon}\sum_{j=0}^{n}(-1)^j\sum_{\ell=0}^{[j/2]}\frac{j!}{\ell!(j-2\ell)!}\left(\frac{k^2}{m^2}\right)^{j-\ell}\frac{J_{1,1+j-\ell}(1)}{(2-\epsilon)_\ell}I_{1,1+\ell-j}(1)\\
&+\sum_{j=0}^{2n}(-1)^j\int_p\frac{(2(p\cdot k)+k^2)^j}{(p^2)^{j+2}}\int_q\frac{1}{(q^2+m^2)(q+p)^2}\Bigg|_{(k^2)^n}+\mathcal{O}((k^2)^{n+1})\\
&= (k^2m^2)^{-\epsilon}\sum_{j=0}^{n}(-1)^j\sum_{\ell=0}^{[j/2]}\frac{j!}{\ell!(j-2\ell)!}\left(\frac{k^2}{m^2}\right)^{j-\ell}\frac{J_{1,1+j-\ell}(1)}{(2-\epsilon)_\ell}I_{1,1+\ell-j}(1)\\
&+\sum_{j=0}^{2n}(-1)^j\sum_{\ell=0}^{j}\frac{j!}{\ell!(j-\ell)!}(k^2)^{j-\ell}\int_p\frac{(2\,p\cdot k)^\ell}{(p^2)^{j+2}}\int_q\frac{1}{(q^2+m^2)(q+p)^2}\Bigg|_{(k^2)^n}\\
&+\mathcal{O}((k^2)^{n+1})\,.
\end{aligned} \tag{F.25}$$

Since the inner integral is a function of p^2, we can then use the identity from Eq. (F.12) again to obtain

$$\begin{aligned}
U_{00m0}(k^2) &= (k^2m^2)^{-\epsilon}\sum_{j=0}^{n}(-1)^j\sum_{\ell=0}^{[j/2]}\frac{j!}{\ell!(j-2\ell)!}\left(\frac{k^2}{m^2}\right)^{j-\ell}\frac{J_{1,1+j-\ell}(1)}{(2-\epsilon)_\ell}I_{1,1+\ell-j}(1)\\
&+\sum_{j=0}^{2n}(-1)^j\sum_{\ell=0}^{[j/2]}\frac{j!}{\ell!(j-2\ell)!}\frac{(k^2)^{j-\ell}}{(d/2)_\ell}\int_p\frac{1}{(p^2)^{j+2-\ell}}\int_q\frac{1}{(q^2+m^2)(q+p)^2}\Bigg|_{(k^2)^n}\\
&+\mathcal{O}((k^2)^{n+1})\,.
\end{aligned} \tag{F.26}$$

The double integral is

$$I_{1,1,j+2-\ell}(m^2) = (m^2)^{d-4-j+\ell}J_{1,1+\epsilon+j-\ell}(1)B_{1,j+2-\ell}(1), \tag{F.27}$$

therefore,

$$U_{00m0}(k^2) = (k^2m^2)^{-\epsilon}\sum_{j=0}^{n}(-1)^j\sum_{\ell=0}^{[j/2]}\frac{j!}{\ell!(j-2\ell)!}\left(\frac{k^2}{m^2}\right)^{j-\ell}\frac{J_{1,1+j-\ell}(1)}{(2-\epsilon)_\ell}B_{1,1+\ell-j}(1)$$
$$+ (m^4)^{-\epsilon}\sum_{j=0}^{2n}(-1)^j\sum_{\ell=0}^{[j/2]}\frac{j!}{\ell!(j-2\ell)!}\left(\frac{k^2}{m^2}\right)^{j-\ell}\frac{J_{1,1+\epsilon+j-\ell}(1)}{(2-\epsilon)_\ell}B_{1,j+2-\ell}(1)\Bigg|_{(k^2)^n}$$
$$+ \mathcal{O}((k^2)^{n+1})\,. \tag{F.28}$$

F.0.3 Small k^2 expansion of $U_{0mm0}(k^2)$

In this section we work with the integral

$$U_{0mm0}(k^2) \equiv \int_p \frac{1}{p^2}\frac{1}{(p+k)^2+m^2}\int_q \frac{1}{q^2}\frac{1}{(q+p)^2+m^2}\,. \tag{F.29}$$

In this case it is convenient to write

$$\frac{1}{(q+k)^2+m^2} = \frac{1}{q^2+m^2+2(q\cdot k)+k^2}\sum_{j=0}^{\infty}(-1)^j\frac{(2(q\cdot k)+k^2)^j}{(q^2+m^2)^{j+1}}, \tag{F.30}$$

then,

$$U_{0mm0}(k^2) = \sum_{j=0}^{\infty}(-1)^j\int_p\frac{1}{p^2}\frac{(2(p\cdot k)+k^2)^j}{(p^2+m^2)^{j+1}}\int_q\frac{1}{q^2}\frac{1}{(q+p)^2+m^2}$$
$$= \sum_{j=0}^{\infty}(-1)^j\sum_{\ell=0}^{j}\frac{j!}{\ell!(j-\ell)!}(k^2)^{j-\ell}\int_p\frac{1}{p^2}\frac{(2\,p\cdot k)^\ell}{(p^2+m^2)^{j+1}}\int_q\frac{1}{q^2}\frac{1}{(q+p)^2+m^2}\,.$$

By using Eq. (F.12) we arrive at

$$U_{0mm0}(k^2) = \sum_{j=0}^{\infty}(-1)^j\sum_{\ell=0}^{[j/2]}\frac{j!}{\ell!(j-2\ell)!}\frac{(k^2)^{j-\ell}}{(d/2)_\ell}\int_p\frac{(p^2)^\ell}{p^2(p^2+m^2)^{j+1}}$$
$$\times\int_q\frac{1}{q^2}\frac{1}{(q+p)^2+m^2} = \sum_{j=0}^{\infty}(-1)^j\sum_{\ell=0}^{[j/2]}\frac{j!}{(j-2\ell)!}\frac{(k^2)^{j-\ell}}{(d/2)_\ell}\sum_{h=0}^{\ell}\frac{(-1)^{\ell-h}(m^2)^{\ell-h}}{h!(\ell-h)!}$$
$$\times\int_p\frac{1}{p^2(p^2+m^2)^{j-h+1}}\int_q\frac{1}{q^2}\frac{1}{(q+p)^2+m^2}\,. \tag{F.31}$$

Now it is convenient to separate the propagators $G_0(p)$ and $G_m(p)$ in the following way

$$\frac{1}{p^2(p^2+m^2)^{j-h+1}} = \frac{1}{m^2p^2(p^2+m^2)^{j-h}} - \frac{1}{m^2(p^2+m^2)^{j-h+1}}$$
$$= \frac{1}{m^4p^2(p^2+m^2)^{j-h-1}} - \frac{1}{m^4(p^2+m^2)^{j-h}} - \frac{1}{m^2(p^2+m^2)^{j-h+1}}$$
$$= \frac{1}{(m^2)^{j-h+1}p^2} - \sum_{i=0}^{j-h}\frac{1}{(m^2)^{i+1}(p^2+m^2)^{j-h+1-i}}\,, \tag{F.32}$$

which leads to

$$U_{0mm0}(k^2) = \sum_{j=0}^{\infty}(-1)^j \sum_{\ell=0}^{[j/2]} \frac{j!}{(j-2\ell)!} \frac{(k^2)^{j-\ell}}{(d/2)_\ell} \sum_{h=0}^{\ell} \frac{(-1)^{\ell-h}(m^2)^{\ell-j-1}}{h!(\ell-h)!} I_{1,1,1}(m^2)$$
$$- \sum_{j=0}^{\infty}(-1)^j \sum_{\ell=0}^{[j/2]} \frac{j!}{(j-2\ell)!} \frac{(k^2)^{j-\ell}}{(d/2)_\ell} \sum_{h=0}^{\ell} \frac{(-1)^{\ell-h}(m^2)^{\ell-h}}{h!(\ell-h)!} \sum_{i=0}^{j-h} \frac{I_{j-h+1-i,1,1}(m^2,m^2)}{(m^2)^{i+1}} . \tag{F.33}$$

Bu using $I_{\alpha,\beta,\gamma}(1) = B_{\beta,\gamma}(1) J_{\alpha,\beta+\gamma-2+\epsilon}(1)$, we get

$$U_{0mm0}(k^2)$$
$$= (m^2)^{-2\epsilon} \sum_{j=0}^{\infty}(-1)^j \sum_{\ell=0}^{[j/2]} \frac{j!}{(j-2\ell)!} \left(\frac{k^2}{m^2}\right)^{j-\ell} \sum_{h=0}^{\ell} \frac{(-1)^{\ell-h}}{h!(\ell-h)!} \frac{J_{1,2-d/2}(1) B_{1,1}(1)}{(2-\epsilon)_\ell}$$
$$- (m^2)^{-2\epsilon} \sum_{j=0}^{\infty}(-1)^j \sum_{\ell=0}^{[j/2]} \frac{j!}{(j-2\ell)!} \left(\frac{k^2}{m^2}\right)^{j-\ell} \sum_{h=0}^{\ell} \frac{(-1)^{\ell-h}}{h!(\ell-h)!} \sum_{i=0}^{j-h} \frac{I_{j-h+1-i,1,1}(1,1)}{(2-\epsilon)_\ell} . \tag{F.34}$$

F.0.4 Small k^2 expansion of $S_{m00}(k^2)$

Let us consider the master integral

$$S_{m00}(k^2) = \int_p \frac{1}{p^2+m^2} \int_q \frac{1}{q^2(q+p+k)^2} \tag{F.35}$$

and thus

$$\frac{S_{m00}(k^2)}{I_{1,1}(1)} = \int_p \frac{(p+k)^{-\epsilon}}{p^2+m^2} . \tag{F.36}$$

If we leave the momentum k in the massless propagator, we have to be careful with the generation of potential IR divergent terms. This can be done by taking into account the previous considerations. We start by writing

$$\frac{S_{m00}(k^2)}{I_{1,1}(1)} = \frac{1}{m^2} \left[\sum_{j=0}^{n}(-1)^j \frac{(k^2)^{2+j-2\epsilon}}{(m^2)^j} B_{\epsilon,-j}(1) - \frac{(-1)^n}{(m^2)^n} \int_p ((p+k)^2)^{-\epsilon} \frac{(p^2)^{n+1}}{p^2+m^2} \right]$$
$$= \frac{1}{m^2} \left[\sum_{j=0}^{n}(-1)^j \frac{(k^2)^{2+j-2\epsilon}}{(m^2)^j} B_{\epsilon,-j}(1) + \mathcal{O}((k^2)^{n+3}) \right.$$
$$\left. - \frac{(-1)^n}{(m^2)^n} \sum_{j=0}^{2n+4} \frac{\Gamma(1-\epsilon)}{\Gamma(j+1)\Gamma(1-j-\epsilon)} \int_p (2(p\cdot k)+k^2)^j \frac{(p^2)^{1+n-j-\epsilon}}{p^2+m^2} \Bigg|_{(k^2)^{n+2}} \right]$$
$$= \frac{1}{m^2} \left[\sum_{j=0}^{n}(-1)^j \frac{(k^2)^{2+j-2\epsilon}}{(m^2)^j} B_{\epsilon,-j}(1) + \mathcal{O}((k^2)^{n+3}) \right.$$
$$\left. - \frac{(-1)^n}{(m^2)^n} \sum_{j=0}^{2n+4} \frac{\Gamma(1-\epsilon)}{\Gamma(1-j-\epsilon)} \sum_{\ell=0}^{[j/2]} \frac{1}{\ell!(j-2\ell)!} \frac{(k^2)^{j-\ell}}{(d/2)_\ell} \int_p \frac{(p^2)^{1+n-j+\ell-\epsilon}}{p^2+m^2} \Bigg|_{(k^2)^{n+2}} \right] , \tag{F.37}$$

where we have used Eq. (F.12). Consequently,

$$\frac{S_{m00}(k^2)}{I_{1,1}(1)} = \frac{1}{m^2}\left[\sum_{j=0}^{n}(-1)^j\frac{(k^2)^{2+j-2\epsilon}}{(m^2)^j}B_{\epsilon,-j}(1) + \mathcal{O}((k^2)^{n+3})\right.$$
$$- (-1)^n(m^2)^{2-2\epsilon}\sum_{j=0}^{2n+4}\frac{\Gamma(1-\epsilon)}{\Gamma(1-j-\epsilon)}\sum_{\ell=0}^{[j/2]}\frac{1}{\ell!(j-2\ell)!}\left(\frac{k^2}{m^2}\right)^{j-\ell}$$
$$\left.\times\frac{J_{1,-1-n+j-\ell+\epsilon}(1)}{(d/2)_\ell}\bigg|_{(k^2)^{n+2}}\right] = (k^2)^{1-2\epsilon}\sum_{j=0}^{n}(-1)^j\left(\frac{k^2}{m^2}\right)^{j+1}B_{\epsilon,-j}(1) + \mathcal{O}((k^2)^{n+3})$$
$$- (-1)^n(m^2)^{1-2\epsilon}\sum_{j=0}^{2n+4}\frac{\Gamma(1-\epsilon)}{\Gamma(1-j-\epsilon)}\sum_{\ell=0}^{[j/2]}\frac{1}{\ell!(j-2\ell)!}\left(\frac{k^2}{m^2}\right)^{j-\ell}\frac{J_{1,\epsilon-1-n+j-\ell}(1)}{(2-\epsilon)_\ell}\bigg|_{(k^2)^{n+2}}, \tag{F.38}$$

Since $B_{\epsilon,-i} = 0$, see Eq. (E.7), we can write

$$\frac{S_{m00}(k^2)}{I_{1,1}(1)} = (-1)^{n+1}(m^2)^{1-2\epsilon}\sum_{j=0}^{2n+4}\frac{\Gamma(1-\epsilon)}{\Gamma(1-j-\epsilon)}\sum_{\ell=0}^{[j/2]}\frac{1}{\ell!(j-2\ell)!}\left(\frac{k^2}{m^2}\right)^{j-\ell}$$
$$\times\frac{J_{1,\epsilon-1-n+j-\ell}(1)}{(2-\epsilon)_\ell}\bigg|_{(k^2)^{n+2}} + \mathcal{O}((k^2)^{n+3})\,. \tag{F.39}$$

We can now use the formula $J_{1,\beta}(1) = -J_{1,\beta-1}(1)$, see discussion below Eq. (F.8), to get

$$\frac{S_{m00}(k^2)}{I_{1,1}(1)} = (m^2)^{1-2\epsilon}\sum_{j=0}^{2n+4}\frac{\Gamma(1-\epsilon)}{\Gamma(1-j-\epsilon)}\sum_{\ell=0}^{[j/2]}\frac{1}{\ell!(j-2\ell)!}\left(\frac{k^2}{m^2}\right)^{j-\ell}\frac{J_{1,\epsilon+j-\ell}(1)}{(2-\epsilon)_\ell}\bigg|_{(k^2)^{n+2}}$$
$$+ \mathcal{O}((k^2)^{n+3})\,, \tag{F.40}$$

which can be seen simply as the order $(k^2)^{n+2}$ of

$$\frac{S_{m00}(k^2)}{I_{1,1}(1)} = (m^2)^{1-2\epsilon}\sum_{j=0}^{\infty}\frac{\Gamma(1-\epsilon)}{\Gamma(1-j-\epsilon)}\sum_{\ell=0}^{[j/2]}\frac{1}{\ell!(j-2\ell)!}\left(\frac{k^2}{m^2}\right)^{j-\ell}\frac{J_{1,\epsilon+j-\ell}(1)}{(2-\epsilon)_\ell}\,. \tag{F.41}$$

F.0.5 Small k^2 expansion of $S_{mm0}(k^2)$

We end this section with the master integral

$$S_{mm0}(k^2) = \int_p \frac{1}{p^2}\frac{1}{(q+p)^2+m^2}\int_q \frac{1}{(q+k)^2+m^2}\,. \tag{F.42}$$

By means of Eq. (F.30) we obtain

$$
\begin{aligned}
S_{mm0}(k^2) &= \sum_{j=0}^{\infty}(-1)^j \int_p\int_q \frac{1}{p^2}\frac{1}{(q+p)^2+m^2}\frac{(2(q\cdot k)+k^2)^j}{(q^2+m^2)^{j+1}} \\
&= \sum_{j=0}^{\infty}(-1)^j \sum_{\ell=0}^{j}\frac{j!}{\ell!(j-\ell)!}(k^2)^{j-\ell}\int_q \frac{(2\,q\cdot k)^\ell}{(q^2+m^2)^{j+1}}\int_p \frac{1}{p^2}\frac{1}{(q+p)^2+m^2} \\
&= \sum_{j=0}^{\infty}(-1)^j \sum_{\ell=0}^{[j/2]}\frac{j!}{\ell!(j-2\ell)!}\frac{(k^2)^{j-\ell}}{(d/2)_\ell}\int_q \frac{(q^2)^\ell}{(q^2+m^2)^{j+1}}\int_p \frac{1}{p^2}\frac{1}{(q+p)^2+m^2} \\
&= \sum_{j=0}^{\infty}(-1)^j \sum_{\ell=0}^{[j/2]}\frac{j!}{(j-2\ell)!}\frac{(k^2)^{j-\ell}}{(d/2)_\ell}\sum_{h=0}^{\ell}\frac{(-1)^{\ell-h}(m^2)^{\ell-h}}{h!(\ell-h)!} \\
&\qquad \times \int_q \frac{1}{(q^2+m^2)^{j+1-h}}\int_p \frac{1}{p^2}\frac{1}{(q+p)^2+m^2} \\
&= (m^2)^{1-2\epsilon}\sum_{j=0}^{\infty}(-1)^j \sum_{\ell=0}^{[j/2]}\frac{j!}{(j-2\ell)!}\left(\frac{k^2}{m^2}\right)^{j-\ell}\sum_{h=0}^{\ell}\frac{(-1)^{\ell-h}}{h!(\ell-h)!}\frac{I_{j+1-h,1,1}(1,1)}{(2-\epsilon)_\ell}\,.
\end{aligned}
\tag{F.43}
$$

We could have proceeded in the same manner in the case of $S_{m00}(k^2)$, with the difference that in the step

$$
S_{m00}(k^2) = \sum_{j=0}^{\infty}(-1)^j \sum_{\ell=0}^{[j/2]}\frac{j!}{\ell!(j-2\ell)!}\frac{(k^2)^{j-\ell}}{(d/2)_\ell}\int_q \frac{(q^2)^\ell}{(q^2+m^2)^{j+1}}\int_p \frac{1}{p^2}\frac{1}{(q+p)^2}
\tag{F.44}
$$

we get the result

$$
\begin{aligned}
\frac{S_{m00}(k^2)}{I_{1,1}(1)} &= \sum_{j=0}^{\infty}(-1)^j \sum_{\ell=0}^{[j/2]}\frac{j!}{\ell!(j-2\ell)!}\frac{(k^2)^{j-\ell}}{(d/2)_\ell}\int \frac{d^dq}{(2\pi)^d}\frac{(q^2)^{-\epsilon+\ell}}{(q^2+m^2)^{j+1}} \\
&= (m^2)^{1-2\epsilon}\sum_{j=0}^{\infty}(-1)^j \sum_{\ell=0}^{[j/2]}\frac{j!}{\ell!(j-2\ell)!}\left(\frac{k^2}{m^2}\right)^{j-\ell}\frac{J_{j+1,\epsilon-\ell}(1)}{(2-\epsilon)_\ell}\,.
\end{aligned}
\tag{F.45}
$$

Because of

$$
\frac{J_{j+a,b}(1)}{J_{a,j+b}(1)} = \frac{\Gamma(d/2-b)}{\Gamma(d/2-j-b)}\frac{\Gamma(a)}{\Gamma(j+a)}\,,
\tag{F.46}
$$

we can write

$$
\frac{J_{j+1,\epsilon-\ell}(1)}{J_{1,j+\epsilon-\ell}(1)} = \frac{\Gamma(2-2\epsilon+\ell)}{\Gamma(2-2\epsilon+\ell-j)}\frac{1}{j!}\,,
\tag{F.47}
$$

and thus

$$
\begin{aligned}
\frac{S_{m00}(k^2)}{I_{1,1}(1)} &= \sum_{j=0}^{\infty}(-1)^j \sum_{\ell=0}^{[j/2]}\frac{j!}{\ell!(j-2\ell)!}\frac{(k^2)^{j-\ell}}{(d/2)_\ell}\int \frac{d^dq}{(2\pi)^d}\frac{(q^2)^{-\epsilon+\ell}}{(q^2+m^2)^{j+1}} \\
&= (m^2)^{1-2\epsilon}\sum_{j=0}^{\infty}(-1)^j \sum_{\ell=0}^{[j/2]}\frac{1}{\ell!(j-2\ell)!}\frac{\Gamma(2-2\epsilon+\ell)}{\Gamma(2-2\epsilon+\ell-j)}\left(\frac{k^2}{m^2}\right)^{j-\ell}\frac{J_{1,j+\epsilon-\ell}(1)}{(2-\epsilon)_\ell}\,.
\end{aligned}
\tag{F.48}
$$

This expression does not look exactly like (F.41). Nonetheless, we checked with MATHEMATICA that the two expressions actually coincide for various values of n.

Appendix G

Small mass expansion

In this appendix we present an example which shows that a standard expansion in powers of the mass does not lead to the correct small mass expansion, since it can introduce spurious IR divergences. However, as we discuss at the end of this appendix, such naive Taylor expansion could yield the right result under certain conditions. This seems to be the case of the ghost-antighost-gluon vertex function, as we explained in Chapter 4.

To begin with, let us consider the integral

$$B_{m0}(p^2) \equiv \int \frac{d^d q}{(2\pi)^d} \frac{1}{q^2+m^2} \frac{1}{(q+p)^2} \,. \tag{G.1}$$

If we carry out a naive Taylor expansion in powers of the mass, we find

$$B_{m0}(p^2) \to \int \frac{d^d q}{(2\pi)^d} \frac{1}{q^2} \frac{1}{(q+p)^2} - m^2 \int \frac{d^d q}{(2\pi)^d} \frac{1}{q^4} \frac{1}{(q+p)^2} + \mathcal{O}\left(\frac{m^4}{p^4}\right). \tag{G.2}$$

Despite both integrals are well defined, this result should be taken with a grain of salt since the second integral introduces an extra pole $1/\epsilon$, which is indicating a misuse of IR divergent integrals, as occurred in Eq. (F.5)[1]

In order to avoid this problematic behavior it is useful to introduce the relation

$$\frac{1}{(q+p)^2} = \frac{1}{p^2} + \left[\frac{1}{(q+p)^2} - \frac{1}{p^2}\right] \tag{G.3}$$

which leads to

$$B_{m0}(p^2) = \frac{1}{p^2} \int \frac{d^d q}{(2\pi)^d} \frac{1}{q^2+m^2} + \int \frac{d^d q}{(2\pi)^d} \frac{1}{q^2+m^2} \left[\frac{1}{(q+p)^2} - \frac{1}{p^2}\right]. \tag{G.4}$$

The first term is proportional to $(m^2)^{d/2-1} = (m^2)^{1-\epsilon}$ and such it does not admit any low mass Taylor expansion. In the second term, the naive Taylor expansion can be pushed to order m^2 without introducing IR divergences. We find

$$\begin{aligned} B_{m0}(p^2) = \frac{1}{p^2} \int \frac{d^d q}{(2\pi)^d} \frac{1}{q^2+m^2} + \int \frac{d^d q}{(2\pi)^d} \frac{1}{q^2} \left[\frac{1}{(q+p)^2} - \frac{1}{p^2}\right] \\ - m^2 \int \frac{d^d q}{(2\pi)^d} \frac{1}{q^4} \left[\frac{1}{(q+p)^2} - \frac{1}{p^2}\right] + \mathcal{O}\left(\frac{m^4}{p^4}\right). \end{aligned} \tag{G.5}$$

[1] Note that the pole of $B_{m0}(p^2)$ is already present in the first integral in (G.2). We are reasoning under the assumption that the ϵ and low-m expansions commute. We will check below that this assumption is indeed correct, at least for the example of $B_{m0}(p^2)$.

which, after the cancellation of some dimensional regularization zeros, gives

$$\begin{aligned} B_{m0}(p^2) &= \int \frac{d^dq}{(2\pi)^d}\frac{1}{q^2}\frac{1}{(q+p)^2} - m^2\int \frac{d^dq}{(2\pi)^d}\frac{1}{q^4}\frac{1}{(q+p)^2} \\ &+ \frac{1}{p^2}\int \frac{d^dq}{(2\pi)^d}\frac{1}{q^2+m^2} + \mathcal{O}\left(\frac{m^4}{p^4}\right). \end{aligned} \tag{G.6}$$

The only difference between this expression and (G.2) is given by the last term. We note that the problematic integral there is also present in Eq. (G.6). However, the pole introduced for such integral is exactly canceled by the pole of the last integral in Eq. (G.6). As a result, the only pole present in the right hand side of Eq. (G.6) comes from the first term, as it should be.

With the purpose of testing this result, in what follows we evaluate the low mass expansion of $B_{m0}(p^2)$ by using an alternative approach. More precisely, we exploit the fact that, provided that there is only one mass scale, the low mass expansion is equivalent to the UV-expansion, see Eq. (4.57). The latter can be determined by means of Weinberg's theorem. We remind the reader that this theorem classifies the various contributions that make the large momentum asymptotic expansion according to the possible ways the momentum can flow inside the diagram. For each of such contributions one must expand in powers of any scale (momentum or mass) that appear in the propagator whose total momentum is large. Applying these ideas to our example, we obtain

$$\begin{aligned} B_{m0}(p^2) \to & \left[\int \frac{d^dq}{(2\pi)^d}\frac{1}{q^2+m^2}\frac{1}{(q+p)^2}\right]_m \\ & + \int \frac{d^dq}{(2\pi)^d}\frac{1}{q^2+m^2}\left[\frac{1}{(q+p)^2}\right]_q + \int \frac{d^dq}{(2\pi)^d}\frac{1}{q^2}\left[\frac{1}{(q+p)^2+m^2}\right]_{q,m}, \end{aligned} \tag{G.7}$$

where $[\dots]_{\mu,\nu,\dots}$ indicates that the quantity inside the square brackets should be expanded in powers of the scales μ, ν. It is easy to check that expanding each term in Eq. (G.7) in that way yields the expansion (G.6) and not (G.2).

A last method confirming the result (G.6) rests on the comparison between the ϵ-expansion of that result with the small mass expansion of the analytic result for the ϵ-expansion of $B_{m0}(p^2)$, which is

$$B_{m0}(p^2) = \frac{1}{16\pi^2}\left[\frac{1}{\epsilon} + 2 + \ln\frac{\bar{\mu}^2}{m^2} - \left(1+\frac{m^2}{p^2}\right)\ln\left(1+\frac{p^2}{m^2}\right)\right] \tag{G.8}$$

In line with the previous analysis, we find that (G.6) is the correct starting point whereas (G.2) misses one contribution. As a result, we can conclude that this example strongly suggests that a naive Taylor expansion in the mass does not lead to the correct low mass expansion.

To end this section, we introduce a final example to illustrate that, under some circumstances, a naive mass expansion is enough in order to find the correct low mass expansion. Let us consider the integral

$$\mathcal{I}_m(p^2) \equiv \int \frac{d^dq}{(2\pi)^d}\frac{1}{q^2+m^2}\frac{3q^2+2(p\cdot q)}{(q+p)^2(2q+p)^2}. \tag{G.9}$$

Because of the presence of enough powers of q in the numerator, it can be Taylor expanded up to order m^2, leading to

$$\begin{aligned}\mathcal{I}_m(p^2) &= \int \frac{d^dq}{(2\pi)^d}\frac{1}{q^2}\frac{3q^2+2(p\cdot q)}{(q+p)^2(2q+p)^2} \\ &- m^2\int \frac{d^dq}{(2\pi)^d}\frac{1}{q^4}\frac{3q^2+2(p\cdot q)}{(q+p)^2(2q+p)^2} + \mathcal{O}\left(\frac{m^4}{p^4}\right). \end{aligned} \tag{G.10}$$

On the other hand, this integral can be decomposed in terms of master integrals as

$$\mathcal{I}_m(p^2) = \int \frac{d^dq}{(2\pi)^d}\frac{1}{q^2+m^2}\frac{1}{(q+p)^2} - \int \frac{d^dq}{(2\pi)^d}\frac{1}{q^2+m^2}\frac{1}{(2q+p)^2}. \tag{G.11}$$

As we saw above, for each of these master integrals, the Taylor expansion cannot be pushed to order m^2. It can be easily checked, however, that if one proceeds anyway with this ill-defined Taylor expansion, at the end of the day one gets the right expansion (G.10). The reason behind this is that the problematic contribution for both integrals, the one coming from $(1/p^2)\int d^dq/(2\pi)^d 1/(q^2+m^2)$, cancels in the difference (G.11).

In general terms, we could speculate with the following rule for a quantity Q_m. Assuming that the following conditions hold:

1. Q_m is regular in the $m \to 0$ limit,
2. The first n derivatives $\partial^k Q_m/\partial(m^2)^k$ are regular in the $m \to 0$ limit,
3. Q_m can be split into many pieces $Q_m = \sum_i Q_m^i$ (which are basically master integrals times some prefactors), where each $Q_m^{(i)}$ which could lead to IR divergences when performing a naive Taylor expansion.

Then, the mass expansion of Q_m to order n is nothing but its Taylor expansion to order n, and it can be obtained by Taylor expanding formally the $Q_m^{(i)}$ to the same order, even though for the latter this does not correspond to their mass expansion. This is possible due to cancellations among the potential IR divergent when considered altogether. We believe this explains why we could obtain the correct limit $\lim_{m\to 0} v_{m^2}(k^2)$ by simply using a naive Taylor expansion for that quantity.

Appendix H

IR structure of the CF model

This appendix is devoted to the analysis of the IR structure of correlation functions from the CF model in the quenched approximation. We are particularly interested in the application of such ideas to the investigation of the zero-crossing of the three-gluon vertex, see Chapter 5. We begin by presenting some general notions regarding small momentum expansions of Feynman graphs.

H.1 IR expansion of Feynman graphs

H.1.1 Asymptotic irreducible graphs

To begin with, let us denote by $\mathcal{G}$ certain Feynman graph and by $G(p_i, m)$ its corresponding Feynman integral, where p_i indicate the external momenta and m is the gluon mass. As we mentioned in Appendix F, when one aims at obtaining an IR expansion of $G(p_i, m)$, a naive Taylor expansion in p_i possibly will yield to the appearance of IR divergences. These are the result of the impossibility of routing the external momenta in such a way that they avoid the massless lines of $\mathcal{G}$. Even though such divergent integrals are regularized in dimensional regularization, their presence is a manifestation of the invalidity of a naive Taylor expansion beyond certain order.

The appropriate form of performing the IR expansion is given by the formula [240]:

$$\mathcal{A}_{p_i} G(p_i, m) = \sum_{\bar{\mathcal{G}} \subset \mathcal{G}} \int_{q_j} R(q_j, p_i) \mathcal{T} q_j, p_i \bar{G}(q_j, p_i, m). \tag{H.1}$$

In this relation $\mathcal{A}_{p_i} G(p_i, m)$ denotes the IR asymptotic expansion and $\mathcal{T}_{p_i} G(p_i, m)$ refers to the Taylor expansion of $G(p_i, m)$ in powers of the momenta p_i. The sum is taken over the *asymptotic irreducible (AI) subgraphs* $\bar{\mathcal{G}}$ of the original graph with associated Feynman integral $\bar{G}(q_j, p_i, m)$. An asymptotic irreducible subgraph is defined as any subgraph that contains all the massive lines of the original graph and that is 1-PI with respect to the massless lines. With this definition we can safely perform a Taylor expansion on $\bar{G}(q_j, p_i, m)$ with respect to *all* the external momenta of the subgraph.

Before continuing, let us mention that AI subgraphs are not necessarily connected. However, its connected components appear as trees of 1-PI subgraphs with respect to all types of lines, linked to each other by massive lines. We denote

the 1-PI subgraphs as the nodes of the tree whereas we refer to the massive links as branches.

H.1.2 Taylor and asymptotic power mass

In what follows, and in relation with the calculations presented in this thesis, we will be interested in configurations of momenta depending only on one external momentum, denoted as p, with $p \to 0$. For later convenience, we introduce the notion of Taylor asymptotic and mass powers.

The low momenta Taylor expansion of an AI subgraph yields to terms of the form $m^\omega P^n$, where P^n is a shorthand notation for a monomial in the external momentum of the subgraph and n a natural number. Thus, we have the relation

$$\omega + n = \delta_{\bar{\mathcal{G}}}, \tag{H.2}$$

where $\delta_{\bar{\mathcal{G}}}$ is the mass dimension of the subgraph. We will call ω the *Taylor mass power*. As $n \geq 0$, then $\omega \leq 0$. Moreover, increasing orders in the Taylor expansion correspond to decreasing Taylor mass power. Then, the leading term of the expansion corresponds to the term with the highest Taylor mass power $\omega_{\bar{\mathcal{G}}}$, referred to as the *Taylor mass power of the subgraph*. In the absence of symmetries we will usually have $\omega_{\bar{\mathcal{G}}} = \delta_{\bar{\mathcal{G}}}$. In contrast, symmetries can decrease the value of $\omega_{\bar{\mathcal{G}}}$ strictly below $\delta_{\bar{\mathcal{G}}}$, as we will see explicitly later in this appendix.

As for the asymptotic expansion of the original graph, according to Eq. (H.1), it will lead to terms of the form $m^\nu p^\alpha$, where $\nu + \alpha = \delta_{\mathcal{G}}$. Again, the leading term in the asymptotic expansion corresponds to the highest value of ν. Such quantity will be denoted as $\nu_{\mathcal{G}}$ and we will be referred as the *asymptotic mass power of the graph*. In this case, since α is not restricted to take positive values, ν is not bounded from above.

The various elements we have introduced can be exploited to determine the various contributions to the asymptotic expansion of a given graph $\mathcal{G}$. More precisely, the leading contribution of an AI subgraph to $\mathcal{A}_p G(p,m)$ will be given by $\omega_{\bar{\mathcal{G}}}$, and therefore, the leading contribution of the $p \to 0$ expansion of $G(p,m)$ will be determined by the AI subgraphs with the highest $\omega_{\bar{\mathcal{G}}}$. The next-to-leading order contribution will be determined by the next-to-leading order contribution of the AI subgraphs with highest $\omega_{\bar{\mathcal{G}}}$ and also by the AI subgraphs with next-to highest $\omega_{\bar{\mathcal{G}}}$, and so on and so forth.

H.2 Asymptotic expansion in the CF model

H.2.1 AI subgraphs

In order to apply these ideas to the CF model, we first note that the ghost field is massless whereas the gluon propagator can be written as

$$\frac{P^\perp_{\mu\nu}}{q^2+m^2} = \frac{1}{q^2+m^2}\left[\delta_{\mu\nu} + \frac{q_\mu q_\nu}{m^2}\right] - \frac{1}{m^2}\frac{q_\mu q_\nu}{q^2}, \tag{H.3}$$

which shows that it contains both a massive and a massless component. In order to distinguish between these two components in a certain AI subgraph, we can

replicate the graph by choosing which gluon line is associated with a massive component and which one with a massless component.

This can be achieved by proceeding in the following manner. First, we leave out certain gluon lines. Second, we look all the other graphs which contain the other gluon lines and whose connected components form trees, the branches of these trees being some of the gluon lines we did not leave out. The gluon lines inside the nodes of the trees correspond to fully transverse propagators (H.3). The gluon lines corresponding to branches are the massive components whereas the gluon lines left out of the graph correspond to the massless components. By exhausting the possibilities of gluon lines left out we can generate all possible AI subgraphs of a given graph.

H.2.2 Taylor mass power of an AI subgraph

We will represent the various nodes of $\bar{\mathcal{G}}$ as $\bar{\mathcal{G}}_i$ and by I_A the total number of gluon lines excluding those inside the nodes. Since each of these gluon lines contributes with a -2 to the Taylor mass power of the AI subgraph, we have

$$\omega_{\bar{\mathcal{G}}} = -2I_A + \sum_i \omega_{\bar{\mathcal{G}}_i}. \tag{H.4}$$

Thus, in order to continue with the analysis we need to find the Taylor mass power of the nodes, i.e. the 1-PI vertices.

Let us consider a generic vertex function $\Gamma^{(m+2n)}_{A^m(c\bar{c})^n}$ with $m + 2n \geq 2$. We denote its Taylor mass power as ω_{mn}. Without symmetries ω_{mn} must be equal to the mass dimension of the vertex, this is $4 - m - 2n$. The derivative nature of the ghost-antighost-gluon vertex (related to the antighost shift symmetry) adds a factor p for each antighost leg. Moreover, the same derivative nature combined with the transverse nature of the gluon propagator also add an extra factor p for each ghost leg (in the presence of loops). Finally, for odd values of m, because of Lorentz symmetry we have another extra factor p. Therefore, we can conclude

$$\begin{aligned} \omega_{mn} &= 4 - m - 4n, \quad \text{with } m \text{ even;} \\ \omega_{mn} &= 3 - m - 4n, \quad \text{with } m \text{ odd.} \end{aligned} \tag{H.5}$$

The exception to such relations is the tree level ghost-antighost-gluon vertex, since its Taylor mass power is zero. However, since such vertex can only appear as a node at the edge of a tree, we can decide not to include it in the AI subgraph. So, we can assume without loss of generality $\omega_{11} = -2$.

From the identities (H.5), we can classify the vertex functions according to its decreasing Taylor power mass. By restricting our analysis to original graphs which are connected and 1-PI with $m + 2n \geq 2$, the highest Taylor mass power corresponds to $\Gamma^{(2)}_{AA}$ and takes a value of two. The next highest value is zero and corresponds to the vertices $\Gamma^{(4)}_{AAAA}$, $\Gamma^{(3)}_{AAA}$, $\Gamma^{(2)}_{c\bar{c}}$ and $\Gamma^{(3),\text{tree}}_{Ac\bar{c}}$.

In general terms, the Taylor mass power $\omega = -2k$, with $k \geq 1$ will correspond to $\Gamma^{(4+2k)}_{A^{4+2k}}$ and $\Gamma^{(3+2k)}_{A^{3+2k}}$. By replacing tetrads of gluon fields by pairs of ghost-antighost legs in such functions we generate the same value $\omega = -2k$. There are no other possibilities for an odd value of k. When k is even (and therefore $4 + 2k$ is a multiple of 4), there is one extra function generated from $\Gamma^{(4+2k)}_{A^{4+2k}}$, namely $\Gamma^{(2+k)}_{(c\bar{c})^{1+k/2}}$. Several examples are displayed in Fig. H.1.

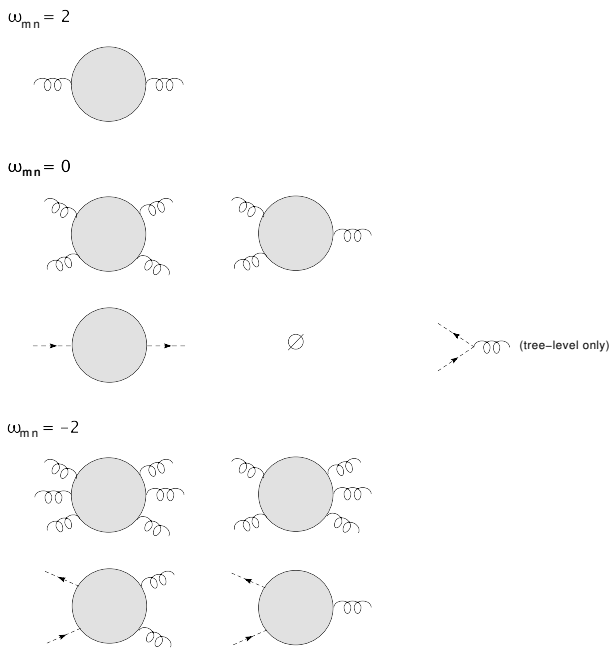

Figure H.1: Classification of the vertex functions according to their Taylor mass power.

H.2.3 Highest asymptotic mass power

As we just saw, the nodes can have at most a Taylor mass power of 2, corresponding to $\Gamma^{(2)}_{AA}$. Therefore, the only possible way of creating positive mass powers is by inserting gluon self-energies in the nodes. Nonetheless, except when we are looking at a graph that is a contribution to the gluon two-point function, each of these insertions will come accompanied by two gluon lines. Since each of these gluon lines contributes with a -2 to the Taylor mass power, gluon self-energy insertions actually contribute with a -2. As a result, the only case with a strictly positive asymptotic mass power is the gluon two-point function i.e. the case where the considered AI subgraph is the two-point function itself, expanded at leading order.

H.2.4 Next-to-highest asymptotic mass power

The next-to-highest asymptotic mass power corresponds to zero. Of course, this could be generated by taking the next-to-leading order in the asymptotic expansion of the gluon two-point function with an AI subgraph equal to the graph itself.

Leaving aside this case, we note that the nodes of the AI subgraph corresponding to gluon self-energy insertions always appear with other two gluon lines, contributing, when considered as a whole, with a -2 to the Taylor mass power. As a result, we can include gluon chains connecting gluon self-energies insertions in our definition of I_A in Eq. (H.4). By doing this modification, it is now clear that all possible contributions to the Taylor mass power are negative or zero. Therefore, the only chance to have a vanishing $\omega_{\bar{\mathcal{G}}}$ is by combining the various vertices with vanishing Taylor mass power. These are $\Gamma^{(4)}_{AAAA}$, $\Gamma^{(3)}_{AAA}$ and $\Gamma^{(2)}_{c\bar{c}}$.

The latter are trivial cases in the sense that correspond to the situation where

the AI subgraph coincides with the graph, expanded at leading order. Non-trivial AI subgraphs are quite restricted, since no gluon chains are allowed. This means that the trees of the AI are single nodes and that these nodes cannot be nor $\Gamma^{(4)}_{AAAA}$ neither $\Gamma^{(3)}_{AAA}$. Consequently, we are only allowed to use self-energy insertions of the type $\Gamma^{(2)}_{c\bar{c}}$ connected by ghost lines or tree level ghost-antighost-gluon vertices (which do not belong to the AI subgraph) in order reconstruct the original graph. Since this is assumed to be 1-PI, the only possibility is to form a single ghost loop connecting ghost self-energies and with an arbitrarily number of tree level ghost-antighost-gluon vertices. In brief, the only structure generating a vanishing asymptotic mass power is an effective ghost loop contributing to $\Gamma^{(m)}_{m}$. Such structure is illustrated in Fig. H.2.

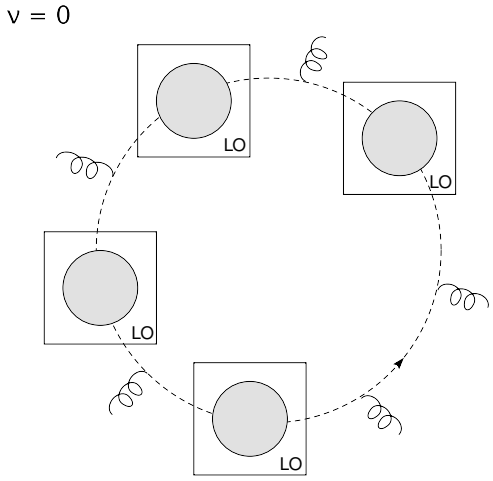

Figure H.2: Origin of the Taylor mass power $\nu = 0$. The boxes surrounding the subgraphs represent the Taylor expansion operators with respect to the external momenta of each subgraph. In addition, there are trivial cases leading to $\nu = 0$ which we do not show here.

A similar analysis can be done for lower order of the asymptotic mass power. We skip it in the present analysis, since it is not relevant for the study of the zero-crossing of the three-gluon dressing function.

H.2.5 Structure of leading logs

The leading asymptotic behavior of a vertex function is given by $m^\nu p^\alpha$ where $\nu + \alpha = \delta$, with δ the mass dimension of the vertex. Both ν and α are integers modulo possible terms proportional to ϵ. From Eq. (H.1) we know that such terms come multiplied by two integrals that contain potential poles in $1/\epsilon$. However, we just saw that one of these integrals has a one-loop structure, so it contains at most a simple pole $1/\epsilon$ in the case of primitively divergent vertex functions. The remaining poles are associated to self-energies insertions and as such they correspond to UV divergences, which are removed after renormalization.

Therefore, we can conclude that the leading $p \to 0$ behavior of any primitively divergent vertex function is given at most by a simple logarithm in p at all orders of perturbation theory. In contrast, the powers of logarithms in m is not bounded and can grow with the number of loops. As a result, in order to ensure a controlled perturbative expansion in the IR, we must choose a renormalization scale of the

type $\mu(p) \to m$ rather than $\mu(p) \to p$, as $p \to 0$. This was what we actually did when evaluating the three-gluon vertex in Chapter 5.

Appendix I

Asymptotic behavior of anomalous dimensions in the presence of quarks

In this appendix we show the UV- and IR- asymptotic expansions of the two-loop $\gamma-$functions from the CF model we used to control the renormalization group flow in these regimes in Chapter 6.

I.1 UV asymptotic behaviour

$$\begin{aligned}
\gamma_A = \lambda &\left\{\left[-\frac{13}{3}+\left(\frac{65}{4}+\frac{3}{2}\ln\frac{\mu^2}{m^2}\right)\frac{m^2}{\mu^2}\right]+\frac{N_f}{N}\left[\frac{4}{3}-8\frac{M^2}{\mu^2}\right]\right\} \\
&+\lambda^2\left\{-\frac{85}{6}+\left(\frac{18343}{96}+\frac{\pi^2}{48}-\frac{891}{16}S_2+\frac{205}{16}\ln\frac{\mu^2}{m^2}\right.\right. \\
&\left.+\frac{35}{8}\ln^2\frac{\mu^2}{m^2}+\frac{171}{4}\zeta(3)\right)\frac{m^2}{\mu^2}+\frac{N_f}{N}\left[\frac{17}{3}-\left(\frac{8}{3}+48\zeta(3)\right)\frac{m^2}{\mu^2}\right. \\
&-\left(\frac{281}{3}+16\zeta(3)\right)\frac{M^2}{\mu^2}+2\left(\frac{m^2}{\mu^2}-2\frac{M^2}{\mu^2}\left(1+\frac{M^2}{m^2}\right)\right)\tilde{I}_{mMM} \\
&+\left(2\ln\frac{\mu^2}{m^2}-2\ln\frac{\mu^2}{m^2}\ln\frac{\mu^2}{M^2}+\ln^2\frac{\mu^2}{M^2}\right)\frac{m^2}{\mu^2}-2\left(\ln\frac{\mu^2}{m^2}+2\ln\frac{\mu^2}{M^2}\right)\frac{M^2}{\mu^2}\Bigg] \\
&\left.+\frac{N_f}{N}\frac{C_F}{N}\left[4-\left(\frac{128}{3}-32\zeta(3)\right)\frac{m^2}{\mu^2}-48\frac{M^2}{\mu^2}\right]\right\}+\mathcal{O}\left(\frac{m^2}{\mu^2},\frac{M^2}{\mu^2}\right) \qquad \text{(I.1)}
\end{aligned}$$

where

$$\begin{aligned}
\tilde{I}_{mMM} = &-m\ \mathrm{Re}\left\{\frac{\sqrt{m^2-4M^2}}{m^2-4M^2}\left[\frac{\pi^2}{6}-\frac{1}{2}\ln^2\frac{M^2}{m^2}+\ln^2\left(\frac{1}{2}-\frac{\sqrt{m^2-4M^2}}{2m}\right)\right.\right. \\
&\left.\left.-2\mathrm{Li}_2\left(\frac{1}{2}-\frac{\sqrt{m^2-4M^2}}{2m}\right)\right]\right\} \qquad \text{(I.2)}
\end{aligned}$$

$$
\begin{aligned}
\gamma_c =&\lambda\left\{-\frac{3}{2}-\left(\frac{3}{4}-\frac{3}{2}\ln\frac{\mu^2}{m^2}\right)\frac{m^2}{\mu^2}\right\}\\
&+\lambda^2\left\{-\frac{17}{4}+\left(-\frac{211}{8}+\frac{\pi^2}{48}-\frac{891}{16}S_2+\frac{103}{8}\ln\frac{\mu^2}{m^2}+\frac{35}{8}\ln^2\frac{\mu^2}{m^2}+\frac{3}{4}\zeta(3)\right)\frac{m^2}{\mu^2}\right.\\
&\frac{N_f}{N}\left[\frac{1}{2}+\frac{3}{2}\frac{m^2}{\mu^2}+11\frac{M^2}{\mu^2}+2\left(\frac{m^2}{\mu^2}-2\left(1+\frac{M^2}{m^2}\right)\frac{M^2}{\mu^2}\right)\tilde{I}_{mMM}\right.\\
&\left.\left.+\left(\ln^2\frac{\mu^2}{M^2}-2\ln\frac{\mu^2}{m^2}\ln\frac{\mu^2}{M^2}+\ln\frac{\mu^2}{m^2}\right)\frac{m^2}{\mu^2}-2\left(\ln\frac{\mu^2}{m^2}+2\ln\frac{\mu^2}{M^2}\right)\frac{M^2}{\mu^2}\right]\right\}\\
&+\mathcal{O}\left(\frac{m^2}{\mu^2},\frac{M^2}{\mu^2}\right)
\end{aligned}
\tag{I.3}
$$

$$
\begin{aligned}
\gamma_\psi =&\lambda\frac{C_F}{N}\left(\frac{9}{2}-3\ln\frac{\mu^2}{m^2}\right)\frac{m^2}{\mu^2}\\
&+\lambda^2\frac{C_F}{N}\left\{\frac{25}{2}+\left(\frac{695}{8}-\frac{\pi^2}{24}+\frac{891}{8}S_2-45\zeta(3)-\frac{47}{2}\ln\frac{\mu^2}{m^2}-\frac{35}{4}\ln^2\frac{\mu^2}{m^2}\right)\frac{m^2}{\mu^2}\right.\\
&+(-31+18\zeta(3))\frac{M^2}{\mu^2}+\frac{C_F}{N}\left[-3+24\frac{M^2}{\mu^2}+(-40+48\zeta(3))\frac{m^2}{\mu^2}\right]\\
&\frac{N_f}{N}\left[-2-5\frac{m^2}{\mu^2}-18\frac{M^2}{\mu^2}+2\left(-\ln\frac{\mu^2}{m^2}+2\ln\frac{\mu^2}{m^2}\ln\frac{\mu^2}{M^2}-\ln^2\frac{\mu^2}{M^2}\right)\frac{m^2}{\mu^2}\right.\\
&\left.\left.+4\left(\ln\frac{\mu^2}{m^2}+2\ln\frac{\mu^2}{M^2}\right)\frac{M^2}{\mu^2}-4\left(\frac{m^2}{\mu^2}-2\left(1+\frac{M^2}{m^2}\right)\frac{M^2}{\mu^2}\right)\tilde{I}_{mMM}\right]\right\}\\
&+\mathcal{O}\left(\frac{m^2}{\mu^2},\frac{M^2}{\mu^2}\right)
\end{aligned}
\tag{I.4}
$$

$$
\begin{aligned}
\gamma_M =&\lambda\frac{C_F}{N}\left[6-\left(\frac{9}{2}+3\ln\frac{\mu^2}{m^2}\right)\frac{m^2}{\mu^2}-6\frac{M^2}{\mu^2}\ln\frac{\mu^2}{M^2}\right]\\
&+\lambda^2\frac{C_F}{N}\left\{\frac{67}{2}-\left(\frac{\pi^2}{24}+69\zeta(3)+\frac{41}{2}-\frac{891}{8}S_2\right)\frac{m^2}{\mu^2}+(3-36\zeta(3))\frac{M^2}{\mu^2}\right.\\
&-\left(\frac{49}{4}\ln\frac{\mu^2}{m^2}+\frac{35}{4}\ln^2\frac{\mu^2}{m^2}\right)\frac{m^2}{\mu^2}-46\frac{M^2}{\mu^2}\ln\frac{\mu^2}{M^2}\\
&+\frac{N_f}{N}\left[-2+\left(5-2\ln\frac{\mu^2}{m^2}+4\ln\frac{\mu^2}{m^2}\ln\frac{\mu^2}{M^2}-2\ln^2\frac{\mu^2}{M^2}\right)\frac{m^2}{\mu^2}\right.\\
&\left.+\left(-10+4\ln\frac{\mu^2}{m^2}+12\ln\frac{\mu^2}{M^2}\right)\frac{M^2}{\mu^2}-4\left(\frac{m^2}{\mu^2}-2\left(1+\frac{M^2}{m^2}\right)\frac{M^2}{\mu^2}\right)\tilde{I}_{mMM}\right]\\
&+\frac{C_F}{N}\left[3+\left(-\frac{35}{2}+48\zeta(3)-45\ln\frac{\mu^2}{m^2}\right)\frac{m^2}{\mu^2}\right.\\
&\left.\left.+\left(14-24\zeta(3)+54\ln\frac{\mu^2}{M^2}-36\ln^2\frac{\mu^2}{M^2}-72\tilde{I}_{mMM}\right)\frac{M^2}{\mu^2}\right]\right\}
\end{aligned}
$$

$$+\mathcal{O}\left(\frac{m^2}{\mu^2},\frac{M^2}{\mu^2}\right) \tag{I.5}$$

I.2 IR asymptotic behaviour

$$\begin{aligned}
\gamma_A =&\lambda\left\{\frac{1}{3}-\frac{217}{180}\frac{\mu^2}{m^2}+\frac{4N_f}{5N}\frac{\mu^2}{M^2}\right\}\\
&\lambda^2\frac{\mu^2}{m^2}\left\{\frac{N_f}{N}\left[\left(\frac{8}{9}m^8-16m^6M^2+\frac{994}{9}m^4M^4-\frac{2756}{9}m^2M^6+\frac{520}{9}M^8\right.\right.\right.\\
&\left.+\frac{7216}{9}\frac{M^{10}}{m^2}-\frac{1984}{3}\frac{M^{12}}{m^4}\right)\frac{\tilde{I}_{mMM}}{(m^2-4M^2)^4}\\
&-\frac{25m^8+1122m^6M^2-12128m^4M^4+36760m^2M^6-44640M^8}{270m^2(m^2-4M^2)^3}\\
&+\left(-\frac{151}{90}m^8+\frac{3334}{135}m^6M^2-\frac{3280}{27}m^4M^4+\frac{33112}{135}m^2M^6-\frac{3112}{9}M^8\right.\\
&\left.\left.+\frac{992}{3}\frac{M^{10}}{m^2}\right)\frac{\ln\left(m^2/M^2\right)}{(m^2-4M^2)^4}\right]+\frac{C_F}{N}\frac{N_f}{N}\left[\left(-\frac{16}{9}m^8+32m^6M^2\right.\right.\\
&\left.-\frac{1952}{9}m^4M^4+\frac{5888}{9}m^2M^6-\frac{1664}{3}M^8-\frac{1280}{9}\frac{M^{10}}{m^2}\right)\frac{\tilde{I}_{mMM}}{(m^2-4M^2)^4}\\
&-\frac{4m^8-416m^6M^2+3904m^4M^4-5376m^2M^6+4800M^8}{135(m^2-4M^2)^3(m^2-M^2)}\\
&+\frac{\ln\left(m^2/M^2\right)}{135(m^2-4M^2)^6}\left(4m^{12}+504m^{10}M^2-8056m^8M^4+47792m^6M^6\right.\\
&\left.\left.-78432m^4M^8+19840m^2M^{10}+9600M^{12}\right)\right]+\frac{38687}{25920}-\frac{38167}{69984}\pi^2\\
&\left.-\frac{179}{360}\ln\frac{\mu^2}{m^2}+\frac{13}{144}\ln^2\frac{\mu^2}{m^2}+\frac{3647}{8748}\pi^2+\frac{3647}{288}S_2\right\}\\
&+\mathcal{O}\left(\frac{\mu^2}{m^2},\frac{\mu^2}{M^2}\right)
\end{aligned} \tag{I.6}$$

$$\begin{aligned}
\gamma_c =&\lambda\frac{\mu^2}{m^2}\left(-\frac{5}{12}+\frac{1}{2}\ln\frac{\mu^2}{m^2}\right)\\
&+\lambda^2\frac{\mu^2}{m^2}\left\{\frac{N_f}{N}\left[\frac{5}{9}+4\frac{M^2}{m^2}+4\frac{M^4}{m^4}\tilde{I}_{mMM}-\left(\frac{1}{3}+2\frac{M^2}{m^2}\right)\ln\frac{m^2}{M^2}\right]\right.\\
&\left.-\frac{4295}{576}-\frac{7}{8}\pi^2+\frac{1}{12}\ln\frac{\mu^2}{m^2}+\frac{17}{48}\left(\psi_1\left(\frac{1}{6}\right)+\psi_1\left(\frac{1}{3}\right)\right)\right\}+\mathcal{O}\left(\frac{\mu^2}{m^2},\frac{\mu^2}{M^2}\right)
\end{aligned} \tag{I.7}$$

$$
\begin{aligned}
\gamma_\psi =& \lambda \frac{C_F}{N} \frac{m^2\mu^2}{(m^2-M^2)^4} \left\{ m^4 - 8m^2M^2 + 7M^4 - \left(m^4 - 4m^2M^2 - 3M^4\right) \ln \frac{m^2}{M^2} \right\} \\
& \lambda^2 \frac{C_F}{N} \left\{ \frac{\mu^2}{M^2} \left[\left(\frac{7}{4} m^{10} + \frac{m^{14}}{12M^4} - \frac{5}{6} \frac{m^{12}}{M^2} + \frac{47}{12} m^8 M^2 - \frac{475}{12} m^6 M^4 + \frac{295}{3} m^4 M^6 \right.\right. \right. \\
& \left. + \frac{184}{3} m^2 M^8 - 32 M^{10} \right) \frac{\tilde{I}_{mMM}}{(M^2-m^2)^5} + \left(\frac{7}{24} m^{10} + \frac{m^{14}}{24M^4} - \frac{m^{12}}{3M^2} + \frac{49}{24} m^8 M^2 \right. \\
& \left. - \frac{415}{24} m^6 M^4 + \frac{685}{24} m^4 M^6 + \frac{167}{8} m^2 M^8 - \frac{11}{6} M^{10} \right) \frac{\ln^2 (m^2/M^2)}{(M^2-m^2)^5} \\
& + \left(\frac{3}{4} - \frac{m^4}{12M^4} + \frac{m^2}{8M^2} - \frac{25}{24} \frac{M^2}{m^2} \right) \left(\ln \left(\frac{M^2}{m^2} - 1 \right)^2 \ln \frac{m^2}{M^2} - 2 \operatorname{Re} \left[\operatorname{Li}_2 \left(\frac{M^2}{m^2} \right) \right] \right) \\
& - \frac{\ln \frac{m^2}{M^2}}{24(m^2-M^2)^5 (4m^2-M^2)^2} (32 m^{14} + 656 m^{12} M^2 - 5038 m^{10} M^4 \\
& . + 46433 m^8 M^6 + 16497 m^6 M^8 - 15787 m^4 M^{10} + 2013 M^2 m^{12} + 50 M^{14}) \\
& + \frac{m^2 M^6 \left(3m^2 + M^2\right)}{(m^2-M^2)^5} \ln \frac{\mu^2}{M^2} \ln \frac{m^2}{M^2} \\
& + \frac{324 m^8 M^2 - 1311 m^6 M^4 - 2754 m^4 M^6 + 45 m^2 M^8 + 240 M^{10}}{8(m^2-M^2)^5} S_2 \\
& + \left(-12 m^{14} + 204 m^{12} M^2 - \frac{3238}{3} m^{10} M^4 + \frac{6371}{3} m^8 M^6 - \frac{6098}{3} m^6 M^8 \right. \\
& \left. + \frac{5995}{6} m^4 M^{10} - \frac{1585}{6} m^2 M^{12} + \frac{437}{12} M^{14} - \frac{25}{12} \frac{M^{16}}{m^2} \right) \frac{\tilde{I}_{Mmm}}{(m^2-M^2)^5 (4m^2-M^2)^2} \\
& + \frac{m^2 M^2 \left(m^4 - 8m^2M^2 - 17M^4\right)}{6 \left(m^2-M^2\right)^4} \ln \frac{\mu^2}{M^2} \\
& - \frac{24 m^{10} + 1294 m^8 M^2 - 9840 m^6 M^4 - 17937 m^4 M^6 + 3680 m^2 M^8 + 351 M^{10}}{36 \left(m^2-M^2\right)^4 \left(4m^2-M^2\right)} \\
& \left. + \left(18 - \frac{m^6 - 3m^4M^2 + 25M^6}{m^2M^4} \right) \frac{\pi^2}{72} \right] \\
& + \frac{N_f}{N} \frac{\mu^2}{m^2} \left[\frac{24 m^8 M^2 - 54 m^6 M^4 - 450 m^4 M^6 - 168 m^2 M^8}{(m^2-M^2)^5} S_2 \right. \\
& + \left(60 m^4 M^6 - 20 m^6 M^4 + 96 m^2 M^8 + 8 M^{10} \right) \frac{\tilde{I}_{mMM}}{(M^2-m^2)^5} \\
& + \frac{10 m^8 - 8 m^6 M^2 - 494 m^4 M^4 - 324 m^2 M^6}{9 \left(m^2-M^2\right)^4} \\
& \left. + \left(-\frac{2}{3} m^{10} - \frac{2}{3} m^8 M^2 + \frac{118}{3} m^6 M^4 + \frac{146}{3} m^4 M^6 + 4 m^2 M^8 \right) \frac{\ln (m^2/M^2)}{(m^2-M^2)^5} \right] \\
& \frac{C_F}{N} \frac{\mu^2}{m^2} \left[\frac{24 m^8 M^2 - 54 m^6 M^4 - 234 m^4 M^6 - 60 m^2 M^8}{(m^2-M^2)^5} S_2 \right. \\
& + \left(-144 m^{16} + 48 \frac{m^{18}}{M^2} + \frac{995}{3} m^{14} M^2 - \frac{4655}{6} m^{12} M^4 - \frac{4357}{3} m^{10} M^6 \right.
\end{aligned}
$$

$$
\begin{aligned}
&+\frac{5183}{6}m^8M^8-\frac{629}{3}m^6M^{10}+\frac{145}{3}m^4M^{12}-6m^2M^{14}\Big)\\
&\times\frac{\ln\left(m^2/M^2\right)}{\left(m^2-M^2\right)^6\left(4m^2-M^2\right)^2}\\
&+\left(3-\frac{3}{2}\frac{m^4}{M^4}\right)\left(\ln\left(\frac{M^2}{m^2}-1\right)^2\ln\frac{m^2}{M^2}-2\ \mathrm{Re}\left[\mathrm{Li}_2\left(\frac{M^2}{m^2}\right)\right]\right)\\
&+\frac{m^2}{6M^2\left(M^2-4m^2\right)\left(M^2-m^2\right)^5}(72m^{12}-518m^{10}M^2-1325m^8M^4\\
&+1867m^6M^6+1670m^4M^8-457m^2M^{10}-13M^{12})+\left(1-\frac{m^4}{2M^4}\right)\pi^2\\
&+\left(\frac{175}{3}m^{10}+\frac{3}{4}\frac{m^{14}}{M^4}-21\frac{m^{12}}{M^2}-m^8M^2-382m^6M^4-\frac{28}{3}m^4M^6\right.\\
&\left.+64m^2M^8\right)\frac{\tilde{I}_{mMM}}{(M^2-m^2)^5}\left(-316m^{14}+96\frac{m^{16}}{M^2}-\frac{15022}{3}m^{12}M^2\right.\\
&+\frac{1691}{3}m^{10}M^4+\frac{8525}{3}m^8M^6-\frac{5759}{3}m^6M^8+\frac{1765}{3}m^4M^{10}\\
&\left.\left.-\frac{278}{3}m^2M^{12}+6M^{14}\right)\frac{\tilde{I}_{Mmm}}{\left(4m^2-M^2\right)^2\left(m^2-M^2\right)^5}\right]\Bigg\}+\mathcal{O}\left(\frac{\mu^2}{m^2},\frac{\mu^2}{M^2}\right)
\end{aligned}
\tag{I.8}
$$

$$
\begin{aligned}
\gamma_M=&\lambda\frac{C_F}{N}\frac{\mu^2}{(m^2-M^2)^4}\left\{2m^6+5m^4M^2-10m^2M^4+3M^6\right.\\
&\left.+\left(m^6-10m^4M^2+3m^2M^4\right)\ln\frac{m^2}{M^2}\right\}\\
&+\lambda^2\frac{C_F}{N}\left\{\frac{\mu^2}{m^2}\left[-\frac{3}{8}\frac{m^2}{(m^2-M^2)^5}\left(108m^8-1055m^6M^2-558m^4M^4\right.\right.\\
&\left.+285m^2M^6+68M^8\right)S_2+\left(\frac{58}{3}m^{14}+\frac{4m^{16}}{3M^2}+\frac{927}{4}m^{12}M^2+\frac{75499}{24}m^{10}M^4\right.\\
&\left.-\frac{13207}{8}m^8M^6+\frac{1141}{24}m^6M^8+\frac{2041}{24}m^4M^{10}-\frac{131}{12}m^2M^{12}\right)\\
&\times\frac{\ln\left(m^2/M^2\right)}{\left(m^2-M^2\right)^5\left(4m^2-M^2\right)^2}\\
&+\left(-\frac{35}{24}m^{10}-\frac{m^{16}}{12M^6}+\frac{13}{24}\frac{m^{14}}{M^4}-\frac{35}{24}\frac{m^{12}}{M^2}-\frac{229}{24}m^8M^2+\frac{1261}{24}m^6M^4\right.\\
&\left.-\frac{65}{8}m^4M^6+\frac{5}{12}m^2M^8-\frac{5}{8}M^{10}+\frac{M^{12}}{8m^2}\right)\frac{\ln^2\left(m^2/M^2\right)}{\left(m^2-M^2\right)^5}\\
&+\left(-\frac{m^8}{6}+\frac{23}{6}m^6M^2+\frac{5}{6}m^4M^4-\frac{m^2M^6}{2}\right)\frac{\ln\left(\mu^2/M^2\right)}{\left(m^2-M^2\right)^4}\\
&-\frac{m^4M^2\left(m^4+4m^2M^2-M^4\right)}{\left(m^2-M^2\right)^5}\ln\frac{\mu^2}{M^2}\ln\frac{m^2}{M^2}
\end{aligned}
$$

$$+\frac{24m^{12}-2426m^{10}M^2+55179m^8M^4-72m^6M^6-9331m^4M^8+1482m^2M^{10}}{72M^2\left(m^2-M^2\right)^4\left(M^2-4m^2\right)}$$
$$+\left(\frac{13}{72}-\frac{m^6}{36M^6}+\frac{m^4}{24M^4}-\frac{M^2}{8m^2}\right)\pi^2$$
$$+\left(\frac{13}{24}-\frac{m^6}{8M^6}+\frac{m^4}{8M^4}-\frac{M^2}{4m^2}\right)\left(\ln\frac{m^2}{M^2}\ln\left(\frac{M^2}{m^2}-1\right)^2-2\ \mathrm{Re}\left[\mathrm{Li}_2\left(\frac{M^2}{m^2}\right)\right]\right)$$
$$+\left(-\frac{17}{12}m^{10}+\frac{m^{16}}{6M^6}-\frac{17m^{14}}{12M^4}+\frac{19m^{12}}{4M^2}+\frac{133}{12}m^8M^2-\frac{809}{6}m^6M^4\right.$$
$$\left.-\frac{10}{3}m^4M^6+32m^2M^8\right)\frac{\tilde{I}_{mMM}}{\left(M^2-m^2\right)^5}$$
$$+\left(-6m^{14}+36\frac{m^{16}}{M^2}+\frac{601}{3}m^{12}M^2-\frac{2258}{3}m^{10}M^4+\frac{2897}{3}m^8M^6-\frac{3451}{6}m^6M^8\right.$$
$$\left.+\frac{584}{3}m^4M^{10}-\frac{485}{12}m^2M^{12}+\frac{29}{6}M^{14}-\frac{M^{16}}{4m^2}\right)\frac{\tilde{I}_{Mmm}}{\left(m^2-M^2\right)^5\left(4m^2-M^2\right)^2}\Bigg]$$
$$+\frac{N_f}{N}\frac{\mu^2}{m^2}\left[\frac{324m^4M^6-42m^6M^4-9m^2M^8+51M^{10}}{(m^2-M^2)^5}S_2\right.$$
$$+\left(\frac{2}{3}m^{10}-10m^8M^2-78m^6M^4-\frac{22}{3}m^4M^6+4m^2M^8\right)\frac{\ln\left(m^2/M^2\right)}{\left(m^2-M^2\right)^5}$$
$$+\frac{176m^6M^2-10m^8+770m^4M^4-120m^2M^6}{9\left(m^2-M^2\right)^4}$$
$$\left.+\left(4m^8M^2+16m^6M^4-156m^4M^6-16m^2M^8+8M^{10}\right)\frac{\tilde{I}_{mMM}}{\left(M^2-m^2\right)^5}\right]$$
$$+\frac{C_F}{N}\frac{\mu^2}{M^2}\left[\frac{-42m^6M^4+324m^4M^6-9m^2M^8+51M^{10}}{\left(m^2-M^2\right)^5}S_2\right.$$
$$+\left(-16m^{16}-80m^{14}M^2+\frac{943}{3}m^{12}M^4+\frac{7295}{6}m^{10}M^6+\frac{1012}{3}m^8M^8\right.$$
$$\left.-\frac{3611}{6}m^6M^{10}+\frac{374}{3}m^4M^{12}+\frac{11}{3}m^2M^{14}-2M^{16}\right)\frac{\ln\left(m^2/M^2\right)}{\left(m^2-M^2\right)^6\left(4m^2-M^2\right)^2}$$
$$+\left(-\frac{7}{2}m^{14}+\frac{m^{16}}{2M^2}+\frac{119}{3}m^{12}M^2-137m^{10}M^4-\frac{43}{2}m^8M^6+\frac{117}{2}m^6M^8\right.$$
$$\left.-m^4M^{10}-\frac{9}{2}m^2M^{12}-\frac{37}{6}M^{14}+\frac{7}{2}\frac{M^{16}}{m^2}-\frac{M^{18}}{2m^4}\right)\frac{\ln^2\left(m^2/M^2\right)}{\left(m^2-M^2\right)^7}$$
$$+\left(\frac{m^2}{6M^2}+\frac{M^4}{2m^4}\right)\pi^2-\frac{1}{6\left(m^2-M^2\right)^5\left(4m^2-M^2\right)}\left(24m^{12}-1586m^{10}M^2\right.$$
$$\left.+541m^8M^4+2560m^6M^6+281m^4M^8-622m^2M^{10}+98M^{12}\right)$$
$$+\left(\frac{m^2}{2M^2}+\frac{M^4}{m^4}\right)\left(\ln\frac{m^2}{M^2}\ln\left(\frac{M^2}{m^2}-1\right)^2-2\ \mathrm{Re}\left[\mathrm{Li}_2\left(\frac{M^2}{m^2}\right)\right]\right)$$
$$\left(-288m^{14}+3748m^{12}M^2+\frac{6292}{3}m^{10}M^4-\frac{7403}{3}m^8M^6-\frac{1370}{3}m^6M^8\right.$$

$$
\begin{aligned}
&+\frac{2744}{3}m^4M^{10}-\frac{1177}{8}m^2M^{12}+\frac{296}{3}M^{14}-15\frac{M^{16}}{m^2}+\frac{M^{18}}{m^4}\Bigg)\\
&\times\frac{\tilde{I}_{Mmm}}{\left(m^2-M^2\right)^5\left(4m^2-M^2\right)^2}\\
&+\Bigg(-7m^{10}+\frac{m^{12}}{M^2}+\frac{229}{3}m^8M^2-263m^6M^4-174m^4M^6\\
&+\frac{44}{3}m^2M^8+64M^{10}\Bigg)\frac{\tilde{I}_{mMM}}{\left(m^2-M^2\right)^5}\Bigg]\Bigg\}+\mathcal{O}\left(\frac{\mu^2}{m^2},\frac{\mu^2}{M^2}\right). \qquad \text{(I.9)}
\end{aligned}
$$

In the above expressions we have used $S_2=\frac{4}{9\sqrt{3}}\,\mathrm{Im}(\mathrm{Li}(e^{i\pi/3}))$.

Bibliography

[1] C. N. Yang and R. L. Mills. "Conservation of Isotopic Spin and Isotopic Gauge Invariance". *Physical Review* 96.1 (1954), pp. 191–195. DOI: 10.1103/physrev.96.191.

[2] L. Faddeev and V. Popov. "Feynman diagrams for the Yang-Mills field". *Physics Letters B* 25.1 (1967), pp. 29–30. ISSN: 0370-2693. DOI: https://doi.org/10.1016/0370-2693(67)90067-6.

[3] G. Hooft. "Renormalizable Lagrangians for massive Yang-Mills fields". *Nuclear Physics B* 35.1 (1971), pp. 167–188. ISSN: 0550-3213. DOI: https://doi.org/10.1016/0550-3213(71)90139-8.

[4] D. J. Gross and F. Wilczek. "Ultraviolet Behavior of Non-Abelian Gauge Theories". *Phys. Rev. Lett.* 30 (1973), pp. 1343–1346. DOI: 10.1103/PhysRevLett.30.1343.

[5] H. D. Politzer. "Reliable Perturbative Results for Strong Interactions?" *Phys. Rev. Lett.* 30 (1973), pp. 1346–1349. DOI: 10.1103/PhysRevLett.30.1346.

[6] S. Coleman and D. J. Gross. "Price of Asymptotic Freedom". *Physical Review Letters* 31.13 (1973), pp. 851–854. DOI: 10.1103/physrevlett.31.851.

[7] V. N. Gribov. "Quantization of Nonabelian Gauge Theories". *Nucl. Phys. B* 139 (1978). Ed. by J. Nyiri, p. 1. DOI: 10.1016/0550-3213(78)90175-X.

[8] I. M. Singer. "Some remarks on the Gribov ambiguity". *Communications in Mahtematical Physics* 60 (1978). DOI: 10.1007/BF01609471.

[9] Z. Fodor and C. Hoelbling. "Light Hadron Masses from Lattice QCD". *Rev. Mod. Phys.* 84 (2012), p. 449. DOI: 10.1103/RevModPhys.84.449. arXiv: 1203.4789 [hep-lat].

[10] M. Lüscher and P. Weisz. "Quark confinement and the bosonic string". *Journal of High Energy Physics* 2002.07 (2002), pp. 049–049. DOI: 10.1088/1126-6708/2002/07/049.

[11] O. Oliveira et al. "Quark propagator with two flavors of O(a)-improved Wilson fermions". *Phys. Rev. D* 99.9 (2019), p. 094506. DOI: 10.1103/PhysRevD.99.094506. arXiv: 1809.02541 [hep-lat].

[12] F. J. Dyson. "The S matrix in quantum electrodynamics". *Phys. Rev.* 75 (1949), pp. 1736–1755. DOI: 10.1103/PhysRev.75.1736.

[13] J. Schwinger. "On the Green's Functions of Quantized Fields. I". *Proceedings of the National Academy of Sciences of the United States of America* 37.7 (1951), pp. 452–455. ISSN: 00278424. DOI: 10.1073/pnas.37.7.455.

[14] J. Schwinger. "On the Green's functions of quantized fields. II". *Proceedings of the National Academy of Sciences* 37.7 (1951), pp. 455–459. DOI: 10.1073/pnas.37.7.455.

[15] R. Alkofer and L. von Smekal. "The Infrared behavior of QCD Green's functions: Confinement dynamical symmetry breaking, and hadrons as relativistic bound states". *Phys. Rept.* 353 (2001), p. 281. DOI: 10.1016/S0370-1573(01)00010-2. arXiv: hep-ph/0007355.

[16] A. C. Aguilar, D. Binosi, and J. Papavassiliou. "Gluon and ghost propagators in the Landau gauge: Deriving lattice results from Schwinger-Dyson equations". *Physical Review D* 78.2 (2008), p. 025010. DOI: 10.1103/physrevd.78.025010. arXiv: 0802.1870.

[17] A. Aguilar, D. Binosi, and J. Papavassiliou. "Yang-Mills two-point functions in linear covariant gauges". *Physical Review D* 91.8 (2015), p. 085014. DOI: 10.1103/physrevd.91.085014. arXiv: 1501.07150.

[18] M. Q. Huber. "Correlation functions of Landau gauge Yang-Mills theory". *Physical Review D* 101.11 (2020), p. 114009. DOI: 10.1103/physrevd.101.114009. arXiv: 2003.13703.

[19] A. Aguilar et al. "Infrared facets of the three-gluon vertex". *Physics Letters B* 818 (2021), p. 136352. DOI: 10.1016/j.physletb.2021.136352. arXiv: 2102.04959.

[20] B.-J. Schaefer and J. Wambach. "Renormalization group approach towards the QCD phase diagram". *Phys. Part. Nucl.* 39 (2008), pp. 1025–1032. DOI: 10.1134/S1063779608070083. arXiv: hep-ph/0611191.

[21] J. M. Pawlowski. "Aspects of the functional renormalisation group". *Annals Phys.* 322 (2007), pp. 2831–2915. DOI: 10.1016/j.aop.2007.01.007. arXiv: hep-th/0512261.

[22] A. K. Cyrol et al. "Nonperturbative quark, gluon, and meson correlators of unquenched QCD". *Phys. Rev. D* 97.5 (2018), p. 054006. DOI: 10.1103/PhysRevD.97.054006. arXiv: 1706.06326 [hep-ph].

[23] N. Dupuis et al. "The nonperturbative functional renormalization group and its applications". *Phys. Rept.* 910 (2021), pp. 1–114. DOI: 10.1016/j.physrep.2021.01.001. arXiv: 2006.04853 [cond-mat.stat-mech].

[24] L. von Smekal, R. Alkofer, and A. Hauck. "The Infrared behavior of gluon and ghost propagators in Landau gauge QCD". *Phys. Rev. Lett.* 79 (1997), pp. 3591–3594. DOI: 10.1103/PhysRevLett.79.3591. arXiv: hep-ph/9705242.

[25] L. von Smekal, A. Hauck, and R. Alkofer. "A Solution to Coupled Dyson–Schwinger Equations for Gluons and Ghosts in Landau Gauge". *Annals Phys.* 267 (1998). [Erratum: Annals Phys. 269, 182 (1998)], pp. 1–60. DOI: 10.1006/aphy.1998.5806. arXiv: hep-ph/9707327.

[26] A. C. Aguilar and A. A. Natale. "A dynamical gluon mass solution in a coupled system of the Schwinger-Dyson equations". *Journal of High Energy Physics* 2004.08 (2004), pp. 057–057. DOI: 10.1088/1126-6708/2004/08/057.

[27] A. C. Aguilar and A. A. Natale. "A dynamical gluon mass solution in Mandelstam's approximation". *International Journal of Modern Physics A* 20.32 (2005), pp. 7613–7632. DOI: 10.1142/s0217751x05025061.

[28] F. D. R. Bonnet et al. "Infrared behavior of the gluon propagator on a large volume lattice". *Phys. Rev. D* 62 (2000), p. 051501. DOI: 10.1103/PhysRevD.62.051501. arXiv: hep-lat/0002020.

[29] A. Cucchieri, A. Maas, and T. Mendes. "Three-point vertices in Landau-gauge Yang-Mills theory". *Phys. Rev. D* 77 (2008), p. 094510. DOI: 10.1103/PhysRevD.77.094510. arXiv: 0803.1798 [hep-lat].

[30] A. G. Duarte, O. Oliveira, and P. J. Silva. "Lattice gluon and ghost propagators and the strong coupling in pure SU(3) Yang-Mills theory: Finite lattice spacing and volume effects". *Physical Review D* 94.1 (2016), p. 014502. DOI: 10.1103/physrevd.94.014502. arXiv: 1605.00594.

[31] T. Mendes. "Numerical test of the Gribov-Zwanziger scenario in landau gauge". *Proceedings of International Workshop on QCD Green's Functions, Confinement and Phenomenology — PoS(QCD-TNT09)*. Sissa Medialab, 2010. DOI: 10.22323/1.087.0026.

[32] I. L. Bogolubsky et al. "Lattice gluodynamics computation of Landau gauge Green's functions in the deep infrared". *Phys. Lett. B* 676 (2009), pp. 69–73. DOI: 10.1016/j.physletb.2009.04.076. arXiv: 0901.0736 [hep-lat].

[33] F. D. R. Bonnet et al. "Infinite volume and continuum limits of the Landau gauge gluon propagator". *Phys. Rev. D* 64 (2001), p. 034501. DOI: 10.1103/PhysRevD.64.034501. arXiv: hep-lat/0101013.

[34] V. G. Bornyakov, V. K. Mitrjushkin, and M. Muller-Preussker. "SU(2) lattice gluon propagator: Continuum limit, finite-volume effects and infrared mass scale m(IR)". *Phys. Rev. D* 81 (2010), p. 054503. DOI: 10.1103/PhysRevD.81.054503. arXiv: 0912.4475 [hep-lat].

[35] T. Iritani, H. Suganuma, and H. Iida. "Gluon-propagator functional form in the Landau gauge in SU(3) lattice QCD: Yukawa-type gluon propagator and anomalous gluon spectral function". *Phys. Rev. D* 80 (2009), p. 114505. DOI: 10.1103/PhysRevD.80.114505. arXiv: 0908.1311 [hep-lat].

[36] A. Maas. "Describing gauge bosons at zero and finite temperature". *Phys. Rept.* 524 (2013), pp. 203–300. DOI: 10.1016/j.physrep.2012.11.002. arXiv: 1106.3942 [hep-ph].

[37] O. Oliveira and P. J. Silva. "The lattice Landau gauge gluon propagator: lattice spacing and volume dependence". *Phys. Rev. D* 86 (2012), p. 114513. DOI: 10.1103/PhysRevD.86.114513. arXiv: 1207.3029 [hep-lat].

[38] A. Ilderton, M. Lavelle, and D. McMullan. "Colour, copies and confinement". *JHEP* 03 (2007), p. 044. DOI: 10.1088/1126-6708/2007/03/044. arXiv: hep-th/0701168.

[39] D. Zwanziger. "Fundamental modular region, Boltzmann factor and area law in lattice gauge theory". *Nucl. Phys. B* 412 (1994), pp. 657–730. DOI: 10.1016/0550-3213(94)90396-4.

[40] D. Dudal et al. "A Refinement of the Gribov-Zwanziger approach in the Landau gauge: Infrared propagators in harmony with the lattice results". *Phys. Rev. D* 78 (2008), p. 065047. DOI: 10.1103/PhysRevD.78.065047. arXiv: 0806.4348 [hep-th].

[41] G. Curci and R. Ferrari. "On a class of Lagrangian models for massive and massless Yang-mills fields". *Il Nuovo Cimento A* 32.2 (1976), pp. 151–168. DOI: 10.1007/bf02729999.

[42] M. Tissier and N. Wschebor. "Infrared propagators of Yang-Mills theory from perturbation theory". *Physical Review D* 82.10 (2010), p. 101701. DOI: 10.1103/physrevd.82.101701. arXiv: 1004.1607.

[43] M. Tissier and N. Wschebor. "Infrared safe perturbative approach to Yang-Mills correlators". *Physical Review D* 84.4 (2011), p. 045018. DOI: 10.1103/physrevd.84.045018. arXiv: 1105.2475.

[44] F. Delduc and S. Sorella. "A note on some non-linear covariant gauges in Yang-Mills theory". *Physics Letters B* 231.4 (1989), pp. 408–410. DOI: 10.1016/0370-2693(89)90684-9.

[45] J. de Boer et al. "On the renormalizability and unitarity of the Curci-Ferrari model for massive vector bosons". *Physics Letters B* 367.1-4 (1996), pp. 175–182. DOI: 10.1016/0370-2693(95)01455-1. arXiv: hep-th/9510167.

[46] M. Tissier and N. Wschebor. "Gauged supersymmetries in Yang-Mills theory". *Physical Review D* 79.6 (2009), p. 065008. DOI: 10.1103/physrevd.79.065008. arXiv: 0809.1880.

[47] I. Ojima. "Comments on massive and massless Yang-Mills lagrangians with a quartic coupling of Faddeev-Popov ghosts". *Zeitschrift fr Physik C Particles and Fields* 13.2 (1982), pp. 173–177. DOI: 10.1007/bf01547683.

[48] A. Cucchieri, T. Mendes, and A. R. Taurines. "SU(2) Landau gluon propagator on a 140**3 lattice". *Physical Review D* 67.9 (2003), p. 091502. DOI: 10.1103/physrevd.67.091502. arXiv: hep-lat/0302022.

[49] A. Cucchieri, T. Mendes, and A. R. Taurines. "Positivity violation for the lattice Landau gluon propagator". *Physical Review D* 71.5 (2005), p. 051902. DOI: 10.1103/physrevd.71.051902. arXiv: hep-lat/0406020.

[50] A. Cucchieri and T. Mendes. "Constraints on the IR behavior of the ghost propagator in Yang-Mills theories". *Phys. Rev. D* 78 (2008), p. 094503. DOI: 10.1103/PhysRevD.78.094503. arXiv: 0804.2371 [hep-lat].

[51] P. O. Bowman et al. "Scaling behavior and positivity violation of the gluon propagator in full QCD". *Physical Review D* 76.9 (2007), p. 094505. DOI: 10.1103/physrevd.76.094505. arXiv: hep-lat/0703022.

[52] A. Maas. "Two- and three-point Green's functions in two-dimensional Landau-gauge Yang-Mills theory". *Physical Review D* 75.11 (2007), p. 116004. DOI: 10.1103/physrevd.75.116004. arXiv: 0704.0722.

[53] U. Reinosa et al. "How nonperturbative is the infrared regime of Landau gauge Yang-Mills correlators?" *Physical Review D* 96.1 (2017), p. 014005. DOI: 10.1103/physrevd.96.014005. arXiv: 1703.04041.

[54] J. A. Gracey et al. "Two-loop calculation of Yang-Mills propagators in the Curci-Ferrari model". *Physical Review D* 100.3 (2019), p. 034023. DOI: 10.1103/physrevd.100.034023. arXiv: 1905.07262.

[55] A. Sternbeck. "The Infrared behavior of lattice QCD Green's functions". PhD thesis. 2006. arXiv: hep-lat/0609016.

[56] P. Boucaud et al. "The Infrared Behaviour of the Pure Yang-Mills Green Functions". *Few Body Syst.* 53 (2012), pp. 387–436. DOI: 10.1007/s00601-011-0301-2. arXiv: 1109.1936 [hep-ph].

[57] M. Peláez, M. Tissier, and N. Wschebor. "Three-point correlation functions in Yang-Mills theory". *Physical Review D* 88.12 (2013), p. 125003. DOI: 10.1103/physrevd.88.125003. arXiv: 1310.2594.

[58] M. Peláez, M. Tissier, and N. Wschebor. "Two-point correlation functions of QCD in the Landau gauge". *Physical Review D* 90.6 (2014), p. 065031. DOI: 10.1103/physrevd.90.065031. arXiv: 1407.2005.

[59] N. Barrios et al. "Ghost-antighost-gluon vertex from the Curci-Ferrari model: Two-loop corrections". *Physical Review D* 102.11 (2020), p. 114016. DOI: 10.1103/physrevd.102.114016. arXiv: 2009.00875.

[60] N. Barrios, M. Peláez, and U. Reinosa. "Two-loop three-gluon vertex from the Curci-Ferrari model and its leading infrared behavior to all loop orders" (2022). arXiv: 2207.10704 [hep-ph].

[61] N. Barrios et al. "Two-loop corrections to the QCD propagators within the Curci-Ferrari model". *Physical Review D* 104.9 (2021), p. 094019. DOI: 10.1103/physrevd.104.094019. arXiv: 2103.16218.

[62] M. E. Peskin and D. V. Schroeder. *An Introduction to Quantum Field Theory.* Westview Press, 1995. DOI: 10.1201/9780429503559.

[63] S. Weinberg. *The Quantum Theory of Fields.* Vol. 2. Cambridge University Press, 1996. DOI: 10.1017/cbo9781139644174.

[64] J. Zinn-Justin. *Quantum Field Theory and Critical Phenomena; 4th ed.* International series of monographs on physics. Oxford: Clarendon Press, 2002. DOI: 10.1093/acprof:oso/9780198509233.001.0001.

[65] T. Muta. *Foundations of Quantum Chromodynamics: An Introduction to Perturbative Methods in Gauge Theories, (3rd ed.)* 3rd. Vol. 78. World scientific Lecture Notes in Physics. Hackensack, N.J.: World Scientific, 2010. ISBN: 978-981-279-353-9.

[66] A. Zee. *Quantum field theory in a nutshell.* second edition. Princeton University Press, 2010.

[67] W. Heisenber and W. Pauli. "Zur Quantendynamik der Wellenfelder". *Zeitschrift fur Physik* 56.1 (1929), pp. 1–61. DOI: 10.1007/978-3-322-90270-2_33.

[68] G. Parisi and Y.-s. Wu. "Perturbation theory without gauge fixing". *Scientia Sinica* 24 (1981), p. 483.

[69] R. Feynamn. "Space-time approach to nonrelativistic quantum mechanics". *Reviews of Modern Physics* 20.2 (1948), pp. 367–387.

[70] S. Weinberg. *The Quantum Theory of Fields*. Vol. 1. Cambridge University Press, 1995. DOI: 10.1017/CBO9781139644167.

[71] N. Vandersickel and D. Zwanziger. "The Gribov problem and QCD dynamics". *Phys. Rept.* 520 (2012), pp. 175–251. DOI: 10.1016/j.physrep.2012.07.003. arXiv: 1202.1491 [hep-th].

[72] N. Nakanishi. "Covariant Quantization of the Electromagnetic Field in the Landau Gauge". *Progress of Theoretical Physics* 35.6 (1966), pp. 1111–1116. DOI: 10.1143/ptp.35.1111.

[73] G. Hooft. "Renormalization of massless Yang-Mills fields". *Nuclear Physics B* 33.1 (1971), pp. 173–199. ISSN: 0550-3213. DOI: https://doi.org/10.1016/0550-3213(71)90395-6.

[74] G. Leibbrandt. "Introduction to noncovariant gauges". *Reviews of Modern Physics* 59.4 (1987), pp. 1067–1119. DOI: 10.1103/revmodphys.59.1067.

[75] T. Shinohara, T. Imai, and K.-i. Kondo. "The most general and renormalizable maximal abelian gauge". *International Journal of Modern Physics A* 18.31 (2003), pp. 5733–5756. DOI: 10.1142/s0217751x03016008. arXiv: hep-th/0105268.

[76] C. Becchi, A. Rouet, and R. Stora. "Renormalization of the abelian Higgs-Kibble model". *Communications in Mathematical Physics* 42.2 (1975), pp. 127–162. DOI: 10.1007/bf01614158.

[77] C. Becchi, A. Rouet, and R. Stora. "Renormalization of gauge theories". *Annals of Physics* 98.2 (1976), pp. 287–321. ISSN: 0003-4916. DOI: https://doi.org/10.1016/0003-4916(76)90156-1.

[78] I. V. Tyutin. "Gauge Invariance in Field Theory and Statistical Physics in Operator Formalism" (1975). arXiv: 0812.0580 [hep-th].

[79] M. Henneaux and C. Teitelboim. *Quantization of gauge systems*. 1992. ISBN: 978-0-691-03769-1. DOI: 10.1515/9780691213866.

[80] N. Nakanishi and I. Ojima. *Covariant operator formalism of gauge theories and quantum gravity*. Vol. 27. 1990. DOI: 10.1142/0362.

[81] M. Srednicki. *Quantum field theory*. Cambridge University Press, 2007. ISBN: 978-0-521-86449-7, 978-0-511-26720-8. DOI: 10.1017/cbo9780511813917.

[82] R. P. Feynman. "The Theory of Positrons". *Physical Review* 76.6 (1949), pp. 749–759. DOI: 10.1103/physrev.76.749.

[83] A. Bilal. *Advanced quantum field theory: renormalization, non-abelian gauge theories and anomalies*. Lecture notes. Brussels doctoral school, 2014.

[84] D. Binosi et al. "JaxoDraw: A Graphical user interface for drawing Feynman diagrams. Version 2.0 release notes". *Comput. Phys. Commun.* 180 (2009), pp. 1709–1715. DOI: 10.1016/j.cpc.2009.02.020. arXiv: 0811.4113 [hep-ph].

[85] M. Peláez. "Infrared correlation functions in Quantum Chromodynamics". PhD thesis. Paris U., VI, LPTL, 2015.

[86] J. Taylor. "Ward identities and charge renormalization of the Yang-Mills field". *Nuclear Physics B* 33.2 (1971), pp. 436–444. DOI: 10.1016/0550-3213(71)90297-5.

[87] A. A. Slavnov. "Ward identities in gauge theories". *Theoretical and Mathematical Physics* 10.2 (1972), pp. 99–104. DOI: 10.1007/bf01090719.

[88] G. '. Hooft and M. Veltman. "Regularization and renormalization of gauge fields". *Nuclear Physics B* 44.1 (1972), pp. 189–213. ISSN: 0550-3213. DOI: https://doi.org/10.1016/0550-3213(72)90279-9.

[89] R. Brandt. "Gauge invariance and renormalization". *Nuclear Physics B* 116.2 (1976), pp. 413–448. DOI: 10.1016/0550-3213(76)90357-6.

[90] J. C. Collins. *Renormalization*. Cambridge University Press, 1984. DOI: 10.1017/cbo9780511622656.

[91] M. Gell-Mann and F. E. Low. "Quantum Electrodynamics at Small Distances". *Physical Review* 95.5 (1954), pp. 1300–1312. DOI: 10.1103/physrev.95.1300.

[92] C. G. Callan. "Broken Scale Invariance in Scalar Field Theory". *Physical Review D* 2.8 (1970), pp. 1541–1547. DOI: 10.1103/physrevd.2.1541.

[93] K. Symanzik. "Small distance behaviour in field theory and power counting". *Communications in Mathematical Physics* 18.3 (1970), pp. 227–246. DOI: 10.1007/bf01649434.

[94] S. Weinberg. "New Approach to the Renormalization Group". *Physical Review D* 8.10 (1973), pp. 3497–3509. DOI: 10.1103/physrevd.8.3497.

[95] W. E. Caswell. "Asymptotic Behavior of Non-Abelian Gauge Theories to Two-Loop Order". *Phys. Rev. Lett.* 33 (4 1974), pp. 244–246. DOI: 10.1103/PhysRevLett.33.244.

[96] D. R. T. Jones. "Two Loop Diagrams in Yang-Mills Theory". *Nucl. Phys. B* 75 (1974), p. 531. DOI: 10.1016/0550-3213(74)90093-5.

[97] W. Celmaster and R. J. Gonsalves. "Renormalization-prescription dependence of the quantum-chromodynamic coupling constant". *Phys. Rev. D* 20 (6 1979), pp. 1420–1434. DOI: 10.1103/PhysRevD.20.1420.

[98] J. Greensite. *An introduction to the confinement problem*. Vol. 821. 2011. DOI: 10.1007/978-3-642-14382-3.

[99] Nash, T. and Yamanouchi, T. and Nease, D. and Sculli, J. "Search for Fractionally Charged Quarks Produced by 200- and 300-GeV Proton-Nuclear Interactions". *Phys. Rev. Lett.* 32 (15 1974), pp. 858–862. DOI: 10.1103/PhysRevLett.32.858.

[100] D. Antreasyan et al. "Search for Quarks Produced with Large Transverse Momentum in 400-GeV Proton-Nucleus Collisions". *Phys. Rev. Lett.* 39 (9 1977), pp. 513–515. DOI: 10.1103/PhysRevLett.39.513.

[101] M. L. Stevenson. "Search for massive, long-lived, fractionally charged particles produced by 300-GeV protons". *Phys. Rev. D* 20 (1 1979), pp. 82–86. DOI: 10.1103/PhysRevD.20.82.

[102] R. L. Delgado, C. Hidalgo-Duque, and F. J. Llanes-Estrada. "To What Extent is Gluon Confinement an Empirical Fact?" *Few Body Syst.* 54 (2013), pp. 1705–1717. DOI: 10.1007/s00601-012-0500-5. arXiv: 1106.2462 [hep-ph].

[103] R. Alkofer and J. Greensite. "Quark Confinement: The Hard Problem of Hadron Physics". *J. Phys. G* 34 (2007), S3. DOI: 10.1088/0954-3899/34/7/S02. arXiv: hep-ph/0610365.

[104] J. Greensite. "The Confinement problem in lattice gauge theory". *Prog. Part. Nucl. Phys.* 51 (2003), p. 1. DOI: 10.1016/S0146-6410(03)90012-3. arXiv: hep-lat/0301023.

[105] A. Bassetto, I. Lazzizzera, and R. Soldati. "Absence of Gribov Copies in the Space - Like Planar Gauge". *Phys. Lett. B* 131 (1983), pp. 177–178. DOI: 10.1016/0370-2693(83)91115-2.

[106] F. S. Henyey. "Gribov ambiguity without topological charge". *Phys. Rev. D* 20 (6 1979), pp. 1460–1462. DOI: 10.1103/PhysRevD.20.1460.

[107] P. van Baal. "More (thoughts on) Gribov copies". *Nucl. Phys. B* 369 (1992), pp. 259–275. DOI: 10.1016/0550-3213(92)90386-P.

[108] R. F. Sobreiro et al. "Gribov horizon in the presence of dynamical mass generation in Euclidean Yang-Mills theories in the Landau gauge". *Phys. Lett. B* 590 (2004), pp. 265–272. DOI: 10.1016/j.physletb.2004.03.084. arXiv: hep-th/0403135.

[109] A. Cucchieri. "Gribov copies in the minimal Landau gauge: The Influence on gluon and ghost propagators". *Nucl. Phys. B* 508 (1997), pp. 353–370. DOI: 10.1016/S0550-3213(97)00629-9. arXiv: hep-lat/9705005.

[110] M. Q. Huber. "Nonperturbative properties of Yang Mills theories". *Phys. Rept.* 879 (2020), pp. 1–92. DOI: 10.1016/j.physrep.2020.04.004. arXiv: 1808.05227 [hep-ph].

[111] J. Greensite, S. Olejnik, and D. Zwanziger. "Coulomb energy, remnant symmetry, and the phases of nonAbelian gauge theories". *Phys. Rev. D* 69 (2004), p. 074506. DOI: 10.1103/PhysRevD.69.074506. arXiv: hep-lat/0401003.

[112] J. Greensite, S. Olejnik, and D. Zwanziger. "Center vortices and the Gribov horizon". *JHEP* 05 (2005), p. 070. DOI: 10.1088/1126-6708/2005/05/070. arXiv: hep-lat/0407032.

[113] D. Zwanziger. "Vanishing of zero momentum lattice gluon propagator and color confinement". *Nucl. Phys. B* 364 (1991), pp. 127–161. DOI: 10.1016/0550-3213(91)90581-H.

[114] D. Dudal et al. "Gribov no-pole condition, Zwanziger horizon function, Kugo-Ojima confinement criterion, boundary conditions, BRST breaking and all that". *Phys. Rev. D* 79 (2009), p. 121701. DOI: 10.1103/PhysRevD.79.121701. arXiv: 0904.0641 [hep-th].

[115] S. P. Sorella. "Gribov horizon and BRST symmetry: A Few remarks". *Phys. Rev. D* 80 (2009), p. 025013. DOI: 10.1103/PhysRevD.80.025013. arXiv: 0905.1010 [hep-th].

[116] L. Baulieu et al. "Gribov horizon and i-particles: About a toy model and the construction of physical operators". *Phys. Rev. D* 82 (2010), p. 025021. DOI: 10.1103/PhysRevD.82.025021. arXiv: 0912.5153 [hep-th].

[117] S. P. Sorella et al. "Gribov Horizon and BRST Symmetry: A Pathway to Confinement". *AIP Conf. Proc.* 1361.1 (2011). Ed. by A. Ayala et al., pp. 272–276. DOI: 10.1063/1.3622713. arXiv: 1003.0086 [hep-th].

[118] D. Dudal, S. P. Sorella, and N. Vandersickel. "Dynamical origin of the refinement of the Gribov-Zwanziger theory". *Physical Review D* 84.6 (2011), p. 065039. DOI: 10.1103/physrevd.84.065039. arXiv: 1105.3371.

[119] J. A. Gracey. "Alternative refined Gribov-Zwanziger Lagrangian". *Phys. Rev. D* 82 (2010), p. 085032. DOI: 10.1103/PhysRevD.82.085032. arXiv: 1009.3889 [hep-th].

[120] J. A. Gracey. "Loop calculations in the three dimensional Gribov-Zwanziger Lagrangian". *Eur. Phys. J. C* 70 (2010), pp. 451–477. DOI: 10.1140/epjc/s10052-010-1473-5. arXiv: 1010.1104 [hep-th].

[121] D. Dudal, O. Oliveira, and N. Vandersickel. "Indirect lattice evidence for the Refined Gribov-Zwanziger formalism and the gluon condensate $<A^2>$ in the Landau gauge". *Phys. Rev. D* 81 (2010), p. 074505. DOI: 10.1103/PhysRevD.81.074505. arXiv: 1002.2374 [hep-lat].

[122] D. Dudal, M. S. Guimaraes, and S. P. Sorella. "Glueball Masses from an Infrared Moment Problem". *Physical Review Letters* 106.6 (2011), p. 062003. DOI: 10.1103/physrevlett.106.062003.

[123] D. Dudal, M. S. Guimaraes, and S. P. Sorella. "Pade approximation and glueball mass estimates in $3d$ and $4d$ with $N_c = 2, 3$ colors". *Phys. Lett. B* 732 (2014), pp. 247–254. DOI: 10.1016/j.physletb.2014.03.056. arXiv: 1310.2016 [hep-ph].

[124] B. W. Mintz et al. "Ghost-gluon vertex in the presence of the Gribov horizon". *Phys. Rev. D* 97.3 (2018), p. 034020. DOI: 10.1103/PhysRevD.97.034020. arXiv: 1712.09633 [hep-th].

[125] C. S. Fischer, A. Maas, and J. M. Pawlowski. "On the infrared behavior of Landau gauge Yang-Mills theory". *Annals Phys.* 324 (2009), pp. 2408–2437. DOI: 10.1016/j.aop.2009.07.009. arXiv: 0810.1987 [hep-ph].

[126] F. Gao, J. Papavassiliou, and J. M. Pawlowski. "Fully coupled functional equations for the quark sector of QCD". *Physical Review D* 103.9 (2021), p. 094013. DOI: 10.1103/physrevd.103.094013. arXiv: 2102.13053.

[127] M. Q. Huber, C. S. Fischer, and H. Sanchis-Alepuz. "Spectrum of scalar and pseudoscalar glueballs from functional methods". *Eur. Phys. J. C* 80.11 (2020), p. 1077. DOI: 10.1140/epjc/s10052-020-08649-6. arXiv: 2004.00415 [hep-ph].

[128] A. Bashir et al. "Collective perspective on advances in Dyson-Schwinger Equation QCD". *Commun. Theor. Phys.* 58 (2012), pp. 79–134. DOI: 10.1088/0253-6102/58/1/16. arXiv: 1201.3366 [nucl-th].

[129] D. Binosi. "Emergent Hadron Mass in Strong Dynamics". *15th International Conference on the Structure of Baryons*. 2022. DOI: 10.1007/s00601-022-01740-6. arXiv: 2203.00942 [hep-ph].

[130] R. Jackiw. "Functional evaluation of the effective potential". *Phys. Rev. D* 9 (1974), p. 1686. DOI: 10.1103/PhysRevD.9.1686.

[131] J. M. Cornwall, R. Jackiw, and E. Tomboulis. "Effective Action for Composite Operators". *Phys. Rev. D* 10 (1974), pp. 2428–2445. DOI: 10.1103/PhysRevD.10.2428.

[132] J. Berges. "N-particle irreducible effective action techniques for gauge theories". *Phys. Rev. D* 70 (2004), p. 105010. DOI: 10.1103/PhysRevD.70.105010. arXiv: hep-ph/0401172.

[133] M. E. Carrington and Y. Guo. "Techniques for n-Particle Irreducible Effective Theories". *Phys. Rev. D* 83 (2011), p. 016006. DOI: 10.1103/PhysRevD.83.016006. arXiv: 1010.2978 [hep-ph].

[134] D. Schutte. "Nonperturbative many body techniques applied to a Yang-Mills field theory". *Phys. Rev. D* 31 (1985), pp. 810–821. DOI: 10.1103/PhysRevD.31.810.

[135] C. Feuchter and H. Reinhardt. "Variational solution of the Yang-Mills Schrodinger equation in Coulomb gauge". *Phys. Rev. D* 70 (2004), p. 105021. DOI: 10.1103/PhysRevD.70.105021. arXiv: hep-th/0408236.

[136] H. Reinhardt and W. Schleifenbaum. "Hamiltonian Approach to 1+1 dimensional Yang-Mills theory in Coulomb gauge". *Annals Phys.* 324 (2009), pp. 735–786. DOI: 10.1016/j.aop.2008.09.005. arXiv: 0809.1764 [hep-th].

[137] D. R. Campagnari and H. Reinhardt. "Non-Gaussian wave functionals in Coulomb gauge Yang–Mills theory". *Phys. Rev. D* 82 (2010), p. 105021. DOI: 10.1103/PhysRevD.82.105021. arXiv: 1009.4599 [hep-th].

[138] M. Quandt, H. Reinhardt, and J. Heffner. "Covariant variational approach to Yang-Mills theory". *Phys. Rev. D* 89.6 (2014), p. 065037. DOI: 10.1103/PhysRevD.89.065037. arXiv: 1310.5950 [hep-th].

[139] C. D. Roberts and A. G. Williams. "Dyson-Schwinger equations and their application to hadronic physics". *Prog. Part. Nucl. Phys.* 33 (1994), pp. 477–575. DOI: 10.1016/0146-6410(94)90049-3. arXiv: hep-ph/9403224.

[140] R. Alkofer, M. Q. Huber, and K. Schwenzer. "Infrared singularities in Landau gauge Yang-Mills theory". *Physical Review D* 81.10 (2010), p. 105010. DOI: 10.1103/physrevd.81.105010. arXiv: 0801.2762.

[141] T. Kugo and I. Ojima. "Local Covariant Operator Formalism of Nonabelian Gauge Theories and Quark Confinement Problem". *Prog. Theor. Phys. Suppl.* 66 (1979), pp. 1–130. DOI: 10.1143/PTPS.66.1.

[142] A. Cucchieri and T. Mendes. "What's up with IR gluon and ghost propagators in Landau gauge? A puzzling answer from huge lattices". *PoS* LATTICE2007 (2007). Ed. by G. Bali et al., p. 297. DOI: 10.22323/1.042.0297. arXiv: 0710.0412 [hep-lat].

[143] A. Sternbeck et al. "Comparing SU(2) to SU(3) gluodynamics on large lattices". *PoS* LATTICE2007 (2007). Ed. by G. Bali et al., p. 340. DOI: 10.22323/1.042.0340. arXiv: 0710.1982 [hep-lat].

[144] S. W. Li et al. "Non-perturbative BRST symmetry and the spectral structure of the ghost propagator". *Physics Letters B* 823 (2021), p. 136753. DOI: 10.1016/j.physletb.2021.136753. arXiv: 2109.10942.

[145] K. G. Wilson. "Confinement of Quarks". *Phys. Rev. D* 10 (1974). Ed. by J. C. Taylor, pp. 2445–2459. DOI: 10.1103/PhysRevD.10.2445.

[146] J. Smit. *Introduction to quantum fields on a lattice: A robust mate*. Vol. 15. Cambridge University Press, 2011. ISBN: 978-0-511-89373-5, 978-0-521-89051-9.

[147] H. J. Rothe. *Lattice Gauge Theories : An Introduction (Fourth Edition)*. Vol. 43. World Scientific Publishing Company, 2012. ISBN: 978-981-4365-87-1, 978-981-4365-85-7. DOI: 10.1142/8229.

[148] I. Montvay and G. Munster. *Quantum fields on a lattice*. Cambridge Monographs on Mathematical Physics. Cambridge University Press, 1997. ISBN: 978-0-521-59917-7, 978-0-511-87919-7. DOI: 10.1017/CBO9780511470783.

[149] C. Davies. "Lattice QCD: A Guide for people who want results". *58th Scottish Universities Summer School in Physics (SUSSP58): A NATO Advanced Study Institute and EU Hadron Physics 13 Summer Institute*. 2005, pp. 233–272. arXiv: hep-lat/0509046.

[150] S. Borsanyi et al. "Full result for the QCD equation of state with 2+1 flavors". *Phys. Lett. B* 730 (2014), pp. 99–104. DOI: 10.1016/j.physletb.2014.01.007. arXiv: 1309.5258 [hep-lat].

[151] A. Bazavov, P. Petreczky, and J. H. Weber. "Equation of State in 2+1 Flavor QCD at High Temperatures". *Phys. Rev. D* 97.1 (2018), p. 014510. DOI: 10.1103/PhysRevD.97.014510. arXiv: 1710.05024 [hep-lat].

[152] D. Sexty. "New algorithms for finite density QCD". *PoS* LATTICE2014 (2014), p. 016. DOI: 10.22323/1.214.0016. arXiv: 1410.8813 [hep-lat].

[153] L. Scorzato. "The Lefschetz thimble and the sign problem". *PoS* LATTICE2015 (2016), p. 016. DOI: 10.22323/1.251.0016. arXiv: 1512.08039 [hep-lat].

[154] C. Gattringer and K. Langfeld. "Approaches to the sign problem in lattice field theory". *Int. J. Mod. Phys. A* 31.22 (2016), p. 1643007. DOI: 10.1142/S0217751X16430077. arXiv: 1603.09517 [hep-lat].

[155] G. Aarts et al. "The QCD phase diagram in the limit of heavy quarks using complex Langevin dynamics". *JHEP* 09 (2016), p. 087. DOI: 10.1007/JHEP09(2016)087. arXiv: 1606.05561 [hep-lat].

[156] M. Peláez et al. "A window on infrared QCD with small expansion parameters". *Rept. Prog. Phys.* 84.12 (2021), p. 124202. DOI: 10.1088/1361-6633/ac36b8. arXiv: 2106.04526 [hep-th].

[157] J. E. Mandula and M. Ogilvie. "The Gluon Is Massive: A Lattice Calculation of the Gluon Propagator in the Landau Gauge". *Phys. Lett. B* 185 (1987), pp. 127–132. DOI: 10.1016/0370-2693(87)91541-3.

[158] A. G. Duarte, O. Oliveira, and P. J. Silva. "Further Evidence For Zero Crossing On The Three Gluon Vertex". *Phys. Rev. D* 94.7 (2016), p. 074502. DOI: 10.1103/PhysRevD.94.074502. arXiv: 1607.03831 [hep-lat].

[159] A. Maas and M. Vujinović. "More on the three-gluon vertex in SU(2) Yang-Mills theory in three and four dimensions" (2020). DOI: 10.21468/scipostphyscore.5.2.019. arXiv: 2006.08248 [hep-lat].

[160] P. O. Bowman et al. "Unquenched gluon propagator in Landau gauge". *Phys. Rev. D* 70 (2004), p. 034509. DOI: 10.1103/PhysRevD.70.034509. arXiv: hep-lat/0402032.

[161] P. O. Bowman et al. "Unquenched quark propagator in Landau gauge". *Phys. Rev. D* 71 (2005), p. 054507. DOI: 10.1103/PhysRevD.71.054507. arXiv: hep-lat/0501019.

[162] P. J. Silva and O. Oliveira. "Unquenching the Landau Gauge Lattice Propagators and the Gribov Problem". *PoS* LATTICE2010 (2010). Ed. by G. Rossi, p. 287. DOI: 10.22323/1.105.0287. arXiv: 1011.0483 [hep-lat].

[163] A. Sternbeck et al. "Determination of LambdaMS from the gluon and ghost propagators in Landau gauge". *PoS* LATTICE2012 (2012). Ed. by D. Leinweber et al., p. 243. DOI: 10.22323/1.164.0243. arXiv: 1212.2039 [hep-lat].

[164] A. Kızılersü et al. "Quark-gluon vertex from Nf=2 lattice QCD". *Phys. Rev. D* 103.11 (2021), p. 114515. DOI: 10.1103/PhysRevD.103.114515. arXiv: 2103.02945 [hep-lat].

[165] P. O. Bowman et al. "Quark propagator from LQCD and its physical implications". *Lect. Notes Phys.* 663 (2005). Ed. by A. C. Kalloniatis, D. B. Leinweber, and A. G. Williams, pp. 17–63. DOI: 10.1007/11356462_2.

[166] J. B. Kogut and L. Susskind. "Hamiltonian Formulation of Wilson's Lattice Gauge Theories". *Phys. Rev. D* 11 (1975), pp. 395–408. DOI: 10.1103/PhysRevD.11.395.

[167] T. Banks, L. Susskind, and J. B. Kogut. "Strong Coupling Calculations of Lattice Gauge Theories: (1+1)-Dimensional Exercises". *Phys. Rev. D* 13 (1976), p. 1043. DOI: 10.1103/PhysRevD.13.1043.

[168] L. Susskind. "Lattice Fermions". *Phys. Rev. D* 16 (1977), pp. 3031–3039. DOI: 10.1103/PhysRevD.16.3031.

[169] R. Frezzotti et al. "Lattice QCD with a chirally twisted mass term". *JHEP* 08 (2001), p. 058. DOI: 10.1088/1126-6708/2001/08/058. arXiv: hep-lat/0101001.

[170] C. F. J. Wu. "Jackknife, Bootstrap and Other Resampling Methods in Regression Analysis". *The Annals of Statistics* 14.4 (1986), pp. 1261–1295. DOI: 10.1214/aos/1176350142.

[171] J. Skullerud and A. Kizilersu. "Quark gluon vertex from lattice QCD". *JHEP* 09 (2002), p. 013. DOI: 10.1088/1126-6708/2002/09/013. arXiv: hep-ph/0205318.

[172] J. I. Skullerud et al. "Nonperturbative structure of the quark gluon vertex". *JHEP* 04 (2003), p. 047. DOI: 10.1088/1126-6708/2003/04/047. arXiv: hep-ph/0303176.

[173] A. Kizilersu et al. "Quark-gluon vertex in general kinematics". *Eur. Phys. J. C* 50 (2007), pp. 871–875. DOI: 10.1140/epjc/s10052-007-0250-6. arXiv: hep-lat/0610078.

[174] D. Atkinson and P. W. Johnson. "Chiral Symmetry Breaking in QCD. 1. The Infrared Domain". *Phys. Rev. D* 37 (1988), pp. 2290–2295. DOI: 10.1103/PhysRevD.37.2290.

[175] J. M. Cornwall. "Dynamical mass generation in continuum quantum chromodynamics". *Physical Review D* 26.6 (1982), pp. 1453–1478. DOI: 10.1103/physrevd.26.1453.

[176] A. Aguilar et al. "Gluon mass scale through nonlinearities and vertex interplay". *Physical Review D* 100.9 (2019), p. 094039. DOI: 10.1103/physrevd.100.094039. arXiv: 1909.09826.

[177] H. Verschelde et al. "The non-perturbative groundstate of QCD and the local composite operator A_μ^2". *Physics Letters B* 516.3-4 (2001), pp. 307–313. DOI: 10.1016/s0370-2693(01)00929-7.

[178] R. E. Browne and J. A. Gracey. "Two loop effective potential for $<A_\mu^2>$ in the Landau gauge in quantum chromodynamics". *Journal of High Energy Physics* 2003.11 (2003), pp. 029–029. DOI: 10.1088/1126-6708/2003/11/029.

[179] J. Horak et al. "Gluon condensates and effective gluon mass" (2022). arXiv: 2201.09747 [hep-ph].

[180] J. Serreau and M. Tissier. "Lifting the Gribov ambiguity in Yang–Mills theories". *Physics Letters B* 712.1-2 (2012), pp. 97–103. DOI: 10.1016/j.physletb.2012.04.041.

[181] M. Tissier. "Gribov copies, avalanches and dynamic generation of a gluon mass". *Physics Letters B* 784 (2018), pp. 146–150. DOI: 10.1016/j.physletb.2018.07.043. arXiv: 1711.08694.

[182] P. Dall'Olio and A. Weber. "Exploiting the scheme dependence of the renormalization group improvement in infrared Yang–Mills theory". *Annals Phys.* 439 (2022), p. 168801. DOI: 10.1016/j.aop.2022.168801. arXiv: 2012.02389 [hep-th].

[183] F. Siringo. "Analytical study of Yang–Mills theory in the infrared from first principles". *Nuclear Physics B* 907 (2016), pp. 572–596. DOI: 10.1016/j.nuclphysb.2016.04.028.

[184] F. Siringo and G. Comitini. "Gluon propagator in linear covariant R_ξ gauges". *Physical Review D* 98.3 (2018), p. 034023. DOI: 10.1103/physrevd.98.034023.

[185] F. Siringo. "Calculation of the nonperturbative strong coupling from first principles". *Physical Review D* 100.7 (2019), p. 074014. DOI: 10.1103/physrevd.100.074014. arXiv: 1902.04110.

[186] G. Comitini and F. Siringo. "One-loop RG improvement of the screened massive expansion in the Landau gauge". *Physical Review D* 102.9 (2020), p. 094002. DOI: 10.1103/physrevd.102.094002. arXiv: 2007.04231.

[187] G. Comitini et al. "Screened massive expansion of the quark propagator in the Landau gauge". *Physical Review D* 104.7 (2021), p. 074020. DOI: 10.1103/physrevd.104.074020. arXiv: 2108.00417.

[188] R. Browne and J. Gracey. "The Curci Ferrari model with massive quarks at two loops". *Physics Letters B* 540.1-2 (2002), pp. 68–74. DOI: 10.1016/s0370-2693(02)02131-7. arXiv: hep-th/0206111.

[189] J. Gracey. "Three loop MS renormalization of the Curci Ferrari model and the dimension two BRST invariant composite operator in QCD". *Physics Letters B* 552.1-2 (2003), pp. 101–110. DOI: 10.1016/s0370-2693(02)03077-0. arXiv: hep-th/0211144.

[190] N. Wschebor. "Some nonrenormalization theorems in Curci-Ferrari model". *International Journal of Modern Physics A* 23.19 (2008), pp. 2961–2973. DOI: 10.1142/s0217751x08040469. arXiv: hep-th/0701127.

[191] F. Figueroa and M. Peláez. "One-loop unquenched three-gluon and ghost-gluon vertices in the Curci-Ferrari model". *Physical Review D* 105.9 (2022), p. 094005. DOI: 10.1103/physrevd.105.094005. arXiv: 2110.09561.

[192] M. Peláez et al. "Spontaneous chiral symmetry breaking in the massive Landau gauge: Realistic running coupling". *Physical Review D* 103.9 (2021), p. 094035. DOI: 10.1103/physrevd.103.094035. arXiv: 2010.13689.

[193] U. Reinosa et al. "Two-loop study of the deconfinement transition in Yang-Mills theories: SU(3) and beyond". *Physical Review D* 93.10 (2016), p. 105002. DOI: 10.1103/physrevd.93.105002. arXiv: 1511.07690.

[194] U. Reinosa et al. "Deconfinement transition in SU(2) Yang-Mills theory: A two-loop study". *Physical Review D* 91.4 (2015), p. 045035. DOI: 10.1103/physrevd.91.045035. arXiv: 1412.5672.

[195] U. Reinosa et al. "Deconfinement transition in SU(N) theories from perturbation theory". *Physics Letters B* 742 (2015), pp. 61–68. DOI: 10.1016/j.physletb.2015.01.006. arXiv: 1407.6469.

[196] U. Reinosa, J. Serreau, and M. Tissier. "Perturbative study of the QCD phase diagram for heavy quarks at nonzero chemical potential". *Physical Review D* 92.2 (2015), p. 025021. DOI: 10.1103/physrevd.92.025021.

[197] J. Maelger, U. Reinosa, and J. Serreau. "Universal aspects of the phase diagram of QCD with heavy quarks". *Physical Review D* 98.9 (2018), p. 094020. DOI: 10.1103/physrevd.98.094020. arXiv: 1805.10015.

[198] J. Maelger, U. Reinosa, and J. Serreau. "Perturbative study of the QCD phase diagram for heavy quarks at nonzero chemical potential: Two-loop corrections". *Physical Review D* 97.7 (2018), p. 074027. DOI: 10.1103/physrevd.97.074027. arXiv: 1710.01930.

[199] D. M. van Egmond et al. "A novel background field approach to the confinement-deconfinement transition". *SciPost Physics* 12.3 (2022). DOI: 10.21468/scipostphys.12.3.087. arXiv: 2104.08974.

[200] J. Maelger, U. Reinosa, and J. Serreau. "Localized rainbows in the QCD phase diagram". *Physical Review D* 101.1 (2020), p. 014028. DOI: 10.1103/physrevd.101.014028. arXiv: 1903.04184.

[201] C. G. Bollini and J. J. Giambiagi. "Dimensional renorinalization : The number of dimensions as a regularizing parameter". *Il Nuovo Cimento B* 12.1 (1972), pp. 20–26. DOI: 10.1007/bf02895558.

[202] C. Bollini and J. Giambiagi. "Lowest order "divergent" graphs in v-dimensional space". *Physics Letters B* 40.5 (1972), pp. 566–568. DOI: 10.1016/0370-2693(72)90483-2.

[203] D. Dudal, O. Oliveira, and P. J. Silva. "High precision statistical Landau gauge lattice gluon propagator computation vs. the Gribov–Zwanziger approach". *Annals of Physics* 397 (2018), pp. 351–364. DOI: 10.1016/j.aop.2018.08.019.

[204] A. G. Duarte, O. Oliveira, and P. J. Silva. "Reply to "Comment on 'Lattice gluon and ghost propagators and the strong coupling in pure $SU(3)$ Yang-Mills theory: Finite lattice spacing and volume effects' "". *Physical Review D* 96.9 (2017), p. 098502. DOI: 10.1103/physrevd.96.098502.

[205] A. Aguilar et al. "Ghost dynamics in the soft gluon limit". *Physical Review D* 104.5 (2021), p. 054028. DOI: 10.1103/physrevd.104.054028. arXiv: 2107.00768.

[206] L. Corell et al. "Correlation functions of three-dimensional Yang-Mills theory from the FRG". *SciPost Physics* 5.6 (2018). DOI: 10.21468/scipostphys.5.6.066. arXiv: 1803.10092.

[207] A. K. Cyrol et al. "Landau gauge Yang-Mills correlation functions". *Phys. Rev. D* 94.5 (2016), p. 054005. DOI: 10.1103/PhysRevD.94.054005. arXiv: 1605.01856 [hep-ph].

[208] A. C. Aguilar, D. Ibáñez, and J. Papavassiliou. "Ghost propagator and ghost-gluon vertex from Schwinger-Dyson equations". *Physical Review D* 87.11 (2013), p. 114020. DOI: 10.1103/physrevd.87.114020. arXiv: 1303.3609.

[209] W. Schleifenbaum et al. "Infrared behavior of the ghost-gluon vertex in Landau gauge Yang-Mills theory". *Physical Review D* 72.1 (2005), p. 014017. DOI: 10.1103/physrevd.72.014017. arXiv: hep-ph/0411052.

[210] A. Aguilar et al. "Nonperturbative structure of the ghost-gluon kernel". *Physical Review D* 99.3 (2019), p. 034026. DOI: 10.1103/physrevd.99.034026. arXiv: 1811.08961.

[211] A. Cucchieri, A. Maas, and T. Mendes. "Exploratory study of three-point Green's functions in Landau-gauge Yang-Mills theory". *Physical Review D* 74.1 (2006), p. 014503. DOI: 10.1103/physrevd.74.014503. arXiv: hep-lat/0605011.

[212] E.-M. Ilgenfritz et al. "Landau gauge gluon and ghost propagators from lattice QCD". *Brazilian Journal of Physics* 37.1b (2007). DOI: 10.1590/s0103-97332007000200006.

[213] N. V. Smolyakov. "Furry theorem for non-abelian gauge Lagrangians". *Theoretical and Mathematical Physics* 50.3 (1982), pp. 225–228. DOI: 10.1007/bf01016449.

[214] S. P. Martin and D. G. Robertson. "TSIL: a program for the calculation of two-loop self-energy integrals". *Computer Physics Communications* 174.2 (2006), pp. 133–151. DOI: 10.1016/j.cpc.2005.08.005. arXiv: hep-ph/0501132.

[215] S. P. Martin. "Evaluation of two-loop self-energy basis integrals using differential equations". *Physical Review D* 68.7 (2003), p. 075002. DOI: 10.1103/physrevd.68.075002. arXiv: hep-ph/0307101.

[216] A. Davydychev and J. Tausk. "Two-loop self-energy diagrams with different masses and the momentum expansion". *Nuclear Physics B* 397.1-2 (1993), pp. 123–142. DOI: 10.1016/0550-3213(93)90338-p.

[217] J. Fleischer, M. Kalmykov, and A. Kotikov. "Two-loop self-energy master integrals on shell". *Physics Letters B* 462.1-2 (1999), pp. 169–177. DOI: 10.1016/s0370-2693(99)00892-8. arXiv: hep-ph/9905249.

[218] O. Tarasov. "Generalized recurrence relations for two-loop propagator integrals with arbitrary masses". *Nuclear Physics B* 502.1-2 (1997), pp. 455–482. DOI: 10.1016/s0550-3213(97)00376-3. arXiv: hep-ph/9703319.

[219] D. J. Broadhurst. "The master two-loop diagram with masses". *Zeitschrift für Physik C Particles and Fields* 47.1 (1990), pp. 115–124. DOI: 10.1007/bf01551921.

[220] A. Smirnov. "Algorithm FIRE—Feynman Integral REduction". *Journal of High Energy Physics* 2008.10 (2008), pp. 107–107. DOI: 10.1088/1126-6708/2008/10/107.

[221] A. Smirnov and V. Smirnov. "FIRE4, LiteRed and accompanying tools to solve integration by parts relations". *Computer Physics Communications* 184.12 (2013), pp. 2820–2827. DOI: 10.1016/j.cpc.2013.06.016. arXiv: 1302.5885.

[222] S. Laporta. "High-precision calculation of multiloop Feynman integrals by difference equations". *International Journal of Modern Physics A* 15.32 (2000), pp. 5087–5159. DOI: 10.1142/s0217751x00002159.

[223] A. V. Smirnov. "An algorithm to construct Gröbner bases for solving integration by parts relations". *Journal of High Energy Physics* 2006.04 (2006), pp. 026–026. DOI: 10.1088/1126-6708/2006/04/026.

[224] K. Chetyrkin and F. Tkachov. "Integration by parts: The algorithm to calculate β-functions in 4 loops". *Nuclear Physics B* 192.1 (1981), pp. 159–204. DOI: 10.1016/0550-3213(81)90199-1.

[225] S. Weinberg. "High-Energy Behavior in Quantum Field Theory". *Physical Review* 118.3 (1960), pp. 838–849. DOI: 10.1103/physrev.118.838.

[226] A. Davydychev, V. Smirnov, and J. Tausk. "Large momentum expansion of two-loop self-energy diagrams with arbitrary masses". *Nuclear Physics B* 410.2 (1993), pp. 325–342. DOI: 10.1016/0550-3213(93)90436-s. arXiv: hep-ph/9307371.

[227] F. Berends et al. "Zero-threshold expansion of two-loop self-energy diagrams". *Nuclear Physics B* 439.3 (1995), pp. 536–560. DOI: 10.1016/0550-3213(95)00018-n. arXiv: hep-ph/9410232.

[228] A. I. Davydychev, P. Osland, and O. V. Tarasov. "Two-loop three-gluon vertex in the zero-momentum limit". *Physical Review D* 58.3 (1998), p. 036007. DOI: 10.1103/physrevd.58.036007. arXiv: hep-ph/9801380.

[229] *WebPlotDigitizer (version 4.3, July 2020) by Anki Rohatgi.*

[230] G. T. R. Catumba, O. Oliveira, and P. J. Silva. "Another look at the Landau gauge three-gluon vertex". *EPJ Web of Conferences* 258 (2022). Ed. by A. Rothkopf et al., p. 02008. DOI: 10.1051/epjconf/202225802008. arXiv: 2111.10312.

[231] A. Athenodorou et al. "On the zero crossing of the three-gluon vertex". *Physics Letters B* 761 (2016), pp. 444–449. DOI: 10.1016/j.physletb.2016.08.065. arXiv: 1607.01278.

[232] M. Vujinović and T. Mendes. "Probing the tensor structure of lattice three-gluon vertex in Landau gauge". *Physical Review D* 99.3 (2019), p. 034501. DOI: 10.1103/physrevd.99.034501. arXiv: 1807.03673.

[233] A. L. Blum et al. "Gluonic three-point correlations in pure Landau gauge QCD". *Physical Review D* 89.6 (2014), p. 061703. DOI: 10.1103/physrevd.89.061703. arXiv: 1401.0713.

[234] G. Eichmann et al. "Three-gluon vertex in Landau gauge". *Physical Review D* 89.10 (2014), p. 105014. DOI: 10.1103/physrevd.89.105014. arXiv: 1402.1365.

[235] A. Blum et al. "Unquenching the Three-gluon Vertex: A Status Report". *Acta Physica Polonica B Proceedings Supplement* 8.2 (2015), p. 321. DOI: 10.5506/aphyspolbsupp.8.321.

[236] P. Boucaud et al. "Refining the detection of the zero crossing for the three-gluon vertex in symmetric and asymmetric momentum subtraction schemes". *Physical Review D* 95.11 (2017), p. 114503. DOI: 10.1103/physrevd.95.114503.

[237] A. C. Aguilar et al. "Gluon propagator and three-gluon vertex with dynamical quarks". *The European Physical Journal C* 80.2 (2020). DOI: 10.1140/epjc/s10052-020-7741-0.

[238] A. Aguilar et al. "Nonperturbative Ball-Chiu construction of the three-gluon vertex". *Physical Review D* 99.9 (2019), p. 094010. DOI: 10.1103/physrevd.99.094010. arXiv: 1903.01184.

[239] A. Pak and A. Smirnov. "Geometric approach to asymptotic expansion of Feynman integrals". *The European Physical Journal C* 71.4 (2011). DOI: 10.1140/epjc/s10052-011-1626-1.

[240] V. A. Smirnov. *Applied asymptotic expansions in momenta and masses*. Vol. 177. Springer, 2003.

[241] P. Nogueira. "Automatic Feynman Graph Generation". *Journal of Computational Physics* 105.2 (1993), pp. 279–289. DOI: 10.1006/jcph.1993.1074.

[242] A. Smirnov and F. Chukharev. "FIRE6: Feynman Integral REduction with modular arithmetic". *Computer Physics Communications* 247 (2020), p. 106877. DOI: 10.1016/j.cpc.2019.106877. arXiv: 1901.07808.

[243] C. S. Fischer and R. Alkofer. "Nonperturbative propagators, running coupling, and the dynamical quark mass of Landau gauge QCD". *Physical Review D* 67.9 (2003), p. 094020. DOI: 10.1103/physrevd.67.094020.

[244] C. S. Fischer and R. Alkofer. "Dynamical Chiral Symmetry Breaking in Landau gauge QCD". *AIPConf.Proc.756:275-277,2005* (2004). DOI: 10.1063/1.1920965. arXiv: hep-ph/0411347 [hep-ph].

[245] A. Aguilar et al. "New method for determining the quark-gluon vertex". *Physical Review D* 90.6 (2014), p. 065027. DOI: 10.1103/physrevd.90.065027. arXiv: 1405.3506.

[246] R. Williams, C. S. Fischer, and W. Heupel. "Light mesons in QCD and unquenching effects from the 3PI effective action". *Physical Review D* 93.3 (2016), p. 034026. DOI: 10.1103/physrevd.93.034026. arXiv: 1512.00455.

[247] A. Aguilar et al. "Quark gap equation with non-Abelian Ball-Chiu vertex". *Physical Review D* 98.1 (2018), p. 014002. DOI: 10.1103/physrevd.98.014002. arXiv: 1804.04229.

[248] O. Oliveira et al. "Lattice Landau Gauge Quark Propagator and the Quark–Gluon Vertex". *Acta Physica Polonica B Proceedings Supplement* 9.3 (2016), p. 363. DOI: 10.5506/aphyspolbsupp.9.363. arXiv: 1605.09632.

[249] A. Ayala et al. "Quark flavor effects on gluon and ghost propagators". *Physical Review D* 86.7 (2012), p. 074512. DOI: 10.1103/physrevd.86.074512. arXiv: 1208.0795.

[250] M. Peláez et al. "Small parameters in infrared quantum chromodynamics". *Physical Review D* 96.11 (2017), p. 114011. DOI: 10.1103/physrevd.96.114011. arXiv: 1703.10288.

[251] G. '. Hooft. "A two-dimensional model for mesons". *Nuclear Physics B* 75.3 (1974), pp. 461–470. DOI: 10.1016/0550-3213(74)90088-1.

[252] E. Witten. "Baryons in the expansion". *Nuclear Physics B* 160.1 (1979), pp. 57–115. DOI: 10.1016/0550-3213(79)90232-3.

[253] T. DeGrand and Y. Liu. "Lattice study of large N_c QCD". *Phys. Rev. D* 94.3 (2016). [Erratum: Phys.Rev.D 95, 019902 (2017)], p. 034506. DOI: 10.1103/PhysRevD.94.034506. arXiv: 1606.01277 [hep-lat].

[254] C. Studerus. "Reduze - Feynman Integral Reduction in C++". *Comput. Phys. Commun.* 181 (2010), pp. 1293–1300. DOI: 10.1016/j.cpc.2010.03.012. arXiv: 0912.2546 [physics.comp-ph].

[255] A. von Manteuffel and C. Studerus. "Reduze 2 - Distributed Feynman Integral Reduction" (2012). arXiv: 1201.4330 [hep-ph].

[256] C. Bauer, A. Frink, and R. Kreckel. "Introduction to the GiNaC Framework for Symbolic Computation within the C++ Programming Language". *Journal of Symbolic Computation* 33.1 (2002), pp. 1–12. DOI: 10.1006/jsco.2001.0494.

[257] J. A. M. Vermaseren. "New features of FORM" (2000). arXiv: math-ph/0010025 [math-ph].

[258] M. Tentyukov and J. Vermaseren. "The multithreaded version of FORM". *Computer Physics Communications* 181.8 (2010), pp. 1419–1427. DOI: 10.1016/j.cpc.2010.04.009. arXiv: hep-ph/0702279.

[259] O. V. Tarasov and A. A. Vladimirov. "Two Loop Renormalization of the Yang-Mills Theory in an Arbitrary Gauge". *Sov. J. Nucl. Phys.* 25 (1977), p. 585.

[260] E. Egorian and O. V. Tarasov. "Two Loop Renormalization of the QCD in an Arbitrary Gauge". *Teor. Mat. Fiz.* 41 (1979), pp. 26–32.

[261] M. Caffo et al. "The Master differential equations for the two loop sunrise selfmass amplitudes". *Nuovo Cim. A* 111 (1998), pp. 365–389. arXiv: hep-th/9805118.

[262] M. L. Bellac. *Quantum and Statistical Field Theory*. OUP Oxford, 1992. 612 pp. ISBN: 0198539649.

ECOLE DOCTORALE

Titre: Fonctions de corrélation de Yang-Mills et de la Chromodynamique Quantique dans le modèle de Curci-Ferrari à deux boucles

Mots clés: Chromodynamique Quantique à basse énergie, fonctions de corrélation, modèle de Curci-Ferrari, deux boucles

Résumé: La Chromodynamique Quantique (QCD) est une théorie de jauge bien établie qui décrit la dynamique des quarks et des gluons. Au niveau analytique, les observables physiques ne peuvent être calculées que lorsque la jauge est fixée. La méthode standard pour y parvenir est la méthode de Faddeev-Popov (FP), qui introduit comme sous-produit des champs auxiliaires non physiques, les "fantômes". D'autre part, le couplage de jauge de la QCD devient faible pour des impulsions très élevées, ce qui fait de la théorie des perturbations (TP) un outil de calcul approprié dans cette limite. L'approche perturbative dans le cadre de la méthode de FP s'est avérée extrêmement utile et a été testée expérimentalement à de nombreuses reprises. Cependant, dans la gamme opposée d'impulsions, la méthode de FP n'est plus entièrement valide en raison de la présence de copies de Gribov. Par conséquent, pour accéder à l'infrarouge de la QCD, une approche alternative est nécessaire.

Cette thèse est consacrée à une de ces approches : le modèle de Curci-Ferrari (CF) dans la jauge de Landau. Elle consiste en une simple extension de la théorie de FP, à laquelle est ajouté un terme de masse pour le champ de gluons. Sa principale motivation provient des simulations numériques de fonctions de corrélation dans la jauge de Landau, qui indiquent clairement que le gluon acquiert une masse dans l'infrarouge profond. En plus de ce phénomène frappant, les simulations numériques montrent un couplage de jauge compatible avec une analyse perturbative pour toute la gamme d'impulsions, au moins pour le secteur pure jauge - ou de Yang-Mills (YM). Ainsi, afin de tester le modèle, plusieurs fonctions de corrélation à deux et trois points ont été évaluées de manière perturbative à une boucle. D'une manière générale, ces résultats montrent un bon accord avec leurs homologues numériques. Plus récemment, les fonctions à deux points de la théorie YM pure ont été évaluées à deux boucles, améliorant ainsi l'accord avec les données des simulations. L'objectif de cette thèse est d'étendre les calculs à deux boucles à d'autres fonctions de corrélation. Il s'agira ainsi de tester plus avant l'approche perturbative dans le modèle de CF, tout en clarifiant ses limites.

Dans le cas de la théorie YM pure, nous évaluons le vertex fantôme-antifantôme-gluon et le vertex à trois gluons dans une configuration cinématique particulière, en quatre dimensions, pour les groupes de jauge SU(2) et SU(3). Ces deux quantités sont une pure prédiction du modèle de CF, puisque les deux paramètres libres du modèle sont déterminés à partir de l'ajustement des fonctions à deux points. De manière générale, les corrections à deux boucles améliorent l'accord avec les numériques par rapport aux corrections à une boucle. La dépendance de nos prédictions par rapport au schéma de renormalisation, diminue également une fois les corrections à deux boucles incluses, ce qui conforte l'approche perturbative. En ce qui concerne le vertex à trois gluons, le calcul nous permet notamment d'obtenir des informations sur le passage à zéro ainsi que de tester une prédiction sur le comportement dominant exact de cette quantité dans l'infrarouge.

Nous concluons cette étude en calculant les fonctions à deux boucles pour le fantôme, le gluon et le quark dans le cadre de la QCD, en présence deux saveurs dégénérées de quarks, et en les comparant aux données des simulations numériques. Les résultats à deux boucles montrent un accord au résultats numériques systématiquement meilleur par rapport aux évaluations à une boucle, à l'exception de la fonction de masse des quarks légers. Ce résultat est particulièrement pertinent pour la fonction d'habillage des quarks, puisque les calculs à une boucle est incapable de reproduire les données des simulations. Cette incohérence est levée à deux boucles tant sur le plan qualitatif que quantitatif.

Title: Yang-Mills and Quantum Chromodynamics correlation functions from the Curci-Ferrari model at two-loop accuracy

Keywords: Low-energy Quantum Chromodynamics, correlation functions, Curci-Ferrari model, two-loop

Abstract: Quantum Chromodynamics (QCD) is a well established gauge theory which describes the dynamics of quarks and gluons. At the analytical level, physical observables can be computed only after the gauge is fixed. The textbook procedure to do so is the Faddeev-Popov (FP) method, which introduces, as a byproduct, auxiliary non-physical fields known as ghosts. Moreover, the QCD gauge coupling becomes small at very high momenta, making of perturbation theory (PT) a suitable calculation tool within that region of momenta. The combination of the FP theory and PT has turned out to be extremely useful and has been tested experimentally in many occasions. However, in the opposite momentum range, the FP method is no longer fully valid due to the presence of Gribov copies. Consequently, in order to access QCD in the infrared, new approaches are needed.

This thesis is devoted to one of such approaches: the Curci-Ferrari (CF) model in Landau gauge. It consists in a simple gluon mass extension of the FP theory. Its main motivation comes from the lattice simulations for correlation functions in the Landau gauge, which clearly indicate that the gluon acquires a mass in the deep infrared. In addition to this striking phenomenon, lattice simulations feature a gauge coupling compatible with a perturbative analysis for the whole range of momenta, at least in the pure gauge - or Yang-Mills (YM) - sector. Thus, with the purpose of testing the model, several two- and three-point correlation functions have been perturbatively evaluated at one-loop order. In general terms, the results show a very good agreement with the lattice data. More recently, the two-point functions from the pure YM theory were evaluated at two-loop order, improving the agreement with lattice data. The goal of this thesis is to extend the two-loop calculations to other correlation functions. This is a way to further test the perturbative use of the model as well as to clarify its limits.

In the case of pure YM theory, we evaluate the ghost-antighost-gluon vertex and the three-gluon vertex in a particular kinematical configuration in four dimensions, for the SU(2) and SU(3) gauge groups. Both quantities emerge as a pure prediction of the CF model, since its two free parameters are determined by fitting the two-point functions. Broadly speaking, the predicted vertices are able to improve the agreement with their numerical counterparts in comparison with the one-loop correction. We also investigate the renormalization scheme dependence of our results, which shows consistency with the perturbative approach. As for the three-gluon vertex, the calculation allows us in particular to gain insight on the zero-crossing as well as to test an exact prediction for its leading behavior in the infrared.

We end this investigation by fitting the ghost, gluon and quark two-point functions in QCD, with two degenerate quark flavors, to available lattice data. Our evaluation is consistent with such data in all cases, except for the quark mass function in the case of light quarks. The result is particularly relevant for the quark dressing function, since the CF model is unable to reproduce the lattice data at one-loop order. This discrepancy is corrected by the two-loop evaluation, which agrees with the data both at a qualitative and at a quantitative level.

Institut Polytechnique de Paris
91120 Palaiseau, France